INAUGURALDISSERTATION
zur Erlangung der Doktorwürde der
Naturwissenschaftlich-Mathematischen Gesamtfakultät
der
Ruprecht-Karls-Universität
Heidelberg

vorgelegt von
Diplom-Biologe Christian Stoy
geboren in Marktheidenfeld

Tag der mündlichen Prüfung:

____. ____. _____

Transcriptional co-regulators TBL1X and TBL1XR1 control tumor growth and tumor cell metabolism in pancreatic cancer

Gutachter:

PD Dr. Karin Müller-Decker

Prof. Dr. Stephan Herzig

Statement of authorship (Selbstständigkeitserklärung)

I hereby declare that this thesis has been written only by the undersigned, without any unauthorized use of services of a third party. No sources or aids have been used in the preparation of this thesis other than those indicated in the thesis itself. Where the work of others has been quoted or reproduced, the source is always given. This thesis, in same or similar form, has not been available to any audit authority yet.

Ich erkläre hiermit, dass ich die vorliegende Arbeit selbstständig und ohne unzulässige Hilfe Dritter verfasst habe. Ich habe keine anderen als die angegebenen Hilfsmittel und Quellen verwendet. Insbesondere habe ich wörtlich oder sinngemäß aus anderen Werken übernommene Inhalte als solche kenntlich gemacht. Die Arbeit ist in dieser oder ähnlicher Form noch nicht als Prüfungsarbeit eingereicht worden.

Christian Stoy,
Heidelberg (Germany), 2014

πάντες ἄνθρωποι τοῦ εἰδέναι ὀρέγονται φύσει.

All men by nature desire to know.

Aristotle
(Metaphysics, 980a, 21)

This document was typeset with XeLaTeX using the Linux Libertine font family.
The word cloud on the cover page was created with Wordle™ (www.wordle.net) based on chapters 1–4.

Contents

List of Figures

List of Tables

Abbreviations and chemical formulae

2-DG 2-deoxy-D-glucose

ACLY ATP citrate lyase

AGE advanced glycation endproduct

Akt protein kinase B

AMP adenosine monophosphate

AMPK 5'-AMP-activated protein kinase catalytic subunit alpha-2

ANOVA analysis of variance

AP-1 activator protein 1

APS ammonium persulfate

AR androgen receptor

Arf cyclin-dependent kinase inhibitor 2A

ATCC American Type Culture Collection

ATP adenosine triphosphate

BCA bicinchoninic acid

BMI body mass index; BMI = $\frac{\text{weight in kg}}{(\text{height in m})^2}$

BRCA2 breast cancer type 2 susceptibility protein

BrdU 5-bromo-2'-deoxyuridine

BSA bovine serum albumin

$CaCl_2$ calcium chloride

$CaCO_3$ calcium carbonate

$CaHPO_4$ calcium monohydrogen phosphate

cAMP 3'-5'-cyclic adenosine monophosphate

CARM1 coactivator-associated arginine methyltransferase 1

Cat. No. catalogue number

CDA cytidine deaminase

CDC Centers for Disease Control and Prevention

CDK cyclin-dependent kinase

cDNA complementary DNA

$CHCl_3$ chloroform / trichloromethane

ChIP chromatin immunoprecipitation

CI confidence interval

CK1 casein kinase I

c-Kit mast/stem cell growth factor receptor Kit

CO_2 carbon dioxide

CoA coenzyme A

COX-2 cyclooxygenase 2

CP chronic pancreatits

CPT1A carnitine palmitoyl transferase 1, liver isoform

CPT1B carnitine palmitoyl transferase 1, muscle isoform

Cre Cre-recombinase

CREB cyclic AMP-responsive element-binding protein 1

CRHR corticotropin-releasing factor receptor

CRTC2 CREB-regulated transcription coactivator 2

C_T cycle threshold

CtBP C-terminal-binding protein

$CuSO_4$ copper (II) sulfate

DAB diaminobenzidine

DAPI 4',6-diamidino-2-phenylindole

DCK deoxycytidine kinase

ddH_2O double-distilled water

DEPC diethylpyrocarbonate

DKFZ Deutsches Krebsforschungszentrum (German Cancer Research Center)

DMEM Dulbecco's modified Eagle's medium

DMSO dimethyl sulfoxide

DNA deoxyribonucleic acid

DPBS Dulbecco's phosphate buffered saline

DPPHR duodenum-preserving pancreatic head resection

DTT DL-dithiothreitol

ECAR extracellular acidification rate

ECL enhanced chemoluminescence

EDTA ethylenediaminetetraacetic acid

EdU 5-ethynyl-2'-deoxyuridine

EGFR epidermal growth factor receptor

EGTA ethylene glycol tetraacetic acid

Ela elastase

ELISA enzyme-linked immunosorbent assay

EMAP endothelial monocyte activating polypeptide II

EMT epithelial-mesenchymal transition

ER estrogen receptor

Erk extracellular signal-regulated kinase

ERT estrogen receptor, T variant

ERT2 estrogen receptor, T2 variant

ETV6 ETS translocation variant 6

FAM 6-carboxyfluorescein

FASN fatty acid synthase

FBS fetal bovine serum

FCCP carbonyl cyanide-4-(trifluoromethoxy)phenylhydrazone

fl floxed, i. e. flanked by LoxP sites

G12D glycine to aspartic acid mutation at position 12

G12V glycine to valine mutation at position 12

G6PD glucose-6-phosphate dehydrogenase

GDP guanosine diphosphate

GEM gemcitabine

GLP1 glucagon-like peptide 1

GLP1R glucagon-like peptide 1 receptor

GLS2 glutaminase 2

GLUT1 glucose transporter 1

GLUT2 glucose transporter 2

GO Gene Ontology

GOBP Gene Ontology Biological Process

GR glucocorticoid receptor

GSEA gene set enrichment analysis

GSK3 glycogen synthase kinase-3

Gsk3β glycogen synthase kinase-3 beta

GTP guanosine triphosphate

H2B histone 2B

H_2O water

H_2O_2 hydrogen peroxide

H_3BO_3 boric acid

H4 histone 4

HCl hydrochloric acid

HDAC histone deacetylase

H & E hematoxilin and eosin

hENT1 human equilibrative nucleoside transporter-1

HEPES 4-(2-hydroxyethyl)piperazine-1-ethanesulfonic acid

HFD high fat diet

HIF-1α hypoxia-inducible factor 1-alpha

HIV human immunodeficiency virus

HK2 hexokinase 2

HRE hormone-response element

HRP horseradish peroxidase

IB immunoblot

ifu infectious unit

IGF-I insulin-like growth factor I

IGF-IR insulin-like growth factor I receptor

IGFBP IGF-I binding protein

IgG immunoglobulin G

IHC immunohistochemistry

IL interleukin

Ink4a/Arf cyclin-dependent kinase inhibitor 2A

IRS1 insulin receptor substrate 1

IVC individually ventilated cages

KCl potassium chloride

KEGG Kyoto encyclopedia of genes and genomes

KH_2PO_4 potassium dihydrogen phosphate

Kras Kirsten rat sarcoma viral oncogene homologue

LacZ gene encoding β-galactosidase

LDHa L-Lactate dehydrogenase A chain

LFD low fat diet

LiCl lithium chloride

LisH lis homology

LoxP locus of X-over P1 (recombination target sequence derived from bacteriophage P1)

LSL LoxP-STOP-LoxP cassette

MAPK mitogen-activated protein kinase

$MgCl_2$ magnesium chloride

$MgSO_4$ magnesium sulfate

miRNA micro-RNA

Mist1 class A basic helix-loop-helix protein 15

MOI multiplicity of infection (MOI = $\frac{\text{number of infectious particles}}{\text{number of cells to infect}}$)

MOPS 3-(*N*-morpholino)propanesulfonic acid

mRNA messenger RNA

n. d. not detectable

n. s. not significant

Na_2HPO_4 di-sodium hydrogen phosphate

Na_2MoO_4 sodium molybdate

Na_3VO_4 sodium orthovanadate

NaF sodium fluoride

$NaHCO_3$ sodium carbonate

NaOH sodium hydroxide

NC negative control

NCoR nuclear receptor co-repressor

NF-κB nuclear factor 'kappa-light-chain-enhancer' of activated B-cells

NMR nuclear magnetic resonance

NRIP1 nuclear receptor-interacting protein 1

OCR oxygen consumption rate

OD optical density

OR odds ratio OR = $\frac{P(A)\cdot(1-P(B))}{P(B)\cdot(1-P(A))}$ with $P(A)$ and $P(B)$ being the probabilities for the occurrence of events A and B. In this context an OR of ≥1 means increased odds for the occurrence of event A whereas an OR ≤1 means decreased odds for the occurrence of event A.

ORA overrepresentation analysis

Ⓟ phosphorylated

p48 Ptf1a / p48 DNA-binding subunit of transcription factor PTF1

p53 cellular tumor antigen p53

PanIN pancreatic intraepithelial neoplasia

PBS phosphate buffered saline

PCR polymerase chain reaction

PDAC pancreatic ductal adenocarcinoma

PDGFR platelet derived growth factor receptor

PDK1 pyruvate dehydrogenase kinase 1

PDK4 pyruvate dehydrogenase kinase 4

Pdx1 pancreas/duodenum homeobox protein 1

PGC1α peroxysome proliferator-activated receptor gamma coactivator 1-alpha

PI(3)P phosphatidylinositol-3-phosphate

$PI(3,4)P_2$ phosphatidylinositol-(3,4)-bisphosphate

$PI(3,4,5)P_3$ phosphatidylinositol-(3,4,5)-trisphosphate

PI3K phosphatidylinositol-4,5-bisphosphate 3-kinase

PIK3CA gene encoding for phosphatidylinositol 4,5-bisphosphate 3-kinase catalytic subunit alpha isoform

PKC protein kinase C

pp pylorus-preserving

PPARα peroxysome proliferator-activated receptor alpha

PPARγ peroxysome proliferator-activated receptor gamma

PPARGC1A gene encoding for PGC1α

PR progesteron receptor

PRMT4 protein arginine *N*-methyltransferase 4 (synonym name for CARM1)

PTEN phosphatase and tensin homolog

PTF1 pancreas transcription factor 1

PVDF polyvinylidene fluoride

R172H arginine to histidine mutation at position 172

Raf rapidly accelerated fibrosarcoma proto-oncogene serine/threonine-protein kinase

RAGE receptor of advanced glycation endproducts

RAR retinoic acid receptor

Ras rat sarcoma viral oncogene homolog

RET proto-oncogene tyrosine-protein kinase receptor Ret

Rip recombinant insulin promoter

RIP140 receptor-interacting protein 140 (synonym for NRIP1)

RIPA radioimmunoprecipitation assay

RNA ribonucleic acid

RNR ribonucleotide reductase

ROS reactive oxygen species

RR relative risk RR = $\frac{P(\text{event when exposed to risk factor})}{P(\text{event when not exposed to risk factor})}$. An RR ≥1 indicates an increased risk to suffer from a given disease when exposed to a risk factor and an RR ≤1 indicates a decreased risk.

RRM1 ribonucleotide reductase M1

RRM2 ribonucleotide reductase M2

RUNX1 Runt-related transcription factor 1

RXR retinoid X receptor

SCD1 stearyl-CoA desaturase

SD standard deviation $SD = \sqrt{\frac{1}{n-1}\sum_{i=1}^{n}(x_i - \bar{x})}$

SDS sodium dodecylsulfate

SEM standard error of the mean $SEM = \frac{SD}{\sqrt{n}}$

shNC negative control shRNA

shRNA short hairpin RNA

siNC negative control siRNA

siRNA small interfering RNA

Smad mothers against decapentaplegic homologue

SMRT silencing mediator of retinoid and thyroid hormone receptors

SRB sulforhodamine B

STAT3 signal transducer and activator of transcription 3

SUMO small ubiquitin-related modifier

TAMRA tetramethylrhodamine

TBL1X transducin-beta-like 1, X-linked

TBL1XR1 transducin-beta-like 1X-related protein 1

TBP TATA-box-binding protein

TEMED *N,N,N',N'*-tetramethylethane-1,2-diamine

TetO tetracycline operator

tet-OFF tetracycline-off inducible expression (gene expression is active in the absence of tetracycline or doxycycline)

TGFβ transforming growth factor beta

TNFα tumor necrosis factor alpha

TNFR tumor necrosis factor alpha receptor

TORC2 transducer of regulated cAMP response element-binding protein 2 (synonym for CRTC2)

TR thyroid hormone receptor

Tris tris(hydroxymethyl)aminomethane

Triton® X-100 octylphenolpoly(ethyleneglycolether)$_n$

Trp53 gene encoding for cellular tumor antigen p53

TSC22D4 transforming growth factor-beta-stimulated clone-22 domain family protein 4

tTA tetracycline transactivator

Tween® 20 polyethylene glycol sorbitan monolaurat

UbcH5 ubiquitin-conjugating enzyme E2 D1

UbcH7 ubiquitin-conjugating enzyme E2 L3

UCN3 urocortin 3

UCP1 mitochondrial brown fat uncoupling protein 1

VCP valosin-containing protein / transitional endoplasmic reticulum ATPase

VEGF-C vascular endothelial growth factor C

VEGFR vascular endothelial growth factor receptor

WAT white adipose tissue

WD40 repeat *a short structural motif of approximately 40 amino acids, often terminating in a tryptophan-aspartic acid (W-D) dipeptide*

Whipple partial pancreatoduodenectomy according to Kausch and Whipple

WHO World Health Organization

Wnt wingless-related integration site

wt wild type

Summary

Pancreatic ductal adenocarcinoma (PDAC) is among the ten most frequent cancers in the western world, and also one of the most lethal. The mortality rate approximately equals the incidence rate and the five-year survival rate is only around 5 %, mainly due to advanced stage at diagnosis, non-resectability, and frequent chemotherapy resistance. Epidemiological studies show that obesity and/or type 2 diabetes increase the risk of PDAC. Both conditions have been increasing world wide during the last 20–30 years, and have become a global health hazard.

The transcriptional co-regulators TBL1X (transducin-beta-like 1, X-linked) and TBL1XR1 (transducin-beta-like 1X-related protein 1) mediate the exchange of co-repressors to co-activators on target gene promoters. They have been shown by previous work in our lab to regulate lipid metabolism in liver and white adipose tissue. Furthermore, they interact with Wnt/β-catenin signaling, a pathway frequently altered in cancers. Recent studies have shown a growth-regulating role of TBL1XR1 in various cancer entities, but not in pancreatic cancer.

The aim of the present study was therefore to investigate whether TBL1X and/or TBL1XR1 play a role in pancreatic cancer and might link tumor initiation or progression with obesity or type 2 diabetes.

While the latter could not be confirmed, the present study was able to show that TBL1X and TBL1XR1 were highly expressed in human and murine pancreatic cancer. The expression was specific for PanIN precursor lesions and carcinoma cells, while healthy tissue showed little to no expression. In human patients, multiple genes involved in metabolic processes showed a high correlation with *TBL1X* and *TBL1XR1* expression. *In vitro* studies revealed a growth-promoting effect of TBL1X and TBL1XR1 in pancreatic cancer cells and gene expression microarrays indicated cell cycle and p53 signaling as the most prominently regulated pathways. Furthermore, both proteins, especially TBL1X, affected tumor cell glucose metabolism and cellular response to glucose withdrawal.

Application of a syngeneic subcutaneous allograft mouse model confirmed the growth-regulating effect of Tbl1x *in vivo*. Ablation of Tbl1x additionally sensitized murine Panc02 tumor cells to gemcitabine, the most commonly used chemotherapeutic agent for pancreatic cancer. Tbl1x-deficient cells had markedly reduced levels of PI3 kinase, a major regulator of cell growth and metabolism, as well as downstream mediators. TBL1X was confirmed to bind to PI3 kinase promoter region and its expression correlated with PI3 kinase in human patients.

Taken together, this study is the first to show a role of TBL1X in cancer, and of TBL1XR1 in pancreatic cancer, both in humans and in mice. The control of PI3 kinase by TBL1X on the transcriptional level is a plausible explanation for the observed sensitization to gemcitabine, making TBL1X an attractive target for future cancer therapies to enhance treatment response and patient survival.

Zusammenfassung

Das duktale Adenokarzinom des Pankreas gehört zu den zehn häufigsten Tumorarten in der westlichen Welt und ist zugleich eine der tödlichsten. Die Mortalität entspricht in etwa der Inzidenz, die Fünfjahresüberlebensrate beträgt nur rund 5 %. Dies rührt hauptsächlich daher, dass die Tumoren zum Zeitpunkt der Diagnose meist in einem fortgeschrittenen Stadium und oft nicht resektierbar sind. Zudem sprechen sie häufig nicht auf Chemotherapie an. Epidemiologische Studien zeigen, dass Fettleibigkeit und/oder Typ-2-Diabetes mit einem erhöhten Risiko für Pankreaskrebs einhergehen. Beide Stoffwechselstörungen haben in den letzten 20–30 Jahren weltweit zugenommen und entwickeln sich mehr und mehr zu einer Bedrohung für die globale Gesundheit.

Die transkriptionellen Koregulatoren TBL1X (transducin-beta-like 1, X-linked) und TBL1XR1 (transducin-beta-like 1X-related protein 1) vermitteln den Austausch von Korepressoren gegen Koaktivatoren auf den Promotoren von Zielgenen. Frühere Untersuchungen in unserer Arbeitsgruppe konnten zeigen, dass sie den Fettstoffwechsel in der Leber und in weißem Fettgewebe regulieren. Des weiteren interagieren sie mit dem Wnt/β-catenin-Signalweg, der in Krebszellen häufig fehlreguliert ist. Neuere Studien haben für TBL1XR1 eine wachstumsregulierende Funktion in verschiedenen Tumorarten nachgewiesen, jedoch nicht für Pankreaskrebs.

In der vorliegenden Studie sollte deshalb untersucht werden, ob TBL1X und/oder TBL1XR1 im Pankreaskrebs eine Funktion haben und ob sie eine Verbindung herstellen können zwischen Tumorentstehung oder Tumorprogression und Fettleibigkeit oder Typ-2-Diabetes.

Während letzteres nicht bestätigt werden konnte, zeigte die vorliegende Studie, dass TBL1X und TBL1XR1 in Pankreastumoren des Menschen und der Maus stark exprimiert waren. Die Expression war hierbei spezifisch für die PanIN-Vorläuferläsionen und Krebszellen, während gesundes Gewebe keine oder nur eine geringe Expression aufwies. In humanen Patienten besaß eine Vielzahl an stoffwechselrelevanten Genen eine starke Korrelation ihrer Expression mit derjenigen von TBL1X und TBL1XR1. *In-vitro*-Studien konnten nachweisen, dass TBL1X und TBL1XR1 einen wachstumsfördernden Effekt auf Krebszellen haben und Genexpressions-Microarrays brachten Zellzyklus und den p53-Signalweg als stark regulierte zelluläre Signalwege zu Tage. Des weiteren beeinflussten beide Proteine, und speziell TBL1X, den Glucosestoffwechsel von Pankreaskrebszellen sowie ihr Wachstumsverhalten in Abwesenheit von Glucose.

Mittels eines syngenen subkutanen Allotransplantat-Modells in der Maus konnte die wachstumsregulierende Funktion von Tbl1x *in vivo* bestätigt werden. Darüber hinaus waren Tbl1x-defiziente murine Panc02-Pankreaskrebszellen sensitiver gegenüber dem bei Pankreaskrebs meist verwendeten Chemotherapeutikum Gemcitabin. Diese Zellen wiesen zudem geringere Mengen des Proteins PI3-Kinase auf, eines wichtigen Regulators für Zellwachstum und Stoffwechsel, und auch in der PI3-Kinase-Signalkette nachgeschaltete Proteine waren in ihrer Menge reduziert. Nachfolgend konnte gezeigt werden, dass TBL1X an die Promotorregion des PI3-Kinase-Gens bindet und dass in humanen Tumoren die Expression von TBL1X mit derjenigen von PI3-Kinase korreliert.

Die vorliegende Studie ist die erste, die eine Funktion von TBL1X in Krebs und von TBL1XR1 im Pankreaskrebs aufzeigt, sowohl im Menschen als auch in der Maus. Die Kontrolle von PI3-Kinase durch TBL1X auf transkriptioneller Ebene ist eine plausible Erklärung für die beobachtete Sensitivierung gegenüber Gemcitabin. TBL1X ist somit ein attraktives Ziel für zukünftige Krebstherapien zur Verbesserung des Ansprechens auf Chemotherapie und des Überlebens der Patienten.

1 Introduction

1.1 The pancreas

The pancreas is located in the upper abdomen. It has a length of 16–20 cm, a width of 3–4 cm, a thickness of 1–2 cm and a weight of 70–100 g. The head lies in the bend of the duodenum with the main body reaching behind the stomach and the tail touching the spleen (see figure 1.1 on the following page).

It is both an exocrine and endocrine organ. The exocrine part constitutes the majority of the pancreatic tissue and consists of acinar tissue producing pancreatic fluid rich in digestive enzymes (lipases, proteases, amylases) that is released to the duodenum via the main and accessory pancreatic duct. The acini are clustered in a grape-like manner and are located at the ends of the highly branched ductal system. The ductal cells enrich the pancreatic fluid with mucous and bicarbonate. Embedded into the exocrine tissue are the islets of Langerhans that constitute the endocrine part of the organ. They contain several cell types secreting various hormones, namely α-cells (15–20 % of total islet cells, producing glucagon), β-cells (65–80 %, producing insulin and amylin), δ-cells (3–10 %, producing somatostatin), PP-cells (3–5 %, producing pancreatic polypeptide) and ε-cells (<1 %, producing ghrelin) [1]. These hormones are distributed throughout the body via the bloodstream (see figure 1.2C). Insulin and glucagon are the major regulators of glucose homeostasis in the body. During fasting, when blood glucose levels are low, glucagon is secreted promoting glycogenolysis in the liver and glucose release into the blood. After a meal, blood glucose rises which in turn stimulates insulin secretion promoting energy storage by means of glucose uptake and glycogen synthesis in liver and muscle, as well as fat uptake and lipid synthesis in adipose tissue.

1.2 Pancreatic cancer

Tumors arising from the exocrine tissue of the pancreas comprise about 95 % of all pancreatic cancers [4]. Of these, the vast majority (85–90 %) are pancreatic ductal adenocarcinoma (PDAC), whereas islet tumors and other non-adenocarcinoma tumors only account for less than 15 % of pancreatic cancers [3]. The tumor commonly arises in the head of the pancreas, is characterized by a dense stroma, and is prone to infiltrate surrounding tissues, including lymph nodes, lymphatic vessels, spleen, peritoneal cavity, liver, and lung. In the early stages it often is asymptomatic or accompanied by unspecific symptoms such as diffuse pain in the upper abdomen, anorexia, nausea and vomiting, weight loss (can be associated with anorexia, early satiety, diarrhea, steatorrhea, or in later stages also chachexia), painless jaundice, or diabetes mellitus. Furthermore, the early precursor lesions are too small to be detected with imaging technologies and can only be discerned under the microscope, thus requiring a biopsy. Therefore, PDAC is in most cases diagnosed late and in an advanced stage, resulting in a dismal prognosis (see section 1.2.1). The time range between the original gene mutation (see section 1.2.2) until the establishment of a primary tumor is estimated at 11.7±3.1 years. It then takes another 6.8±3.4 years to develop metastases and patients die 2.7±1.2 years later [5].

1.2.1 Epidemiology

In Germany, as of 2009/10, 3.2 % of all newly diagnosed cancers in men and 3.6 % in women were pancreatic, placing PDAC as the 10th or 6th most frequent cancer entity, respectively. Among cancer mortality, pancreatic cancer was the 4th most common in both sexes with 6.4 % of all cancer deaths in men and 7.9 % in women. The age-standardized incidence rate was 13.8 per 100,000 in men and 10.0 per 100,000 in women, resulting in an estimate of 8,020 men and 8,060 women in total. Mortality was equally high with 12.8 per 100,000 in men and 9.5 per 100,000 in women or 7,537 and 7,950 total cases, respectively. The relative 5-year survival rate was 8 % in both sexes. Both incidence and mortality have been relatively constant since the late 1990s and equally high due to the poor prognosis of the disease [6].

For other industrialized countries the picture looks similar. In the U. S. in 2009, 2.62 % of the total cancer incidence in women and 2.54 % in men was attributed to pancreatic cancer, which ranked it the 12th or 10th most common cancer, respectively. In total, 18,421 women and 18,979 men were diagnosed with pancreatic cancer in that year. Concerning cancer mortality, pancreatic cancer ranked 5th in both sexes, comprising 6.56 % of all cancer deaths in women and 6.02 % in men. Absolute mortality was 17,758 cases among women and 17,870 among men. [7]. When diagnosed with PDAC, 52 % of patients already have distant metastases and 26 % have regional spread [8].

1.2.2 Histopathology and etiology

Pancreatic ductal adenocarcinoma is characterized by cells that re-gained a duct-like phenotype. The disease progresses via precursor lesions called pancreatic intraductal neoplasia (PanIN) that are categorized in stages 1–3 of increasing cellular and nuclear atypia (see table 1.1 on page 3 and figure 1.3 on page 4).

Mutations of the small GTPase Kras are found in about 95 % of human PDAC. They affect the glycine at codon 12 (usually G12D or G12V mutations), thus compromising the GTPase function. The mutant protein is therefore highly

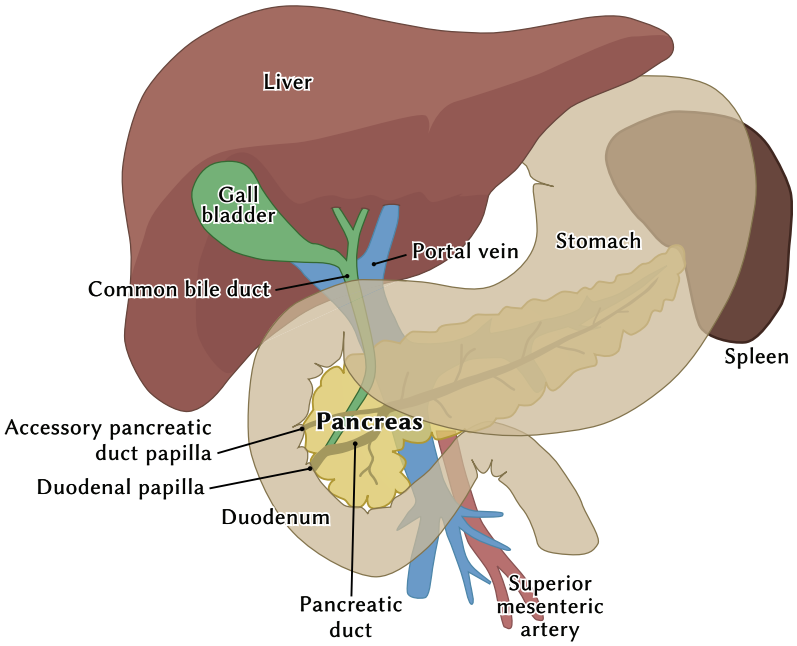

Figure 1.1: Location of the pancreas in the abdominal cavity

The pancreas is located behind the stomach with the tail touching the spleen and the head lying in the bend of the duodenum. The highly branched pancreatic duct system collects the digestive fluid produced in the exocrine tissue and releases it into the duodenum via the duodenal and the accessory pancreatic duct papilla. The terminal part of the main pancreatic duct merges with the terminal part of the common bile duct so that bile and digestive fluid are released together via the duodenal papilla; adapted from [2]

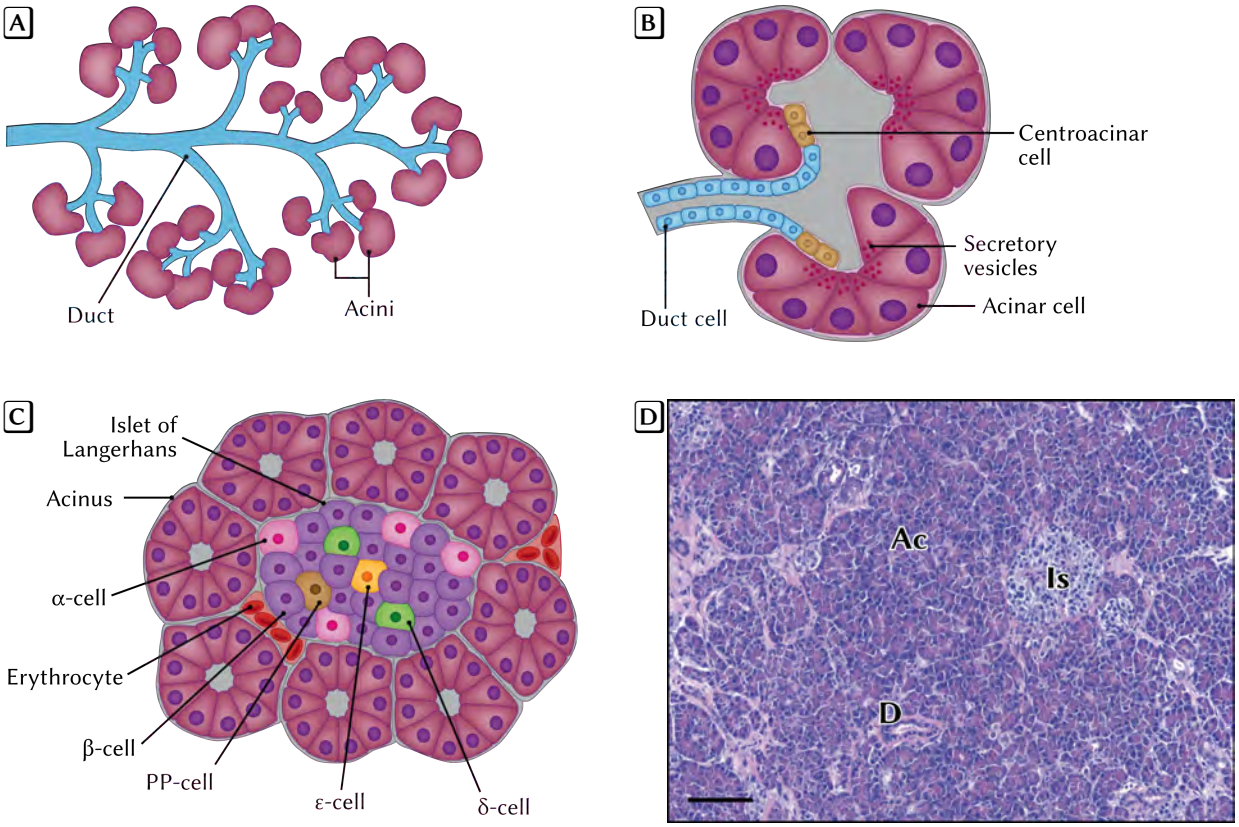

Figure 1.2: Anatomy of the pancreas

A Pancreatic ducts with acini; B Detailed structure of acini and efferent pancreatic duct; C islet of Langerhans surrounded by acinar tissue; D H & E staining of human pancreas; Ac: acinar tissue – Is: islet of Langerhans; D: pancreatic duct; scale bar 100 µm; panels A–C adapted from [3]

Table 1.1: Characterization of PanIN lesions according to Hruban et al. [11]

Normal duct	Morphology: cuboidal to low-columnar epithelium; amphophilic[1] cytoplasm; no mucinous cytoplasm; Nuclei: regularly shaped; no nuclear crowding or atypia
PanIN-1A	Morphology: flat, epithelial lesions; tall cells of columnar shape; high in supranuclear mucin Nuclei: small, round to oval, located at basal membrane Mutations: Kras mutations in 35–36 % of lesions [12, 13]; p16/Ink4a inactivation in 31 % of lesions [14]
PanIN-1B	Morphology: epithelial lesions; (micro)papillary or basally pseudostratified[2] architecture; otherwise identical to PanIN-1A Mutations: Kras mutations in 43–44 % of lesions [12, 13] p16/Ink4a inactivation in 44 % of lesions [14]
PanIN-2	Morphology: Flat or mostly papillary mucinous epithelial lesions Nuclei: some nuclear abnormalities (some loss of polarity, nuclear crowding, enlarged nuclei, pseudo-stratification[2] and hyperchromasia[3]); mitoses are rare and non-apical (non-luminal) and not atypical Mutations: Kras mutations in 87 % of PanIN-2–3 lesions [13] p16/Ink4a inactivation in 50 % of lesions [14]
PanIN-3	Morphology: papillary or micropapillary, rarely flat; cribriforming[4]; small clusters of epithelial cells budding off into the lumen; potentially luminal necroses Nuclei: loss of polarity; goblet cells with nuclei oriented towards the lumen and mucin-rich cytoplasm towards the basal membrane; mitoses potentially abnormal; nuclear irregularities; prominent (macro)nucleoli Mutations: Kras mutations in 87 % of PanIN-2–3 [13] or in 86 % of PanIN-3 lesions [12] p16/Ink4a inactivation in 85 % of lesions [14] p53 mutations in 57 % of lesions [14] loss of Smad4 in 28 % of lesions [14]

impeded in its ability to hydrolyze bound GTP. Once activated by upstream signaling events, it remains in its active state for much longer periods of time than wild type Kras [9] and can initiate a feed-forward loop of inflammation [10].

The capability of mutant Kras to reprogram pancreatic cells to a ductal phenotype giving rise to PanIN lesions progressing with age has been shown and elaborated in various mouse models, the first ones being the $p48^{+/Cre}$; $Kras^{+/LSL\text{-}G12D}$ and *Pdx1-Cre;* $Kras^{+/LSL\text{-}G12D}$ models by Hingorani et al. [15] in 2003. Despite the universal occurrence of mutant Kras in human PDAC and its capability of reprogramming pancreatic cells in mouse models, Kras signaling alone is not sufficient for a progression to fully developed PDAC. It rather relies on sequential tuning of other signaling pathways and loss of function of tumor suppressors such as p53, p16/Ink4a (Ink4a/Arf) or Smad4 which are also observed in higher-grade PanIN lesions with increasing frequency (see table 1.1). In the original model of Hingorani et al. [15] only 2 out of 29 mice (one $p48^{+/Cre}$; $Kras^{+/LSL\text{-}G12D}$ and one *Pdx1-Cre;* $Kras^{+/LSL\text{-}G12D}$) at the age of 8.25 and 6.25 months, respectively, spontaneously developed and succumbed to invasive PDAC. Therefore, in a second model, the authors crossed *Pdx1-Cre;* $Kras^{+/LSL\text{-}G12D}$ mice with *Pdx1-Cre;* $Trp53^{+/LSL\text{-}R172H}$ mice to create *Pdx1-Cre;* $Kras^{+/LSL\text{-}G12D}$; $Trp53^{+/LSL\text{-}R172H}$ mice expressing both G12D-mutant Kras and R172H-mutant p53 specifically in the pancreas [16]. These animals showed a much more rapid disease progression with a high frequency of metastases resulting in a median survival of 5 months and 100 % mortality after 12 months whereas $p48^{+/Cre}$; $Kras^{+/LSL\text{-}G12D}$ animals had a median survival rate of 15 months. During progression from pre-invasive to invasive disease the cells lost the wild type p53 allele thus becoming hemizygous for the mutant R172H allele, a feature also observed in humans. This loss of heterozygosity might be triggered by the mutant allele via chromosomal instability that is then further aggravated once the wild type allele is lost [16]. In another model, Aguirre et al. [17] created triple-transgenic *Pdx1-Cre;* $Kras^{+/LSL\text{-}G12D}$; $Ink4a/Arf^{fl/fl}$ mice with pancreas-specific expression of mutant $Kras^{G12D}$ and homozygous deletion of Ink4a/Arf. These animals were clinically normal

[1] staining with either acid or basic dyes
[2] describing a type of layered epithelium in which the nuclei of adjacent cells are at different levels
[3] increased staining capacity of nuclei for hematoxylin due to an increase in chromatin
[4] perforated like a sieve

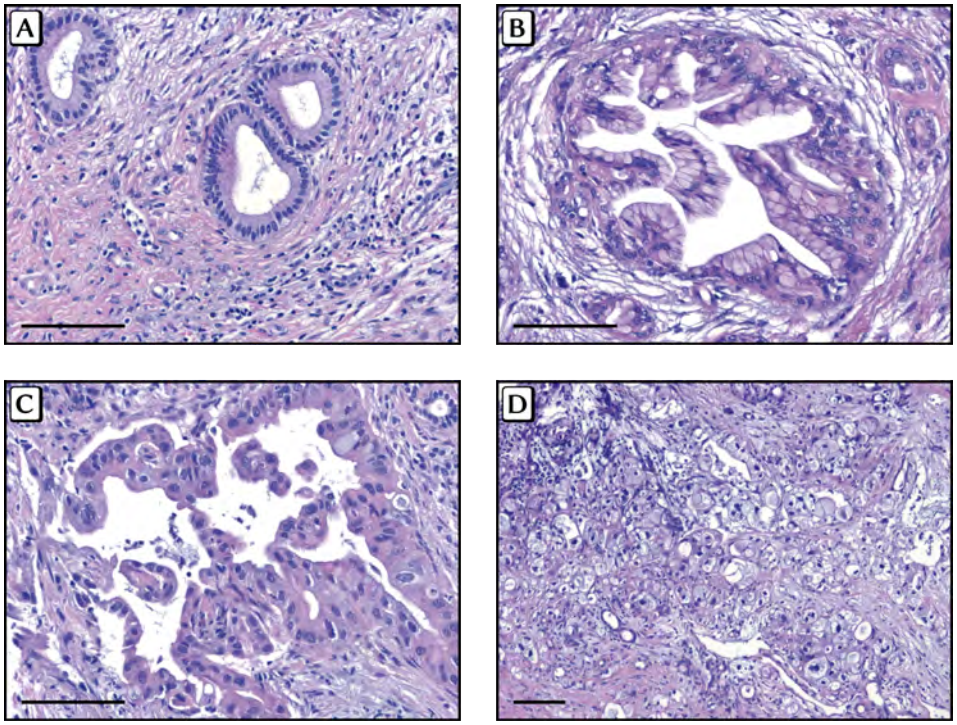

Figure 1.3: Progression from PanINs to PDAC
A PanIN-1 lesion. B PanIN-2 lesion. C PanIN-3 lesion. D invasive carcinoma embedded in extensive fibrotic stromal tissue. Scale bars 100 µm.

until 7 weeks of age but falling moribund between weeks 7–11 with symptoms of weight loss, ascites and jaundice. Necropsy revealed tumors between 4–20 mm in size that were highly invasive, frequently affecting the duodenum and spleen and occasionally obstructing the common bile duct. On the other hand, *Pdx1-Cre; Ink4a/Arf* $^{fl/fl}$ mice did not develop pancreatic tumors. At the age of 5 weeks all examined *Pdx1-Cre; Ink4a/Arf* $^{fl/fl}$ mice had developed small PDACs while still clinically asymptomatic. In contrast, *Pdx1-Cre; Ink4a/Arf* $^{fl/+}$ mice hemizygous for Ink4a/Arf only showed low-grade PanIN lesions. Taken together, these two mouse models as well as others (see [18, Tab. 1]) support the idea of a two-hit model of human PDAC with initiating Kras mutations and progression to PDAC after subsequent loss of function of tumor suppressors p16/Ink4a (Ink4a/Arf) and p53.

The cell type of origin for pancreatic cancer is still under debate, however, epithelial, acinar and islet cells are the likeliest candidates as they have been implicated in several mouse models. Carrière et al. [19] used *Nestin-Cre; Kras* $^{+/LSL\text{-}G12D}$ mice where Cre-recombinase triggers recombination and expression of mutant Kras in pancreatic exocrine progenitors and descending acinar and some rare ductal cells, but also in the central nervous system. This model was sufficient to invoke PanIN lesions. In *Ela-tTA; tetO-Cre; Kras* $^{+/LSL\text{-}G12V}$ mice, Cre is both under the control of the elastase promoter and the tet-OFF system. In the absence of doxycycline, recombination of mutant Kras takes place resulting in its expression in acinar and centroacinar cells. These animals also were capable of developing PanIN lesions [20]. Habbe et al. [21] used three different mouse models where Cre was induced by tamoxifen injection allowing to trigger mutant Kras expression in adult mice. In the *Ela-Cre* ^{ERT2}*; Kras* $^{+/LSL\text{-}G12D}$ and *Mist1-Cre* ^{ERT2}*; Kras* $^{+/LSL\text{-}G12D}$ animals the recombination took place in mature acinar cells whereas in *Pdx1-Cre* ^{ERT2}*; Kras* $^{+/LSL\text{-}G12D}$ mice Cre was activated in mature β-cells. Both acinar models showed the full spectrum of PanIN lesions while the *Pdx1-Cre* ^{ERT2}*; Kras* $^{+/LSL\text{-}G12D}$ β-cell model did not present any neoplasms during a follow-up of 12 months. Insulin-expressing cells can however give rise to PanIN lesions when stressed with cerulein-induced pancreatitis as was shown by Gidekel Friedlander et al. [22] using *Rip-Cre* ^{ERT}*; Kras* $^{+/LSL\text{-}G12D}$*; LSL-LacZ* mice. Because there are no conditionally inducible Kras models available that are specific for ductal and centroacinar cells, these are still under debate regarding their capability to undergo transformation. Since in the *p48* $^{+/Cre}$*; Kras* $^{+/LSL\text{-}G12D}$ and *Pdx1-Cre; Kras* $^{+/LSL\text{-}G12D}$ mouse models Kras recombination is triggered in pancreatic progenitors resulting in mutant Kras expression throughout the entire organ, these two remaining cell types can however not be entirely excluded to potentially give rise to PanIN lesions.

1.2.3 Risk factors

1.2.3.1 Smoking, alcohol and pancreatitis

The most prominent risk factor for PDAC is cigarette smoking. Meta-analysis showed that current smokers are at a 2.2-fold (95 % CI: 1.71–2.83) higher risk for pancreatic cancer [23, 24]. Roughly 25 % of pancreatic tumors can be attributed to cigarette smoking [25]. Other frequent risk factors are alcohol abuse and pancreatitis. Individuals who consumed more than 6 drinks per day had an OR of 1.46 (95 % CI: 1.16–1.83) compared to those who took less than one drink per day [26]. Having a history of chronic pancreatitis resulted in a 2.71-fold (95 % CI: 1.96–3.74) increased OR for pancreatic cancer when the interval between the two diagnoses was more than two years [27].

1.2.3.2 Genetic predisposition

A familial history of pancreatic cancer with two or more first degree relatives being diagnosed with PDAC is a strong indicator of a genetic predisposition. This may be the case in up to 10 % of patients [28] and often involves the *BRCA2* gene that is well known for its role in hereditary breast cancer [29]. In cases with familial background, genetic testing should be considered to allow preventive measures. In such high-risk individuals, screening measures that would otherwise be too expensive or burdensome, such as endoscopic ultrasound and nuclear magnetic resonance (NMR) imaging, are advisable to detect tumors in an early stage.

1.2.3.3 Metabolic syndrome

In recent years it has become evident that constituents of the metabolic syndrome, namely obesity and type 2 diabetes, are risk factors for various cancer entities, including PDAC.

Several prospective cohort studies showed an increased risk for obese individuals (BMI ≥30) compared to normal-weight individuals (BMI <25) with RR from 1.2–3.0 (summarized by Giovannucci and Michaud [30, p. 2215f and fig. 4]). Four case-control studies from the U. S. and Canada using direct interviews reported elevated risks for pancreatic cancer in obese individuals with OR from 1.3–2.0 [31–34]. Calle et al. [35] also observed an elevated risk of mortality from pancreatic and other cancers with increasing BMI in a large prospective cohort study.

For diabetic patients, it is important to clearly distinguish between long-lasting and recent-onset cases of type 2 diabetes. PDAC patients are often diagnosed with type 2 diabetes several months to several years before cancer diagnosis. In these cases it is likely that the previously undetected pancreatic cancer caused the recent onset of diabetes. A meta-analysis by Everhart [36] concluded that diabetes of 5 years or more increases the RR for PDAC by a factor of 2 (95 % CI: 1.2–3.2). In a further meta-study, Huxley et al. reported an OR of 1.5 (95 % CI: 1.3–1.8) for individuals with a diabetes history of >5 years compared to an OR of 2.1 (95 % CI: 1.9–2.3) for those with <4 years of diabetes [37, p. 2079]. These and other findings [38] support both the role of diabetes as a risk factor for PDAC as well as the effect of reverse causality in patients with recent-onset diabetes. Further evidence is provided by the Whitehall study [39] and the Chicago Heart Association Detection Project [40] where individuals with blood glucose levels of ≥11.1 mM/≥200 $^{mg}/_{dl}$ 1 h [40] or 2 h [39] after a 50 g oral glucose load had a 2- to 4-fold increased risk of pancreatic cancer death during a follow-up period of 25 years. Even when omitting deaths within the first 10 years of follow up, the 4-fold risk increase in the Whitehall study was only slightly reduced [39].

1.2.4 Pancreatic cancer and metabolic syndrome

Possible mechanisms to explain the higher risks of pancreatic cancer in obesity and type 2 diabetes have been widely discussed [30, 41, 42] and are the subject of ongoing research. In particular, the insulin/IGF-I axis as well as oxidative stress and inflammation are considered key pathways.

The activation of IGF-I (insulin-like growth factor I) receptor (IGF-IR) leads to enhanced proliferation, invasive growth, expression of angiogenic mediators, and reduced apoptosis in pancreatic cancer cells *in vitro* [43]. When the IGF-I receptor was being blocked, growth of human pancreatic cancer cells in nude mice was reduced and radiation- or chemotherapy-induced apoptosis of tumor cells was upregulated [44]. Further evidence for the role of insulin signaling was provided by a case-control study from Li et al. [45]. They could show that diabetic patients treated with metformin, a drug that lowers hepatic gluconeogenesis and enhances insulin sensitivity, had a lower risk for pancreatic cancer with an RR of 0.38 (95 % CI: 0.22–0.69). On the other hand, an increased risk for pancreatic cancer was observed in patients that had been treated with insulin or insulin secretagogues compared to those who had never taken one of these drugs. Diabetic patients treated with insulin had an overall RR for PDAC of 4.99 (95 % CI: 2.59–9.61) and an RR of 5.04 (95 % CI: 2.38–10.7) when only considering those with >2 years of diabetes. Patients treated with insulin secretagogues had an overall RR of 2.52 (95 % CI: 1.32–4.84) while those that had not been previously treated with insulin had an RR of 3.82 (95 % CI: 1.78–8.20) and those with >2 years of diabetes history had an RR of 1.74 (95 % CI: 0.80–3.77).

This is interesting considering the nature of insulin and IGF-I signaling. The insulin receptor is highly expressed in adipose tissue, muscle and kidney whereas the IGF-I receptor is found in all tissue types. The insulin receptor is a heterotetrameric aggregate of two extracellular α-subunits that are responsible for ligand binding and two intracellular β-subunits responsible for signal transduction. The two receptors have a sequence homology of >50 % and also the two ligands, insulin and IGF-I, are 40–50 % homologous. Therefore, both ligands can interact with either receptor, albeit the affinity of insulin to the insulin receptor is 1000 times higher than to the IGF-I receptor and vice versa IGF-I binds to its cognate receptor with 100–500 higher affinity than to the insulin receptor [46]. In settings of hyperinsulinemia, as observed in metabolic syndrome, high insulin levels could thus also activate IGF-IR signaling and promote tumor growth. Furthermore, high concentrations of insulin decrease the levels of IGF-I binding proteins IGFBP1 and IGFBP2 resulting in increased amounts of unbound and thus bioactive IGF-I [41].

Hyperglycemia in diabetic patients has been found to raise levels of superoxide by the mitochondrial electron transport chain in susceptible cells [47]. This process is considered a key mechanism to downstream damaging events in diabetes. Particularly the formation of advanced glycation end products (AGE) and their binding to the receptor of AGE (RAGE) are a focus of ongoing research. AGE form under conditions of high blood glucose by spontaneous chemical reaction of protein amino acids with the oxo group of glucose or other carbohydrates. Binding of AGE to RAGE can lead to increased inflammation via the NF-κB (nuclear factor kappa-light-chain-enhancer of activated B cells) pathway leading to formation of intracellular ROS (reactive oxygen species). Interestingly, RAGE were found to be expressed in several pancreatic cancer cell lines [48, 49]. This upregulation of RAGE could also be shown in *Pdx1-Cre; Kras*$^{+/LSL\text{-}G12D}$ mice [50]. Crossing these animals with *RAGE*$^{-/-}$ mice resulted in delayed carcinogenesis. Furthermore, shRNA-mediated RAGE knockdown *in vitro* resulted in decreased IL-6 (interleukin 6) secretion, reduced IL-6-induced proliferation and STAT3 (signal transducer and activator of transcription 3) phosphorylation as well as decreased autophagy.

The above mentioned protective effect of metformin on tumor growth observed by Li et al. [45] could also be demonstrated in a mouse model of obesity and hyperinsulinemia by Algire et al. [51] using subcutaneous allografts. Later studies by the same group [52] could show that metformin action on tumors was not only indirect by its effects on lowering blood glucose and insulin levels. In fact, the drug was capable of reducing endogenous Ras-induced ROS levels, DNA damage, and mutations in cells *in vitro* and ameliorating ROS-induced toxicity in mice.

The effect of obesity on pancreatic cancer was also studied in a transgenic mouse model (*p48*$^{+/Cre}$*; Kras*$^{+/LSL\text{-}G12D}$) under high fat diet (HFD) conditions [53]. The authors observed an accelerated progression of PanIN lesions. Since obesity is known to cause low-grade inflammation [54, 55], the levels of circulating TNFα (tumor necrosis factor alpha) and IL-6 were measured and indeed found to be elevated in *p48*$^{+/Cre}$*; Kras*$^{+/LSL\text{-}G12D}$ mice on HFD. Crossing *p48*$^{+/Cre}$*; Kras*$^{+/LSL\text{-}G12D}$ mice with TNF-receptor 1 deficient (*TNFR*$^{-/-}$) mice led to attenuated PanIN progression under the obesogenic regimen and reversed pancreatic insufficiency observed in *p48*$^{+/Cre}$*; Kras*$^{+/LSL\text{-}G12D}$ animals on a HFD.

Another study examining the effects of HFD on tumor growth in the pancreas was done by Philip et al. [56] using *Ela-Cre*^{ERT}*; Kras*$^{+/LSL\text{-}G12D}$ mice expressing mutant Kras in acinar cells after tamoxifen-induced activation of Cre. Here, the HFD exacerbated Kras activity and downstream signaling and resulted in enhanced PanIN lesions, pancreatic inflammation, and fibrosis. Moreover, these mice showed elevated levels of COX-2 (cyclooxygenase 2) and increased recruitment of F4/80^{+} macrophages under HFD conditions. Crossing *Ela-Cre*^{ERT}*; Kras*$^{+/LSL\text{-}G12D}$ mice with *COX-2*$^{fl/fl}$ mice resulted in mice with acinar cell specific expression of mutant Kras and concomitant deletion of COX-2. With this model it was possible to reverse the HFD-induced effects observed previously in *Ela-Cre*^{ERT}*; Kras*$^{+/LSL\text{-}G12D}$ mice, namely enhanced PanIN progression, fibrosis, inflammation, Kras activity, and macrophage infiltration. The COX-2 inhibitor celecoxib was also able to lower the levels of inflammation, fibrosis, and PanIN formation in *Ela-Cre*^{ERT}*; Kras*$^{+/LSL\text{-}G12D}$ animals. Moreover, the HFD could provoke the progression of PanINs to cancer in both *Ela-Cre*^{ERT}*; Kras*$^{+/LSL\text{-}G12D}$ and *Pdx1-Cre; Kras*$^{+/LSL\text{-}G12D}$ mice resulting in decreased median survival rates compared to animals on a normal diet.

1.2.4.1 Global perspective

Obesity and diabetes have been constantly rising worldwide during the last 3–4 decades [57–59]. They are now not only a problem in developed countries (figure 1.4 on the facing page) but are also on the rise in middle- and low-income countries [60]. According to the World Health Organization (WHO), the global obesity prevalence has almost doubled from 1980–2008 [61]. Approximately 1.4 billion or 35 % of adults over 20 years of age were overweight (BMI ≥25) and around 500 million or 12 % were obese (BMI ≥30) in 2008 [62] (see also appendix A on page 79). Concomitantly, 347 million people worldwide had diabetes in 2013 (see also appendix A on page 79) of which 80 % lived in low- and middle-income countries [63].

Regarding this worldwide dramatic trend and the fatal nature of pancreatic cancer it is of great scientific and public interest to learn more about the underlying mechanisms and identify distinct molecular pathways linking metabolic perturbations to initiation and promotion of tumors.

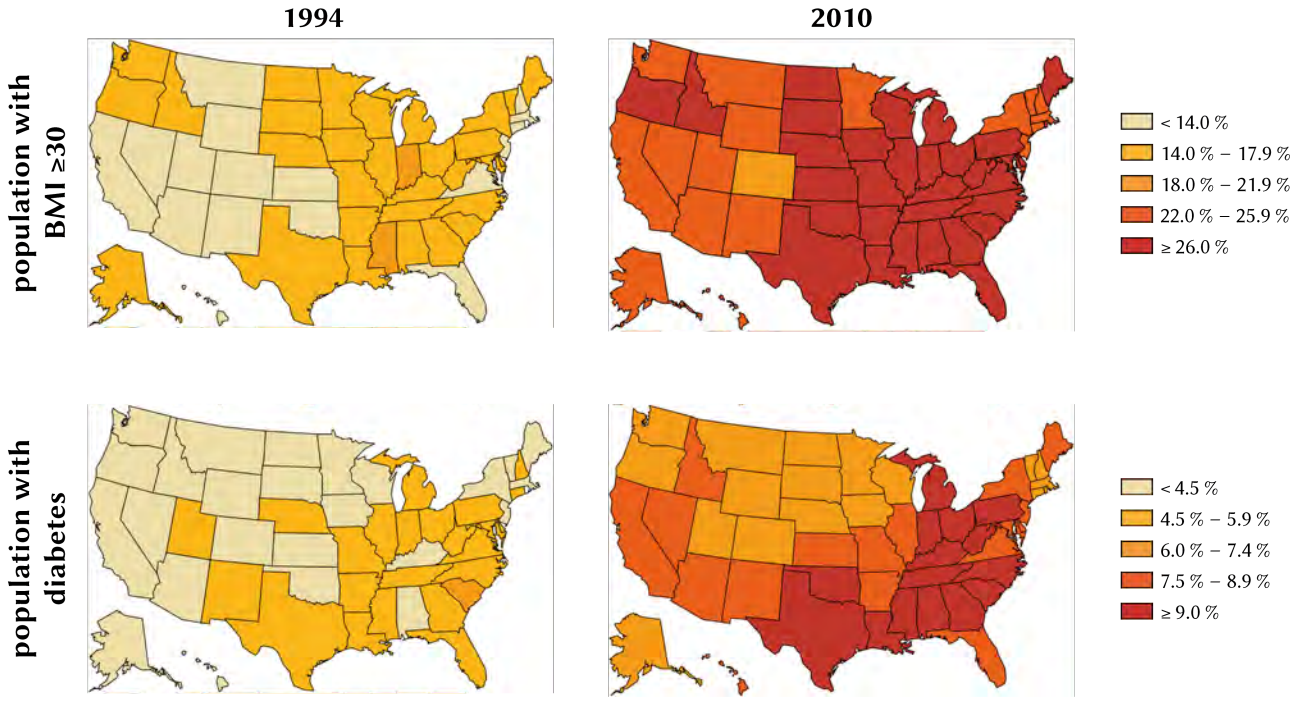

Figure 1.4: Trends of obesity and diabetes in the U. S.
Overview of obesity (BMI ≥30) and diabetes prevalence in the U. S. from 1994–2010. Data obtained from CDC [64].

1.2.5 Therapy

According to the recent S3 guideline [65], surgery is the only potentially curative measure of therapy. Only localized cancers, which occur in approximately 20 % of PDAC patients [66], are considered suitable for surgery with curative intent. Non-resectable tumors are treated with neoadjuvant chemotherapy to reduce tumor size in attempts to reach resectability. After surgery, adjuvant chemotherapy with gemcitabine or a combination of 5-fluorouracil and folinic acid has been shown to increase the 5-year survival rate from approximately 10 to 20 % [65, 67–72]. Many tumors, however, are resistant to gemcitabine in the first place or become resistant during therapy. On the other hand, a survival of 5 years after diagnosis does not guarantee a cure, as death of recurrent disease is still possible. Most patients eventually succumb to the consequences of local invasion or metastases. Long term cures of the disease are very rare.

1.2.6 Gemcitabine resistance

Gemcitabine (2',2'-difluoro-2'-deoxycytidine) is a DNA base analog. It is transported into the cell via the transmembrane transporter hENT1 (human equilibrative nucleoside transporter-1) and intracellularly converted to either the inactive compound 2',2'-difluoro-2'-deoxyuridine by cytidine deaminase (CDA) or to its corresponding triphosphate by deoxycytidine kinase (DCK). The triphosphate is then incorporated into newly synthesized DNA instead of cytidine. This causes an arrest of strand elongation during DNA replication leading to apoptosis. It can also bind to the active site of ribonucleotide reductase (RNR) thus irreversibly deactivating the enzyme [73]. When RNR is inhibited, the cell can no longer produce deoxyribonucleotides required for DNA replication and repair resulting in apoptosis.

Poor response of a tumor to gemcitabine can be attributed to multiple factors including accessibility of tumor cells to the drug, uptake into cells, intracellular metabolism or shuttling the drug out of the cell. Changes in the expression of hENT1 as well as downstream gemcitabine metabolizing enzymes, including DCK and ribonucleoside reductases M1 (RRM1) and M2 (RRM2), have been shown to play a role in gemcitabine resistance [74, 75]. Gemcitabine incorporation into cells was diminished with low expression levels of the transporter hENT1 or with dense stroma, indicating an involvement of the extracellular matrix [75].

Other studies suggest that the picture is more complex and the cell's capability to take up gemcitabine can not be attributed to the up- or downregulation of a single gene but rather the ratios of several genes have to be considered [76]. Wang et al. [77] have shown an association of gemcitabine resistance with an epithelial-mesenchymal transition (EMT) phenotype and with induction of HIF-1α (hypoxia-inducible factor 1-alpha). The PI3 kinase/Akt pathway that is often dysregulated in pancreatic cancer has also been connected to gemcitabine resistance [78–80]. Overall, gemcitabine resistance of PDAC remains a complex issue and a focus of ongoing research.

1.3 Transcriptional co-regulators TBL1X and TBL1XR1

1.3.1 Nuclear receptors

The efficient and fine tuned regulation of gene transcription is of fundamental importance in complex multicellular organisms. One class of such regulators are nuclear receptors which intracellularly bind to lipophilic signaling molecules capable of passing the cellular membrane and then exert their function.

Type I nuclear receptors bind their ligands in the cytosol, form homodimers, translocate to the nucleus and bind to specific DNA sequences (hormone-response elements, HRE) on target gene promoters. They then recruit co-activator complexes and RNA polymerase to exert target gene transcription. Members of type I nuclear receptors include androgen receptor (AR), estrogen receptors (ER), glucocorticoid receptor (GR), and progesteron receptor (PR).

Type II nuclear receptors always reside in the nucleus and bind as heterodimers (usually with retinoid X receptor RXR) to their HREs. In the unliganded state they are often associated with co-repressor complexes, such as NCoR (nuclear receptor co-repressor) and SMRT (silencing mediator of retinoid and thyroid hormone receptors) [81] or CtBP1/2 (C-terminal-binding protein 1/2) [82, 83]. These co-repressors recruit HDAC3 (histone deacetylase 3) [84], a chromatin-remodeling enzyme, that leads to hypoacetylation of histones resulting in densely packed chromatin that is inaccessible to the transcription machinery. After ligand binding, the co-repressor complexes dissociate from the nuclear receptors and co-activators and subsequently RNA polymerase are recruited to initiate target gene transcription. Type II nuclear receptors include retinoic acid receptor (RAR), retinoid X receptor (RXR) and thyroid hormone receptor (TR).

1.3.2 TBL1X and TBL1XR1 as nuclear receptor co-regulators

The two proteins TBL1X (Transducin β-like protein 1X) and TBL1XR1 (Transducin β-like 1X-related protein 1) are part of the transcriptional co-repressor complexes associated with nuclear receptors of the steroid, thyroid hormone, and retinoic acid receptor family. Their sequences are highly homologous. They consist of an N-terminal LisH and F-box-like domain followed by eight WD40 repeat domains (see figure B.1 on page 81).

1.3.2.1 Genomic location and first description

The *TBL1X* gene is located on the X-chromosome in human and mouse, and was first described by Bassi et al. [85] as being associated with X-linked ocular albinism with late-onset sensorineural deafness. Later studies identified it as part of the large co-repressor complex containing NCoR, SMRT and HDAC3 [86, 87].

TBL1XR1 is genetically encoded on chromosome 3 in human and mouse and was first identified by Zhang et al. [88] as part of that complex. TBL1X and TBL1XR1 directly interact with SMRT and NCoR whereas their interaction with HDAC3 is bridged by SMRT [87–89]. They are functionally redundant but necessary for SMRT/NCoR/HDAC3-mediated repression by unliganded TR, possibly by their ability to bind to histones H2B and H4 via their N-terminal domain [89].

1.3.2.2 TBL1X and TBL1XR1 as exchange factors

Perissi et al. [90] further delineated the function of TBL1X and TBL1XR1 showing that they act as exchange factors for nuclear receptor-associated co-repressor complexes. After ligand binding, TBL1XR1 mediated the recruitment of the E2-ubiquitin ligase UbcH5 and the 19S-proteasome resulting in degradation of the repressing SMRT/NCoR/HDAC3 complex followed by recruitment of co-activator complexes and target gene transcription. TBL1XR1 was required for the ligand-induced transcriptional activation of RAR, TR, PPARγ (peroxisome proliferator-activated receptor gamma), and ER as well as AP-1 (activator protein 1) and NF-κB, whereas TBL1X was only required for transcriptional activation of TR, PPARγ, ER, and NF-κB. The N-terminal F-box domain of TBL1X and TBL1XR1 was required for binding of UbcH5.

Interestingly, even in the absence of NCoR and SMRT, TBL1X was required for signal-dependent transcriptional activation but not in the absence of CtBP1/2 [91]. These different roles of TBL1X and TBL1XR1 on signal-induced transcriptional activation are at first sight surprising regarding their high sequence similarity (figure B.1 on page 81). Their specificity lies within distinct phosphorylation sites. The two proteins are phosphorylated after recruitment to promoter sites and then either lead to TBL1XR1-dependent degradation of NCoR/SMRT or TBL1X-dependent degradation of CtBP1/2 on target-gene promoters [91]. Since many promoters are simultaneously occupied by NCoR/SMRT and CtBP1/2, this provides a dual checkpoint for transcriptional activation (figure 1.5 on the next page).

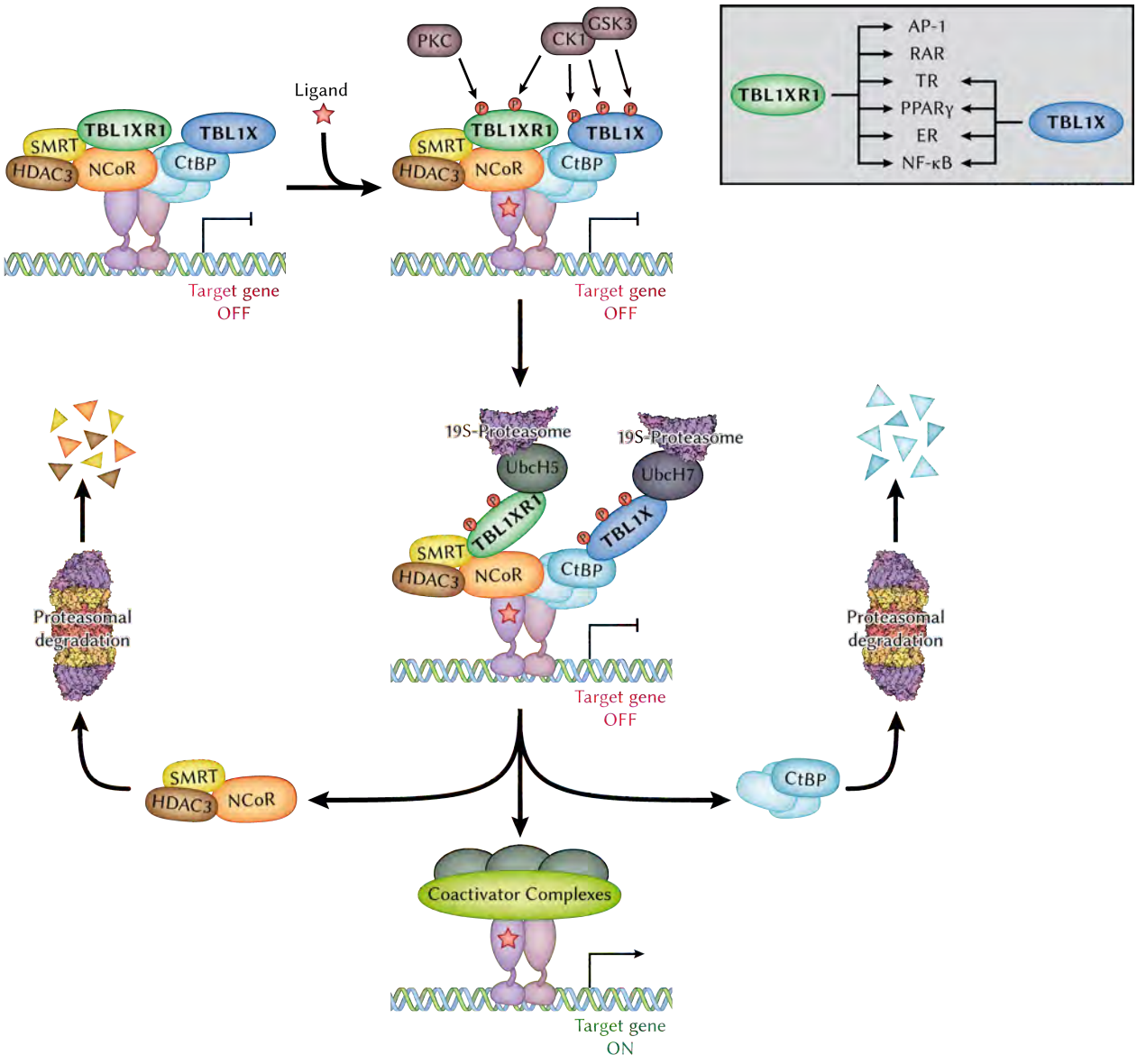

Figure 1.5: Model of TBL1X and TBL1XR1 action in transcriptional regulation

TBL1XR1 is associated with NCoR/SMRT/HDAC3 and TBL1X with CtBP co-repressor complexes on unliganded nuclear receptors. Upon ligand binding, they get phosphorylated by PKC, CK1 or GSK3. This leads to engagement of ubiquitin E2 ligases UbcH5 or UbcH7 and the 19S-proteasomal subunit resulting in degradation of the NCoR/SMRT/HDAC3 or CtBP co-repressor complexes by the 26S-proteasome and subsequent recruitment of co-activator complexes triggering target gene expression.
Grey box: TBL1X and TBL1XR1 are associated with different nuclear receptors as well as some non-nuclear receptor signaling pathways. Images are a combined adaptation of figures 4H and 7 from Perissi et al. (2004) [90] and figure 5E from Perissi et al. (2008) [91]. Proteasome 3D models were taken from PDB website (`http://www.pdb.org/pdb/101/motm.do?momID=166`).

1.3.3 TBL1X and TBL1XR1 as regulators of Wnt/β-catenin signaling

Li and Wang [92] identified the TBL1X/TBL1XR1 complex as critical players in Wnt/β-catenin-mediated signal transduction. Activation of Wnt signaling led to an interaction of the arm repeats 1–8 of β-catenin with the N-terminal domain of TBL1X and TBL1XR1 and recruitment to Wnt target gene promoters. Depletion of either TBL1X or TBL1XR1 abrogated expression of Wnt target genes. Interestingly, β-catenin still shuttled to the nucleus in the absence of TBL1X/ TBL1XR1 but was unable to bind to target gene promoters. A later study [93] could demonstrate that TBL1X/TBL1XR1 only bound to β-catenin when they were SUMOylated whereas binding to the NCoR/SMRT complex only occurred when they were not SUMOylated.

The interplay of TBL1X/TBL1XR1 with β-catenin is particularly interesting, as the Wnt/β-catenin pathway plays a critical role in development in general and also in pancreatic development [94]. It is often aberrantly regulated in cancers [95, 96], including pancreatic tumors [18, 97–99]. Concordantly, HT29 cells expressing shRNA against TBL1X or TBL1XR1 were unable to form colonies in a soft agar assay. Similarly manipulated UMSCC1 cells showed impeded invasiveness in a Matrigel migration assay and reduced growth rates in nude mice [92]. Amplification, upregulation, deletion, or mutation of *TBL1XR1* has also been detected in various tumors [100–104].

1.3.4 TBL1X and TBL1XR1 in metabolism

Two recent studies in our own group highlighted a previously unobserved role of TBL1X [105] and TBL1XR1 [106] in metabolism. Ablation of TBL1X in the liver of mice led to hypertriglyceridemia, hepatic steatosis and inhibition of fatty acid oxidation. Conversely, overexpression resulted in decreased liver triglycerides and enhanced fatty acid oxidation. Moreover, *TBL1X* mRNA levels were found to negatively correlate with liver triglyceride content in humans. These effects of TBL1X on hepatic lipid metabolism were mediated via PPARα (peroxisome proliferator-activated receptor alpha) [105]. Lack of TBL1XR1 in white adipose tissue resulted in decreased lipolysis via perturbation of cAMP-dependent signal transduction. Adipocyte-specific knockout of TBL1XR1 in mice led to impaired lipid mobilization during fasting and aggravated adiposity on HFD due to increased adipocyte cell size. Human patients that underwent a weight-loss program showed increased *TBL1XR1* mRNA expression in their visceral white adipose tissue which positively correlated with serum levels of adiponectin and free fatty acids [106].

2 Aim of the study

Due to the reported epidemiological correlation of pancreatic cancer with obesity and type 2 diabetes, it was of interest to identify transcriptional co-regulators that may explain these observations on the basis of distinct cellular mechanisms.

The two proteins TBL1X and TBL1XR1 were chosen as promising candidates as they were known regulators of lipid metabolism in the liver [105] and adipose tissue [106] as well as in Wnt/β-catenin signaling [92], a known pro-proliferative pathway in cancer.

The aim of the present study was to investigate whether TBL1X and/or TBL1XR1 play a role in pancreatic cancer and might link tumor initiation or progression with obesity or type 2 diabetes.

To do so, human patient samples from tumor and adjacent non-tumor tissue of lean and obese patients were screened for expression of transcriptional co-regulators, including TBL1X and TBL1XR1, to identify differences between tumor vs. non-tumor tissue and lean vs. obese patients. The transgenic *p48*$^{+/Cre}$*; Kras*$^{+/LSL\text{-}G12D}$ mouse model [15] was subjected to a high fat diet regime to test tumor-promoting effects of obesity and metabolic syndrome on pancreatic cancer, and to validate observations made in human samples regarding TBL1X and TBL1XR1 expression.

For detailed mechanistic studies *in vitro*, the human pancreatic cancer cell lines Capan-1, BxPC-3, AsPC-1 and Capan-2 were used. The role of TBL1X and TBL1XR1 in cancer cell growth and metabolism was examined by siRNA-mediated knockdown, primarily in Capan-1 cells. Affymetrix gene expression microarrays were employed for high-throughput analysis of genes and cellular pathways regulated by TBL1X or TBL1XR1. Cell growth and proliferation was monitored by cell counting and BrdU or EdU incorporation. Metabolic changes were assessed by glucose consumption, radioactive 2-deoxyglucose uptake, and extracellular flux measurement.

To examine Tbl1x function *in vivo*, the mouse pancreatic cancer cell line Panc02 was subcutaneously injected into the syngeneic C57BL/6 mouse strain. These allograft tumors were then injected with shRNA-carrying adenovirus to monitor effects of Tbl1x on growth of established tumors. For a preventive approach, Panc02 cells were stably transduced with shRNA using lentiviral gene transfer, followed by subcutaneous implantation into C57BL/6 mice. To test a potential role of Tbl1x in chemotherapy resistance, these mice were treated with gemcitabine, the most commonly used chemotherapeutic agent for human pancreatic cancer. Chromatin immunoprecipitation was employed to investigate TBL1X binding to potential target gene promoters.

3 Results

3.1 Human patient screening

3.1.1 TBL1X and TBL1XR1 are upregulated in human pancreatic cancer

In order to identify the role of TBL1X and TBL1XR1 in human pancreatic ductal adenocarcinoma, their expression levels were measured together with that of other transcriptional co-regulators in tumor resection samples. To investigate a potential role in obesity, cancer patients were grouped to lean (BMI ≤25) and obese (BMI ≥30) subgroups. All cancer patients had a tumor staging between T3 N0 M0 and T3 N1 M1 (see appendix C on page 83 for explanation of the TNM grading system). Tissue from organ donors served as a control. Detailed information on patients and organ donors is given in appendix D on page 85. The transcriptional co-regulators *TBL1X* and *TBL1XR1* were significantly upregulated in tumor tissue compared to adjacent non-tumor tissue from the same patient and to controls. Increased expression in tumors was also observed for *TSC22D4*, which was previously identified in our lab as a binding partner of TBL1X/TBL1XR1, as well as the histone-arginine transferase *CARM1* and the transcriptional co-regulators *NRIP1* and *CRTC2* (figure 3.1 on the following page) but not for *PGC1α*. CARM1 methylates histones and is thus involved in regulation of gene expression. It was shown to be dysregulated in lung cancer [107] and to play a role in breast cancer [108]. NRIP1 is a regulator of hepatic triglyceride metabolism [109] and a co-regulator of cytokine promoter activity via the NF-κB pathway [110]. It was furthermore shown to be involved in colorectal cancer [111]. CRTC2 (also known as TORC2) is a transcriptional co-activator for the transcription factor CREB and a central regulator of gluconeogenic gene expression in response to cAMP [112]. PGC1α is a transcriptional co-activator for steroid receptors [113] and nuclear receptors [114, 115]. It is a major regulator of fatty acid oxidation and the brown adipocyte specific uncoupling protein UCP1 and was also shown to have tumor-promoting effects [116, 117].

There was, however, no statistically significant difference between lean and obese patients for any of the genes analyzed.

To check if the upregulation in tumor samples might be due to inflammatory processes, samples from chronic pancreatitis patients were analyzed for *TBL1X*, *TBL1XR1* and *TSC22D4*. Here, expression levels were quite variable compared to healthy tissue samples. H & E stainings of the pancreas of these patients were examined to assess the degree of pancreatitis (table D.1 on page 86) but there was no correlation between disease severity and expression levels. As an additional control, cDNA from cultured primary pancreatic stellate cells was provided by Dr. Oliver Strobel from the European Pancreas Center at Heidelberg University Clinic. Also in these samples there was no difference in *TBL1X* or *TBL1XR1* expression between cells from normal, pancreatitis or tumor tissue (figure 3.2 on the following page).

The upregulation of *TBL1X* and *TBL1XR1* in tumor tissue was also confirmed by immunoblotting protein extracts from the same patient material that was used for mRNA expression analysis (figure 3.3 on page 15). Immunoblot bands from tumor samples were more prominent than bands from adjacent non-tumor tissue of the same patient. Similar to the findings on mRNA level, there was no obvious difference between lean and obese individuals.

3.1.2 TBL1X and TBL1XR1 are highly expressed in human PanINs and carcinoma cells

To gain further knowledge about the cell types responsible for the upregulation of TBL1X and TBL1XR1, paraffin sections of patient tissue were stained for both proteins using immunohistochemistry as described in section 5.13.3.1 on page 62 and section 5.13.3.3 on page 63. Healthy pancreatic tissue showed little to no expression of TBL1X and TBL1XR1 whereas levels were markedly increased in PanIN lesions of all stages as well as carcinoma cells (figure 3.4 on page 15 and figure 3.5 on page 16). Early PanIN lesions showed exclusively nuclear staining for TBL1X and TBL1XR1 whereas higher grade PanINs also had low expression of TBL1XR1 in the cytoplasm. Carcinoma cells showed nuclear and cytoplasmic staining for both TBL1X and TBL1XR1.

3.1.3 Expression of metabolic genes correlates with TBL1X and TBL1XR1

It is a well-established fact that tumors have an altered metabolism characterized by increased glycolysis, which was already described more than 85 years ago by Warburg et al. [118]. The Warburg effect has come back to the focus of research in recent years [119–121]. Previous work in our own group has shown a crucial role for TBL1X and TBL1XR1 in metabolism [105, 106]. Therefore, it was of interest to measure the expression levels of several candidate genes for metabolic reprogramming (table 3.1 on page 17) in patient samples and to investigate if they would correlate with *TBL1X* and *TBL1XR1*. According to literature, mRNA levels of *ACLY* (ATP citrate lyase), *FASN* (fatty acid synthase), *G6PD* (glucose-6-phosphate dehydrogenase), *GLUT1* (glucose transporter 1), *LDHa* (L-lactate dehydrogenase A chain), *PDK1* (pyruvate dehydrogenase kinase 1) and *SCD1* (stearyl-CoA desaturase) were higher in tumors while expression of *GLS2* (glutaminase 2) was lower. *CPT1A* (carnitine palmitoyl transferase 1, liver isoform) was upregulated in tumor

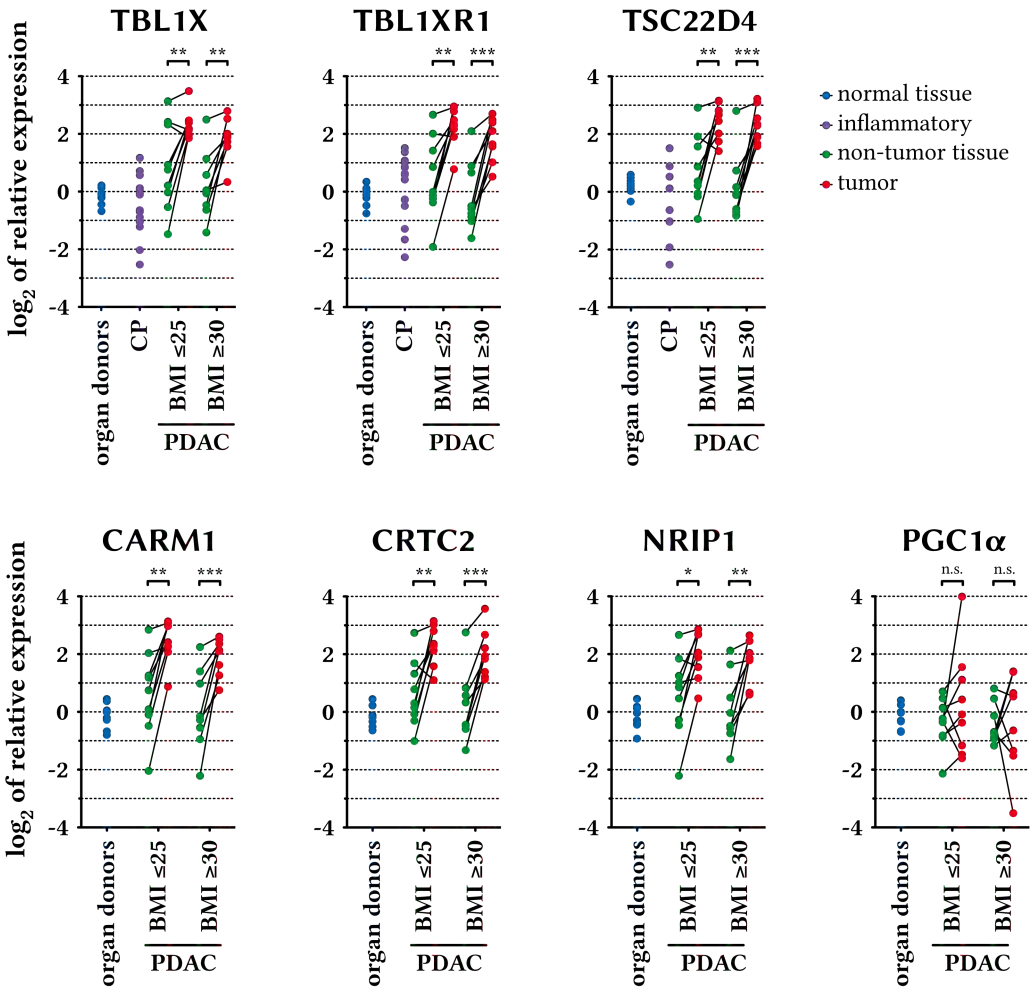

Figure 3.1: Regulation of transcriptional co-regulators in human PDAC

Plots show mRNA expression of individual patients normalized to 18S-rRNA and relative to a pooled organ donor sample. Lines between dots connect samples from the same patient. CP: chronic pancreatitis; BMI: body mass index; PDAC: pancreatic ductal adenocarcinoma; TBL1X: transducin β-like protein 1X; TBL1XR1: transducin β-like 1X-related protein 1; TSC22D4: TSC22 domain family protein 4; CARM1: co-activator-associated arginine methyltransferase 1; CRTC2: CREB-regulated transcription co-activator 2; NRIP1: nuclear receptor-interacting protein 1; PGC1α: peroxisome proliferator-activated receptor gamma co-activator 1-alpha; * $p \leq 0.05$, ** $p \leq 0.01$, *** $p \leq 0.001$ as determined by two-tailed paired Student's *t*-test.

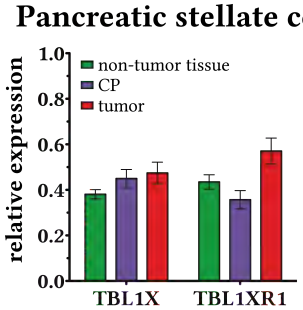

Figure 3.2: mRNA expression of *TBL1X* and *TBL1XR1* in primary human pancreatic stellate cells

Primary stellate cells were isolated from patient material and cultured before extracting RNA and reverse transcribing to cDNA. Expression is displayed relative to the pooled organ donor sample that was also used as a reference in figure 3.1. CP: chronic pancreatitis. Data are plotted as mean ± SEM. No statistical significance was detected by one-way ANOVA.

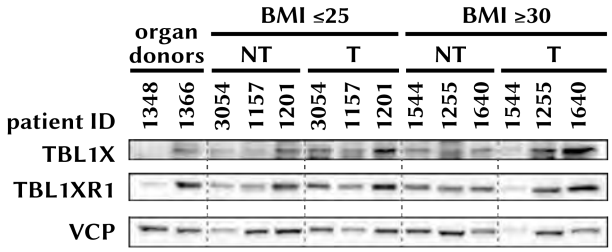

Figure 3.3: Protein expression of TBL1X and TBL1XR1 in pancreas of human patients

Protein extracts of human patients were immunoblotted for TBL1X and TBL1XR1. Expression was higher in tumor samples than in adjacent non-tumor tissue when comparing corresponding bands for each patient. NT: non-tumor; T: tumor; VCP: valosin-containing protein (loading control)

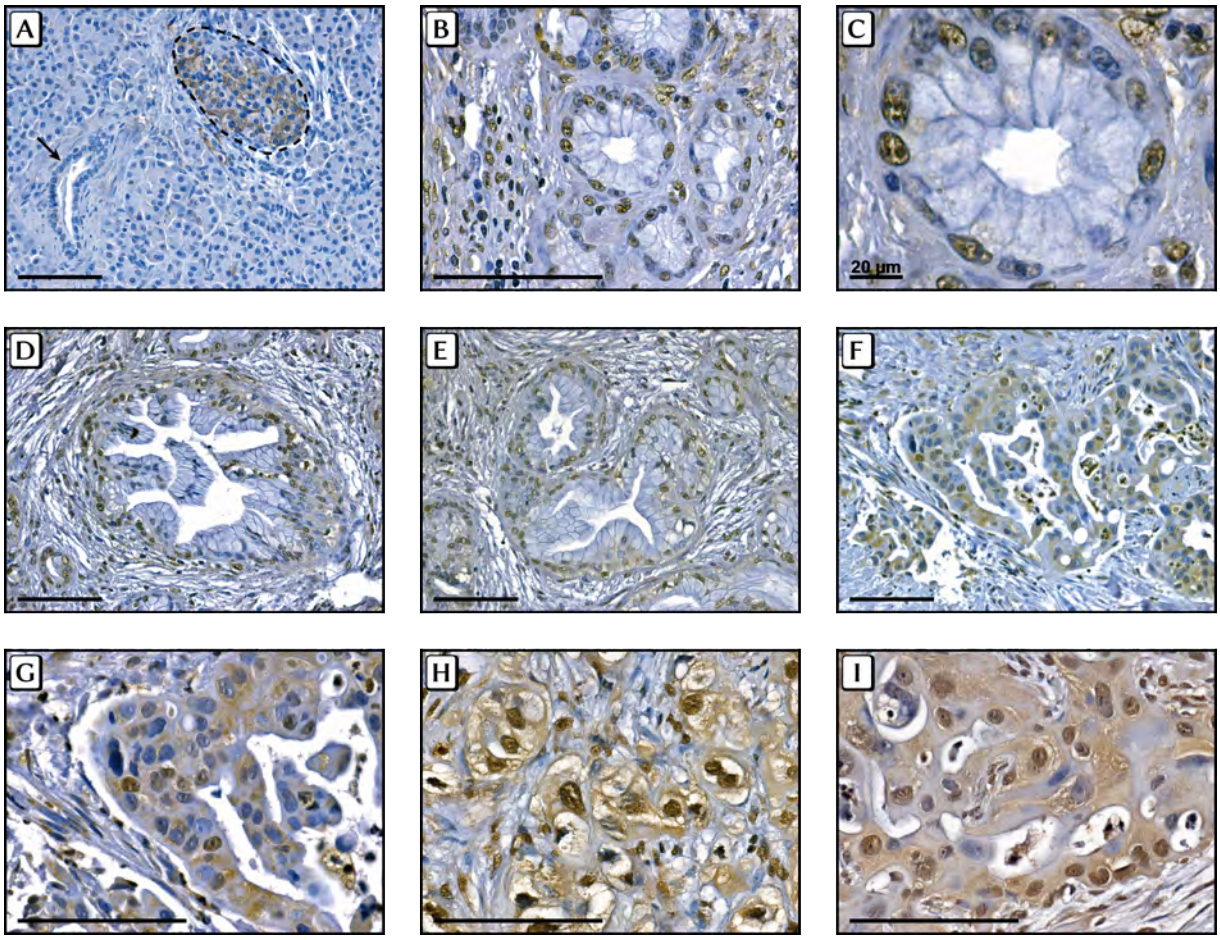

Figure 3.4: Immunohistochemistry staining for TBL1X in human samples

Paraffin-embedded tissue sections from human patients were stained for TBL1X. A healthy tissue with acini, duct (arrow) and islet of Langerhans (dotted line) showing no or only very weak nuclear staining in acinar and ductal tissue and cytoplasmic staining in islet cells; B–C PanIN-1 lesion with nuclear staining; D–E PanIN-2 lesion with nuclear staining; F–G PanIN-3 lesion with nuclear and faint cytoplasmic staining; H–I tumor cells with nuclear and cytoplasmic staining; scale bar 100 µm unless stated otherwise.

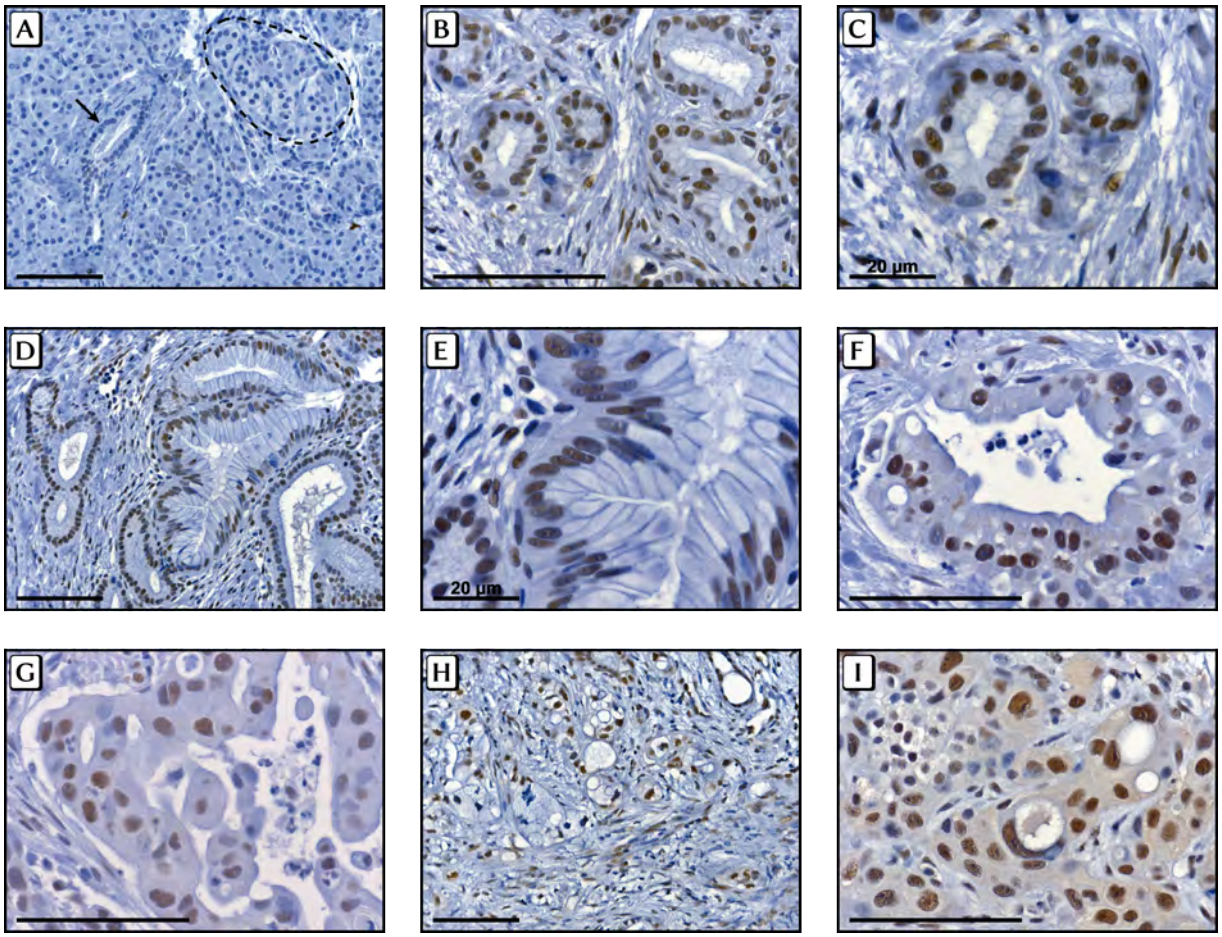

Figure 3.5: Immunohistochemistry staining for TBL1XR1 in human samples

Paraffin-embedded tissue sections from human patients were stained for TBL1XR1. [A] healthy tissue with acini, duct (arrow) and islet of Langerhans (dotted line) showing no or only very weak nuclear staining ; [B]–[C] PanIN-1 lesion with nuclear staining; [D]–[E] PanIN-2 lesion with nuclear staining; [F]–[G] PanIN-3 lesion with nuclear staining; [H]–[I] tumor cells with nuclear and weak cytoplasmic ([I]) staining; scale bar 100 µm unless stated otherwise.

Table 3.1: Candidate genes for cancer-specific metabolic reprogramming

gene	name	process	metabolic function	regulation	references
ACLY	ATP citrate lyase	lipid synthesis; cytosolic acetyl-CoA	conversion of citrate and CoA to acetyl-CoA	↑	[122]
CPT1A/B	carnitine palmitoyl transferase	β-oxidation	transport of fatty acids into mitochondria	↓	[119]
FASN	fatty acid synthase	lipid synthesis	multi-enzyme complex catalyzing multiple reactions in fatty acid chain elongation	↑	[119, 123]
G6PD	glucose-6-phosphate dehydrogenase	pentose phosphate pathway; nucleotide synthesis	conversion of glucose-6-phosphate to 6-phosphogluconolactone	↑	[124]
GLS2	glutaminase 2	citric acid cycle; ROS defense	conversion of L-glutamine to L-glutamate for citric acid cycle	↓	[125]
GLUT1/2 (SLC2A1/2)	glucose transporter 1/2	glucose metabolism	facilitated glucose transport across plasma membrane	↑	[119, 126]
LDHa	L-lactate dehydrogenase A chain	lactate production / proton extrusion	conversion of pyruvate to lactate	↑	[119, 127]
PDK1/4	pyruvate dehydrogenase kinase	fuel selection, reduced oxidative phosphorylation	inactivation of PDH by phosphorylation; reduced flux through citric acid cycle	↑	[119, 128]
SCD1	stearyl-CoA desaturase	lipid metabolism	desaturation of fatty acids	↑	[129]

tissue contrary to reports in literature [119]. *CPT1B* (carnitine palmitoyl transferase 1, muscle isoform), *GLUT2* (glucose transporter 2) and *PDK4* (pyruvate dehydrogenase kinase 4) did not show a significant regulation (figure 3.6 on the following page). In the next step the $\log_2$ expression levels of these metabolic genes were plotted versus the $\log_2$ expression levels of *TBL1X* or *TBL1XR1* (appendix D, figure D.2 on page 88 and figure D.3 on page 89). Linear correlation coefficients and p values are summarized in table 3.2 on page 19. *ACLY*, *CPT1A*, *CPT1B*, *FASN*, *G6PD*, *GLUT1*, *LDHa*, *PDK1* and *SCD1* had a strong and significant positive correlation in gene expression with *TBL1X* and *TBL1XR1*. *GLS2* had a weak negative correlation that was almost significant for *TBL1X* and significant for *TBL1XR1*. *GLUT2* and *PDK4* were not differentially upregulated in tumors and did thus not correlate with either *TBL1X* or *TBL1XR1*.

Taken together, these results showed that TBL1X and TBL1XR1 were highly expressed in human PDAC but not in healthy or chronic pancreatitis tissue. The expression in tumors was specific for PanIN precursor lesions and cancer cells implying a role in tumor initiation or progression. Furthermore, the expression levels of *TBL1X* and *TBL1XR1* correlated with expression levels of genes important for tumor cell metabolism. Even though these correlations do not prove a causal role for TBL1X or TBL1XR1 in the regulation of metabolic genes or vice versa, they are nevertheless an interesting, and so far unobserved, feature of pancreatic ductal adenocarcinoma.

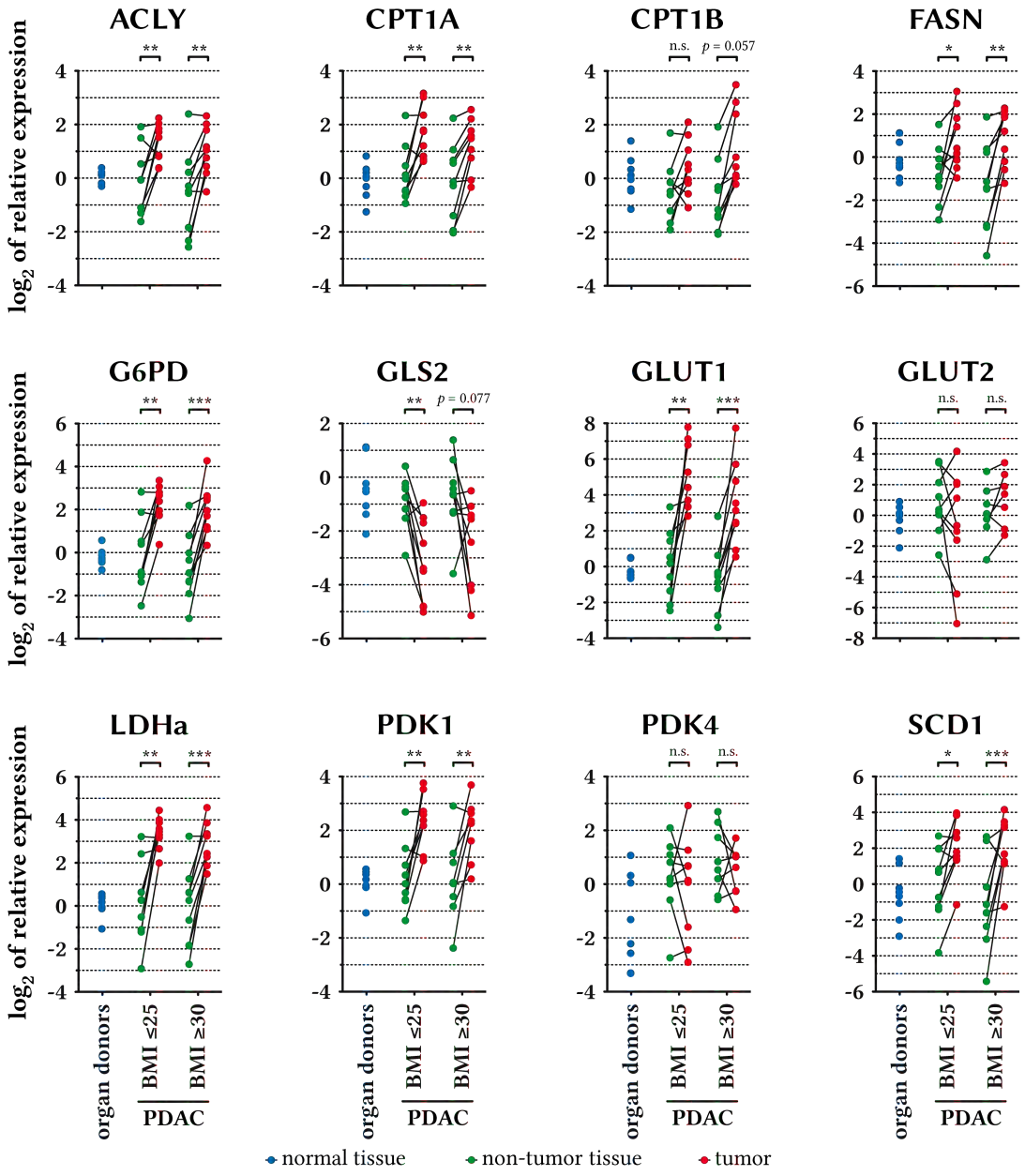

Figure 3.6: mRNA expression of metabolic genes in human PDAC patients

Plots show expression of individual patients normalized to 18S-rRNA and relative to a pooled organ donor sample. Lines between dots connect samples from the same patient. ACLY: ATP citrate lyase; CPT1A: carnitine palmitoyl transferase 1, liver isoform; CPT1B: carnitine palmitoyl transferase 1, muscle isoform; FASN: fatty acid synthase; G6PD: glucose-6-phosphate dehydrogenase; GLS2: glutaminase 2; GLUT1: glucose transporter 1 (SLC2A1); GLUT2: glucose transporter 2 (SLC2A2); LDHa: L-lactate dehydrogenase A chain; PDK1: pyruvate dehydrogenase kinase 1; PDK4: pyruvate dehydrogenase kinase 4; SCD1: stearyl-CoA desaturase. * $p \leq 0.05$, ** $p \leq 0.01$, *** $p \leq 0.001$ as determined by two-tailed paired Student's *t*-test.

Table 3.2: Correlation of metabolic genes with *TBL1X* and *TBL1XR1* expression in human patients

R^2: correlation coefficient of linear regression; p: significance level for slope of regression line different from zero, indicated in green when significant ($p \leq 0.05$).

	TBL1X		TBL1XR1	
gene	R^2	p	R^2	p
ACLY	0.6463	< 0.0001	0.7408	< 0.0001
CPT1A	0.7408	< 0.0001	0.6523	< 0.0001
CPT1B	0.2783	0.0003	0.3765	< 0.0001
FASN	0.4796	< 0.0001	0.5707	< 0.0001
G6PD	0.8074	< 0.0001	0.9083	< 0.0001
GLS2	0.0871	0.0597	0.1122	0.0262
GLUT1 (SLC2A1)	0.6731	< 0.0001	0.7756	< 0.0001
GLUT2 (SLC2A2)	0.0922	0.0568	0.0978	0.0438
LDHa	0.7535	< 0.0001	0.8835	< 0.0001
PDK1	0.7865	< 0.0001	0.8491	< 0.0001
PDK4	0.0499	0.1658	0.0154	0.433
SCD1	0.5723	< 0.0001	0.6598	< 0.0001

3.2 Mouse study on tumor-promoting effects of high fat diet

3.2.1 Body weight and body fat increase during high fat diet feeding

Even though transcriptional co-regulator gene expression levels were equal for lean and obese patients, it may be possible that differences can only be observed at earlier stages of disease development and not in advanced cancer. To this end, wild type and *p48*$^{+/Cre}$*; Kras*$^{+/LSL\text{-}G12D}$ mice were fed with a high fat diet (HFD) or low fat diet (LFD) for 12 weeks as described in section 5.12.4 on page 61 with $n = 5–13$ per group. This regime leads to diet-induced obesity and metabolic disorders and closely mirrors the human situation [130].

During the course of the experiment, animals on HFD became obese as expected. Interestingly, male *p48*$^{+/Cre}$*; Kras*$^{+/LSL\text{-}G12D}$ animals but not females showed decreased weight gain, both on LFD and on HFD. Wild type males gained 49 % of weight compared to the start of the experiment on LFD and 97 % on HFD whereas *p48*$^{+/Cre}$*; Kras*$^{+/LSL\text{-}G12D}$ males only gained 36 % on LFD and 58 % on HFD. Female wild type animals had a weight gain of 18 % on LFD and 77 % on HFD and female *p48*$^{+/Cre}$*; Kras*$^{+/LSL\text{-}G12D}$ mice had similar results with 24 % weight gain on LFD and 74 % on HFD (figure 3.7A on page 21). When calculating the area under curve for weight gain and performing a three-way ANOVA (with factors sex, genotype and diet), a significant main effect for sex and diet alone, and the interaction of genotype and diet was observed. Furthermore, there were almost significant main effects for genotype alone ($p = 0.057$), and for the interaction of sex and genotype ($p = 0.051$, table E.2 on page 93).

Three-way ANOVA in males (with factors time, genotype and diet) showed significant main effects for genotype and diet alone, as well as for the interaction of genotype and diet (table E.3 on page 94). In females there was a significant main effect of diet alone, and the interaction of genotype and diet, but not for genotype alone (table E.4 on page 95).

The increase in body fat was in line with the weight gain. At the beginning of the study, all animals had an average body fat content of 10.6 ± 2.7 %. At the end of the 12-week period, wild type males had 29 % body fat on LFD and 45 % on HFD while *p48*$^{+/Cre}$*; Kras*$^{+/LSL\text{-}G12D}$ males had 19 % on LFD and 33 % on HFD. Female wild type mice had 19 % body fat on LFD and 46 % on HFD whereas *p48*$^{+/Cre}$*; Kras*$^{+/LSL\text{-}G12D}$ females had 13 % on LFD and 34 % on HFD (figure 3.7B).

Three-way ANOVA (with factors sex, genotype and diet) for the area under curve of body fat gave a significant main effect for genotype and diet alone, as well as their interaction, whereas there was no significant main effect for sex ($p = 0.096$, table E.5 on page 96).

When performing a three-way ANOVA in males only (with factors time, genotype and diet), there was a significant main effect for genotype and diet alone, but not for the interaction of both (table E.6 on page 97). In females there was a significant main effect for genotype and diet alone, as well as their interaction (table E.7 on page 98).

Perigonadal white adipose tissue (WAT) at necropsy was heavier in HFD animals compared to LFD animals except for wild type males (figure 3.7C). Three-way ANOVA (with factors sex, genotype and diet) detected a significant main effect for genotype and diet alone, and the interaction of sex and diet, both for absolute fat pad weight (table E.8 on

page 99) and for fat pad weight relative to body weight (table E.9 on page 100). On the other hand, wild type males showed a slight difference in liver weight whereas wild type females and *p48$^{+/Cre}$; Kras$^{+/LSL-G12D}$* males and females had no changes (figure 3.7D). Three-way ANOVA showed significant main effects for sex, genotype, and diet alone, and the interaction of sex and genotype regarding absolute liver weight (table E.10 on page 101). For liver weight relative to body weight there were significant main effects for sex and diet alone, as well as for the interaction of sex and genotype, and the interaction of sex and diet (table E.11 on page 102). Also, contrary to predictions, male wild type animals on LFD had high liver weights and histology revealed fatty livers for all of them. Female wild type mice on LFD, on the other hand, rarely developed fatty livers and if so only to a very mild extend. Possible reasons for this have to be discussed together with the observed differences in body weight and body fat development in male animals (see section 4.1 on page 41).

3.2.2 High fat diet leads to increased fasting blood glucose levels

During the course of the 12-week feeding, animals on HFD showed signs of a pre-diabetic phenotype as expected. Four weeks after diet administration, HFD animals showed slightly increased blood glucose after over night fasting and differences where more pronounced in wild type animals, as was also reflected in three-way ANOVA with significant main effects for genotype and diet (table E.12 on page 103). Eight weeks after diet administration, wild type animals on HFD showed greater differences than at four weeks, especially in males. In *p48$^{+/Cre}$; Kras$^{+/LSL-G12D}$* mice the differences between HFD and LFD animals were smaller than in wild type but slightly bigger than at four weeks. Three-way ANOVA gave significant main effects for sex, genotype, and diet alone, as well as all possible interactions (table E.13 on page 104). Twelve weeks after start of the diet, animals were killed and blood glucose was determined again. This was done in random fed state to not stress the animals by fasting and thus affect the sampled organs. Blood glucose levels under these circumstances were still higher in wild type animals on HFD compared to wild types on LFD even though with a greater variance. No difference was observed in *p48$^{+/Cre}$; Kras$^{+/LSL-G12D}$* animals (figure 3.8A on page 22). Three-way ANOVA did not detect any significant main effects here (table E.14 on page 105).

Parallel to blood glucose measurement, blood was also sampled to determine insulin levels. At four and eight weeks, no clear differences were discernible in the fasted state although some males in both wild type and *p48$^{+/Cre}$; Kras$^{+/LSL-G12D}$* showed relatively high values. In many samples, however, insulin levels were below the detection limit of the ELISA as would be expected during fasting. In the random fed state after 12 weeks of diet, insulin levels were increased in HFD animals compared to LFD with differences being more pronounced in wild types. Especially some of the wild type males on HFD had dramatically high insulin levels (figure 3.8B). Three-way ANOVA, however, did not detect significant main effects, possibly due to the big variance introduced by the wild type males on HFD (tables E.15–E.17 on page 105–106).

3.2.3 High fat diet leads to decreased survival in *p48$^{+/Cre}$; Kras$^{+/LSL-G12D}$* mice

Several *p48$^{+/Cre}$; Kras$^{+/LSL-G12D}$* animals, predominantly males, became moribund during the course of the study. First signs were difficulties in correctly moving the hind legs progressing to overt limping and in some cases complete paralysis of the leg(s) within 2–3 days. This was often accompanied by crouching and apathy, both signs of severe distress, as well as weight loss. The latter might be due to either anorexia or decreased nutrient uptake as a consequence of pancreatic exocrine insufficiency reflected in increased fecal triglycerides and free fatty acids (table 3.3 on page 22).

When such behavior was observed, animals were killed for ethical reasons and blood and organs were sampled as described in section 5.12.4 on page 61. Kaplan-Meier survival curves are shown in figure 3.9 on page 23. Some mice showed structures resembling invasive carcinoma. A thorough analysis by an experienced mouse pathologist will, however, be needed to confirm and quantify these findings to judge if HFD promotes tumorigenesis in *p48$^{+/Cre}$; Kras$^{+/LSL-G12D}$* mice. Details on age and survival time of individual mice are given in appendix E on page 91, table E.1. These results suggested that obesity and diabetes aggravate disease development in pancreatic cancer leading to reduced survival.

3.2.4 Tbl1x and Tbl1xr1 are highly expressed in murine PanIN lesions

In protein extracts from pancreas, Tbl1x and Tbl1xr1 were highly expressed in *p48$^{+/Cre}$; Kras$^{+/LSL-G12D}$* animals compared to wild type mice (figure 3.10 on page 23). This nicely reflects the pattern seen in human samples where expression in tumor tissue was higher. Concomitantly, no differences could be detected between lean (LFD) and obese (HFD) mice for expression of Tbl1x and Tbl1xr1.

Besides, also components of the insulin signaling cascade were examined, namely Irs1 (insulin receptor substrate 1), Akt (protein kinase B) and Ampk (5'-AMP-activated protein kinase catalytic subunit alpha-2) as markers for diabetes and obesity. Irs1 was found to be more expressed in HFD mice. Phosphorylation of Irs1 at tyrosine 895[1] was only

[1]Phosphorylation of tyrosine 895 in IRS-1 generates a binding site for Grb2, which mediates the downstream signaling leading to MAP kinase activation and mitogenesis [131]

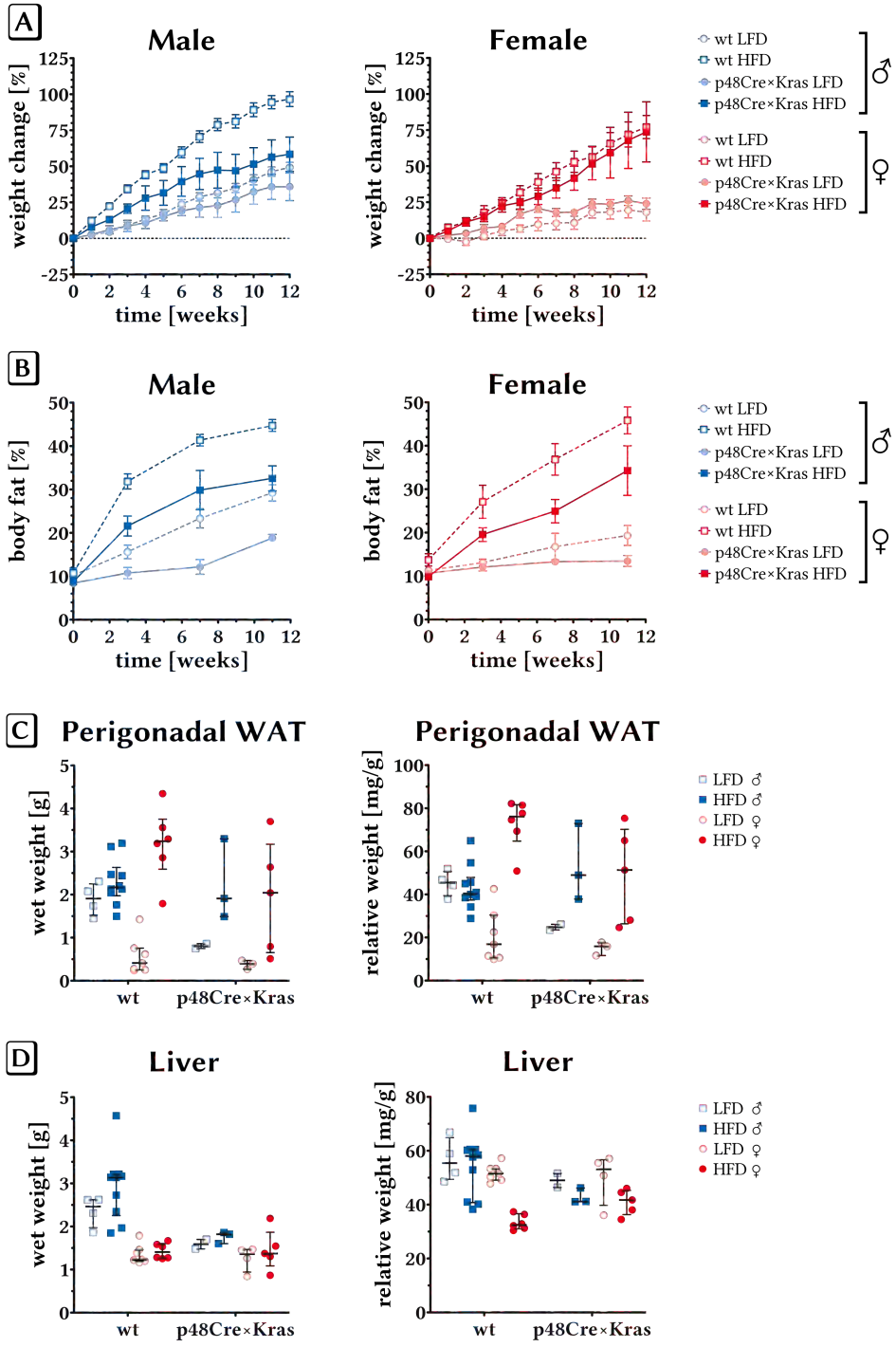

Figure 3.7: Weight and body fat development of *p48*$^{+/Cre}$*; Kras*$^{+/LSL\text{-}G12D}$ and wild type mice on HFD/LFD

5–12 week old wild type and *p48*$^{+/Cre}$*; Kras*$^{+/LSL\text{-}G12D}$ mice were fed a HFD or LFD for 12 weeks. A: change in body weight compared to day zero for males (left panel) and females (right panel); B: percent body fat in males (left panel) and females (right panel) as determined by *in vivo* EchoMRI™ measurement; C: perigonadal white adipose tissue (WAT) at necropsy in wet weight (left panel) and relative to total body weight (right panel, mg tissue per g body weight); D: liver weight at necropsy in wet weight (left panel) and relative to total body weight (right panel, mg tissue per g body weight). Values in A and B plotted as mean ± SEM. Lines and error bars in C and D: median with interquartile range.

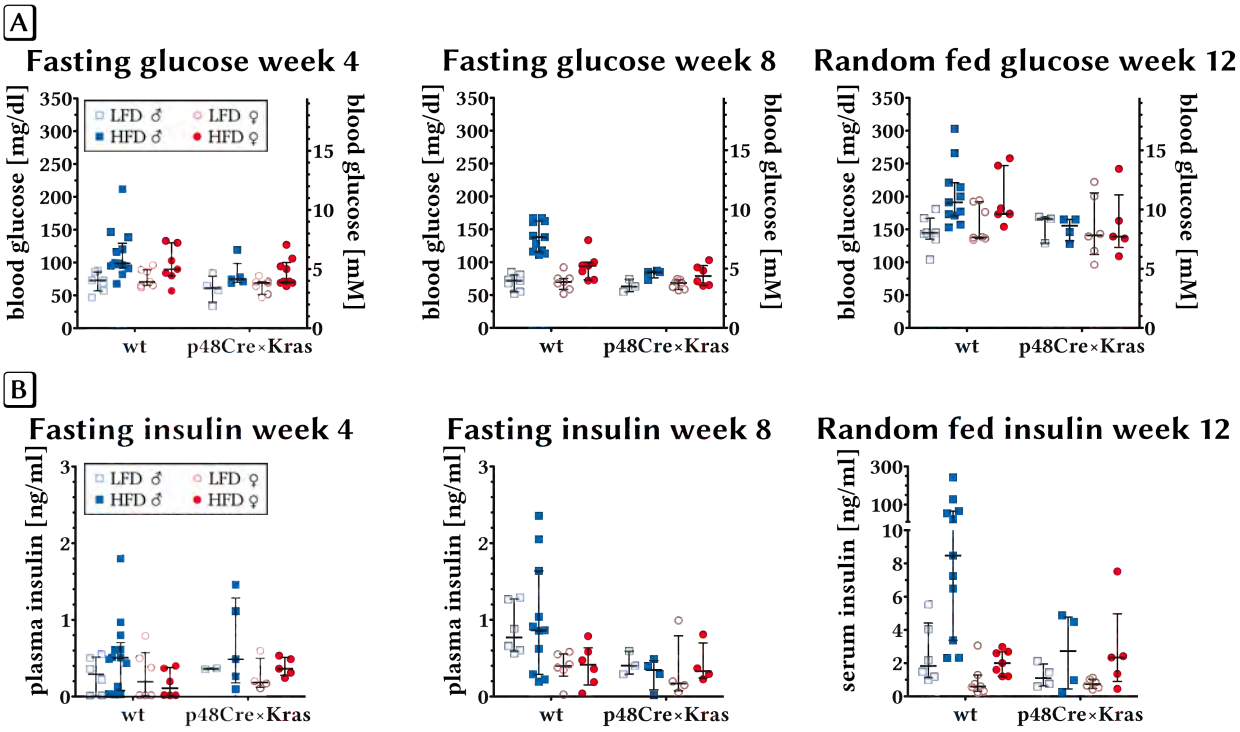

Figure 3.8: Metabolic parameters of *p48*$^{+/Cre}$; *Kras*$^{+/LSL\text{-}G12D}$ and wild type mice on HFD/LFD

5–12 week old wild type and *p48*$^{+/Cre}$; *Kras*$^{+/LSL\text{-}G12D}$ mice were fed a HFD or LFD for 12 weeks. A: blood glucose after over night fasting (16–18 h) at weeks 4 and 8 of HFD/LFD feeding and blood glucose at time of sacrifice (12 weeks of HFD/LFD feeding) in random fed state; B: plasma insulin after over night fasting (16–18 h) at weeks 4 and 8 of HFD/LFD feeding and serum insulin at time of sacrifice (12 weeks of HFD/LFD feeding) in random fed state. Lines and error bars: median with interquartile range.

Table 3.3: Fecal triglycerides and free fatty acids in *p48*$^{+/Cre}$; *Kras*$^{+/LSL\text{-}G12D}$ mice

Mice were put to fresh cages and feces were collected 24 h later from one cage with a male *p48*$^{+/Cre}$; *Kras*$^{+/LSL\text{-}G12D}$ mouse that had been on HFD for 11 weeks, one cage with two male wild type mice on HFD for 11 weeks and one cage with four female mice on LFD for 11 weeks, of which one was wild type and the others were *p48*$^{+/Cre}$; *Kras*$^{+/LSL\text{-}G12D}$. Feces were weighed and lipids were extracted and measured as described in section 5.19 on page 75.

group	total feces [mg]	feces per mouse [mg]	morphology	triglycerides [nmol/mg]	free fatty acids [nmol/mg]
male *p48*$^{+/Cre}$; *Kras*$^{+/LSL\text{-}G12D}$ HFD	112.1	112.1	big pieces, soft, dark in color	382.8	56.2
male wild type HFD	112.5	56.25	small pieces, hard, bright in color	n. d.	28.8
female mixed LFD	102.8	25.7	small pieces, hard, bright in color	n. d	8.8

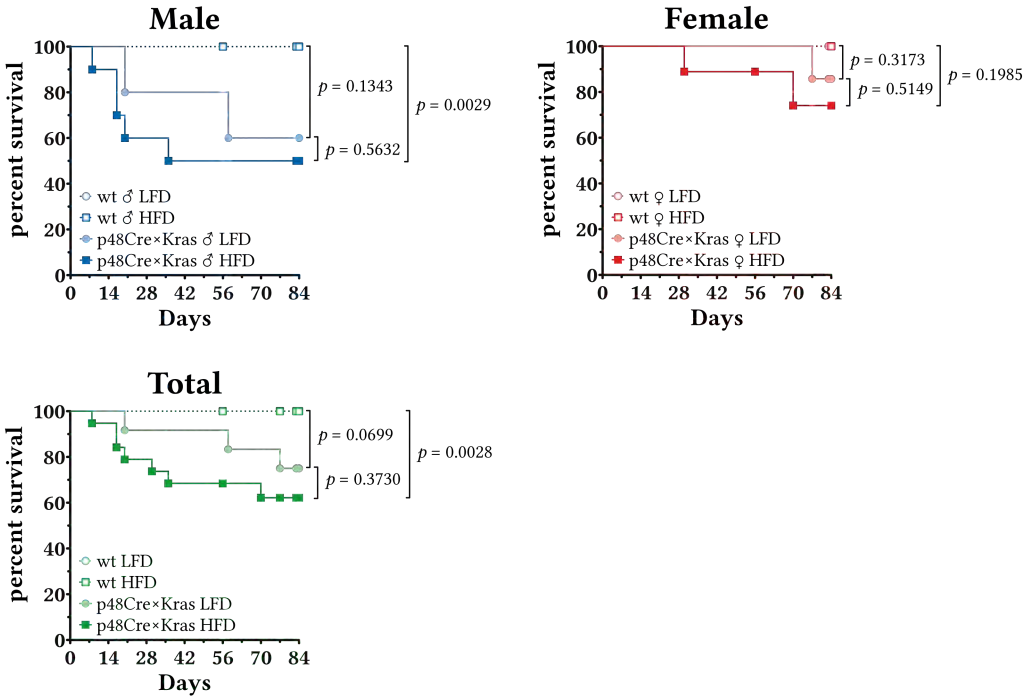

Figure 3.9: Survival curves of *p48$^{+/Cre}$; Kras$^{+/LSL-G12D}$* and wild type mice on HFD/LFD

Mice were killed when becoming moribund and classified as dead for Kaplan-Meier analysis. *p*-values determined by pairwise comparison.

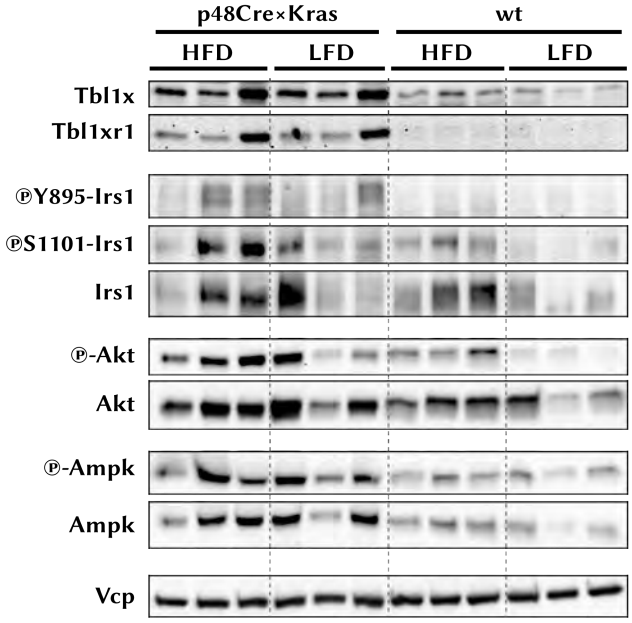

Figure 3.10: Protein expression of pancreas from *p48$^{+/Cre}$; Kras$^{+/LSL-G12D}$* and wild type mice on HFD/LFD

Irs1: insulin receptor substrate 1; Akt: protein kinase B; Ampk: 5'-AMP-activated protein kinase catalytic subunit alpha-2; Vcp: valosin-containing protein (loading control).

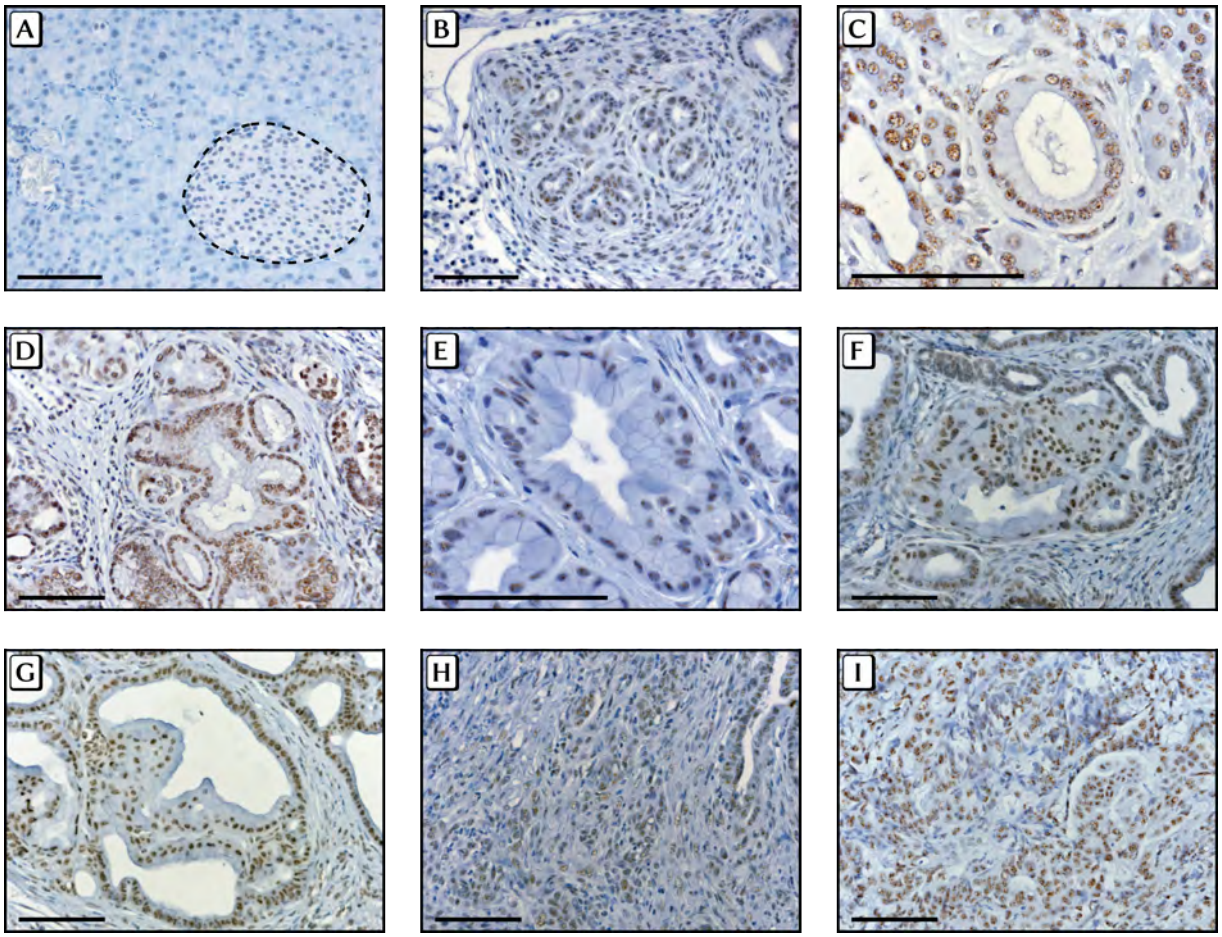

Figure 3.11: Immunohistochemistry staining for Tbl1x in mouse pancreas

Paraffin-embedded tissue sections from wild type (A) or *p48*$^{+/Cre}$; *Kras*$^{+/LSL-G12D}$ mice (B–I) were stained for Tbl1x. A healthy tissue with acini and islet of Langerhans (dotted line) showing weak nuclear staining; B–C PanIN-1 lesion with nuclear staining; D–E PanIN-2 lesion with nuclear staining; F–G PanIN-3 lesion with nuclear staining; H–I tumor cells with nuclear staining; scale bar 100 µm.

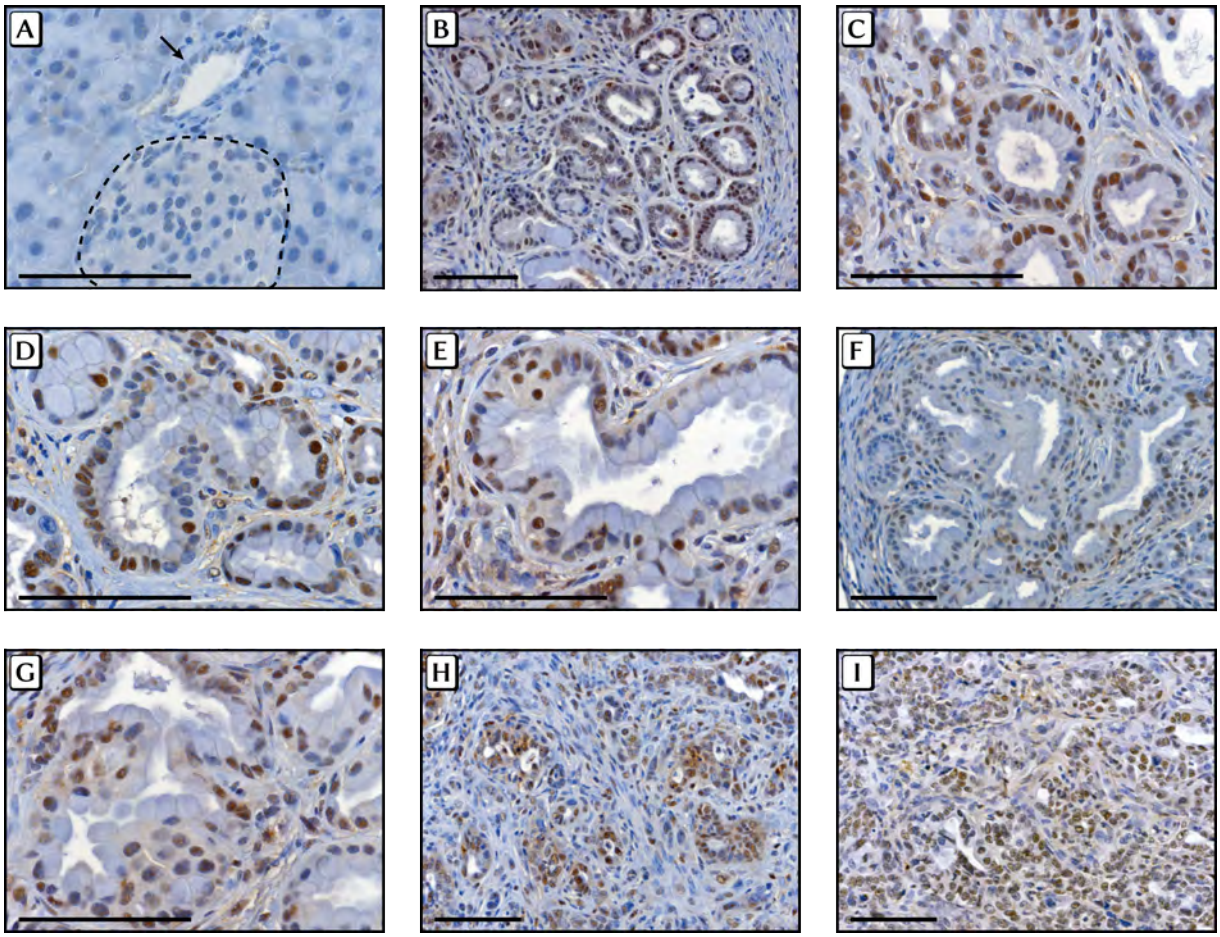

Figure 3.12: Immunohistochemistry staining for Tbl1xr1 in mouse pancreas

Paraffin-embedded tissue sections from wild type (A) or *p48* $^{+/Cre}$*; Kras* $^{+/LSL\text{-}G12D}$ mice (B–I) were stained for Tbl1xr1. A healthy tissue with acini, duct (arrow) and islet of Langerhans (dotted line) showing weak nuclear and partial cytoplasmic staining; B–C PanIN-1 lesion with nuclear staining; D–E PanIN-2 lesion with nuclear and sporadic faint cytoplasmic staining; F–G PanIN-3 lesion with nuclear and faint cytoplasmic staining; H–I tumor cells with nuclear and cytoplasmic staining; scale bar 100 µm.

found in *p48*$^{+/Cre}$*; Kras*$^{+/LSL-G12D}$ animals with reduced levels in HFD animals. Phosphorylation at serine 1101[2] was not markedly changed since the pattern of band intensities mostly resembled that of total Irs1. Akt was slightly more expressed in *p48*$^{+/Cre}$*; Kras*$^{+/LSL-G12D}$ mice compared to wild types and also in HFD animals compared to LFD. Phospho-Akt levels were higher in HFD wild types compared to LFD wild types. Expression of Ampk was also higher in *p48*$^{+/Cre}$*; Kras*$^{+/LSL-G12D}$ compared to wild types, and in HFD animals compared to LFD. Phospho-Ampk band intensities followed the pattern seen for total Ampk (figure 3.10 on page 23) indicating no change in phosphorylation. These data suggested that metabolic signaling was altered in pancreatic tumors, as reflected in elevated levels of phospho-Tyr895-Irs1, Akt and Ampk in *p48*$^{+/Cre}$*; Kras*$^{+/LSL-G12D}$ animals.

Finally, it was of interest which cell types were responsible for increased expression of Tbl1x and Tbl1xr1 in *p48*$^{+/Cre}$*; Kras*$^{+/LSL-G12D}$ mice. To that end paraffin sections were stained for both proteins using immunohistochemistry as described in section 5.13.3.2 on page 63 and section 5.13.3.4 on page 63. In accordance with the observation made in human samples, there was little to no expression in healthy wild type tissue but pronounced staining in PanINs and carcinoma cells of *p48*$^{+/Cre}$*; Kras*$^{+/LSL-G12D}$ animals. Tbl1x showed exclusively nuclear staining while Tbl1xr1 presented nuclear staining in low grade PanINs and slight cytoplasmic staining in high grade PanINs and carcinoma cells (figure 3.11 on page 24 and figure 3.12 on the previous page). Therefore, TBL1X and TBL1XR1 expression in PanIN lesions and carcinoma cells seems to be a conserved feature of PDAC, both in humans and mice.

3.3 *In vitro* studies on proliferation and metabolism

3.3.1 TBL1X and TBL1XR1 regulate proliferation in cell culture

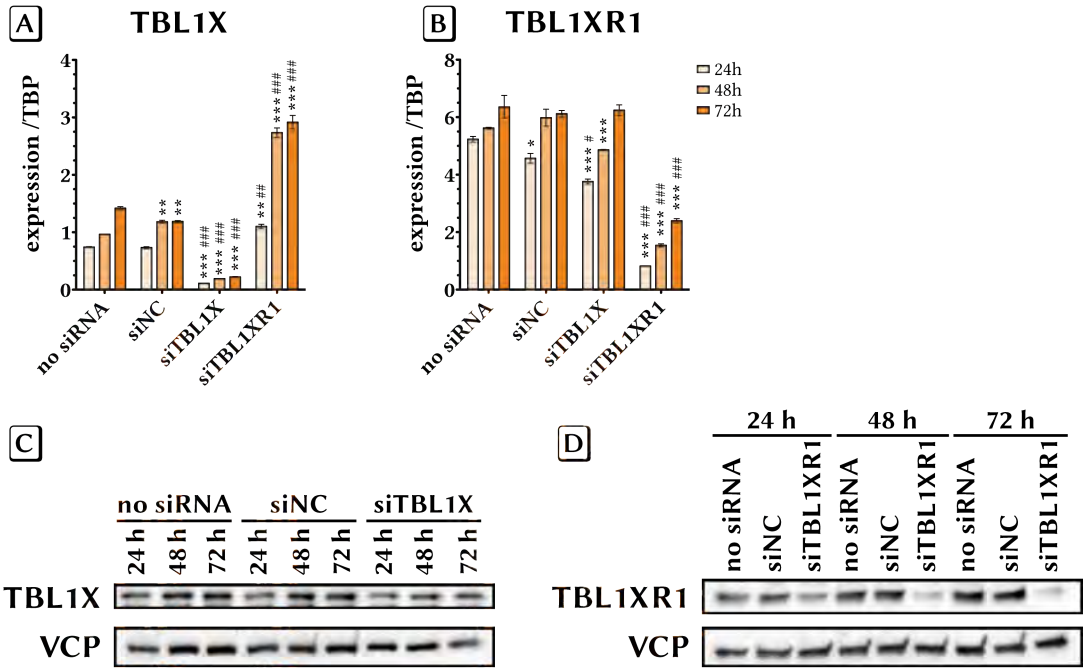

Figure 3.13: Validation of siRNA-mediated knockdown in Capan-1 cells

Capan-1 cells were plated and on the following day transfected with siRNA as described in section 5.14.7 on page 65. 24 h later, cells were either lyzed for RNA or protein extraction or medium was changed and cells were grown further before lysis and RNA or protein extraction. A: mRNA expression levels for *TBL1X* relative to *TBP*. B: mRNA expression levels for *TBL1XR1* relative to *TBP*. C: protein expression of TBL1X. D: protein expression of TBL1XR1. VCP: valosin-containing protein (loading control). Data plotted as mean ± SEM. * $p \leq 0.05$ / ** $p \leq 0.01$ / *** $p \leq 0.001$ vs. no siRNA; # $p \leq 0.05$ / ## $p \leq 0.01$ / ### $p \leq 0.001$ vs. siNC; determined by two-tailed Welch's *t*-test.

The strong upregulation of TBL1X and TBL1XR1 in human and mouse tumors and their known interaction with the Wnt/β-catenin pathway [92, 93] led to the assumption that they might play a role in tumor cell growth. To investigate this question, the human PDAC cell line Capan-1 was transfected with unspecific or *TBL1X*-specific siRNA (figure 3.13) to study cell proliferation. Knockdown of TBL1X and TBL1XR1 led to a significant reduction in BrdU incorporation 72 h

[2]Phosphorylation of IRS-1 at serine 1101 is mediated by PKCθ and results in an inhibition of insulin signaling in the cell, suggesting a potential mechanism for insulin resistance in some models of obesity [132]

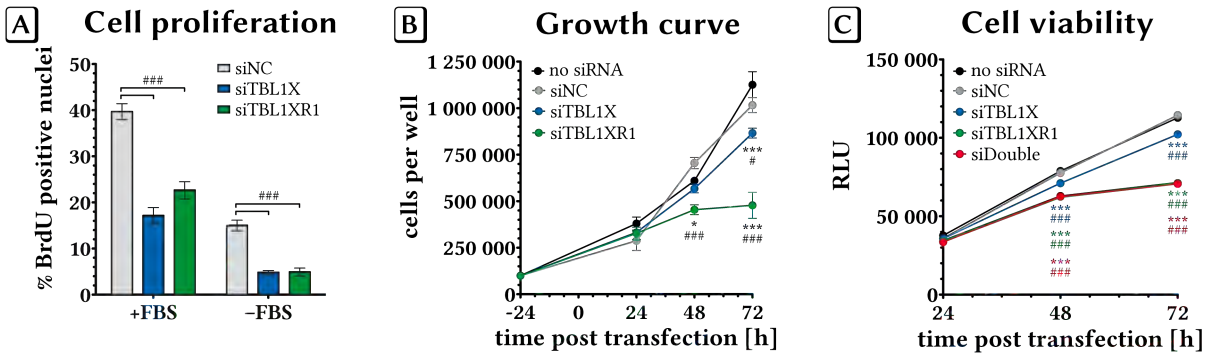

Figure 3.14: TBL1X and TBL1XR1 regulate proliferation in Capan-1 cells

Capan-1 cells were plated and on the following day transfected with siRNA. A: 24 h after transfection, medium was renewed and cells were grown for another 48 h before labeling with BrdU for 45 min followed by fixation and detection as described in section 5.15.1 on page 65. Graph shows a representative experiment with duplicate wells per condition. Three random fields per well were imaged and ≥ 1000 cells counted per condition. B: 24 h after transfection, medium was renewed and cells were grown for another 24 or 48 h before trypsinizing and counting in a Neubauer counting chamber. Graph shows a representative experiment with duplicate wells per condition on 12-well plates. C: 24 h after transfection, medium was renewed and cells were grown for another 24 or 48 h before assessing cell viability with PrestoBlue® Cell Viability Reagent (Life Technologies™) as described in section 5.15.3 on page 66. Graph shows a representative experiment with 8 wells per condition on a 96-well plate. Data plotted as mean ± SEM. * $p \leq 0.05$ / ** $p \leq 0.01$ / *** $p \leq 0.001$ vs. no siRNA; # $p \leq 0.05$ / ## $p \leq 0.01$ / ### $p \leq 0.001$ vs. siNC; determined by two-way ANOVA.

after transfection both in presence or absence of FBS. Accordingly, cell numbers were lower at 48 and 72 h after transfection when counting cells or measuring cell viability via mitochondrial reduction of the resazurin-based dye PrestoBlue® (figure 3.14). This clearly demonstrated that TBL1X and TBL1XR1 play a role in cell growth and proliferation.

To gain further insight, RNA samples from siRNA-mediated knockdown in Capan-1 cells after 24 h were analyzed with Affymetrix gene expression arrays. At a significance level of $p < 10^{-6.04}$, 885 genes were regulated by TBL1X and 864 by TBL1XR1 with an overlap of 183 genes. Overrepresentation analysis and Gene Set Enrichment Analysis of annotated gene sets revealed a significant regulation of cell cycle-associated pathways and p53 signaling. A detailed listing is given in appendix F. Figure 3.15 on the next page shows a heatmap of regulated cell cycle and p53 signaling genes.

3.3.2 TBL1X and TBL1XR1 are regulated by metabolic stimuli

After observing the effect of TBL1X and TBL1XR1 on Capan-1 cell proliferation (figure 3.14) and their correlation with metabolic genes in human samples (table 3.2 on page 19), it was tested whether these genes were regulated after siRNA-mediated knockdown. Therefore, those four metabolic genes were chosen that had the strongest correlation in human samples for both *TBL1X* and *TBL1XR1*, namely *G6PD*, *GLUT1*, *LDHa* and *PDK1*. No relevant change was, however, seen for any of these genes after knockdown of either TBL1X or TBL1XR1 (figure 3.16 on page 29).

Nevertheless, possible links between TBL1X/TBL1XR1 and cell metabolism were further examined, partially based on the observations in $p48^{+/Cre}$; $Kras^{+/LSL\text{-}G12D}$ mice where HFD feeding led to decreased survival. Therefore, it was assessed whether metabolic stimuli were capable of regulating *TBL1X* or *TBL1XR1* expression levels. When culturing Capan-1 and BxPC-3 cells under low-glucose conditions, a significant upregulation of *TBL1X* but not *TBL1XR1* mRNA expression could be observed (figure 3.17 on page 29). Furthermore, *TBL1X* mRNA levels increased over time, possibly due to cell growth-dependent glucose depletion of the media. The upregulation was most striking in BxPC-3 cells that also had a 30–50 fold lower basal expression of *TBL1X* (relative to *TBP* which had similar C_T values in both cell lines).

To investigate *TBL1X* and *TBL1XR1* expression in response to stimulation of metabolic pathways, cells were treated either with insulin or forskolin, the latter raising intracellular cAMP levels thus mimicking glucagon signaling during fasting. In accordance to the findings from the low-glucose experiment, a robust induction of *TBL1X* but not *TBL1XR1* could be seen in three different human pancreatic cancer cell lines after forskolin stimulation. The opposite regulation was observed in response to insulin (figure 3.18 on page 30). This suggested that *TBL1X* expression was regulated in response to cellular energy status.

3.3.3 TBL1X and TBL1XR1 regulate tumor cell metabolism

After observing the effect of metabolic stimulation on *TBL1X* expression, it was examined if the effect of TBL1X and TBL1XR1 knockdown on proliferation is also reflected in tumor cell metabolism. To do so, Capan-1 cells were cultured and glucose consumption was measured. Knockdown of TBL1X and TBL1XR1 did indeed result in decreased glucose

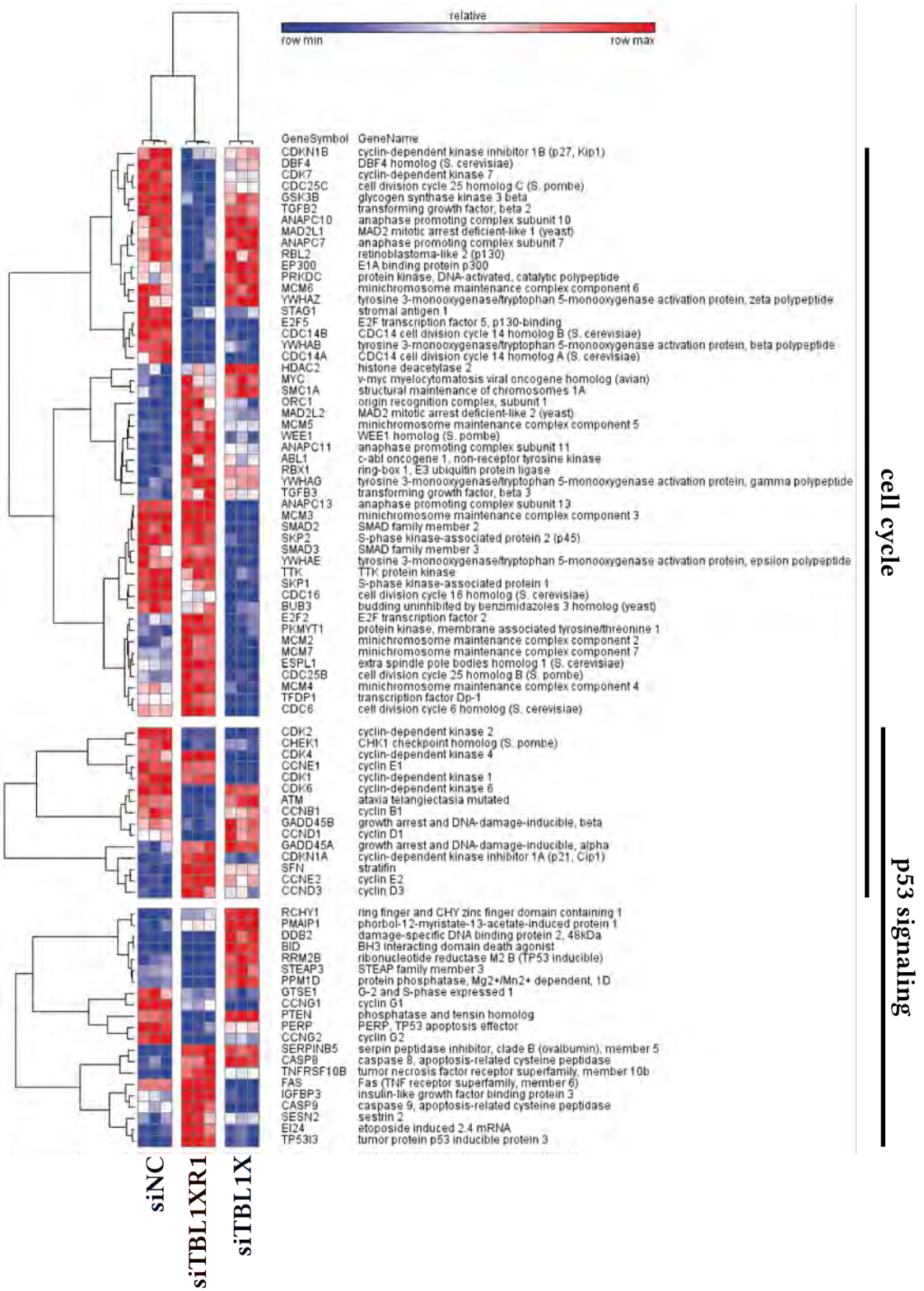

Figure 3.15: Heatmap of cell cycle and p53 signaling

Genes annotated to KEGG pathways "hsa04115 cell cycle" and "hsa04110 p53 signaling" and significantly regulated by either TBL1X or TBL1XR1 at $p < 0.05$ are plotted.

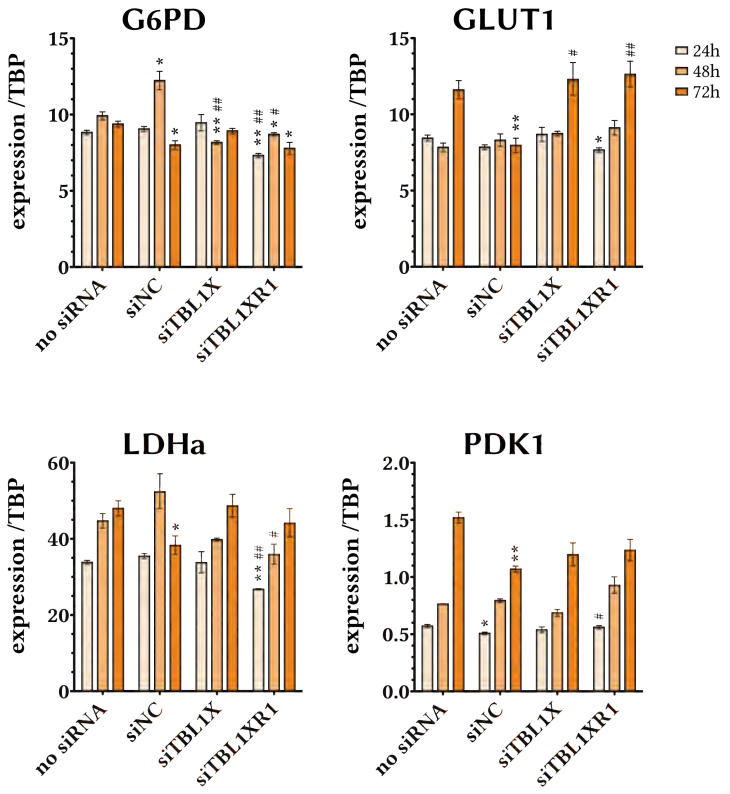

Figure 3.16: Expression levels of metabolic genes after knockdown of TBL1X or TBL1XR1

Metabolic genes that showed the strongest correlation with *TBL1X* and *TBL1XR1* in human PDAC samples were analyzed in Capan-1 cells after siRNA-mediated knockdown. Cells were plated and on the following day transfected with siRNA. 24 h later, cells were either lyzed for RNA extraction or medium was changed and cells were grown further before lysis and RNA extraction. G6PD: glucose-6-phosphate dehydrogenase; GLUT1: glucose transporter 1 (SLC2A1); LDHa: L-lactate dehydrogenase A chain; PDK1: pyruvate dehydrogenase kinase 1. Data plotted as mean ± SEM. * $p \leq 0.05$ / ** $p \leq 0.01$ / *** $p \leq 0.001$ vs. no siRNA; # $p \leq 0.05$ / ## $p \leq 0.01$ / ### $p \leq 0.001$ vs. siNC; determined by two-tailed Welch's *t*-test.

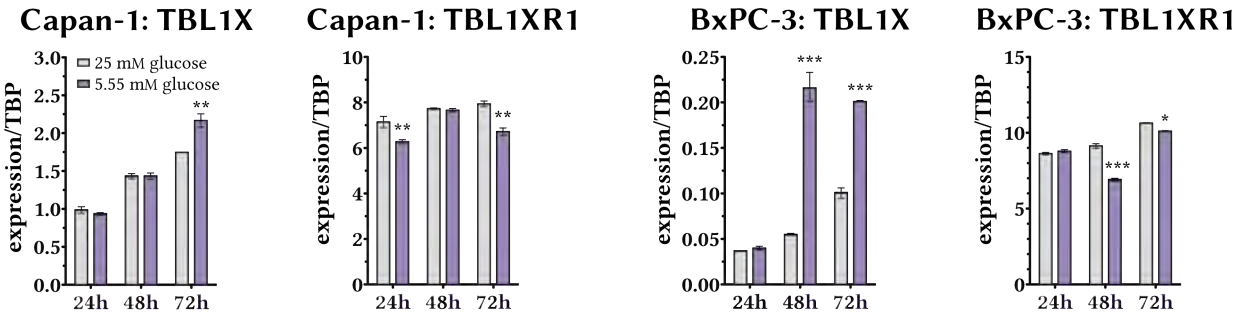

Figure 3.17: Regulation of *TBL1X* and *TBL1XR1* expression by extracellular glucose levels

Capan-1 and BxPC-3 cells were seeded at $1{\times}10^5$ cells per well in 12-well plates in 1 ml DMEM High Glucose Pyruvate (25 mM glucose). The following day, medium was changed to either fresh DMEM High Glucose Pyruvate (25 mM glucose) or DMEM Low Glucose Pyruvate (5.55 mM glucose) and cells were grown for another 24, 48 or 72 h before lyzing and extracting RNA. Data plotted as mean ± SEM. * $p \leq 0.05$ / ** $p \leq 0.01$ / *** $p \leq 0.001$ vs. 25 mM glucose determined by two-way ANOVA.

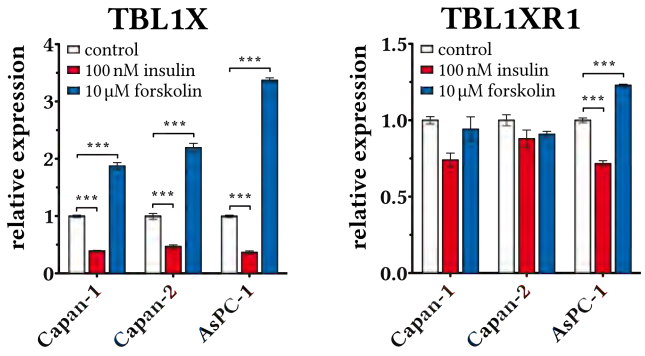

Figure 3.18: Regulation of *TBL1X* and *TBL1XR1* mRNA expression by stimulation with insulin and forskolin

mRNA expression levels of *TBL1X* and *TBL1XR1* in Capan-1, Capan-2 and AsPC-1 human pancreatic cancer cell lines. 24–30 h after seeding, cells were serum-starved over night in DMEM High Glucose Pyruvate (25 mM glucose) with 0.5 % BSA and stimulated with 100 nM insulin or 10 µM forskolin for 6 h in serum-free media (DMEM High Glucose Pyruvate with 0.5 % BSA). Graphs show pooled data from 1–4 experiments per cell line with technical triplicates in each experiment plotted as mean ± SEM. *** $p \leq 0.001$ determined by Welch's *t*-test.

consumption (figure 3.19A and figure 3.19B on the next page). A tracer study with radioactive ^{3}H-2-deoxyglucose further revealed that 48 h after siRNA-transfection, glucose uptake rates were diminished by 25–35 % (figure 3.19D). As these data indicated a reduction in glycolytic activity, extracellular flux measurement was performed using Seahorse technology. This technique measures cellular oxygen consumption (indirect measure of mitochondrial function) and culture media acidification (indirect measure of glycolytic activity) in live cells in a 96-well format. Injection of chemicals allows to assess different functional parameters (see appendix G on page 117). In accordance with the previous findings, a decrease in glycolytic activity could be detected 48 h after siRNA-mediated knockdown of TBL1X. Mitochondrial function, however, was not changed under the same conditions (figure 3.20 on the next page).

Next, the growth behavior of Capan-1 cells was examined under glucose-free conditions following siRNA-mediated knockdown of TBL1X and TBL1XR1 by means of EdU incorporation[3]. Interestingly, Capan-1 cells with TBL1X-knockdown had equal proliferation rates with and without glucose whereas in control-transfected and TBL1XR1-knockdown cells proliferation was markedly reduced in the glucose-free condition (figure 3.21 on page 32). This suggested that TBL1X-deficiency made cells less dependent on glucose.

3.3.4 The Urocortin 3 pathway is not involved in the regulation of TBL1X

A potential way by which insulin and forskolin might regulate the expression of TBL1X is the corticotropin-releasing factor family member urocortin 3 (UCN3). It is expressed in pancreatic β-cells and stimulates insulin and glucagon secretion [133] while being itself secreted after stimulation with high glucose or the insulin secretagogue GLP1 (glucagon-like peptide 1) *in vitro*. Expression is also high in pancreases from HFD or ob/ob mice [134]. Ucn3 exerts its intracellular effects by binding extracellularly to the G protein-coupled 7-transmembrane corticotropin-releasing hormone receptor 2 (CRHR2) while having a very low affinity for CRHR1 [135]. When administered to the central nervous system, it activates the hypothalamic-pituitary-adrenal axis resulting in decreased food intake and elevated blood glucose [136] (figure 3.22 on page 32).

It was hypothesized that metabolic stimuli would induce UCN3 secretion which then activates intracellular signaling regulating TBL1X expression. When checking mRNA levels of GLP1 receptor (GLP1R) as well as CRHR1 and CRHR2 in human samples, no significant regulation was visible except for a slight upregulation of CRHR1 in tumors of lean patients (figure 3.23 on page 33). Moreover, Capan-1 cells did not express neither the Ucn3-specific receptor CRHR2 nor its homolog CRHR1. Therefore, the conclusion was made that this pathway does not play a role in the observed metabolic regulation of TBL1X.

[3]Since the experiments shown in figure 3.14 on page 27 the Click-iT® EdU Imaging Kit (Invitrogen™) had been introduced to the market. Due to its easier and less time consuming handling as well as longer shelf life and better performance, this kit was then applied instead of the previously used BrdU kit.

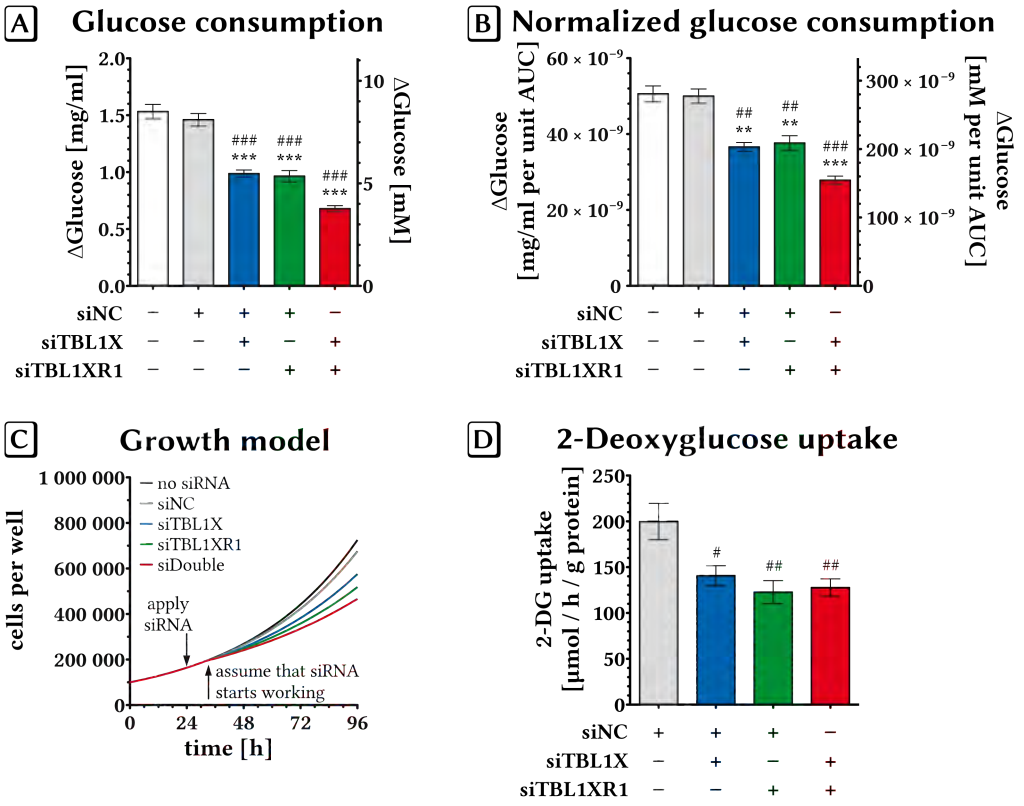

Figure 3.19: TBL1X and TBL1XR1 regulate glucose uptake in Capan-1 cells

Capan-1 cells were treated as described in section 5.15.6 on page 68. A: absolute glucose consumption (mean of 3 independent experiments with technical triplicates for each group). B: glucose consumption was normalized to account for siRNA-affected cell growth by dividing absolute values by area under curve. C: Cell growth model for normalization. Cells were seeded at 1×10^5 cells per well on 12-well plates and counted at end of assay. Cell growth was modeled postulating exponential growth. siRNA was applied 24 h after seeding and assumed to take effect 6 h later, therefore growth rates were considered equal for all groups until this time point and diverging afterwards to reach cell numbers measured at end of assay. Area under curve was calculated for each group and used for normalization. D: radioactive 2-deoxyglucose uptake assay was performed as described in section 5.15.7 on page 68. Data plotted as mean ± SEM. * $p \leq 0.05$ / ** $p \leq 0.01$ / *** $p \leq 0.001$ vs. no siRNA; # $p \leq 0.05$ / ## $p \leq 0.01$ / ### $p \leq 0.001$ vs. siNC, determined by one-way ANOVA.

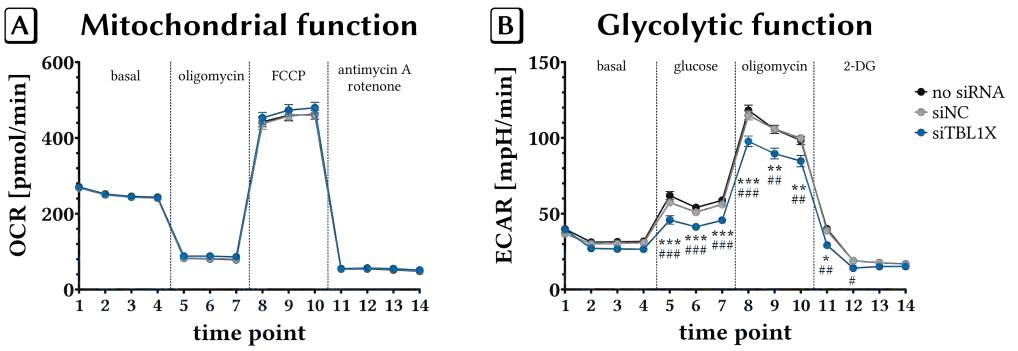

Figure 3.20: TBL1X alters glycolytic function in Capan-1 cells

Capan-1 cells were treated as described in section 5.15.4 on page 66. A: Mitochondrial function measured by oxygen consumption rate (OCR) under basal conditions (time points 1–4) or after injection of indicated chemicals. B: Glycolytic activity function measured by extracellular acidification rate (ECAR) under basal conditions (time points 1–4) or after injection of indicated chemicals. Data plotted as mean ± SEM. $n = 9$ wells per condition; * $p \leq 0.05$ / ** $p \leq 0.01$ / *** $p \leq 0.001$ vs. no siRNA; # $p \leq 0.05$ / ## $p \leq 0.01$ / ### $p \leq 0.001$ vs. siNC, determined by one-way ANOVA.

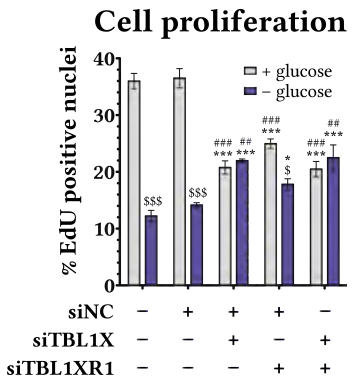

Figure 3.21: TBL1X deficiency enhances growth of Capan-1 cells in the absence of glucose

Cells were seeded on chamber slides and on the following day transfected with siRNA. 24 h after transfection, medium was changed to DMEM with 10 % dialyzed FBS with or without 25 mM glucose. Cells were grown for another 48 h before labeling with EdU for 45 min followed by fixation and staining as described in section 5.15.2 on page 66. Graph shows representative experiment with duplicate wells per condition. 5 random fields per well were imaged and ≥ 870 cells counted per well. Data plotted as mean ± SEM. $^{*}p \leq 0.05$ / $^{**}p \leq 0.01$ / $^{***}p \leq 0.001$ vs. no siRNA; $\#p \leq 0.05$ / $\#\#p \leq 0.01$ / $\#\#\#p \leq 0.001$ vs. siNC; $\$p \leq 0.05$ / $\$\$p \leq 0.01$ / $\$\$\$p \leq 0.001$ vs. +glucose, determined by two-way ANOVA.

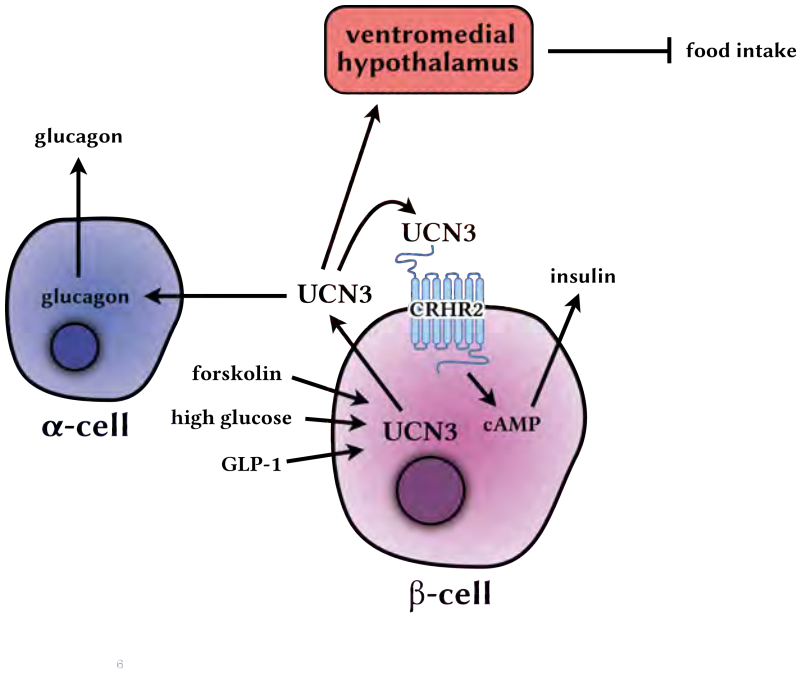

Figure 3.22: Schematic overview of Ucn3 action

Ucn3 is expressed in pancreatic β-cells. Its secretion can be stimulated by high glucose, GLP1 or forskolin. It then stimulates glucagon secretion from α-cells in a paracrine manner or secretion of insulin from β-cells via an autocrine loop through its receptor CRHR2. In the ventromedial hypothalamus it suppresses food intake.

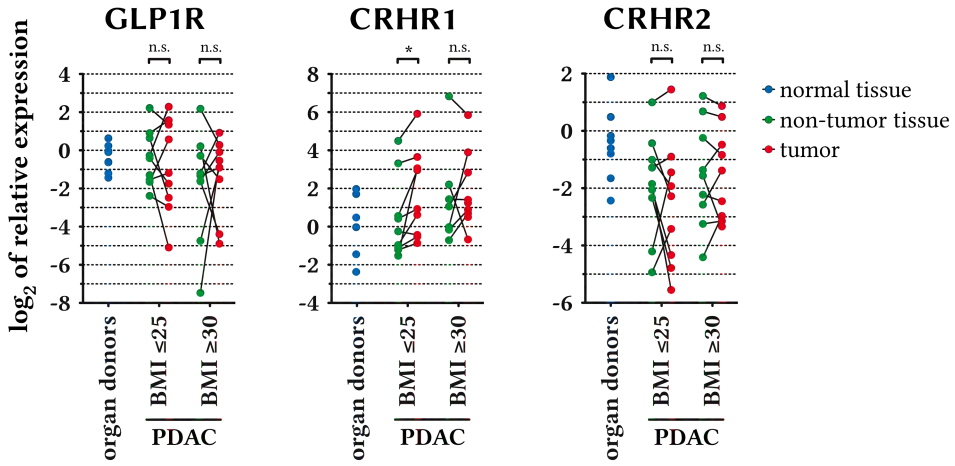

Figure 3.23: Expression of GLP1R, CRHR1 and CRHR2 in human PDAC

Plots show expression of individual patients normalized to 18S-rRNA and relative to a pooled organ donor sample. Lines between dots connect samples from the same patient. GLP1R: glucagon-like peptide 1 receptor; CRHR1: corticotropin-releasing factor receptor 1; CRHR2: corticotropin-releasing factor receptor 2; $^{*}\,p \leq 0.05$, $^{**}\,p \leq 0.01$, $^{***}\,p \leq 0.001$ as determined by two-tailed paired Student's *t*-test.

3.4 Subcutaneous allograft studies

3.4.1 Tbl1x deficiency attenuates growth of established tumors *in vivo*

Based on the findings of TBL1X and TBL1XR1 function in cell proliferation a mouse experiment was designed to test its role in an *in vivo* setting. Since no effect was observable for TBL1XR1 in any of the metabolic experiments, the focus was put on TBL1X alone.

To this end, Panc02 cells were used, which are a well-established syngeneic implantation model for C57BL/6 mice [137]. The cells used in the present study additionally had stable expression of luciferase that had been introduced previously via lentiviral gene transfer (Prof. Dr. Ana Martin-Villalba's lab, DKFZ). This made it possible to monitor tumor growth not only by percutaneous measurement of tumor size but also by means of *in vivo* bioluminescence imaging. The cells were injected subcutaneously into 9-week old male C57BL/6N mice as described in section 5.12.5 on page 61. Four days later, animals were shaved at the site of injection to inspect tumor growth. At this early time point, tumors were very small (≈ 1 mm) and impossible to measure with a digital caliper in a reliable manner. Bioluminescence imaging, however, gave a weak but well-observable signal. At 6 days after implantation, tumors were big enough to be measured with a digital caliper and it was begun to inject 1×10^8 ifu of adenovirus expressing unspecific or *Tbl1x*-specific shRNA directly into the tumors every 2–3 days. This treatment was able to slow tumor growth significantly 9 days after the first viral injection (figure 3.24A–B and figure 3.25 on the next page). Twenty days after implantation, the tumors in the control-shRNA-injected animals had reached the maximum size of 15 mm that is allowed by German Protection of Animals Act (Tierschutzgesetz). Mice were then killed and tumors were excised, weighed and cut in three pieces as depicted in figure 5.1 on page 62 for histology as well as extraction of RNA and proteins. The mass of *Tbl1x*-shRNA-treated tumors was lower than that of control-shRNA-treated ones (figure 3.24C). A reduction in Tbl1x was, however, neither observable on mRNA level nor on protein level or in immunohistochemistry (data not shown), though the adenovirus' capability to induce Tbl1x-knockdown was tested prior to this mouse study in Panc02 cells *in vitro* (figure 3.26 on page 35). Possible explanations for the lack of detectable knockdown in the established tumors will be discussed later (section 4.3.1 on page 43).

3.4.2 Tbl1x deficiency sensitizes established tumors towards gemcitabine

Based on the observations in cell culture of TBL1X affecting cellular glucose metabolism it was of interest if deficiency of the protein could render pancreatic cancer cells sensitive to chemotherapeutic agents as has been suggested by previous work from others [138, 139]. *In vitro* studies in a collaboration project had shown that knockdown of TBL1X resulted in increased apoptotic cell death after treatment with DNA damage-inducing drugs doxorubicin or gemcitabine (Vera Greiner and Dr. Thomas Hofmann, DKFZ, unpublished).

Therefore, Panc02 cells were infected with a lentivirus expressing unspecific or *Tbl1x*-specific shRNA and a population with stable integration of the viral construct was selected (see section 5.16.4 on page 69). Already *in vitro*, Tbl1x-deficient cells had a slower growth rate than control-shRNA-transduced cells (20 % less EdU positive cells). These cells were then

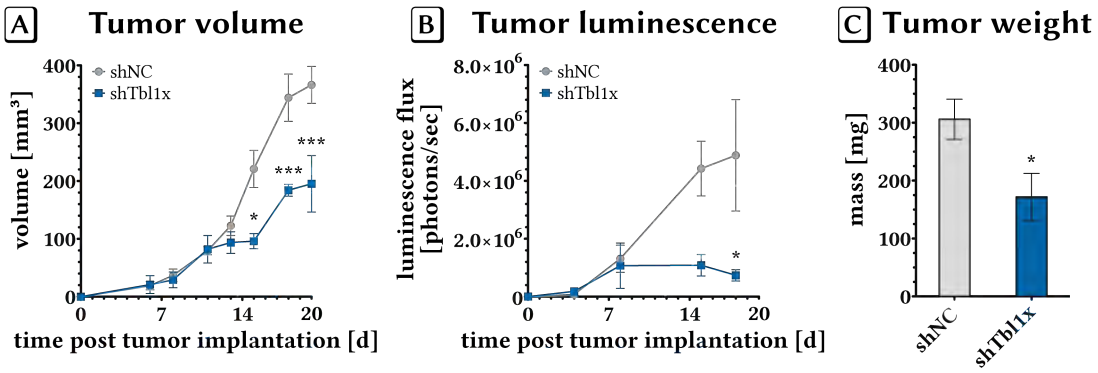

Figure 3.24: Tumor growth of adenovirus-treated subcutaneous Panc02 allografts

Luciferase-expressing Panc02 cells were injected subcutaneously into the right flank of C57BL/6N mice and tumor growth was monitored by percutaneous measurement and bioluminescence as described in section 5.12.5 on page 61. At days 8, 11, 13, 15 and 18 after implantation, 1×10^8 ifu of shRNA-expressing adenovirus were injected directly into the tumors as described in section 5.12.8 on page 61. At day 20 after implantation, animals were killed and tumors were sampled for further analysis. A: tumor volume; B: tumor luminescence (see also figure 3.25); C: tumor weight at necropsy. All values plotted as mean ± SEM. $n = 3–4$ animals per group. $^*p \le 0.05$, $^{**}p \le 0.01$, $^{***}p \le 0.001$ as determined by two-way ANOVA with Bonferroni post-test (A, B) or by one-tailed Welch's t-test (C).

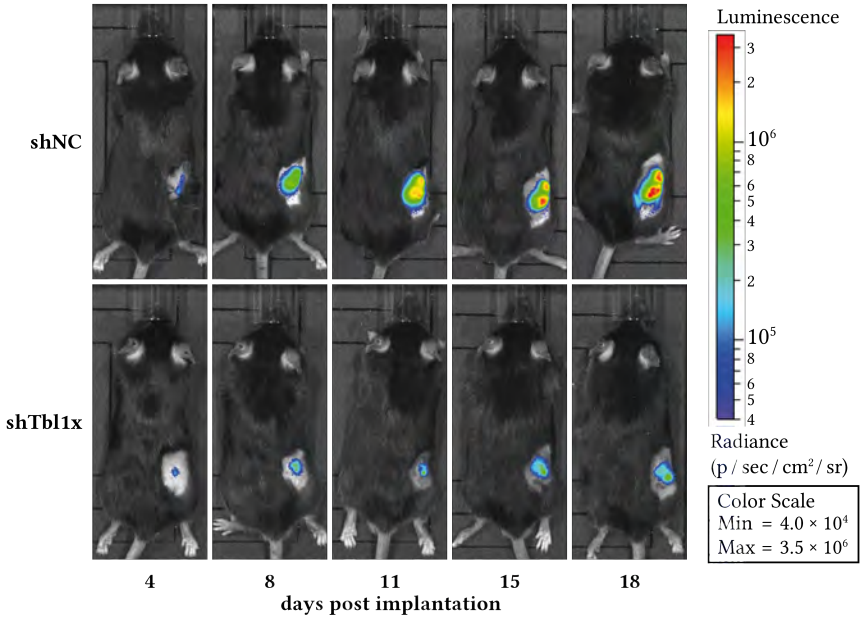

Figure 3.25: Tumor luminescence of adenovirus-treated subcutaneous Panc02 allografts

Bioluminescence images of two representative mice from the experiment described in figure 3.24 are shown.

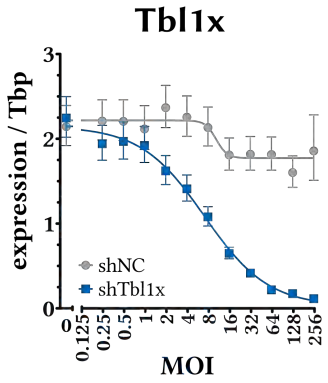

Figure 3.26: Adenoviral knockdown in Panc02 cells *in vitro*

Panc02 cells were seeded and the following day infected as described in section 5.16.5 on page 69 with a 1:2 serial dilution series of adenovirus expressing a negative control (NC) or *Tbl1x*-specific shRNA ranging from an MOI of 250 down to 0.244. Cells were lyzed 48 h after infection and RNA was extracted for quantitative PCR analysis.

implanted subcutaneously into male C57BL/6N mice as before. When tumors had grown to a palpable size, mice were injected three times per week intraperitoneally with three different dosages of gemcitabine (20, 60 and 120 $^{mg}/_{kg}$), which is the most commonly used chemotherapeutic drug in the treatment of human pancreatic cancer. Tbl1x-knockdown alone already resulted in reduced growth as was previously also observed in the intratumoral adenovirus-injection study. Gemcitabine showed a dose-dependent effect on tumor growth as expected. Furthermore, a synergistic effect of Tbl1x-deficiency and chemotherapeutic treatment could be seen. The lowest gemcitabine dosage of 20 $^{mg}/_{kg}$ was already able to provoke a stall of tumor growth in Tbl1x-knockdown tumors whereas in control tumors this was only achieved with the highest dose of 120 $^{mg}/_{kg}$ (figure 3.27 on the next page). The effect became clearest when plotting the volume of each tumor relative to its volume on day 7 post implantation (figure 3.27B) and calculating the area under curve (figure 3.27D). The effect of Tbl1x-knockdown and gemcitabine dosage was also reflected in final tumor weight at necropsy (figure 3.27E).

When analyzing mRNA extracted from tumors, a knockdown of *Tbl1x* between 33 and 48 % (figure 3.28 on the following page) could be measured while knockdown-efficiency in Panc02 cells directly before implantation was 75 %.

Furthermore, a significant reduction in proliferating (Ki-67 expressing) cells could be detected after Tbl1x knockdown in the NaCl-treated group. In the group treated with 20 $^{mg}/_{kg}$ gemcitabine, the effect of Tbl1x deficiency was not significant ($p = 0.149$), but a trend towards reduced proliferation was visible (figure 3.29 on page 37).

3.4.3 Tbl1x deficiency leads to reduction of PI3 kinase and downstream effectors

In search of a possible mechanism explaining these observations, the microarray data from Capan-1 cells were examined and *PIK3CA* mRNA, encoding for PI3 kinase catalytic subunit p110α, was found to be reduced 1.64-fold in cells treated with siRNA against *TBL1X*. When examining protein and RNA samples from Capan-1 cells by immunoblot and quantitative PCR, the reduction of PI3 kinase could be confirmed (figure 3.30 on page 37).

Based on these observations, protein expression was evaluated in the subcutaneous tumor allografts and in Panc02 cells directly before implantation. Since the synergistic effect of Tbl1x-knockdown and chemotherapeutic treatment was most prominent in the animals treated with 20 $^{mg}/_{kg}$ gemcitabine, it was decided to focus on these samples (figure 3.31 on page 38). First of all, the knockdown of Tbl1x could be confirmed both in allograft tumors and cells prior to injection. Furthermore, PI3 kinase was reduced in Tbl1x-knockdown samples in accordance to the findings in Capan-1 cells. Interestingly, the amounts of downstream effectors of PI3 kinase, namely Akt and Gsk3β (glycogen synthase kinase-3 beta) were also reduced. Levels of phosphorylated Akt were higher relative to total Akt in shTbl1x-tumors compared to shNC-tumors and in gemcitabine-treated tumors compared to untreated tumors. Phosphorylated Gsk3β was slightly reduced relative to total Gsk3β in shTbl1x-tumors compared to shNC-tumors and slightly elevated in gemcitabine-treated tumors relative to untreated tumors. Since PI3 kinase is known to interact with Kras [140, 141], also Kras downstream effectors Erk-1 and Erk-2 were examined. Levels of total Erk-1 were slightly reduced in gemcitabine-treated tumors and in shTbl1x-tumors. Erk-2 showed reduction in shTbl1x-tumors. Phosphorylation of Erk-1 and Erk-2 was slightly higher in gemcitabine-treated and in shTbl1x-tumors (figure 3.31 on page 38 and figure 3.32 on page 39).

On the other hand, the PI3 kinase antagonist Pten (Phosphatidylinositol 3,4,5-trisphosphate 3-phosphatase and dual-specificity protein phosphatase) was only slightly elevated in gemcitabine-treated shTbl1x-tumors whereas in all other groups no differences could be observed. Phosphorylation of Pten was reduced in gemcitabine-treated shTbl1x-tumors (figure 3.31 on page 38 and figure 3.32 on page 39). These data indicated that Tbl1x regulated the expression of PI3 kinase and downstream mediators.

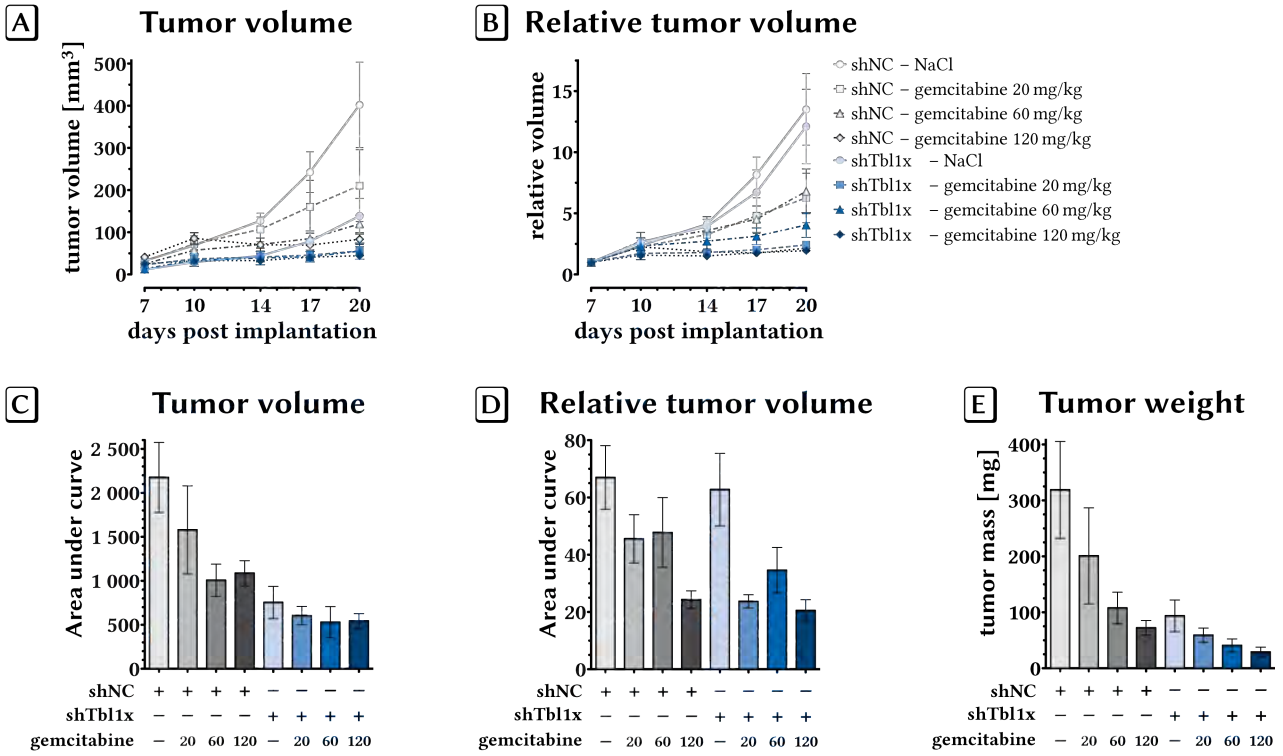

Figure 3.27: Tumor growth of subcutaneous shTbl1x-Panc02 allografts

Panc02 cells with stable expression of *Tbl1x*-specific shRNA (via lentiviral gene transfer) were injected subcutaneously into the right flank of C57BL/6N mice as described in section 5.12.5 on page 61. Starting 7 days after implantation, site of injection was shaved and tumor volume was monitored by percutaneous measurement with a digital caliper followed by intraperitoneal injection of 0.9 % NaCl or indicated dosages of gemcitabine in 0.9 % NaCl. At day 21 after implantation, animals were killed and tumors were sampled for further analysis. A: absolute tumor growth; B: tumor volume relative to day 7 post implantation; C: area under curve of absolute tumor growth; D: area under curve of tumor volume relative to day 7 post implantation; E: tumor weight at necropsy. All values plotted as mean ± SEM. $n = 4–5$ animals per group. For statistical analysis see table H.1 on page 119.

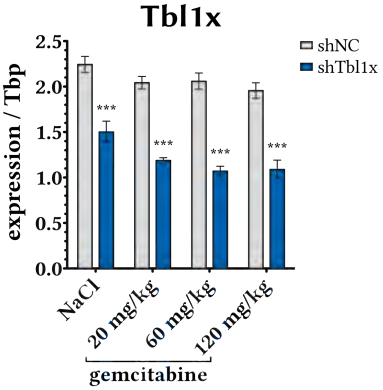

Figure 3.28: mRNA expression of *Tbl1x* in subcutaneous shTbl1x-Panc02 allografts

Data are plotted as mean ± SEM; *** $p \leq 0.001$ vs. shNC determined by two-way ANOVA with Bonferroni post-test.

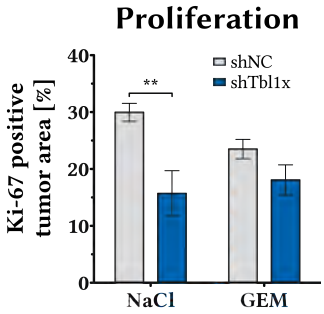

Figure 3.29: Proliferation in subcutaneous shTbl1x-Panc02 allografts

Paraffin sections from 4–5 tumors per group were stained for expression of the proliferative marker Ki-67 as described in section 5.13.3.5 on page 64. Evaluation of Ki-67 positive tumor area was performed as described in section 5.13.4 on page 64. Data are plotted as mean ± SEM; ** $p \leq 0.01$ determined by two-way ANOVA (detailed analysis shown in table H.2 on page 120).

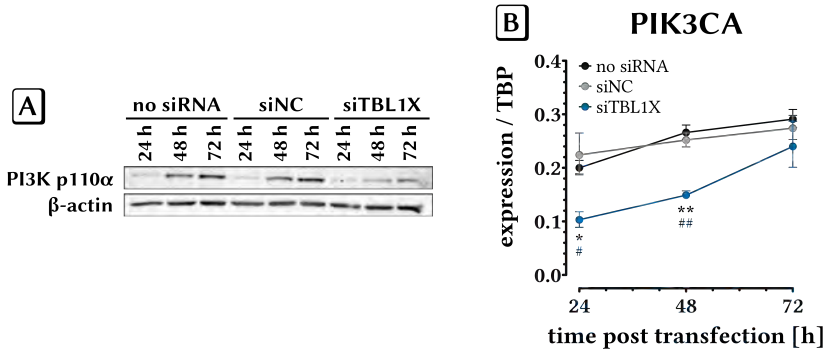

Figure 3.30: Expression of PI3 kinase in siRNA-treated Capan-1 cells

A: Protein samples of Capan-1 cells with siRNA-mediated knockdown of TBL1X were immunoblotted. The samples were from the same experiment as shown in figure 3.13C on page 26; PI3K p110α: phosphatidylinositol 4,5-bisphosphate 3-kinase catalytic subunit alpha isoform; β-actin served as loading control. B: mRNA expression levels for *PIK3CA* relative to *TBP*. The samples were from the same experiment as shown in figure 3.13A on page 26; PIK3CA: gene encoding for PI3K p110α.

In the microarray data from siRNA-mediated TBL1X knockdown in Capan-1 cells also the cell cycle regulators *CDK2* and *CDK4* were downregulated. This was also observed in the subcutaneous tumors and pre-implantation cells expressing *Tbl1x*-shRNA, albeit Cdk2 only showed a slight reduction. Since Gsk3β can phosphorylate cyclin D1 and thus enhance its ubiquitinylation and proteasomal degradation [142], an immunoblot was performed for this protein and it was found to be reduced in Tbl1x-knockdown tumors and Panc02 cells prior to injection (figure 3.31 and figure 3.32 on the facing page).

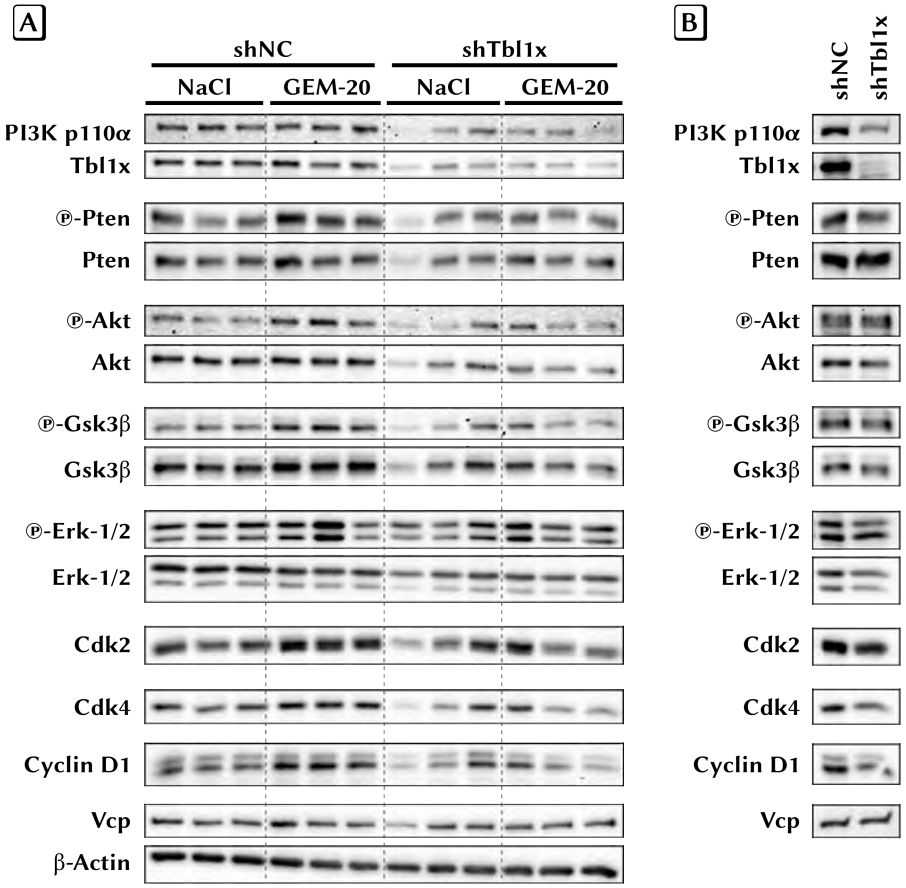

Figure 3.31: Protein expression in subcutaneous shTbl1x-Panc02 allografts

A: immunoblots from implanted tumors after necropsy; B: immunoblots from stable Panc02 cell clones before implantation. PI3K p110α: phosphatidylinositol 4,5-bisphosphate 3-kinase catalytic subunit alpha isoform; Akt: protein kinase B; Gsk3β: glycogen synthase kinase-3 beta; Erk: extracellular signal-regulated kinase; Cdk2: cyclin-dependent kinase 2; Cdk4: cyclin-dependent kinase 4; Vcp: valosin-containing protein (loading control).

3.4.4 PI3 kinase is upregulated in human tumors and correlates with TBL1X and TBL1XR1

To test the relevance of PI3 kinase regulation by TBL1X in human PDAC, patient material was analyzed and there was indeed an increased expression of *PIK3CA* mRNA in tumors compared to normal tissue and a strong and significant correlation with both *TBL1X* and *TBL1XR1* expression levels (figure 3.33 on the next page).

3.4.5 TBL1X binds to PI3 kinase promoter region

Data from a previous chromatin immunoprecipitation coupled with massively parallel DNA sequencing (ChIP-Seq) experiment from mouse liver with TBL1X-antibody (performed by Dr. Xiaoyue Wang in our lab) showed an enrichment peak in the 20 kbp upstream region of the *PIK3CA* gene. This region was mapped to the corresponding human region (figure 3.34A on page 40) and specific primers (figure 3.34B) were designed. Next, a chromatin immunoprecipitation was performed on Capan-1 cells as described in section 5.18.6 on page 72 with TBL1X-specific antibody and a 2.3-fold enrichment of the *PIK3CA* promoter region peak was detected, indicating a binding of TBL1X upstream of the *PIK3CA* gene. This suggested that TBL1X acted as a direct transcriptional (co-)regulator of PI3 kinase.

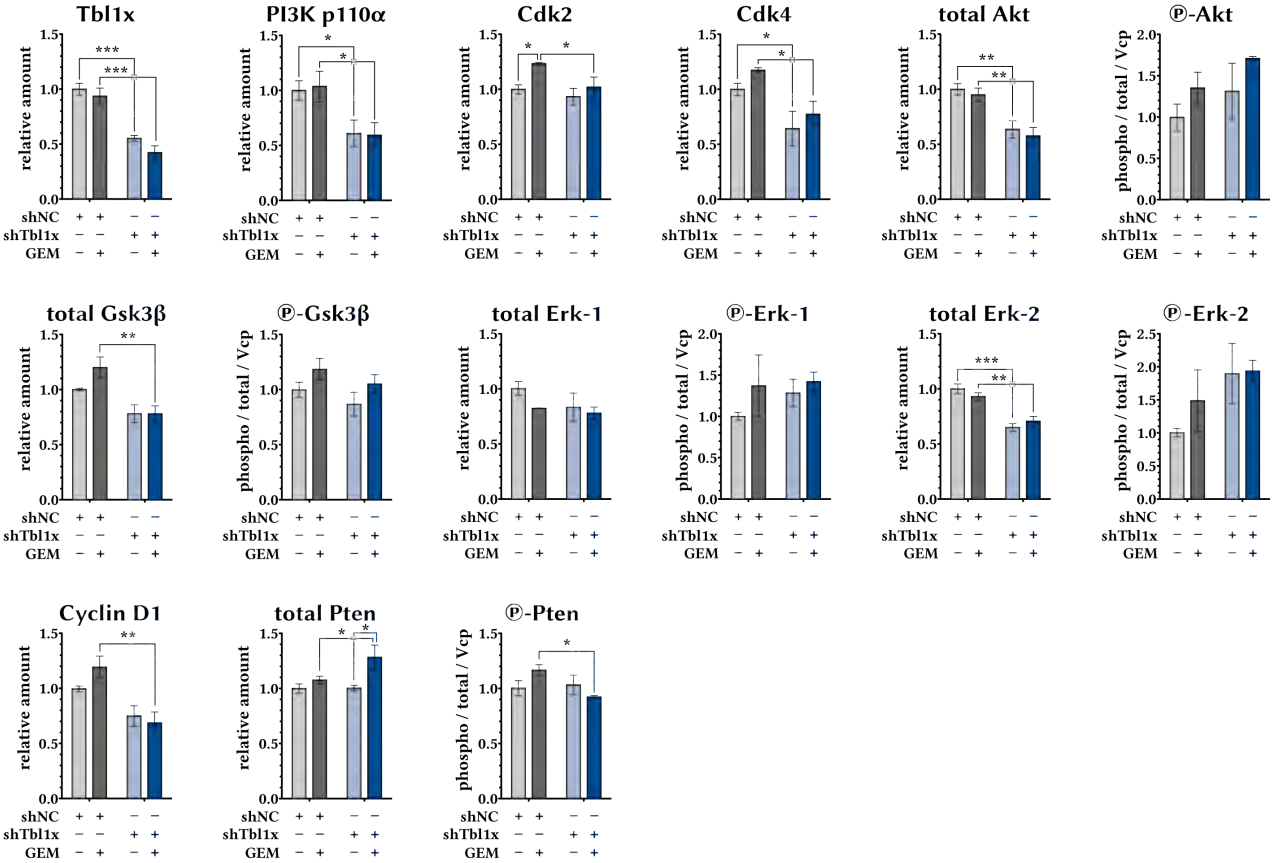

Figure 3.32: Quantification of protein expression in subcutaneous shTbl1x-Panc02 allografts

Immunoblots from implanted tumors after necropsy were quantified using Image Lab™ software (Bio-Rad). Band intensities are normalized to Vcp and relative to shNC-tumors not treated with gemcitabine. Data plotted as mean ± SEM; * $p \leq 0.05$, ** $p \leq 0.01$, *** $p \leq 0.001$ as determined by two-way ANOVA with Bonferroni post test.

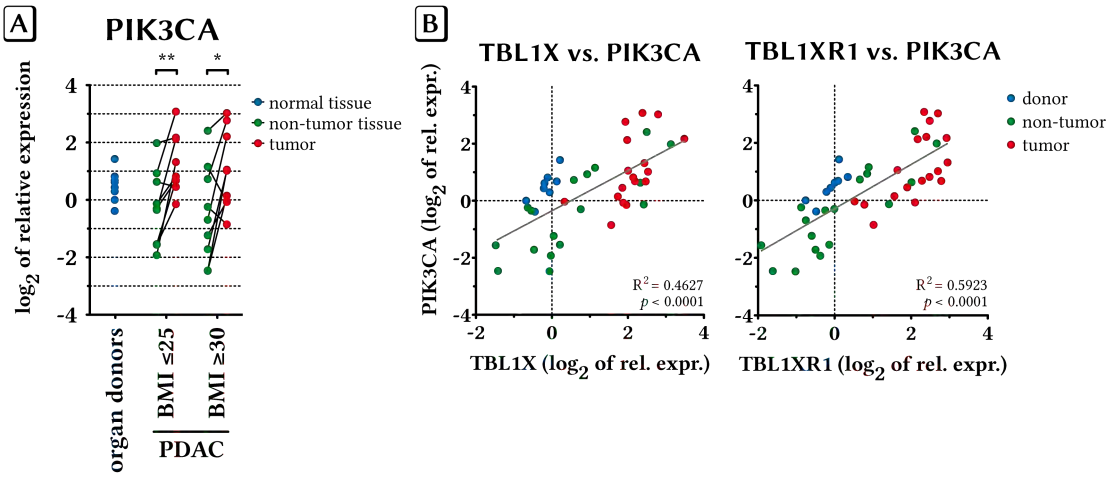

Figure 3.33: Expression of PI3 kinase in human PDAC and correlation with *TBL1X* and *TBL1XR1*

Plots show mRNA expression of individual patients normalized to 18S-rRNA and relative to a pooled organ donor sample. A: Expression of *PIK3CA* in tissue from organ donors or healthy and tumor tissue of PDAC patients. Lines between dots connect samples from the same patient. B: Correlation of *PIK3CA* mRNA with expression levels of *TBL1X* and *TBL1XR1*. BMI: body mass index; PDAC: pancreatic ductal adenocarcinoma; * $p \leq 0.05$, ** $p \leq 0.01$, as determined by two-tailed paired Student's *t*-test.

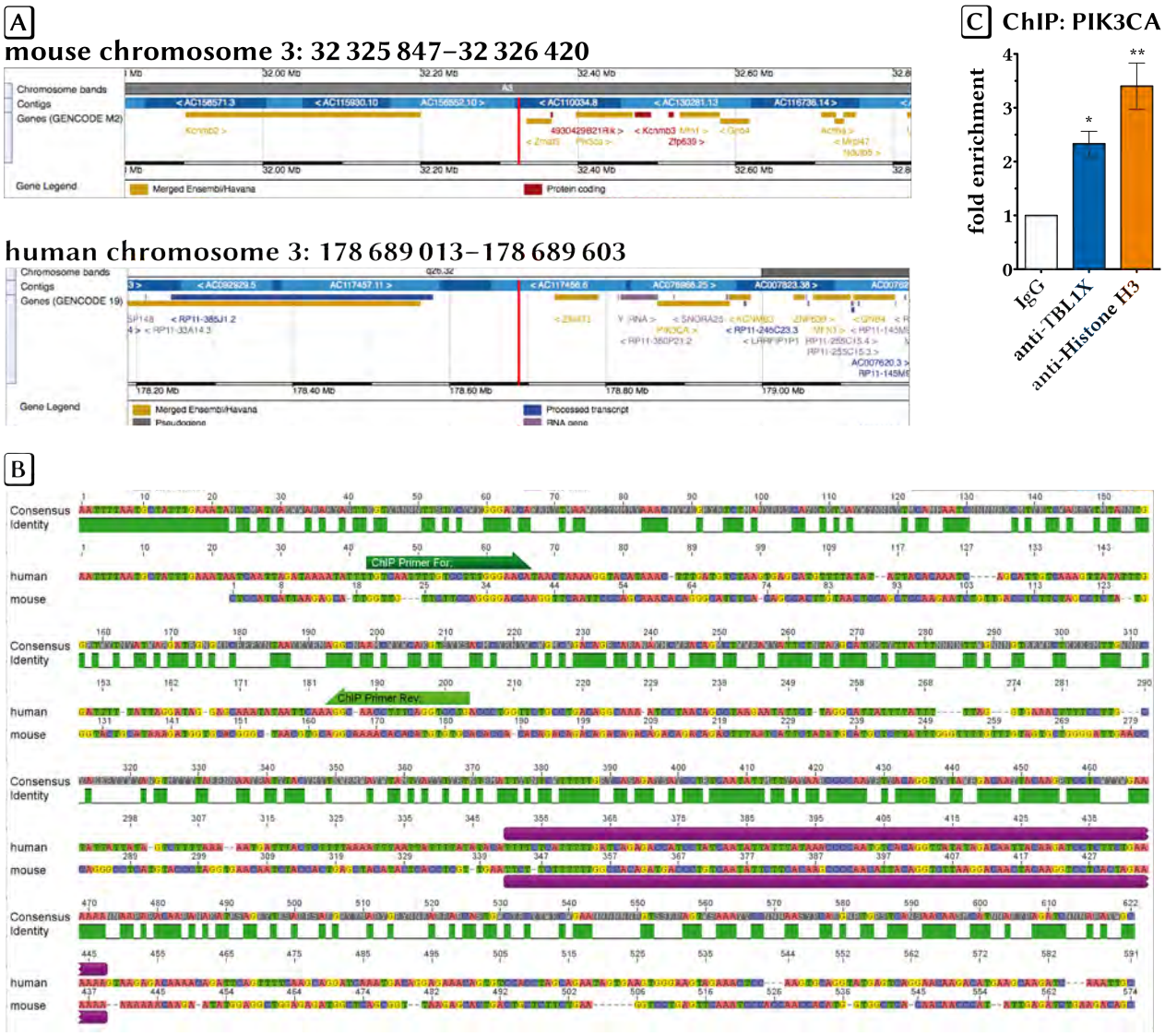

Figure 3.34: TBL1X-binding to *PIK3CA* promoter region

A: an enrichment peak on mouse chromosome 3 upstream of the *PIK3CA* gene was identified with chromatin immunoprecipitation sequencing (ChIP-Seq) with TBL1X-antibody in liver and mapped to the corresponding human region; images were created with Ensembl genome browser (`http://www.ensembl.org`). B: Alignment of mouse and human region with the high-homology core in violet and the primers used for detection in ChIP. Unfortunately, using Primer-Blast (`http://www.ncbi.nlm.nih.gov/tools/primer-blast/`) it was not possible to design suitable primers that would bind closer to the high-homology core and at the same time be specific for that particular genomic region; alignment was created with Geneious software [143]. C: Chromatin immunoprecipitation was performed from Capan-1 cells with TBL1X-antibody (or histone H3 antibody as positive control) and probed for *PIK3CA* promoter region with primers indicated in B. Graph shows results from two independent experiments. $^{*}p \leq 0.05$, $^{**}p \leq 0.01$, as determined by one-way ANOVA.

4 Discussion

4.1 Metabolic phenotype of *p48$^{+/Cre}$; Kras$^{+/LSL-G12D}$* mice on HFD

4.1.1 Male *p48$^{+/Cre}$; Kras$^{+/LSL-G12D}$* mice are partially protected from diet-induced obesity

In recent years, obesity and type 2 diabetes have been implicated as a risk factor for several forms of cancers, including PDAC [30–40]. A distinct mechanistic explanation has, however, not been established yet. Therefore, it was of interest to investigate the role of the transcriptional co-regulator TBL1X and TBL1XR1 as a potential link. To this end, the *p48$^{+/Cre}$; Kras$^{+/LSL-G12D}$* mouse tumor model was subjected to a high fat diet regime.

Surprisingly, male *p48$^{+/Cre}$; Kras$^{+/LSL-G12D}$* mice did not gain as much weight as their wild type litter mates, both on HFD and on LFD (figure 3.7 on page 21). Females, on the other hand did not show such a difference between genotypes. This might at least in part be attributed to exocrine pancreatic insufficiency. Feces samples that were collected from some mice towards the end of the 12-week feeding period suggested that in male *p48$^{+/Cre}$; Kras$^{+/LSL-G12D}$* mice on HFD the uptake of dietary lipids was impeded resulting in high fecal triglycerides and free fatty acids (table 3.3 on page 22). To further investigate this hypothesis, it would be worthwhile to collect feces systematically and to measure fecal triglycerides, free fatty acids and elastase as well as levels of pancreatic lipases.

Pancreatic exocrine insufficiency has been previously described in *p48$^{+/Cre}$; Kras$^{+/LSL-G12D}$* mice on HFD [53]. The authors of this study also observed less weight gain in *p48$^{+/Cre}$; Kras$^{+/LSL-G12D}$* mice compared to controls (although not to the same extent as in the present thesis), increased feces production and fecal energy content. Oil red O staining of stool samples indicated high fat content, but they did not perform a proper lipid extraction and quantification of fecal lipids.

Nevertheless, the fact that this feature was only observed in male animals raises the issue of sex differences that would be interesting to further investigate. Also in humans, pancreatic exocrine insufficiency seems to be more frequent in men [144]. Probably here lifestyle factors such as cigarette smoking and alcohol consumption play a role. Both behaviors are more common among men than women and can lead to pancreatitis, a known cause of pancreatic exocrine insufficiency. Still the fact that mice show similar sex differences should make one consider also genetic and/or hormonal differences between males and females.

4.1.2 Fatty liver development in mice on LFD

Contrary to initial assumptions, male wild type animals on LFD had high liver weights compared to females. Histologically, fatty livers could be identified in all male mice, whereas female wild type mice on LFD rarely developed a fatty liver, and if so, only to a very mild extent. This might be explained by the composition of the HFD and LFD (table 4.1 on the following page). The difference in caloric fat content between the diets is balanced by carbohydrates and here predominantly sucrose and corn starch. Sucrose chemically consists of glucose and fructose, the latter being metabolized exclusively by the liver, where it is converted to triglycerides. Due to this fact, fructose also stands in the focus of research for contributing to the global obesity and diabetes pandemic in humans. Studies in mice have shown that fructose consumption leads to increased adiposity [145]. Additionally, it is known in mice that males are more susceptible to high fat diet-induced obesity than females [146, 147].

4.2 Moribundity of *p48$^{+/Cre}$; Kras$^{+/LSL-G12D}$* mice on HFD

The p48 DNA-binding subunit of transcription factor PTF1, also known as Ptf1a, is a regulator of pancreatic development. It becomes active in early pancreatic buds (around day 9.5 of embryonic development in the mouse) and is involved in determining whether pancreatic bud cells differentiate to pancreatic progenitors or revert back to a duodenal fate [148]. This fact was exploited by Hingorani et al. [15] when they created the *p48$^{+/Cre}$; Kras$^{+/LSL-G12D}$* mouse model for PDAC that was also used in this study.

As described earlier, *p48$^{+/Cre}$; Kras$^{+/LSL-G12D}$* mice, especially males on HFD, frequently fell moribund during the course of the feeding experiment (section 3.2.3 on page 20). The observed symptoms of hind leg limping implied the possibility of neuronal defects. It is indeed known that p48, besides its role in pancreatic development, is also involved in neurogenesis, especially in the cerebellum [149, 150] which is important for motor control. It might therefore be possible that in some mice the mutant Kras also becomes active in neurons potentially leading to the observed locomotive defects. Since the phenomenon occurred most frequently in male *p48$^{+/Cre}$; Kras$^{+/LSL-G12D}$* mice on HFD, both sex and diet-dependent factors, such as obesity-related inflammatory processes, have to be considered as possible variables.

Another symptom sporadically observed in moribund *p48$^{+/Cre}$; Kras$^{+/LSL-G12D}$* mice was weight loss and apathy. This might be due to pancreatic organ failure resulting in impaired food digestion and nutrient uptake. Possible reasons can be either severe pancreatic exocrine insufficiency or obstruction of the main pancreatic and/or bile duct by growing malignancies. The former can be due to loss of exocrine tissue by transformation to PanIN lesions and cancer cells, while

Table 4.1: Composition of HFD and LFD

	LFD		HFD	
component	**weight %**	**kcal %**	**weight %**	**kcal %**
fat	4.3	10	34.9	60
protein	19.2	20	26.2	20
carbohydrates	67.3	70	26.3	20
casein	18.96	19.72	25.84	19.72
L-cystine	0.28	0.30	0.39	0.30
corn starch	29.86	31.06	0	0
maltodextrin 10	3.32	3.45	16.15	12.32
sucrose	33.17	34.51	8.89	6.78
cellulose	4.74	0	6.46	0
soybean oil	2.37	5.55	3.23	5.55
lard	1.90	4.44	31.66	54.35
mineral mix	0.95	0	1.29	0
$CaHPO_4$	1.23	0	1.68	0
$CaCO_3$	0.52	0	0.71	0
potassium citrate hydrate	1.56	0	2.13	0
vitamin mix	0.95	0.99	1.29	0.99
choline bitartrate	0.19	0	0.26	0

the latter results in pancreatic juices to back up into the pancreas, further damaging the organ and causing distress in the animals.

4.3 TBL1X and TBL1XR1 as regulators of tumor cell growth

TBL1X and TBL1XR1 were initially described as components of the SMRT/NCoR/HDAC3 co-repressor complex associated with nuclear receptors [86, 87, 89] where they serve as exchange factors [90] (see section 1.3 on page 8). Later studies then found TBL1XR1 to be upregulated in lung squamous cell carcinoma [100], deleted in ETV6-RUNX1 positive acute lymphoblastic leukemia [101] or amplified in breast cancer [102]. While the first two studies only made the respective observations, the latter paper also further investigated the function and showed that knockdown of TBL1XR1 in breast cancer cells led to reduced migration and invasion *in vitro* and diminished tumorigenesis in a nude mouse xenograft model.

A study published in 2012 found that TBL1XR1 is frequently mutated in central nervous system lymphomas and that the presence of the mutation correlates with shorter survival [104]. But it was not until very recently, that several other studies showed the involvement of TBL1XR1 in various cancers, including lung squamous cell carcinoma [151], prostate cancer [152], acute lymphoblastic leukemia [153, 154], acute promyelocytic leukemia [155], esophageal squamous cell carcinoma [156], and cervical cancer [157]. Of these studies, three showed a correlation between altered TBL1XR1 expression and decreased survival [156, 157] or disease relapse [153].

The study by Liu et al. [156] showed that TBL1XR1 was upregulated in esophageal squamous cell carcinoma and positively correlated with disease progression. Patients with a higher TBL1XR1 expression had a shorter overall survival time. Overexpression of TBL1XR1 promoted lymphangiogenesis and lymphatic metastasis *in vitro* and *in vivo*, whereas downregulation of TBL1XR1 had the opposite effect. This was due to binding of TBL1XR1 to the *VEGFC* promoter, thus inducing gene expression.

Wang et al. [157] found that the expression of TBL1XR1 in cervical cancer cell lines and tissues was significantly upregulated at the mRNA and protein level compared to normal cervical cells. TBL1XR1 could be identified as an independent prognostic factor that was significantly correlated with the clinical stage, survival time and recurrence of patients. Overexpression of TBL1XR1 in HeLa and Siha cell lines promoted invasion *in vitro* and *in vivo*. On the other hand, knockdown of TBL1XR1 inhibited epithelial-mesenchymal transition *in vitro* and *in vivo*.

The present study is the first to show a role for TBL1X in cancer and for TBL1XR1 particularly in pancreatic cancer. The key findings of TBL1X and TBL1XR1 upregulation in pancreatic cancer, both human and murine, and their effects on tumor cell growth *in vitro* and *in vivo* nicely fit into the overall picture set up by the aforementioned publications.

TBL1X and TBL1XR1 have been described to interact with β-catenin and to be required for Wnt-mediated β-catenin signaling and target gene expression [92, 93]. Wnt/β-catenin signaling is an important developmental pathway [94, 158]

that is frequently altered in pancreatic cancer [18, 97–99, 159, 160]. In the microarray data from Capan-1 cells with siRNA-mediated knockdown of TBL1X or TBL1XR1 a significant alteration in the expression of Wnt target genes could, however, not be seen (data not shown). This indicates, that both co-regulators do not exert their pro-proliferative function through the Wnt/β-catenin pathway. It is therefore concluded that not Wnt/β-catenin but PI3 kinase signaling, which will be discussed later, is the major mechanism by which TBL1X (and potentially also TBL1XR1) exerts its function in proliferation and chemotherapy resistance in pancreatic cancer.

4.3.1 TBL1X knockdown efficiency in adenovirus-injected subcutaneous allograft tumors

As was shown in section 3.4.1 on page 33, intratumoral injection of adenovirus with *TBL1X*-specific shRNA attenuated tumor growth. Although the functionality of the virus was validated *in vitro* (figure 3.26 on page 35), a knockdown of TBL1X could not be detected in the tumors after necropsy. This can be attributed to several aspects, namely outgrowth of infected cells by non-infected cells, degradation of the virus by repeated freeze-thaw cycles, and long intervals between injections.

It has been previously described by Possemato et al. [161] that knockdown of genes relevant for growth or survival in an *in vivo* tumor model by viral approaches can lead to a selection process. Cells infected with shRNA against an essential gene underwent growth arrest or apoptosis and were thus outgrown by cells that had not been infected with virus and were therefore not impeded in their growth behavior.

Besides this, also experimental issues have to be considered. The adenovirus used in this experiment was available in three aliquots. For each injection, one aliquot was thawed, virus was used and the remainder frozen at −80 °C. The number of freeze-thaw cycles for each aliquot was marked on the tube and none was freeze-thawed more than three times. It can, however, not be excluded that towards the end of the experiment, when all aliquots had already undergone two freeze-thaw cycles, virus performance was reduced. Furthermore, it was observed that shTBL1X-injected tumors grew slower during the week when injections were performed every 48 h while making a leap in growth over the weekend when the time between injections was 72 h.

4.4 PI3 kinase as a downstream target of TBL1X and mediator of chemoresistance

The lipid kinase family of phosphatidylinositol-4,5-bisphosphate 3-kinases (PI3 kinase) are involved in multiple cellular processes, including cell growth and proliferation, survival, differentiation and intracellular transport. They act as intracellular signal transducers by phosphorylating phosphatidylinositols on the hydroxyl group at position 3 of the inositol ring.

PI3 kinases are grouped in three classes. Members of class I produce phosphatidylinositol-3-phosphate (PI(3)P), phosphatidylinositol-(3,4)-bisphosphate (PI(3,4)P_2), and phosphatidylinositol-(3,4,5)-trisphosphate (PI(3,4,5)P_3). They are heterodimers consisting of a regulatory and catalytic subunit and are activated by receptor tyrosine kinases (class IA) or G protein-coupled receptors (class IB). Members of class IA are formed by one of five isoforms of a p85 or p55 regulatory subunit (p85α, p55α, p50α, p85β, or p55γ) and one of four isoforms of a p110 catalytic subunit (p110α, p110β, p110γ, p110δ). The PI3 kinase products PI(3,4)P_2 and PI(3,4,5)P_3 activate Akt by binding to its pleckstrin-homology domain. Furthermore, it is known that Ras can interact with and activate PI3 kinase [162–164]. A simplified overview of PI3 kinase signaling is given in figure 4.1 on the next page.

In many cancers, including PDAC, the PI3 kinase catalytic subunit isoform p110α is frequently mutated and constitutively active, often coinciding with a loss or reduction of the phosphatidylinositol-(3,4,5)-trisphosphate phosphatase PTEN that antagonizes PI3 kinase signaling [78]. Fresno Vara et al. [165] report that the PI3K/Akt pathway is often disturbed in cancer and that Akt activation is related to apoptosis resistance.

Resistance of pancreatic tumors to gemcitabine treatment is still a major issue that also contributes to the poor survival rates in patients. Several studies have shown that Erk phosphorylation is related to gemcitabine resistance [166, 167]. Inhibition of Erk activity led to a sensitization of cancer cells towards gemcitabine while the expression of a mutant constitutively active MEK provided resistance to the drug. Application of PI3 kinase inhibitors was also able to increase gemcitabine-induced apoptosis in pancreatic cancer cell lines [79, 80].

In this study a reduction in PI3 kinase expression after Tbl1x knockdown could clearly be shown and there was a trend of increased Erk phosphorylation upon gemcitabine treatment and a reduction of Erk-2 levels (figure 3.31 on page 38 and figure 3.32 on page 39) after Tbl1x-knockdown. This suggested that the reduction of PI3 kinase after Tbl1x ablation triggered multiple cellular responses including reduced Erk activity to convey gemcitabine sensitization.

The possibility of a combination treatment of gemcitabine with other drugs to enhance therapy response and patient survival is a focus of ongoing research. One such combination is sorafenib, a potent multi-kinase inhibitor that can be applied orally. It targets Raf serine/threonine kinases and different receptor tyrosine kinases such as vascular endothelial growth factor receptor (VEGFR), platelet derived growth factor receptor (PDGFR), c-Kit, FLT-3 and RET [168, 169]. In a phase I trial of combination treatment of gemcitabine and sorafenib it was well tolerated and 57 % of patients experienced stable disease [170]. A phase II trial, however, did not state a significant clinical benefit of the combination

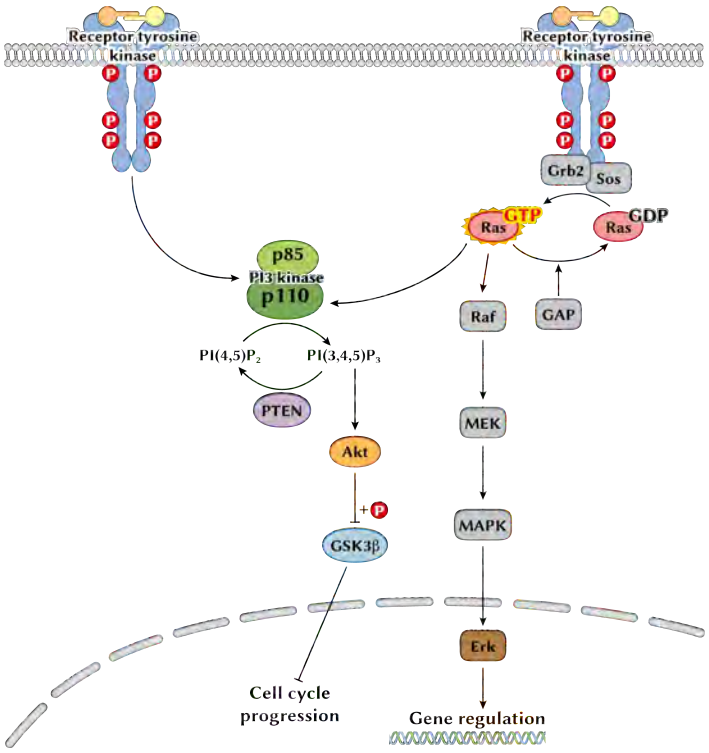

Figure 4.1: PI3 kinase signaling

PI3 kinases of class IA can be directly activated by receptor tyrosine kinases. Alternatively, receptor tyrosine kinases can mediate the exchange of GDP to GTP on Ras, thus activating it. Active Ras can then in turn activate PI3 kinase p110 catalytic subunit or the Raf-MAPK-Erk signaling pathway. The deactivation of Ras by hydrolysis of GTP to GDP can be facilitated by GTPase-activating proteins (GAP). Active PI3 kinase turns phosphatidylinositol-4,5-bisphosphate ($PI(4,5)P_2$) to phosphatidylinositol-3,4,5-trisphosphate ($PI(3,4,5)P_3$) which then activates Akt. This leads to a deactivating phosphorylation of Gsk3β that when active inhibits cell cycle progression. The phosphatase PTEN can dephosphorylate $PI(3,4,5)P_3$ and thus counteracts PI3 kinase activity.

treatment [171]. Therefore, Awasthi et al. [172] combined gemcitabine and sorafenib with endothelial monocyte activating polypeptide II (EMAP), a pro-inflammatory cytokine with antiangiogenic and antiendothelial activities. They could show that, both *in vitro* and *in vivo*, this triple combination provides a benefit over single administration or gemcitabine-sorafenib combination alone. Administration of gemcitabine with LY293111, an antagonist of the Erk1/2-activating leukotriene B_4 receptor, in an orthotopic implantation model in athymic mice also provided a better outcome [173]. A double-blinded, placebo-controlled phase III clinical trial conducted in 2007 [174] with gemcitabine and the EGFR inhibitor erlotinib resulted in a modest increase in median survival (6.24 vs. 5.91 months) while the 1-year survival rate with erlotinib and gemcitabine was 23 % versus 17 % with placebo and gemcitabine.

4.4.1 TBL1X and TBL1XR1 control glucose metabolism in pancreatic tumor cells

One observation that was made in the *in vitro* studies was a decreased glucose uptake and glycolysis after TBL1X and TBL1XR1 knockdown (figure 3.19 and figure 3.20 on page 31). This, however, seems to be a chicken-before-egg-problem of whether glucose consumption is directly regulated by TBL1X/TBL1XR1 or whether it is a secondary consequence of decreased proliferation. Cancer cells usually have high rates of aerobic glycolysis thus meeting their demands in building blocks for new cells. Glycolysis intermediates are shuttled to the pentose phosphate pathway ensuring production of ribose and deoxyribose as components for new RNA and DNA [120, 121]. One explanation could therefore be, that the decrease in proliferation after TBL1X/TBL1XR1 knockdown caused a decreased demand for nucleic acid synthesis and thus a reduction in aerobic glycolysis. On the other hand, it is known that PI3 kinase/Akt signaling is a regulator of metabolic pathways, including glycolysis (reviewed by DeBerardinis et al. [120] and Muñoz-Pinedo et al. [121]). Further studies are therefore required to answer the question whether TBL1X/TBL1XR1 affect glucose metabolism directly via the PI3 kinase/Akt pathway or indirectly via decreased demand for nucleotide building blocks.

The effect of TBL1X/TBL1XR1 on glucose metabolism is furthermore interesting since cancer cells are more sensitive to radiation or chemotherapeutics when glycolysis is inhibited [138, 139]. In Kras-transformed cells glucose starvation has been found to induce cell death via the unfolded protein response [175]. The cellular energy sensor AMPK has recently been found to negatively regulate aerobic glycolysis and thus suppress tumor growth. Inactivation of AMPK

led to an increase in aerobic glycolysis and usage of glucose for lipid and biomass production [176]. Hexokinases catalyze the first step of glycolysis, namely the phosphorylation of glucose to glucose-6-phosphate thus preventing its export out of the cell. Many cancer cells express high levels of hexokinase 2 (HK2) that is otherwise only found in embryonic development or adipose, skeletal, or heart muscle cells. Ablation of HK2 is able to reduce tumor growth in mouse models of lung and breast cancer [177]. HK2-negative cells have less flux of glucose carbon to the citric acid cycle as well as ribonucleotide and fatty acid synthesis. Therapeutic strategies aiming at tumor cell glucose metabolism are therefore a potential candidate for future cancer treatments.

4.5 Outlook

Challenging $p48^{+/Cre}$; $Kras^{+/LSL\text{-}G12D}$ mice with a high fat diet induced structures resembling invasive carcinoma in some of the animals. Thorough analysis by an experienced mouse pathologist is, however, still required to confirm and quantify these findings. Expression levels of TBL1X/TBL1XR1 (and other transcriptional co-regulators) were not altered between lean and obese human patients or between LFD- and HFD-fed mice. Therefore, other mechanisms may link obesity and pancreatic tumor development. For further studies, not only mRNA expression should be studied but also changes on post-transcriptional levels.

A growth-regulating effect of TBL1X in cancer in general and TBL1XR1 on pancreatic cancer in particular has not previously been described and constitutes an interesting basis for future research. To complement the subcutaneous allografts studies with an orthotopic model it would be worthwhile to cross $p48^{+/Cre}$; $Kras^{+/LSL\text{-}G12D}$ mice with $Tbl1x^{fl/fl}$ or $Tbl1xr1^{fl/fl}$ mice to generate animals with a pancreas-specific knockout of Tbl1x or Tbl1xr1 in combination with the tumor-initiating Kras mutation. It would be expected to detect a tumor-preventing effect of Tbl1x and Tbl1xr1 ablation also under these circumstances.

The so far unobserved regulation of PI3 kinase expression by TBL1X provides a novel and promising new target mechanism for PDAC treatment regarding gemcitabine resistance. The action of TBL1X on the PI3 kinase promoter should be further studied with a luciferase reporter gene assay. Also a rescue experiment with ectopic expression of mutant constitutively active PI3 kinase in TBL1X-depleted cancer cells should be carried out to show that the effects of TBL1X on tumor cell growth, metabolism and chemosensitivity are indeed largely dependent on PI3 kinase. TBL1X might nevertheless be an interesting novel drug target upstream of PI3 kinase signaling. This could be done by RNA nanoparticles [178, 179] since it will probably be very difficult to affect Tbl1x/Tbl1xr1 expression or activity with conventional chemical or protein-based drugs *in vivo*. Screening of patients for expression levels of TBL1X in their tumors might help to stratify them to predict therapy response and treatment outcome.

5 Material and Methods

Material

5.1 Instruments and equipment

instrument / equipment	model	company
aspiration adapter, 8-channel		Neolab (Heidelberg, Germany)
bacterial incubator	Heraeus Function Line	ThermoFisher Scientific (Schwerte, Germany)
bacterial shaking incubator	Multitron Standard	Infors HT (Bottmingen, Switzerland)
balance	EW 2200-2NM	Kern & Sohn (Balingen, Germany)
Bunsen burner	Labogaz 206	Campingaz (Hattersheim, Germany)
cell counter, automated	Countess™	Life Technologies™, Invitrogen™ (Darmstadt, Germany)
cell culture hood	Cellgard Class II Biological Safety Cabinet	IBS Integrad Biosciences (Fernwald, Germany)
CO_2 incubator		Sanyo (Etten Leur, The Netherlands)
counting chamber	BLAUBRAND®, Neubauer improved, Cat. No. 717805	Brand (Wertheim, Germany)
digital caliper		Bochem (Weilburg, Germany)
EchoMRI™ Whole Body Composition Analyzer		Echo Medical Systems (Houston, TX, USA)
fluorescence lamp for microscope	HXP 120C	Carl Zeiss (Oberkochen, Germany)
fluorometer	Qubit® 2.0	Life Technologies™, Invitrogen™ (Darmstadt, Germany)
freezer (−20 °C)		Liebherr (Biberach, Germany)
freezer, ultra-low temperature (−80 °C)	New Brunswick U101 Innova	Eppendorf (Hamburg, Germany)
freezing container	Mr. Frosty™, 5100-0001	ThermoFisher Scientific (Schwerte, Germany)
gas anesthesia system	XGI-8	Caliper LifeSciences (Rodgau, Germany)
GeneChip® fluidics station	450	Affymetrix (High Wycombe, United Kingdom)
GeneChip® scanner		Affymetrix (High Wycombe, United Kingdom)
glucometer	OneTouch® Ultra	LifeScan (Neckargemünd, Germany)
immunoblot documentation	ChemiDoc™ XRS+ Molecular Imager® with Image Lab™ Software	Bio-Rad (München, Germany)
IVIS® Optical Imaging System	Lumina II	Caliper LifeSciences (Rodgau, Germany)
LED fluorescence lamp for Axio Imager.M2	Colibri.2	Carl Zeiss (Oberkochen, Germany)
Liquidator™ 96	Rainin Pipetting 360°	Mettler Toledo (Gießen, Germany)
magnetic stirrer	MR 3001 K	Heidolph (Schwabach, Germany)
magnetic stirrer	Duomax 1030	Heidolph (Schwabach, Germany)
magnetic stirrer	444-7076	VWR (Darmstadt, Germany)
microinjector	IM-6	Narishige (London, UK)

instrument / equipment	model	company
microscope	Axio Imager.M2 with AxioCam HRc	Carl Zeiss (Oberkochen, Germany)
microscope	Axiovert 40 CFL with AxioCam ICm1	Carl Zeiss (Oberkochen, Germany)
microscope, automated	Olympus Cell^R	Olympus (Hamburg, Germany)
microscope, motorized	Cell Observer Z1	Carl Zeiss (Oberkochen, Germany)
microplate reader	Mithras LB 940	Berthold Technologies (Bad Wildbad, Germany)
micropipette 0.2–2 µl	P2	Gilson (Limburg-Offheim, Germany)
micropipette 1–10 µl	P10	Gilson (Limburg-Offheim, Germany)
micropipette 2–20 µl	P20	Gilson (Limburg-Offheim, Germany)
micropipette 10–100 µl	P100 N	Gilson (Limburg-Offheim, Germany)
micropipette 50–200 µl	P200	Gilson (Limburg-Offheim, Germany)
micropipette 100–1000 µl	P1000	Gilson (Limburg-Offheim, Germany)
micropipette, 8-channel, 0.5–10 µl	Research plus	Eppendorf (Hamburg, Germany)
micropipette, 8-channel, 10–100 µl	Research	Eppendorf (Hamburg, Germany)
microtome	RM2245	Leica (Wetzlar, Germany)
microwave	700W	Severin (Sundern, Germany)
Mini-PROTEAN® 3 Cell	165-3301	Bio-Rad (München, Germany)
Mini-PROTEAN® Tetra Cell	165-8004	Bio-Rad (München, Germany)
Mini Trans-Blot® Cell	170-3930	Bio-Rad (München, Germany)
mouse cage, 335 cm^2 H-TEMP™ Polysulfon	1144B-00SU	Tecniplast (Hohenpeißenberg, Germany)
mouse cage system	Green Line IVC SealSafe Plus	Tecniplast (Hohenpeißenberg, Germany)
mouse housing cabinet, ventilated		Tecniplast (Hohenpeißenberg, Germany)
multistep pipette	Multipette® plus	Eppendorf (Hamburg, Germany)
multistep pipette	Multipette® M4	Eppendorf (Hamburg, Germany)
Nanodrop	ND-1000	ThermoFisher Scientific (Schwerte, Germany)
orbital shaker	Duomax 1030	Heidolph (Schwabach, Germany)
pH-meter	Qph 70	GHM Messtechnik, Greisinger (Regenstauf, Germany)
pipetboy	acu	Integra (Fernwald, Germany)
power supply for gel electrophoresis	PowerPac Basic™	Bio-Rad (München, Germany)
power supply for Axio Imager.M2	232	Carl Zeiss (Oberkochen, Germany)
precision balance	M-power AZ124	Sartorius (Göttingen, Germany)
real-time PCR system	StepOnePlus	Life Technologies™, Applied Biosystems® (Darmstadt, Germany)
refrigerator (2–8 °C)		Liebherr (Biberach, Germany)
rotating wheel		Neolab (Heidelberg, Germany)
scintillation counter, Tri-Carb Liquid Scintillation analyzer	2200CA	Packard Instruments (Meriden, CT, USA)

instrument / equipment	model	company
sonicator	Bioruptor® Plus	Diagenode (Seraing, Belgium)
tabletop centrifuge	Mikro 22 R	Hettich (Newport Pagnell, United Kingdom)
tabletop centrifuge	Heraeus Fresco 17	ThermoFisher Scientific (Schwerte, Germany)
tabletop centrifuge	Heraeus Biofuge pico	ThermoFisher Scientific (Schwerte, Germany)
tabletop centrifuge	Heraeus Biofuge Primo	ThermoFisher Scientific (Schwerte, Germany)
Thermomixer	comfort	Eppendorf (Hamburg, Germany)
thermocycler	T3000	biometra (Göttingen, Germany)
tissue grinder, all-glass	Dounce 7 ml	Kimble Chase (Meiningen, Germany)
Tissue Lyser	MM 400	Retsch (Haan, Germany)
tissue processor for dehydration	ASP 300	Leica (Wetzlar, Germany)
tissue embedding center	EG1150 H	Leica (Wetzlar, Germany)
titer plate shaker		ThermoFisher Scientific (Schwerte, Germany)
vortex mixer	Genie	Scientific Industries (Bohemia, NY, USA)
water bath		P-D Industriegesellschaft (Dresden, Germany)
water filter system	TKA xCAD	ThermoFisher Scientific (Schwerte, Germany)
XF96 Extracellular Flux Analyzer		Seahorse Bioscience (Copenhagen, Denmark)
XF Prep Station		Seahorse Bioscience (Copenhagen, Denmark)

5.2 Consumable lab ware

product	company	Cat. No.
biopsy foam pad	Simport (Belœil, Québec, Canada)	M476-1
cell scraper	Corning (Wiesbaden, Germany)	3010
chamber slide, 8-well, Nunc Lab-Tek	ThermoFisher Scientific (Schwerte, Germany)	177445
CHROMA SPIN™ 100 columns	Clontech (Saint-Germain-en-Laye, France)	
0.2 ml Combitips advanced®	Eppendorf (Hamburg, Germany)	0030 089.413
0.5 ml Combitips advanced®	Eppendorf (Hamburg, Germany)	0030 089.421
0.5 ml Combitips advanced®, sterile	Eppendorf (Hamburg, Germany)	0030 089.634
5 ml Combitips advanced®	Eppendorf (Hamburg, Germany)	0030 089.456
5 ml Combitips advanced®, sterile	Eppendorf (Hamburg, Germany)	0030 089.669
10 ml Combitips advanced®	Eppendorf (Hamburg, Germany)	0030 089.464
10 ml Combitips advanced®, sterile	Eppendorf (Hamburg, Germany)	0030 089.667
Countess™ cell counting chamber slides	Life Technologies™, Invitrogen™ (Darmstadt, Germany)	C10283
cover slips, 24 × 60 mm #1	Menzel (Braunschweig, Germany)	BB024060A1
2 ml cryogenic vial	StarLab (Hamburg, Germany)	E3110-6122
1.5 ml DNA LoBind tubes	Eppendorf (Hamburg, Germany)	0030 108.051
500 ml filter system 0.22 µm, polystyrene, nonpyrogenic	Corning (Wiesbaden, Germany)	430758

product	company	Cat. No.
10 µl filter tip, graduated	StarLab (Hamburg, Germany)	S1121-3810
20 µl filter tip, beveled	StarLab (Hamburg, Germany)	S1120-1810
100 µl filter tip, beveled	StarLab (Hamburg, Germany)	S1120-1840
200 µl filter tip, graduated	StarLab (Hamburg, Germany)	S1120-8810
1000 µl filter tip	StarLab (Hamburg, Germany)	S1126-7810
folded filters	Munktell (Bärenstein, Germany)	4.303.240
gas cartridge (propane) for Bunsen burner	Campingaz (Hattersheim, Germany)	C 206 Super
GeneChip® Human Genome U133 Plus 2.0 Array	Affymetrix (High Wycombe, United Kingdom)	900466
glucose test stripes, OneTouch® Ultra	LifeScan (Neckargemünd, Germany)	–
histology cassettes	Neolab (Heidelberg, Germany)	7-0014
imaging plate , 96-well clear bottom black wall	BD Falcon™ (Heidelberg, Germany)	353219
injection needle Sterican® 0.4 × 20 mm (27G)	B. Braun (Melsungen, Germany)	4657705
inoculation loops, 1 µl	Sarstedt (Nümbrecht, Germany)	86.1567.050
insulin syringes, Micro-Fine™+ Demi, 0.3 ml	BD Medical (Heidelberg, Germany)	324826
MicroAmp® Fast Optical 96-well Reaction Plate for quantitative PCR	Life Technologies™, Applied Biosystems® (Darmstadt, Germany)	4346906
MicroAmp® Optical Adhesive Film for quantitative PCR	Life Technologies™, Applied Biosystems® (Darmstadt, Germany)	4311971
micro hematocrit capillaries, heparin-coated		Brand (Wertheim, Germany)
microscope slide, SuperFrost® Plus, 25 × 75 mm, 1.0 mm thick	VWR (Darmstadt, Germany)	631-0108
microtiter plate, 96-well (Nunc F96)	ThermoFisher Scientific (Schwerte, Germany)	260836
Millex®-GV filter unit PVDF 0.22 µm	Merck KGaA (Darmstadt, Germany)	SLGV033RS
Millex®-HV filter unit PVDF 0.45 µm	Merck KGaA (Darmstadt, Germany)	SLHV033RS
Millex®-HA filter unit mixed cellulose esters 0.45 µm	Merck KGaA (Darmstadt, Germany)	SLHA033SS
nitrocellulose membrane, Protran BA 85, 0.45 µm	GE Healthcare (Solingen, Germany)	10401196
Parafilm® M	Bemis® (Neenah WI, USA)	PM-996
Pasteur pipette, glass, long	WU Mainz (Bamberg, Germany)	
PCR tubes, 8-strip, 0.2 ml	Greiner Bio-one (Frickenhausen, Germany)	673210
PCR tube lids, flat, 8-strip	Greiner Bio-one (Frickenhausen, Germany)	373250
petri dish for Agar plates	Greiner Bio-one (Frickenhausen, Germany)	632180
200 µl pipette tips, LTS, for Liquidator™	Steinbrenner Laborsysteme (Wiesenbach, Germany)	SL-LT-L200

product	company	Cat. No.
10 µl pipette tip	StarLab (Hamburg, Germany)	S1111-3700
200 µl pipette tip	Steinbrenner Laborsysteme (Wiesenbach, Germany)	TipTower Refill System
1000 µl pipette tip	Steinbrenner Laborsysteme (Wiesenbach, Germany)	TipTower Refill System
0.1–10 µl pipette tips, epT.I.P.S.® LoRetention	Eppendorf (Hamburg, Germany)	0030 072.006
0.5–20 µl pipette tips, epT.I.P.S.® LoRetention	Eppendorf (Hamburg, Germany)	0030 072.014
1–200 µl pipette tips, epT.I.P.S.® LoRetention	Eppendorf (Hamburg, Germany)	0030 072.022
50–1000 µl pipette tips, epT.I.P.S.® LoRetention	Eppendorf (Hamburg, Germany)	0030 072.030
15 ml polypropylene centrifuge tubes	Greiner Bio-one (Frickenhausen, Germany)	188271
50 ml polypropylene centrifuge tubes	Greiner Bio-one (Frickenhausen, Germany)	227261
1.5 ml reaction tubes, black	Carl Roth (Karlsruhe, Germany)	AA80
1.5 ml RNase-free centrifuge tubes, Mµlti® Safe Seal	Carl Roth (Karlsruhe, Germany)	7080
14 ml round-bottom snap-cap tubes, polypropylene	BD Falcon™ (Heidelberg, Germany)	352059
1.5 ml safe-lock tube	Eppendorf (Hamburg, Germany)	0030 120.086
2 ml safe-lock tube	Eppendorf (Hamburg, Germany)	0030 120.094
5 ml safe-lock tube	Eppendorf (Hamburg, Germany)	0030 119.460
scalpel, disposable, sterile, No. 21	Feather (Osaka, Japan)	
scintillation tubes, LDPE	Carl Roth (Karlsruhe, Germany)	5404.1
5 ml serological pipette	BD Falcon™ (Heidelberg, Germany)	357543
10 ml serological pipette	BD Falcon™ (Heidelberg, Germany)	357551
25 ml serological pipette	BD Falcon™ (Heidelberg, Germany)	357525
50 ml serological pipette	BD Falcon™ (Heidelberg, Germany)	357550
5 ml skirted tube	VWR (Darmstadt, Germany)	216-0153
stainless steel beads, 5 mm	Qiagen (Hilden, Germany)	69989
1 ml syringe, Soft-Ject® Tuberkulin	Henke Sass Wolf (Tuttlingen, Germany)	5010-200V0
5 ml syringe	BD (Heidelberg, Germany)	309050
20 ml syringe	BD (Heidelberg, Germany)	300629
50 ml syringe	BD (Heidelberg, Germany)	300865
10 cm tissue culture plate	BD Falcon™ (Heidelberg, Germany)	353003
15 cm tissue culture plate	BD Falcon™ (Heidelberg, Germany)	353025
tissue culture plate, 6-well	BD Falcon™ (Heidelberg, Germany)	353046
tissue culture plate, 12-well	Corning (Wiesbaden, Germany)	3512
tissue culture plate, 24-well	BD Falcon™ (Heidelberg, Germany)	353047
tissue culture plate, 48-well	BD Falcon™ (Heidelberg, Germany)	353230

product	company	Cat. No.
tissue culture plate , 96-well	BD Falcon™ (Heidelberg, Germany)	353072
Venofix® A 0.4 × 10 mm (27G)	B. Braun (Melsungen, Germany)	4056388
waste bags, 200 × 300 mm	Carl Roth (Karlsruhe, Germany)	E706.1
weigh boats 41 × 41 mm	Neolab (Heidelberg, Germany)	1-1124
weigh boats 89 × 89 mm	Neolab (Heidelberg, Germany)	1-1125
Whatman™ paper	GE Healthcare (Solingen, Germany)	3030 917
10–100 µl wide bore tips	Gilson (Limburg-Offheim, Germany)	DFL10ST
XF96 FluxPak 4-port measurement cartridges	Seahorse Bioscience (Copenhagen, Denmark)	102310-001
XF96 Polystyrene Cell Culture Microplates	Seahorse Bioscience (Copenhagen, Denmark)	101085-004

5.3 Kits

product	company	Cat. No.
BioArray HighYield® RNA transcript labeling kit	Enzo Life Sciences (Lörrach, Germany)	ENZ-42655
Cell Proliferation Kit (BrdU Assay)	GE Healthcare (Solingen, Germany)	RPN20
Click-iT® EdU Imaging Kit	Life Technologies™, Invitrogen™ (Darmstadt, Germany)	C10338
DNase Set, RNase-free	Qiagen (Hilden, Germany)	1023460
First strand cDNA Synthesis Kit, Fermentas	ThermoFisher Scientific (Schwerte, Germany)	K1612
Glucose (HK) Assay Kit	Sigma-Aldrich (München, Germany)	GAHK20-1KT
HIV-1 p24 ELISA Assay	XpressBio (Thurmont, MD, USA)	XB-1000
HR Series NEFA-HR (2) kit	Wako Diagnostics (Neuss, Germany)	999-34691
MinElute PCR purification kit	Qiagen (Hilden, Germany)	28004
Mouse Insulin ELISA	Mercodia (Uppsala, Sweden)	10-1247-01
NEFA Standard Solution	Wako Diagnostics (Neuss, Germany)	276-76491
Pierce® BCA Protein Assay Kit	ThermoFisher Scientific (Schwerte, Germany)	23225
PureLink® HiPure Plasmid Maxiprep Kit	Life Technologies™, Invitrogen™ (Darmstadt, Germany)	K2100-06
QIAprep Spin Miniprep Kit	Qiagen (Hilden, Germany)	27104
QIAquick Gel Extraction Kit	Qiagen (Hilden, Germany)	28704
Qubit® dsDNA HS Assay Kit	Life Technologies™, Invitrogen™ (Darmstadt, Germany)	Q32854
RNeasy® Mini Kit	Qiagen (Hilden, Germany)	74106
Serum Triglyceride Determination Kit	Sigma-Aldrich (München, Germany)	TR0100
SuperScript® Choice System for cDNA Synthesis	Life Technologies™, Invitrogen™ (Darmstadt, Germany)	18090-019
VECTASTAIN Elite ABC Kit	Vector Laboratories (Burlingame, CA, USA)	PK-6100
XF Cell Mito Stress Test Kit	Seahorse Bioscience (Copenhagen, Denmark)	101706-100
XF Glycolysis Stress Test Kit	Seahorse Bioscience (Copenhagen, Denmark)	102194-100

5.4 Enzymes

enzyme	company	Cat. No.
micrococcal nuclease	New England Bioloabs® Inc., (Ipswich, MA, USA)	M0247S
proteinase K	ThermoFisher Scientific (Schwerte, Germany)	EO0491
RNase A 10 $^{mg}/_{ml}$	ThermoFisher Scientific (Schwerte, Germany)	EN0531

5.5 Plasmids

plasmid	company	Cat. No.
pLKO.1-shRNA-Mm_Tbl1x	Sigma-Aldrich (München, Germany)	SHCLNG-NM_020601
pLKO.1-shRNA-scrambled	Addgene (Cambridge, MA, USA)	1864
pMD2.G	Addgene (Cambridge, MA, USA)	12259
psPAX2	Addgene (Cambridge, MA, USA)	12260

5.6 Antibodies

5.6.1 Primary antibodies

protein	company	Cat.-No.	origin	usage
AKT	Cell Signaling	9272	rabbit	IB
Ⓟ-AKT Ser-473	Cell Signaling	9271	rabbit	IB
AMPK	Cell Signaling	2532	rabbit	IB
Ⓟ-AMPK Thr-172	Cell Signaling	2535	rabbit	IB
CDK2	Santa Cruz	sc-163	rabbit	IB
CDK4	Cell Signaling	2906	mouse	IB
Cyclin D1	Cell Signaling	2926	mouse	IB
ERK-1/2	Cell Signaling	9102	rabbit	IB
Ⓟ-ERK-1/2 Thr-202/Tyr-204	Cell Signaling	9101	rabbit	IB
GSK3β	Cell Signaling	9315	rabbit	IB
Ⓟ-GSK3β Ser-9	Cell Signaling	9336	rabbit	IB
Histone H3	Cell Signaling	4620	rabbit	ChIP
IRS1	Cell Signaling	3407	rabbit	IB
Ⓟ-IRS1 Tyr-895	Cell Signaling	3070	rabbit	IB
Ⓟ-IRS1 Ser-1101	Cell Signaling	2385	rabbit	IB
Ki-67	Dako	M7249	mouse	IHC
PI3K p110α	Cell Signaling	4249	rabbit	IB
PTEN	Cell Signaling	9552	rabbit	IB
Ⓟ-PTEN Ser-380 / Thr-382/383	Cell Signaling	9549	rabbit	IB
TBL1X	Abcam	ab24548	rabbit	IB, IHC, ChIP
TBL1X	Abcam	ab2243	goat	IHC
TBL1XR1	Novus Biologicals	NB600-270	rabbit	IB
TBL1XR1	Abnova	H00079718-M01	mouse	IHC
β-actin	Sigma	A5441	mouse	IB
VCP	Abcam	11433	mouse	IB

5.6.2 Secondary antibodies

antibody	company	Cat.-No.	origin	usage
anti-goat IgG (H+L), biotinylated	KPL, Inc.	71-00-37	rabbit	IHC
anti-mouse IgG (whole molecule)	Sigma-Aldrich	M8642	goat	IHC
anti-rat IgG, biotinylated, mouse adsorbed	Vector Laboratories	BA-4001	rabbit	IHC
anti-mouse IgG (H+L)-Cy3, MinX	Dianova	715-165-150	donkey	BrdU assay
anti-mouse IgG (H+L)-HRP	Bio-Rad	170-6516	goat	IB
anti-rabbit IgG (H+L)-HRP	Bio-Rad	172-1019	goat	IB
EnVision™⁺ anti-mouse HRP labeled polymer	Dako	K4001		IHC
EnVision™⁺ anti-rabbit HRP labeled polymer	Dako	K4003		IHC
Normal Rabbit IgG	Cell Signaling	2729	rabbit	ChIP
10 % Normal Rabbit Serum	KPL, Inc.	71-00-28	rabbit	IHC

5.7 Chemicals and reagents

product	company	Cat. No.
acetic acid	Sigma-Aldrich (München, Germany)	45731
acrylamide/bisacrylamide 37.5:1, 40 % (Rotiphorese® Gel 40 (37.5:1))	Carl Roth (Karlsruhe, Germany)	T802.1
agarose	Carl Roth (Karlsruhe, Germany)	3810
Alexa Fluor® 555 azide, triethylammonium salt	Life Technologies™, Molecular Probes® (Darmstadt, Germany)	A20012
AllStars Negative control siRNA coupled 3' to Alexa Fluor® 488 on sense-strand	Qiagen (Hilden, Germany)	1027292
ampicillin sodium salt	Sigma-Aldrich (München, Germany)	A9518
Antibody Diluent, Background Reducing	Dako (Hamburg, Germany)	S3022
APS (ammonium persulfate)	Carl Roth (Karlsruhe, Germany)	9592
β-mercaptoethanol	Sigma-Aldrich (München, Germany)	M7154
Biotin-Blocking System (0.1 % avidin solution and 0.01 % biotin solution)	Dako (Hamburg, Germany)	X0590
boric acid (H_3BO_3)	Sigma-Aldrich (München, Germany)	31146
bromophenol blue, sodium salt	Sigma-Aldrich (München, Germany)	114405
BSA for cell culture: Albumin solution from bovine serum, 30 % in DPBS, sterile-filtered	Sigma-Aldrich (München, Germany)	A9576
BSA for immunoblotting and EdU assay: albumin bovine Fraction V	biomol (Hamburg, Germany)	01400.100
BSA for BrdU assay, fatty acid free	Sigma-Aldrich (München, Germany)	A8806
BSA for immunohistochemistry	Sigma-Aldrich (München, Germany)	A7030
$CaCl_2$ (calcium chloride)	Carl Roth (Karlsruhe, Germany)	CN93
chloroform ($CHCl_3$)	Carl Roth (Karlsruhe, Germany)	3313
$CuSO_4$ (copper (II) sulfate pentahydrate)	Sigma-Aldrich (München, Germany)	209198

product	company	Cat. No.
2-deoxy-D-glucose	Sigma-Aldrich (München, Germany)	D8375-5G
1,2-^{3}H-2-deoxy-D-glucose	PerkinElmer (Rodgau, Germany)	NET549001MC
DEPC (diethylpyrocarbonate)	Sigma-Aldrich (München, Germany)	D5758
DMEM High Glucose Pyruvate (+ L-glutamine)	Life Technologies™, Gibco® (Darmstadt, Germany)	41966-029
DMEM Low Glucose Pyruvate (+ L-glutamine)	Life Technologies™, Gibco® (Darmstadt, Germany)	31885-023
DMSO (dimethyl sulfoxide), sterile for cell culture	Sigma-Aldrich (München, Germany)	D2650
DNA marker, GeneRuler 100 bp	ThermoFisher Scientific (Schwerte, Germany)	SM0241
DPBS, no $CaCl_2$, no $MgCl_2$	Life Technologies™, Gibco® (Darmstadt, Germany)	14190-094
DPBS 10×, no $CaCl_2$, no $MgCl_2$	Life Technologies™, Gibco® (Darmstadt, Germany)	14200-067
DTT (dithiothreitol)	Applichem (Darmstadt, Germany)	A2948
ECL™ Western Blotting Detection Reagent	GE Healthcare (Solingen, Germany)	RPN2106
ECL™ Prime Western Blotting Detection Reagent	GE Healthcare (Solingen, Germany)	RPN2232
EDTA (ethylenediaminetetraacetic acid disodium salt dihydrate)	Sigma-Aldrich (München, Germany)	E5134
EdU (5-ethynyl-2'-deoxyuridine)	Life Technologies™, Molecular Probes® (Darmstadt, Germany)	A10044
EGTA (Ethylene glycol-bis(2-aminoethylether)-*N,N,N',N'*-tetraacetic acid)	Sigma-Aldrich (München, Germany)	E4378
ethanol ≥ 99.8 %, denatured with approx. 1 % methyl ethyl ketone (for histology)	Carl Roth (Karlsruhe, Germany)	K928
eosin G	Carl Roth (Karlsruhe, Germany)	7089
ethanol, absolute	Sigma-Aldrich (München, Germany)	32205
ethidium bromide solution 1 % / 10 mg/ml	Carl Roth (Karlsruhe, Germany)	2218
fetal bovine serum (FBS), Dialyzed, US-Origin	Life Technologies™, Gibco® (Darmstadt, Germany)	26400-036
fetal bovine serum (FBS), Qualified, E.U. Approved, South America Origin	Life Technologies™, Gibco® (Darmstadt, Germany)	10270-106
Fluorescent Mounting Medium	Dako (Hamburg, Germany)	S3023
formaldehyde solution 37 %	J. T. Baker (Deventer, The Netherlands)	7040
formamide	Merck KGaA, Calbiochem (Darmstadt, Germany)	344206
forskolin	Sigma-Aldrich (München, Germany)	F3917
gemcitabine 40 mg/ml solution	HEXAL®	–
D-glucose anhydrous	Applichem (Darmstadt, Germany)	A0883
100× L-glutamine 200 mM	Life Technologies™, Gibco® (Darmstadt, Germany)	25030-024
glycerol	Sigma-Aldrich (München, Germany)	15523
glycine	Sigma-Aldrich (München, Germany)	33226

product	company	Cat. No.
HEPES buffer solution 1 M	Life Technologies™, Gibco® (Darmstadt, Germany)	15630-056
H_2O_2 (hydrogen peroxide) 30 % solution	Merck KGaA (Darmstadt, Germany)	1.07209
HCl (hydrochloric acid) 37 %	Sigma-Aldrich (München, Germany)	30721
Hoechst 33342, trihydrochloride trihydrate, 10 mg/ml	Life Technologies™, Molecular Probes® (Darmstadt, Germany)	H3570
IGEPAL® CA-630 (NP-40 substitute)	Sigma-Aldrich (München, Germany)	56741
imidazole	Merck KGaA (Darmstadt, Germany)	4716
insulin human recombinant expressed in yeast	Sigma-Aldrich (München, Germany)	I2643
isoflurane	Baxter (Unterschleißheim, Germany)	I7403
KCl (potassium chloride)	Carl Roth (Karlsruhe, Germany)	A137
KH_2PO_4 (potassium dihydrogen phosphate)	Carl Roth (Karlsruhe, Germany)	3904
LB-Agar (Luria/Miller)	Carl Roth (Karlsruhe, Germany)	X969
LB-Medium (Luria/Miller)	Carl Roth (Karlsruhe, Germany)	X968
LiCl (lithium chloride)	Carl Roth (Karlsruhe, Germany)	3739
Lipofectamine® 2000 Transfection Reagent	Life Technologies™, Invitrogen™ (Darmstadt, Germany)	11668-019
Liquid DAB$^+$ Chromogen and Substrate Buffer	Dako (Hamburg, Germany)	K3468
D-luciferin firefly, potassium salt	Biosynth (Staad, Switzerland)	L-8220
D-mannitol	Sigma-Aldrich (München, Germany)	M4125
1-^{14}C-D-mannitol	PerkinElmer (Rodgau, Germany)	NEC314050UC
Mayer's hemalum solution (hematoxylin)	Merck KGaA (Darmstadt, Germany)	1.09249
methanol	Sigma-Aldrich (München, Germany)	32213
$MgCl_2 \cdot 6\,H_2O$ (magnesium chloride hexahydrate)	Sigma-Aldrich (München, Germany)	M9272
$MgSO_4 \cdot 7\,H_2O$ (magnesium sulfate heptahydrate)	Applichem (Darmstadt, Germany)	A4101
milk powder, skim milk extra grade	Gerbu (Heidelberg, Germany)	1602
MOPS (3-(*N*-morpholino)propanesulfonic acid)	Sigma-Aldrich (München, Germany)	M3183
$Na_2HPO_4 \cdot 2\,H_2O$ (di-sodium hydrogen phosphate dihydrate)	Sigma-Aldrich (München, Germany)	30412
$Na_2MoO_4 \cdot 2\,H_2O$ (sodium molybdate dihydrate)	Sigma-Aldrich (München, Germany)	M1003
Na_3VO_4 (sodium orthovanadate)	Sigma-Aldrich (München, Germany)	S6508
NaCl (sodium chloride)	Sigma-Aldrich (München, Germany)	31434
NaF (sodium fluoride)	Sigma-Aldrich (München, Germany)	S1504
$NaHCO_3 \cdot 10\,H_2O$ (sodium carbonate decahydrate)	Merck KGaA (Darmstadt, Germany)	6391
NaOH (sodium hydroxide)	Sigma-Aldrich (München, Germany)	30620
Opti-MEM® I Reduced Serum Medium	Life Technologies™, Gibco® (Darmstadt, Germany)	31985-047
Orange G	Sigma-Aldrich (München, Germany)	O3756

product	company	Cat. No.
PageRuler™ prestained protein ladder	ThermoFisher Scientific (Schwerte, Germany)	26616
penicillin-streptomycin, liquid, 100×	Life Technologies™, Gibco® (Darmstadt, Germany)	15140-122
Permount Mounting Medium	ThermoFisher Scientific (Schwerte, Germany)	50-277-97
phenol red solution 0.5 % in DPBS, sterile for cell culture	Sigma-Aldrich (München, Germany)	P0290
PMSF (phenylmethanesulfonyl fluoride)	Sigma-Aldrich (München, Germany)	P7626
polybrene (hexadimethrine bromide)	Sigma-Aldrich (München, Germany)	H9268
poly-L-lysine hydrobromide	Sigma-Aldrich (München, Germany)	P2636
Ponceau S solution 0.1 % in 5 % acetic acid	Sigma-Aldrich (München, Germany)	P7170
Power Block™ Universal Blocking Reagent, 10× concentrated	BioGenex (Fremont, CA, USA)	HK085-5KE
Power SYBR® Green PCR Master Mix	Life Technologies™, Applied Biosystems® (Darmstadt, Germany)	4367659
PrestoBlue® cell viability reagent	Life Technologies™, Molecular Probes® (Darmstadt, Germany)	A13261
protease inhibitor cocktail	Sigma-Aldrich (München, Germany)	P8340
protease inhibitor cOmplete	Roche (Mannheim, Germany)	04693116001
protease inhibitor cOmplete, EDTA-free	Roche (Mannheim, Germany)	04693132001
protein G agarose beads, ChIP-grade	Cell Signaling (Leiden, The Netherlands)	9007S
puromycin	Sigma-Aldrich (München, Germany)	P8833
100× pyruvate 100 mM	Life Technologies™, Gibco® (Darmstadt, Germany)	11360-039
RNA*later*™ RNA Stabilization Reagent	Qiagen (Hilden, Germany)	76106
Roti®-Histofix 4 % acid free (pH 7.0) phosphate-buffered formaldehyde solution	Carl Roth (Karlsruhe, Germany)	P087
Roticlear®	Carl Roth (Karlsruhe, Germany)	A538
Rotiszint® eco plus LSC-Universalcocktail	Carl Roth (Karlsruhe, Germany)	0016
RPMI amino acids solution (50×)	Sigma-Aldrich (München, Germany)	R7131
SDS (sodium dodecyl sulfate)	Sigma-Aldrich (München, Germany)	62862
sodium acetate anhydrous	Applichem (Darmstadt, Germany)	A1522
(+)-sodium L-ascorbate	Sigma-Aldrich (München, Germany)	A4034
sodium deoxycholate	Sigma-Aldrich (München, Germany)	D6750
sodium tartrate dibasic dihydrate	Sigma-Aldrich (München, Germany)	71994
spermidine	Sigma-Aldrich (München, Germany)	S0266
spermine	Sigma-Aldrich (München, Germany)	S4264
sucrose	Sigma-Aldrich (München, Germany)	S1888
sulforhodamine B sodium salt (SRB)	Sigma-Aldrich (München, Germany)	S9012
TaqMan® Gene Expression Master Mix	Life Technologies™, Applied Biosystems® (Darmstadt, Germany)	4369016
TEMED (*N,N,N',N'*-tetramethylethane-1,2-diamine)	Carl Roth (Karlsruhe, Germany)	2367
Tris (tris(hydroxymethyl)aminomethane)	Sigma-Aldrich (München, Germany)	T1503

product	company	Cat. No.
Triton® X-100	Applichem (Darmstadt, Germany)	A1388
trypan blue solution 0.4 %	Life Technologies™, Invitrogen™ (Darmstadt, Germany)	T10282
0.25 % Trypsin-EDTA (1×), Phenol Red	Life Technologies™, Gibco® (Darmstadt, Germany)	25200-056
Tween® 20	Sigma-Aldrich (München, Germany)	P9416
water, nuclease-free	Life Technologies™, Gibco® (Darmstadt, Germany)	10977-035
XF Calibrant	Seahorse Bioscience (Copenhagen, Denmark)	100840-000
xylene	Merck KGaA (Darmstadt, Germany)	1.08681

5.8 Animal food

product	company	Cat. No.
standard chow diet	Kliba Nafag (Kaiseraugst, Switzerland)	3437
low fat diet (LFD), 10 % calories from fat, γ-irradiated	Research Diets, Inc. (New Brunswick, NJ, USA)	D12450Bi
high fat diet (HFD), 60 % calories from fat, γ-irradiated	Research Diets, Inc. (New Brunswick, NJ, USA)	D12492i

5.9 Buffers and solutions

Buffers and solutions, including electrophoresis gels, are listed in alphabetical order and subsequently referred to by the names given here. Buffer concentrations are 1× unless stated otherwise.

Citrate buffer 10 mM tri-sodium citrate dihydrate; adjust to pH 6.0 with HCl; add 0.05 % Tween® 20

ChIP buffer 50 mM Tris, pH 8.0; 140 mM NaCl; 1 mM EDTA; 1 % Triton® X-100; 0.1 mM sodium deoxycholate; 0.1 % SDS; 1× protease inhibitor cOmplete (Roche); always prepare fresh

ChIP elution buffer 50 mM Tris, pH 8.0; 1 mM EDTA; 1 % SDS; 50 mM $NaHCO_3$; always prepare fresh

ChIP sucrose buffer A 320 mM sucrose; 15 mM HEPES, pH 7.9; 60 mM KCl; 2 mM EDTA; 0.5 mM EGTA; 0.5 % BSA; 0.5 mM spermidine; 0.15 mM spermine; 0.5 mM DTT; pH adjusted to 7.2; always prepare fresh

ChIP sucrose buffer B 416 mM sucrose; 15 mM HEPES, pH 7.9; 60 mM KCl; 2 mM EDTA; 0.5 mM EGTA; 0.5 mM spermidine; 0.15 mM spermine; 0.5 mM DTT; pH adjusted to 7.2; always prepare fresh

ChIP swelling buffer 25 mM HEPES, pH 7.2; 1 mM $MgCl_2$; 10 mM KCl; 0.1 % IGEPAL (NP-40); 1 mM DTT; 0.5 mM PMSF; 1× protease inhibitor cOmplete (Roche); always prepare fresh

ChIP wash buffer A 50 mM Tris; 140 mM NaCl; 1 mM EDTA; 1 % Triton® X-100; 0.1 % sodium deoxycholate; 0.1 % SDS; always prepare fresh

ChIP wash buffer B 50 mM Tris; 500 mM NaCl; 1 mM EDTA; 1 % Triton® X-100; 0.1 % sodium deoxycholate; 0.1 % SDS; always prepare fresh

ChIP wash buffer C 20 mM Tris; 250 mM LiCl; 1 mM EDTA; 0.5 % IGEPAL (NP-40); 0.1 % sodium deoxycholate; always prepare fresh

DEPC-treated water 1 ml of DEPC was added to 1 l of distilled water, shaken vigorously, incubated over night at room temperature to inactivate RNases and then autoclaved to degrade DEPC. Store at room temperature.

DMEM basic medium 1 vial of DME Base (8.3 g, Sigma, Cat. No. D5030) was dissolved in ddH_2O and supplemented with 3.7 g $NaHCO_3$ and 1.85 g NaCl. pH was adjusted to 7.2, volume filled up to 1 l and medium was 0.22 µm filter-sterilized. Phenol red was added to 15 mg/l as well as 1 mM pyruvate, 2 mM L-glutamine and 10 % dialyzed FBS. Store at 4 °C.
For glucose-withdrawal experiments, 4.5 mg/ml (25 mM) D-glucose was added or left out.

Eosin solution 0.1 % eosin G; 63 % ethanol; 1 % acetic acid; store at room temperature protected from light

LB agar plates 40 g/l LB Agar (Carl Roth) in water, autoclaved, cooled down in water bath to 56 °C, antibiotics added to desired concentration and poured into petri dishes (≈ 20 ml per plate); store at 4 °C for up to 4 weeks

LB medium 25 g/l in water, autoclaved; store at room temperature

Krebs-Ringer-Henseleit (KRH) buffer 118.5 mM NaCl; 24.65 mM $NaHCO_3$; 4.74 mM KCl; 1.18 mM $MgSO_4$; 1.184 mM KH_2PO_4; 2.5 mM $CaCl_2$; pH 7.4; 0.22 µm filter-sterilized; store at 4 °C

MNase digestion buffer 50 mM Tris, pH 7.4; 25 mM KCl; 4 mM $MgCl_2$; 1 mM $CaCl_2$; 1× EDTA-free protease inhibitor cOmplete (Roche); always prepare fresh

MOPS buffer, 10× 200 mM MOPS; 50 mM sodium acetate; 10 mM EDTA; pH 7.0; store at 4 °C

Orange G buffer, 6× 70 % glycerol; 10 mM EDTA; 1 mg/ml Orange G; store at 4 °C

PBS 137 mM NaCl; 2 mM KH_2PO_4; 10 mM Na_2HPO_4; 2.7 mM KCl; pH 7.0; store at room temperature

PBS-T 137 mM NaCl; 2 mM KH_2PO_4; 10 mM Na_2HPO_4; 2.7 mM KCl; 0.1 % Tween® 20; pH 7.0; store at room temperature

Phosphatase inhibitor cocktail, 100× 200 mM imidazole; 100 mM NaF; 115 mM Na_2MoO_4; 100 mM Na_3VO_4; 400 mM sodium tartrate; store in aliquots at −20 °C

Protein extraction buffer 50 mM Tris; 1 mM EDTA; 10 mM NaF; 2 mM Na_3VO_4; 1 mM DTT; 1× protease inhibitor cocktail (Sigma, Cat. No. P8340); 1× phosphatase inhibitor cocktail; always prepare fresh

Protein extraction supplement buffer 150 mM NaCl; 10 % IGEPAL® (NP-40); store at 4 °C

RIPA buffer 50 mM Tris; 250 mM NaCl; 2 % IGEPAL® (NP-40); 2.5 µM EDTA; 0.1 % SDS; 0.5 % sodium deoxycholate; 1× protease inhibitor cocktail (Sigma, Cat. No. P8340); 1× phosphatase inhibitor cocktail; store in aliquots at −20 °C

RNA loading buffer for 100 µl use 0.5 µl of 10 mg/ml ethidium bromide; 5 µl MOPS buffer; 50 µl formamide; 17.5 µl of 37 % formaldehyde; 16.7 µl orange G buffer; 10.3 µl RNase-free water; always prepare fresh

SDS loading dye, 5× 12.5 % β-mercaptoethanol; 10 % SDS; 1 mg/ml bromophenol blue; 300 mM Tris-HCl pH 6.8; 5 mM EDTA; 50 % glycerol; store in aliquots at −20 °C

SDS-polyacrylamide separating gel 8 / 10 / 12 % acrylamide/bisacrylamide (37.5:1); 375 mM Tris-HCl pH 8.8; 0.1 % SDS; 2.66 mM TEMED; 0.1 % APS

SDS-polyacrylamide stacking gel 5 % 5 % acrylamide/bisacrylamide (37.5:1); 125 mM Tris-HCl pH 6.8; 0.1 % SDS; 6.67 mM TEMED; 0.1 % APS

SDS running buffer 200 mM glycine; 25 mM Tris; 0.1 % SDS; store at room temperature

SDS transfer buffer 25 mM Tris; 190 mM glycine; store at 4 °C

Seahorse Assay Medium 1 vial of DME Base (8.3 mg/ml, Sigma, Cat. No. D5030) was dissolved in 1 l of ddH_2O; pH was adjusted to 7.4 and medium was 0.22 µm filter-sterilized and stored at 4 °C
For the Glycolysis Stress Test Kit, medium was freshly supplemented with 15 mg/l phenol red and 2 mM L-glutamine.
For the Mito Stress Test Kit, medium was freshly supplemented with 15 mg/l phenol red, 2 mM L-glutamine, 1 mM pyruvate and 4.5 mg/ml (25 mM) D-glucose.

SRB fixation buffer 5 % acetic acid; 95 % ethanol; store at −20 °C

SRB solution 0.4 % (w/v) sulforhodamine B; 1 % (v/v) acetic acid; store at room temperature protected from light

TBE 45 mM Tris; 45 mM boric acid; 1 mM EDTA; pH 8.0; store at room temperature

TBS 20 mM Tris; 137 mM NaCl; pH 7.6; store at room temperature

TBS-T 20 mM Tris; 137 mM NaCl; 0.1 % Tween® 20; pH 7.6; store at room temperature

TE 10 mM Tris pH 8.0; 1 mM EDTA; store at room temperature

5.10 Nomenclature of genes and proteins

Genes, mRNA and cDNA transcripts of genes and genotypes of mouse strains are addressed using italicized characters (e. g. *Tbl1x*). Proteins are addressed using upright characters (e. g. Tbl1x). Mouse proteins as well as genes and corresponding mRNA and cDNA transcripts are assigned by upper case first letter and subsequent lower case letters (e. g. Tbl1x, *Tbl1x*) whereas human orthologs are assigned by upper case letters (e. g. TBL1X, *TBL1X*).

Methods

5.11 Human patients

Pancreatic tissue from surgical resection of cancer and chronic pancreatitis patients as well as samples from healthy organ donors were provided by Dr. Oliver Strobel from the European Pancreas Center at the Chirurgische Klinik of the University of Heidelberg. Written informed consent was obtained from all patients. In case of cancer patients, tumor tissue and healthy tissue was provided for intra-individual comparison of expression levels. Details on the individual patients are summarized in table D.1 on page 86 in appendix D. RNA was extracted as described in section 5.17.1 on page 69 and reverse-transcribed to cDNA. Proteins were extracted according to section 5.18.1 on page 72.

5.12 Animal experiments

5.12.1 Animal models

p48$^{+/Cre}$*; Kras*$^{+/LSL\text{-}G12D}$ mice [15] use a knock-in of the *Kras*^{G12D} allele, a mutant variant of *Kras* where glycine at position 12 is substituted by aspartic acid which compromises both its intrinsic and extrinsic GTPase activity and results in constitutive downstream signaling of Ras effector pathways. The allele was introduced with an upstream LoxP-Stop-LoxP (LSL) cassette via homologous recombination. Crossing with *p48*$^{+/Cre}$ mice expressing Cre-recombinase under control of the pancreas-specific *p48* promoter resulted in *p48*$^{+/Cre}$*; Kras*$^{+/LSL\text{-}G12D}$ animals expressing the mutant *Kras*^{G12D} allele in pancreatic cells at the same level as the endogenous gene thus mimicking the acquisition of such activating point mutations in human PDACs.
p48$^{+/Cre}$*; Kras*$^{+/LSL\text{-}G12D}$ mice were bred in a C57BL/6N background at the IBF (Interfakultäre Biomedizinische Forschungseinrichtung) of Heidelberg University by Dr. Oliver Strobel and genotyped as described [15].
Wild type C57BL/6N mice were obtained from Charles River Laboratories at the age of 7–9 weeks.

5.12.2 Housing of animals

The animals were housed according to international standards with a 12 h dark / 12 h light cycle and unrestricted access to diet. Animal handling and experimentation was performed in accordance with the German Protection of Animals Act (Tierschutzgesetz) and approved by local authorities (Regierungspräsidium Karlsruhe).

5.12.3 EchoMRI™ measurement

EchoMRI™ analysis allows the determination of whole body fat mass, lean mass and free water in mice. Animals were weighed and then subjected to measurement according to the manufacturer's instructions.

5.12.4 Feeding experiments in *p48$^{+/Cre}$; Kras$^{+/LSL\text{-}G12D}$* mice

At 3–10 weeks of age, *p48$^{+/Cre}$; Kras$^{+/LSL\text{-}G12D}$* mice and wild type litter mates were transferred from Heidelberg University IBF to DKFZ central animal facility and housed in a Green Line IVC SealSafe Plus Mouse Cage system (Tecniplast) with *ad libitum* access to standard chow diet and water. After 1 week of adaptation, food was changed to high fat diet (60 % calories from fat) or low fat diet (10 % calories from fat) for a duration of 12 weeks with *ad libitum* access. Weight of mice was checked weekly. EchoMRI™ (Echo Medical Systems, Houston, TX, USA) measurement was performed before the start of the diet as well as 3, 7 and 11 weeks afterwards. Four and 8 weeks after start of the diet, animals were fasted over night for 16–18 h and then blood glucose was measured with a OneTouch® Ultra glucometer. Blood was collected with heparin-coated micro hematocrit capillaries, stored on ice until all animals were assessed, centrifuged for 1 h at 855 ×g and plasma was used for ELISA measurement of insulin (Mercodia). At the end of the 12-week period, animals were weighed, then killed by cervical dislocation followed by decapitation. Blood glucose was measured from trunk blood with a OneTouch® Ultra glucometer and then collected, stored on ice until all animals were prepared, centrifuged for 1 h at 855 ×g and serum was used for ELISA measurement of insulin (Mercodia). A small piece from the pancreatic tail was taken for protein and RNA extraction and snap-frozen in liquid nitrogen. The rest of the organ was fixed in formalin and embedded in paraffin as described in section 5.13.1 on the following page. Liver, heart, perigonadal white adipose tissue, inguinal white adipose tissue, scapular brown adipose tissue, gastrocnemius muscle, and small intestine were cut into small pieces in PBS, snap-frozen in liquid nitrogen and stored in cryogenic vials or 5 ml skirted tubes at −80 °C.

5.12.5 Subcutaneous tumor cell implantation

Animals were housed in groups of 4 in 335 cm^2 H-TEMP™ Polysulfon cages (Tecniplast) in a ventilated moue housing cabinet (Tecniplast) with *ad libitum* access to standard chow diet and water.
Luciferase-expressing Panc02 cells (see section 5.14.1 on page 64) were grown to sufficient numbers, trypsinized, resuspended in DPBS and counted. Concentration was adjusted to 2×10^6 cells/ml with DPBS and cells were kept on ice. 100 µl of cell suspension containing 2×10^5 cells were injected subcutaneously into the right hind flank of C57BL/6N mice.

5.12.6 Tumor size measurement

Starting at day 4–7 after implantation, the site of injection was shaved and tumor volume was determined by percutaneous measurement with digital a caliper. Tumor volume was calculated by the ellipsoid formula:

$$V = \frac{4}{3}\pi \cdot \left(\frac{\text{width}}{2}\right)^2 \cdot \left(\frac{\text{length}}{2}\right)$$

5.12.7 Bioluminescence imaging

Animals were injected intraperitoneally with 10 µl per g body weight of 15 mg/ml D-luciferin in DPBS using insulin syringes (BD Medical). After 4–6 min, animals were put in a narcotic chamber connected to an XGI-8 Gas Anesthesia System (Caliper LifeSciences). Narcosis was induced with 3 % isoflurane and maintained with 1.5 % isoflurane. 10 min after D-luciferin injection, animals were placed in an IVIS® Lumina II (Caliper LifeSciences) under 1.5 % isoflurane and bioluminescence was measured for 5 min. Data were visualized and analyzed with Living Image software.

5.12.8 Intratumoral injection of adenovirus

Adenovirus was kindly provided by Dr. Maria Rohm from our lab (production described in [180, p77–79] and [181]). Virus was diluted to 1×10^8 infectious particles per 15–20 µl in DPBS with 10 % glycerol and loaded to a 27G Venofix® A injection hose connected to a microinjector (Narishige). 1×10^8 infectious particles were injected into each tumor.

5.12.9 Subcutaneous tumor preparation

At necropsy, tumors were taken out, freed from surrounding skin and other tissue and cut in three pieces as shown in figure 5.1.

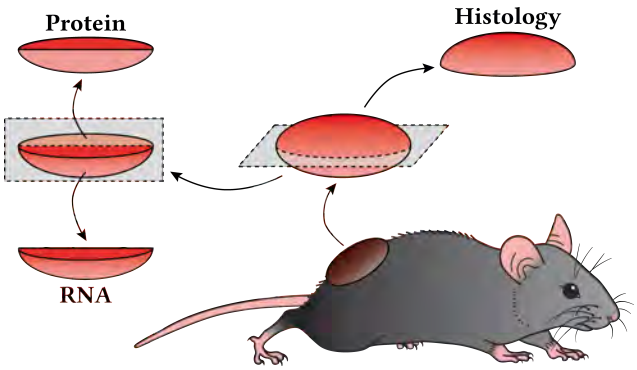

Figure 5.1: Cutting of subcutaneous tumor allografts

The upper half of the tumor (formerly facing the skin) was taken for histology. The cutting surface was placed on a biopsy foam pad in a histology cassette so that after embedding the first sections would be from the middle of the tumor. The lower half (formerly facing towards the peritoneum) was cut longitudinally and the two halves were separately snap-frozen in liquid nitrogen for later extraction of RNA or proteins.

5.13 Histology

Tissues were prepared as described below and imaged on an Axio Imager.M2 with AxioCam HRc (Zeiss).

5.13.1 Paraffin embedding and sectioning of tissue

Upon dissection, organs were placed on a biopsy foam pad in a histology cassette and submerged in Roti®-Histofix for 24 to maximum 48 h, then washed in running deionized water (VE-Wasser) for 2 h and stored in 70 % ethanol for up to 6 weeks. Samples were then dehydrated in a Leica ASP 300 (70 % ethanol 40 min; 95 % ethanol 40 min; 100 % ethanol 35 min; 2 × 100 % ethanol 40 min; 100 % ethanol 60 min; xylene 45 min; xylene 60 min; xylene 75 min; 3 × paraffin wax 60 min) and embedded in paraffin blocks with a Leica EG 1150H. Sections of 4 µm were prepared with a Leica RM2245 microtome, placed on glass cover slides and dried.

5.13.2 Hematoxylin eosin (H & E) staining

Sections were de-paraffinized (3 × 10 min Roticlear®, 3 × 3 min 100 % ethanol, 3 min 96 % ethanol, 10 min 70 % ethanol, 2 min 50 % ethanol, 2 min distilled water), stained for 2 min in Mayer's hemalum solution, washed for 15 min under running tap water, counterstained for 7 sec in eosin solution, briefly washed in distilled water and dehydrated (5 sec 70 % ethanol, 3 min 96 % ethanol, 2 × 3 min 100 % ethanol, 3 × 5 min Roticlear®) and mounted in Permount Mounting Medium.

5.13.3 Immunohistochemistry staining

Sections were de-paraffinized (3 × 10 min Roticlear®, 3 × 10 min 100 % ethanol, 10 min 95 % ethanol, 10 min 75 % ethanol, 10 min 50 % ethanol, 10 min distilled water) and then processed as indicated below.

5.13.3.1 TBL1X (human tissue)

Antigen retrieval was done by heating in the microwave at 500 W for 10 min in citrate buffer pH 6.0 followed by air-cooling for 15 min and settling down to distilled water for 10 min. Endogenous peroxidases were inactivated with 3 % H_2O_2 in methanol for 10 min followed by incubation in distilled water for 10 min and washing 2 × 10 min in TBS with 0.1 % BSA. Slides were blocked with Power Block™ Universal Blocking Reagent for 1 h at room temperature. Primary antibody (rabbit polyclonal to TBL1X, Abcam, Cat. No. ab24548) was applied 1:400 in Dako Antibody Diluent over night at 4 °C in a humid chamber, then washed 2 × 10 min in TBS with 0.1 % BSA and once for 10 min in TBS with 0.1 % BSA and 0.05 % Tween® 20. Secondary antibody (EnVision™+ anti-rabbit HRP, Dako) was added undiluted for 45 min at

room temperature in a humid chamber, then washed 2 × in TBS with 0.1 % BSA and once for 10 min in TBS with 0.1 % BSA and 0.05 % Tween® 20. Color reaction was performed for 15 sec with Dako Liquid DAB+ Chromogen diluted 1:100 in DAB Substrate Buffer, then stopped with distilled water. Slides were counterstained for 12 sec in Mayer's hemalum solution, washed with running tap water for 10 min and then dehydrated (5 min 70 % ethanol, 5 min 95 % ethanol, 3 × 5 min 100 % ethanol, 3 × 5 min Roticlear®) and mounted in Permount Mounting Medium.

5.13.3.2 Tbl1x (mouse tissue)

Antigen retrieval was done by heating in the microwave at 750 W for 10 min in citrate buffer pH 6.0 followed by incubation in water bath for 30 min at 96 °C. Slides were then air-cooled for 15 min and incubated in distilled water for 10 min. Endogenous peroxidases were inactivated with 3 % H_2O_2 in methanol for 10 min followed by incubation in distilled water for 5 min and washing 2 × 5 min in TBS with 0.1 % BSA. Slides were blocked with 10 % Normal Rabbit Serum for 45 min at room temperature, then 0.1 % avidin for 20 min at 37 °C in the dark, washed 2 × 5 min in TBS with 0.1 % BSA, blocked with 0.01 % biotin for 20 min at 37 °C in the dark and washed 2 × 5 min in TBS with 0.1 % BSA. Primary antibody (goat polyclonal to TBL1X, Abcam, Cat. No. ab2243) was applied 1:1000 in Dako Antibody Diluent over night at 4 °C in a humid chamber, then washed 3 × 5 min in TBS with 0.1 % BSA and 0.05 % Tween® 20. Secondary antibody (biotinylated rabbit anti-goat, KPL) was added undiluted for 45 min at room temperature in a humid chamber, then flushed once in TBS with 0.1 % BSA and 0.05 % Tween® 20, washed 2 × 5 min in TBS with 0.1 % BSA and 0.05 % Tween® 20 and once for 5 min in TBS with 0.1 % BSA. Signal was enhanced with ABC reagent from the VECTASTAIN Elite ABC Kit (Vector Laboratories; prepare mixture 30 min before use) for 45 min at room temperature, then washed 2 × 5 min in TBS with 0.1 % BSA. Color reaction was performed for 50 sec with Dako Liquid DAB+ Chromogen diluted 1:100 in DAB Substrate Buffer, then stopped with distilled water. Slides were counterstained for 6 sec in Mayer's hemalum solution, washed with running tap water for 10 min and then dehydrated (5 min 70 % ethanol, 5 min 95 % ethanol, 3 × 5 min 100 % ethanol, 3 × 5 min Roticlear®) and mounted in Permount Mounting Medium.

5.13.3.3 TBL1XR1 (human tissue)

Antigen retrieval was done by heating in the microwave at 500 W for 10 min in citrate buffer pH 6.0 followed by air-cooling for 15 min and settling down to distilled water for 10 min. Endogenous peroxidases were inactivated with 3 % H_2O_2 in methanol for 10 min followed by incubation in distilled water for 10 min and washing 2 × 10 min in TBS with 0.1 % BSA. Slides were blocked with Power Block™ Universal Blocking Reagent for 1 h at room temperature. Primary antibody (TBL1XR1 monoclonal antibody (M01), clone 3G7, Abnova, Cat. No. H00079718-MO1) was applied 1:1000 in Dako Antibody Diluent over night at 4 °C in a humid chamber, then washed 2 × 10 min in TBS with 0.1 % BSA and once for 10 min in TBS with 0.1 % BSA and 0.05 % Tween® 20. Secondary antibody (EnVision™+ anti-mouse HRP, Dako) was added undiluted for 45 min at room temperature in a humid chamber, then washed 2 × in TBS with 0.1 % BSA and once for 10 min in TBS with 0.1 % BSA and 0.05 % Tween® 20. Color reaction was performed for 15 sec with Dako Liquid DAB+ Chromogen diluted 1:100 in DAB Substrate Buffer, then stopped with distilled water. Slides were counterstained for 12 sec in Mayer's hemalum solution, washed with running tap water for 10 min and then dehydrated (5 min 70 % ethanol, 5 min 95 % ethanol, 3 × 5 min 100 % ethanol, 3 × 5 min Roticlear®) and mounted in Permount Mounting Medium.

5.13.3.4 Tbl1xr1 (mouse tissue)

Antigen retrieval was done by heating in the microwave to the boil in citrate buffer pH 6.0, cooling for 5 min, microwaving at 350 W for 3 min and incubating in water bath for 20 min at 96 °C. Slides were then air-cooled for 15 min and incubated in distilled water for 10 min. Endogenous peroxidases were inactivated with 3 % H_2O_2 in methanol for 10 min followed by incubation in distilled water for 5 min and washing 2 × 5 min in TBS with 0.1 % BSA. Slides were blocked with 1 $^{mg}/_{ml}$ goat anti-mouse IgG (Sigma) in 0.9 % NaCl for 1 h at room temperature, then with Power Block™ Universal Blocking Reagent for 1 h at room temperature. Primary antibody (TBL1XR1 monoclonal antibody (M01), clone 3G7, Abnova, Cat. No. H00079718-MO1) was applied 1:500 in Dako Antibody Diluent over night at 4 °C in a humid chamber, then washed 2 × 5 min in TBS with 0.1 % BSA and 2 × 5 min in TBS with 0.1 % BSA and 0.05 % Tween® 20. Secondary antibody (EnVision™+ anti-mouse HRP, Dako) was added undiluted for 45 min at room temperature in a humid chamber, then washed 2 × 5 min in TBS with 0.1 % BSA. Color reaction was performed for 30 sec with Dako Liquid DAB+ Chromogen diluted 1:100 in DAB Substrate Buffer, then stopped with distilled water. Slides were counterstained for 9 sec in Mayer's hemalum solution, washed with running tap water for 10 min and then dehydrated (5 min 70 % ethanol, 5 min 95 % ethanol, 3 × 5 min 100 % ethanol, 3 × 5 min Roticlear®) and mounted in Permount Mounting Medium.

5.13.3.5 Ki-67 (mouse tissue)

Antigen retrieval was done by heating in the microwave to the boil in citrate buffer pH 6.0 followed by incubation in water bath for 30 min at 96 % before air-cooling for 15 min and incubating in distilled water for 10 min. Endogenous peroxidases were inactivated with 3 % H_2O_2 in methanol for 10 min followed by incubation in distilled water for 5 min and washing 2 × 5 min in TBS with 0.1 % BSA. Slides were blocked with 10 % Normal Rabbit Serum for 45 min at room temperature, then 0.1 % avidin for 20 min at 37 °C in the dark, washed 2 × 5 min in TBS with 0.1 % BSA, blocked with 0.01 % biotin for 20 min at 37 °C in the dark and washed 2 × 5 min in TBS with 0.1 % BSA. Primary antibody (Monoclonal mouse anti-rat Ki-67, Dako, Cat. No. M7249) was applied 1:5000 in Dako Antibody Diluent over night at 4 °C in a humid chamber, then flushed in 5 min in TBS with 0.1 % BSA and 0.05 % Tween® 20, washed 3 × 5 min in TBS with 0.1 % BSA and 0.05 % Tween® 20. Secondary antibody (biotinylated rabbit anti-rat IgG antibody, mouse adsorbed, Vector Laboratories) was added at 1 µg/ml in Dako Antibody Diluent for 45 min at room temperature in a humid chamber, then flushed once in TBS with 0.1 % BSA and 0.05 % Tween® 20, washed 2 × 5 min in TBS with 0.1 % BSA and 0.05 % Tween® 20 and once for 5 min in TBS with 0.1 % BSA. Signal was enhanced with ABC reagent from the VECTASTAIN Elite ABC Kit (Vector Laboratories; prepare mixture 30 min before use) for 45 min at room temperature, then washed 2 × 5 min in TBS with 0.1 % BSA. Color reaction was performed for 40 sec with Dako Liquid DAB+ Chromogen diluted 1:100 in Substrate Buffer, then stopped with distilled water. Slides were counterstained for 6 sec in Mayer's hemalum solution, washed with running tap water for 10 min and then dehydrated (5 min 70 % ethanol, 5 min 95 % ethanol, 3 × 5 min 100 % ethanol, 3 × 5 min Roticlear®) and mounted in Permount Mounting Medium.

5.13.4 Quantification of Ki-67 staining

Entire paraffin sections stained for Ki-67 were imaged with a Cell Observer Z1 (Zeiss) with a 20× objective. Images were stitched together with the ZEN software provided with the microscope. Non-tumor tissue such as adhering skin or subcutaneous fat was removed from the image. For ease of processing, the stitched image was sliced into individual images of approximately 1000 × 1000 pixels using ImageJ. These were then loaded to ilastik software which was trained to discriminate background (white), Ki-67 positive nuclei (brown), and counterstained cytoplasm and Ki-67 negative nuclei (blue, hematoxylin-stained). Cell Profiler was then used to quantify the area occupied by tumor cells and by Ki-67 positive nuclei.

5.14 Cell culture

5.14.1 Cell lines

Capan-1, Capan-2, AsPC-1 BxPC-3 and HEK293T cells were obtained from ATCC. Panc02 cells with stable lentivirus-mediated expression of luciferase were kindly provided by Dr. Ana Martin-Villalba (DKFZ).

5.14.2 Cultivation of cells

All cells were cultured on 15 cm-dishes in 20 ml DMEM High Glucose Pyruvate (+ L-glutamine) supplemented with 10 % FBS and 1 % penicillin/streptomycin (all from Gibco®) in a humidified incubator at 37 °C and 5 % CO_2. For sub-culturing, cells were washed with 10 ml DPBS (Gibco®) and detached from culture plate with 3 ml 0.25 % trypsin (Gibco®) for 5–10 min at 37 °C. Trypsin was stopped by adding 10 ml of culture medium. Cells were washed from the plate, centrifuged for 3 min at 550 ×g, re-suspended in culture medium and seeded on a new 15 cm-dish. Cell morphology was monitored with an Axiovert 40 CFL microscope (Zeiss).

For experiments, after the last re-suspension step in culture medium, an aliquot of 10 µl was taken, diluted with 10 µl trypan blue solution. Cells were counted in a Neubauer counting chamber or Countess™ automated cell counter. Concentration of cells was calculated and appropriate amounts of cells were seeded.

5.14.3 Detection of cell culture contamination

1×10^6–1×10^7 cells were harvested, transferred to a 1.5 ml safe-lock tube and pelleted by centrifugation at 2,500 rpm for 5 min. The pellet was resuspended in 100 µl DPBS and placed at 95 °C for 15 min. Lysate was centrifuged at 10,000 rpm for 10 min to remove cellular debris. The supernatant was transferred to a new 1.5 ml safe-lock tube and stored at −20 °C before submission to the company Multiplexion. Multiplexion validated the purity of the cell lines using Multiplex Cell Contamination Test (McCT) [182]. Only non-contaminated cells were used.

5.14.4 Freezing of cells

Cells were washed with 10 ml DPBS (Gibco®) and detached from culture plate with 3 ml 0.25 % trypsin (Gibco®) for 5–10 min at 37 °C. Trypsin was stopped by adding 10 ml of culture medium. Cells were washed from the plate, cen-

trifuged for 3 min at 550 ×g and re-suspended in culture medium. An aliquot was taken, diluted in trypan blue solution and cells were counted in a Neubauer counting chamber or Countess™ automated cell counter. Cell density was adjusted to 2×10^6 cells/ml with culture medium. FBS and sterile DMSO were added to reach a final mixture of 50 % culture medium, 40 % FBS, 10 % DMSO. Cells were aliquoted at 1 ml in cryogenic vials, put into a Mr. Frosty™ freezing container (ThermoFisher Scientific) and placed at −80 °C. The following day, tubes were transferred to a liquid nitrogen storage tank.

5.14.5 Thawing of cells

Cells were taken out of liquid nitrogen storage tank and thawed in a 37 °C water bath, then transferred to 9 ml culture medium, centrifuged for 3 min at 550 ×g, re-suspended in 1 ml culture medium and plated out in 20 ml culture medium on a 15 cm-dish.

5.14.6 Nutrient withdrawal

Capan-1 cells were plated at 5×10^3 cells per well on 96-well clear bottom black wall plates in antibiotic-free culture medium (DMEM High Glucose Pyruvate (+ L-glutamine) with 10 % FBS). On the following day siRNA transfection was done as described in section 5.14.7. 24 h after application of siRNA, medium was changed to DMEM basic medium (59) with or without 4.5 mg/ml D-glucose. Cells were grown for another 48 h before subjecting to EdU assay (see section 5.15.2 on the following page).

5.14.7 siRNA transfection

An overview of the siRNAs used is given in table 5.10. AllStars Negative control siRNA coupled 3' to Alexa Fluor® 488 on sense-strand (Qiagen, Cat. No. 1027292) was used as a non-silencing control and to assess transfection efficiency via green fluorescence. For transfection, cells were plated in antibiotic-free culture medium (DMEM High Glucose Pyruvate (+ L-glutamine) with 10 % FBS) to reach 30–50 % confluence the following day. For each siRNA to be transfected, 0.5 pmol siRNA per 1000 cells plated were dissolved in 1/10 volume Opti-MEM® I (relative to the amount of culture medium on the cells). In case of double transfections, the final amount of siRNA was filled up with AllStars Negative control siRNA to guarantee equal amounts of total siRNA in each group. In a second tube, Lipofectamine® 2000 was dissolved to 3 % in the same amount of Opti-MEM® I. The two mixes were combined and incubated for 20 min at room temperature before adding drop-wise to the culture medium. After 24 h incubation at 37 °C the medium was changed to fresh antibiotic-free culture medium for further culturing or live cell measurements or cells were harvested for RNA or protein extraction.

Table 5.10: Overview on GeneSolution siRNAs from Qiagen

Gene	Species	RefSeq ID	Cat.-No.	Sequence	
TBL1X	human	NM_001139466	SI04329514	target	TGCGTTAGAGTGTACTCTGAA
				sense	GCUUAGAGUGUACUCUGAATT
				antisense	UUCAGAGUACACUCUAACGCA
TBL1XR1	human	NM_024665	SI03025925	target	TTGTTTGATGGTCGACCAATA
				sense	GUUUGAUGGUCGACCAAUATT
				antisense	UAUUGGUCGACCAUCAAACAA

5.15 Cell-based assays

5.15.1 BrdU assay

Cell proliferation was assayed with the Cell Proliferation Kit from GE Healthcare. This assay makes use of the base analogue BrdU that is incorporated into the DNA of proliferating cells instead of thymine and can be detected with a specific antibody. Capan-1 cells were seeded at a density of 1.5×10^4 cells per well on an 8-chamber LabTech Microscopy Slide and subjected to the indicated treatment. Medium was then replaced by fresh pre-warmed medium with 1:1000 Labelling Reagent from the kit and incubated for 1 h at 37 °C. Labelling Reagent medium was then removed and cells were briefly washed with DPBS before fixing for 30 min in 90 % ethanol / 5 % acetic acid / 5 % water at room temperature. Subsequently, cells were rehydrated by washing 3 times 3–5 min with DPBS and 75–100µl reconstituted nuclease/anti-BrdU antibody from the kit was applied for 1 h at room temperature. Cells were then washed 3 times 3–5 min with DPBS before incubating in 100 µl Cy™3-conjugated anti-mouse IgG (Dianova) diluted 1:800 in DPBS with 1 % BSA supplemented with 100 ng/ml Hoechst 33342 for 1 h at room temperature protected from light. Finally, cells were washed

3 times 3–5 min with DPBS protected from light and mounted in Fluorescent Mounting Medium (Dako) after thoroughly aspirating excess DPBS. Microscopy slides were stored at 4 °C before imaging with Cy3 and DAPI channel using an Axio Imager.M2 (Zeiss). Total nuclei (Hoechst 33258 stained) and BrdU-positive nuclei were counted using CellProfiler software [183–185].

5.15.2 EdU assay

Cell proliferation was assayed with a customized modification of the Click-iT® EdU Imaging Kit from Invitrogen™. This assay makes use of the base analogue EdU that is incorporated into the DNA of proliferating cells instead of thymine. With the click reaction performed here, the EdU is covalently coupled to the fluorescent dye Alexa Fluor®-555. Proliferating cells can then be identified by fluorescence microscopy.

Capan-1 cells were seeded at a density of 1.5×10^4 cells per well on 8-chamber LabTech Microscopy Slide or at 6×10^3 cells per well on 96-well clear-bottom black wall microtiter plates and subjected to indicated treatment. Panc02 cells with stable integration of shNC or shTbl1x were seeded at 1×10^3 cells per well on 96-well clear-bottom black wall microtiter plates and grown for 24 h. On the day of assay, ½ volume of medium was aspirated and replaced with an equal amount of fresh pre-warmed medium supplemented with EdU at 20 µM (resulting in a final EdU concentration of 10 µM) and incubated at 37 °C for 45 min (Capan-1) or 30 min (Panc02). Medium was aspirated and cells were fixed with 100[1] or 250 µl[2] Roti®-Histofix (4 % formaldehyde, phosphate-buffered) for 15 min at room temperature, then aspirated and washed twice with 100 or 250 µl of 3 % BSA in DPBS before permeabilizing in 100 or 250 µl of 0.5 % Triton® X-100 in DPBS for 20 min at room temperature. After aspirating and washing twice with 100 or 250 µl of 3 % BSA in DPBS, cells were incubated in 40 or 100 µl Click-iT® reaction cocktail (see table 5.11) for 30 min protected from light. The cocktail was then aspirated, cells were washed once with 100 or 250 µl of 3 % BSA in DPBS, then once with 100 or 250 µl DPBS before incubating in 50 or 125 µl of 5 µg/ml Hoechst 33342 for 30 min at room temperature protected from light. Finally, cells were washed twice with 100 or 250 µl DPBS and (in case of chamber slides) mounted in Fluorescent Mounting Medium (Dako) or (in case of 96-well plates) left in 100 µl DPBS. Cells were imaged in Cy3 and DAPI channel using an Olympus Cell^R automated microscope (Olympus, Hamburg, Germany) with xcellence software. Total nuclei (Hoechst 33258 stained) and EdU-positive nuclei were counted using CellProfiler software [183–185].

Table 5.11: Click-iT® reaction cocktail for EdU assay

It is important to add the components in the exact order listed here and to use the mixture within 15 min after adding sodium ascorbate. The fast and easy reaction is catalyzed by Cu(I) ions but Cu(I) salts are mostly insoluble in water or react with atmospheric oxygen and are thus tricky to handle. Therefore, the easily water soluble Cu(II) salt copper sulfate ($CuSO_4$) is used instead. The Cu(II) ions therein are then reduced *in situ* by ascorbate to Cu(I) ions that then catalyze the reaction. When left standing too long, however, the Cu(I) ions are being oxidized back to Cu(II) by atmospheric oxygen and can no longer catalyze the reaction.

	Volume	
Reaction component	**chamber slide**	**96-well plate**
1× Click-iT® reaction buffer (87.5 mM Tris-HCl pH 7.4, component D)	85.00 µl	34.00 µl
100 mM $CuSO_4$ (component E)	5.00 µl	2.00 µl
1.5 mM Alexa Fluor® 555 azide (component B)	0.25 µl	0.10 µl
1× reaction buffer additive (100 mM sodium ascorbate, component F)	10.00 µl	4.00 µl
Σ	**100.00 µl**	**40.00 µl**

5.15.3 PrestoBlue® cell viability assay

PrestoBlue® is a cell-permeable resazurin derivative that is metabolized by living cells to resazurin. 1/10 volume of PrestoBlue® solution was added to cell culture media and incubated for 2 h at 37 °C and 5 % CO_2 before reading fluorescence at 550 nm excitation / 610 nm emission.

5.15.4 Seahorse extracellular flux measurement

Capan-1 cells were seeded at 1.5×10^4 per well in XF96 Polystyrene Cell Culture Microplates. No cells were plated in the four edge wells (A1, A12, H1, H12) since these served as background-reference. siRNA-mediated knockdown was performed the following day as described under section 5.14.7 on the previous page. 24 h after knockdown, medium was

[1] 96-well plate
[2] chamber-slide

changed to fresh culture medium and cells were grown for another 24 h. An XF96 FluxPak 4-port measurement cartridge was equilibrated over night in the CO_2-free incubator of the XF Prep Station at 37 °C in 150 µl per well XF Calibrant. On the day of assay, medium was carefully aspirated, cells were washed once with 100 µl pre-warmed Seahorse Assay Medium and then incubated in 150 µl pre-warmed Seahorse Assay Medium (see page 60) in the CO_2-free incubator of the XF Prep Station at 37 °C for 1 h. Meanwhile, assay chemicals from either Mito Stress Test Kit or Glycolysis Stress Test Kit were dissolved in Seahorse Assay Medium and were applied to the ports of the equilibrated measurement cartridge according to table 5.12. The loaded cartridge was inserted with the XF Calibrant into the XF96 Extracellular Flux analyzer. After completion of calibration the XF Calibrant plate was ejected by the machine and the plate containing the cells was inserted, equilibrated and the measurements were performed according to the protocol in table 5.13. After completion of the assay the medium was aspirated and the cells were fixed for sulforhodamine B staining (see section 5.15.5). Cell number determined by sulforhodamine B staining for each well was divided by average cell number of all wells to obtain relative cell number. Measurement values were then divided by this relative cell number.

Table 5.12: Compound setup for Seahorse Assays

Mito Stress Test Kit				
compound	**port**	**conc. in port**	**volume in port**	**conc. on cells**
oligomycin	A	14 µM	25 µl	2 µM
FCCP	B	4.0 µM	25 µl	0.5 µM
antimycin A + rotenone	C	9 µM each	25 µl	1 µM each
Seahorse Assay Medium	D	–	25 µl	–

Glycolysis Stress Test Kit				
compound	**port**	**conc. in port**	**volume in port**	**conc. on cells**
D-glucose	A	70 mM	25 µl	10 mM
oligomycin	B	16 µM	25 µl	2 µM
2-deoxy-D-glucose	C	900 mM	25 µl	100 mM
Seahorse Assay Medium	D	–	25 µl	–

Table 5.13: Protocol for Seahorse Assays

1. Calibrate	
2. Equilibrate	
3. Mix 3 min 4. Measure 3 min	4 ×
5. Inject port A	
6. Mix 3 min 7. Measure 3 min	3 ×
8. Inject port B	
9. Mix 3 min 10. Measure 3 min	3 ×
11. Inject port C	
12. Mix 3 min 13. Measure 3 min	4 ×

5.15.5 Sulforhodamine B staining

After Seahorse Extracellular Flux measurement, medium was aspirated and cells were fixed with 100 µl ice cold SRB fixation buffer and incubated for at least 30 min at −20 °C. Cells were washed twice with water before incubating with 50 µl of SRB solution for 30 min at room temperature protected from light with mild shaking on a titer plate shaker. Afterwards, sulforhodamine B was removed and cells were washed four times with 1 % (v/v) acetic acid. For the first wash step, the wells were filled entirely while the following steps were done with 200 µl per well. Sulforhodamine B was resolved from cells by applying 100 µl of 10 mM un-buffered Tris and incubating for 5–10 min at room temperature protected from light with vigorous shaking on a titer plate shaker. Finally, absorbance was measured at 550 nm and

converted to cell number using a standard curve that was determined by seeding defined amounts of cells, allowing them to attach for 5 h and then subjecting them to the staining procedure.

$$\log(\text{cell number}) = 4.632 - \log\left(\frac{\frac{3.859 - 0.005015}{\Delta OD - 0.005015} - 1}{1.324}\right)$$

ΔOD is the blank-corrected OD of sulforhodamine-stained cells.

5.15.6 Glucose consumption assay

$1{\times}10^5$ Capan-1 cells were plated in 1 ml of DMEM High Glucose Pyruvate (+ L-glutamine) with 10 % FBS in 12-well plates in 3 replicates per condition. The following day, cells were transfected with siRNA as described in section 5.14.7 on page 65. 24 h later, medium was changed to fresh DMEM High Glucose Pyruvate (+ L-glutamine) with 10 % FBS and cells were grown for another 48 h. Media was then taken and glucose concentration was determined with the Glucose (HK) Assay Kit (Sigma) following manufacturer's instructions. Glucose consumption was calculated by subtracting cell supernatant concentration from that of fresh media (DMEM High Glucose Pyruvate (+ L-glutamine) with 10 % FBS). Cells were trypsinized and counted for normalization.

5.15.7 2-deoxyglucose uptake assay

1×10^5 Capan-1 cells were plated in 1 ml of DMEM High Glucose Pyruvate (+ L-glutamine) with 10 % FBS in 12-well plates in 6 replicates per condition. The following day, cells were transfected with siRNA as described in section 5.14.7 on page 65. 24 h later, medium was changed to fresh DMEM High Glucose Pyruvate (+ L-glutamine) with 10 % FBS and cells were grown for another 24 h. Media was then changed to pre-gassed and pre-warmed Krebs-Ringer-Henseleit buffer (see page 59) supplemented with 1 mM HEPES (pH 7.4), 25 mM D-glucose, 0.1 % BSA, 1× RPMI amino acids (Sigma-Aldrich), 1 mM pyruvate, 2 mM L-glutamine, 8 mM D-mannitol and cells were incubated at 37 °C and 5 % CO_2 for 2 h. After that, cells were incubated for exactly 15 min in tracer media (pre-gassed and pre-warmed Krebs-Ringer-Henseleit buffer supplemented with 1 mM HEPES (pH 7.4), 25 mM D-glucose, 0.1 % BSA, 1× RPMI amino acids (Sigma-Aldrich), 1 mM pyruvate, 2 mM L-glutamine, 8 mM D-mannitol, ^{14}C-D-mannitol, 1 mM 2-deoxy-D-glucose, ^{3}H-2-deoxy-D-glucose). Tracing was stopped by removing tracer media and immediately adding ice cold pre-incubation media. Cells were then lyzed in 300 µl RIPA buffer with protease inhibitors. 200 µl lysate as well as tracer media (to calculate the specific activity of ^{3}H-2-deoxy-D-glucose and ^{14}C-D-mannitol) and lysis buffer (for background radiation) were mixed each with 4 ml Rotiszint® eco plus in 5 ml LDPE scintillation tubes and scintillation was counted (^{3}H and ^{14}C dual decay per minute). 10 µl of lysate was used in duplicates for protein determination by Pierce® BCA Protein Assay Kit. 2-deoxy-D-glucose uptake rates were calculated based on incorporation of ^{3}H counts into cells versus the specific activity of ^{3}H-2-deoxy-D-glucose in the media with correction for the extracellular space by D-mannitol[3] tracing, divided by time of assay, multiplied by correction factor (200 µl lysate for scintillation counting out of 300 µl total lysate) and divided by total protein amount in well (protein concentration in µg/µl × 300 µl).

5.16 Virus work

5.16.1 Lentiviral shRNA vectors

Lentiviral pLKO.1 vector containing shRNA against murine *Tbl1x* was purchased as bacterial glycerol stock from Sigma-Aldrich (TRCN0000109356, Cat. No. SHCLNG-NM_020601). Control vector pLKO.1 with scrambled shRNA (Cat. No. 1864) as well as lentiviral packaging vectors pMD2.G (Cat. No. 12259) and psPAX2 (Cat. No. 12260) were obtained as stab cultures via Addgene. Bacterial stocks were streaked with sterile inoculation loops on LB agar plates containing 50 µg/ml ampicillin and grown at 37 °C over night. Next day, 5 ml LB medium with 50 µg/ml ampicillin were inoculated in round-bottom snap-cap tubes with some material from glycerol stock or a colony from an LB agar plate using a sterile inoculation loop and grown for 8 h shaking at 37 °C. 200 µl of this pre-culture was inoculated into 200 ml of LB medium with 50 µg/ml ampicillin in a 500 ml Erlenmeyer flask and grown over night at 37 °C shaking at ≈180 rpm before isolating plasmids with the PureLink® HiPure Plasmid Maxiprep Kit from Invitrogen™ following manufacturer's instructions.

5.16.2 Lentivirus production

HEK293T cells were plated in 6-well plates at $2.5{\times}10^5$ cells per well. On the following day, pLKO.1 vectors with scrambled or *Tbl1x*-specific shRNAs were transfected as follows:

[3] D-mannitol can not be taken up by mammalian cells

Table 5.14: shRNAs for lentiviral vectors

Gene	RefSeq ID	TRC Number	Sequence
scrambled (NC)	–	–	*Age*I sense loop/*Xho*I antisense termination CGGTCCTAAGGTTAAGTCGCCCTCGCTCGAGCGAGGGCGACTTAACCTTAGGTTTTTG
Tbl1x	NM_020601.2	TRCN0000109356	*Age*I sense loop/*Xho*I antisense termination CCGGGCGAGGATATGGAACCTTAATCTCGAGATTAAGGTTCCATATCCTCGCTTTTTG

For each cell culture well, 1 µg shRNA vector, 1 µg psPAX2 and 100 ng pMD2.G were diluted in 200 µl of Opti-MEM® I, mixed with 200 µl of Opti-MEM® I supplemented with 2.5 % Lipofectamine® 2000 and incubated for 30 min at room temperature. The plasmid-Lipofectamine mixture (400 µl) was added to the cells drop-wise. On the next day, culture medium was changed to DMEM High Glucose Pyruvate (+ L-glutamine) supplemented with 10 % FBS and 1.1 % BSA (Sigma). 48 h later, supernatant was collected, centrifuged for 3 min at 600 ×g and aliquots were stored at −80 °C. Virus titer of supernatant was determined with HIV-1 p24 ELISA.

5.16.3 Lentivirus titer determination

Titer determination was done with the HIV-1 p24-ELISA (XpressBio). Viral supernatants were diluted 1:5000–1:10,000 and processed following manufacturer's instructions. Resulting concentration of p24 was multiplied by the dilution factor and factor 100 to obtain transducing units per ml.

5.16.4 Lentivirus transduction

3×10^4 cells per well of Panc02 were plated in 12-well plates with antibiotic-free culture medium. On the following day, medium was changed to 200 µl of antibiotic-free culture medium with 8 µg/ml polybrene. An equal volume of Opti-MEM® I with 8 µg/ml polybrene plus lentivirus was added at an MOI of 10–100. 12–14 h later, medium was changed to fresh antibiotic-free culture medium and cells were cultured for additional 24 h. Cells were then trypsinized and 1/10 of the cells were plated onto 6-well plates in antibiotic-free culture medium with 1.5 µg/ml puromycin. Cells were sub-cultured when almost confluent and expanded under constant selective pressure. RNA was isolated (see section 5.17.2), reverse-transcribed to cDNA (see section 5.17.4 on the following page) and knockdown efficiency was measured with TaqMan® quantitative PCR (see section 5.17.5 on the next page).

5.16.5 Adenovirus infection of cells

Adenovirus was generated previously by Dr. Maria Rohm from our lab (see [180, p77–79] and [181]). Sequences were as follows: Tbl1x: `GCGAGGATATGGAACCTTAAT`, unspecific shRNA: `GATCTGATCGACACTGTAATG`. Virus was diluted at desired MOI in DMEM High Glucose Pyruvate (+ L-glutamine) without FBS or antibiotics and with 0.5 µg/ml poly-L-lysine. Culture medium was aspirated and replaced with 1/4 volume of virus-containing media. After 90 min medium was filled up to the usual volume with DMEM High Glucose Pyruvate (+ L-glutamine) supplemented with 10 % FBS and 1 % penicillin/streptomycin. Cells were kept in presence of virus for 48 h before lyzing for RNA or protein extraction.

5.17 RNA methods

5.17.1 RNA extraction from tissue samples

Tissue samples were either snap-frozen in liquid nitrogen or submerged in RNA*later*™ buffer (Qiagen) and stored at −80 °C. Snap-frozen samples were cut into pieces with a disposable scalpel on dry ice whereas RNA*later*™ tissue was thawed and cut with a disposable scalpel at room temperature. Approximately 30 mg were homogenized in 600 µl RLT buffer (RNeasy Mini Kit, Qiagen) supplemented with 1 % β-mercaptoethanol by shaking with a stainless steel bead for 2–5 min at 30 Hz in a Tissue Lyser. Afterwards, the corresponding instructions of the RNeasy Mini Kit (Qiagen) were followed including on-column DNase digest. RNA concentration was measured photometrically with a NanoDrop at 260 and 280 nm.

5.17.2 RNA extraction from cell culture samples

Cells were washed once with DPBS (Gibco®), lyzed on plate with 350 µl per well RLT buffer (RNeasy Mini Kit, Qiagen) supplemented with 1 % β-mercaptoethanol in a 6- or 12-well format and either processed immediately or stored at −80 °C until further use. Lysate was collected from the wells, transferred to a 1.5 ml-tube and passaged 5 times through a 20 G

needle. Afterwards, the corresponding instructions of the RNeasy Mini Kit (Qiagen) were followed including on-column DNase digest. RNA concentration was measured photometrically with a NanoDrop at 260 and 280 nm.

5.17.3 RNA gel electrophoresis

When necessary, RNA integrity was checked by separating 500–1000 ng RNA on a 1 % agarose gel in 1× TBE (prepared in DEPC-treated water). Prior to electrophoresis, RNA was mixed with 10 µl RNA loading buffer, denatured for 10 min at 65 °C on a Thermomixer (Eppendorf) and cooled on ice for 2 min. RNA quality was considered good when the 28S ribosomal RNA band was twice as intense as the 18S band and no smear from degraded RNA was visible.

5.17.4 Reverse transcription of RNA

0.5–2 µg RNA were reverse transcribed to single stranded cDNA in a 20 µl reaction with random hexamer primers using the Fermentas First strand cDNA Synthesis Kit following manufacturer's instructions. Finally, single stranded cDNA was diluted in nuclease-free water (Gibco®) resulting in equivalents of 10 ng/µl of initial RNA.

5.17.5 TaqMan® quantitative PCR

PCR reactions were set up in 20 µl per well in MicroAmp® Fast Optical 96-well Reaction Plates with duplicates for each sample as follows:

commercial TaqMan® probes	
10 ng/µl cDNA	2–5 µl
TaqMan® probe	0.5 µl
TaqMan® Gene Expression Master Mix	10 µl
nuclease-free water	7.5–4.5 µl
total	**20 µl**

self-designed primers and probes	
10 ng/µl cDNA	2–5 µl
10 µM forward primer	1 µl
10 µM reverse primer	1 µl
5 µM self-designed probe	0.5 µl
TaqMan® Gene Expression Master Mix	10 µl
nuclease-free water	5.5–2.5 µl
total	**20 µl**

The plate was sealed with MicroAmp® Optical Adhesive Film, briefly centrifuged and then amplification was done in a StepOne Plus (Applied Biosystems®) as follows: 2 min at 50 °C, 10 min at 95 °C followed by 40–45 cycles of 15 sec at 95 °C, 1 min at 60 °C plus data acquisition. C_T values were determined by the StepOne software.

C_T values of the gene of interest were subtracted form C_T values of a reference gene (TBP or 18S-rRNA) from the same sample, resulting in a ΔC_T value. This ΔC_T was then converted to gene expression relative to TBP or 18S-rRNA using the formula *Relative expression* = $2^{-\Delta C_T}$.

5.17.6 Gene Expression Microarrays

Microarray experiments were performed by Maria Muciek and analyzed by Dr. Carsten Sticht from University Clinic Mannheim. Gene expression profiling was performed using GeneChip® arrays of HGU-133 Plus 2.0 type from Affymetrix. cDNA synthesis was done using the SuperScript® Choice System (Life Technologies™) according to manufacturer's protocol. Biotin-labeled cRNA was produced using ENZO BioArray HighYield® RNA transcript labeling kit. Standard protocol from Affymetrix with 3.3 µl of cDNA was used for the *in vitro* transcription (IVT). Cleanup of the IVT product was done using CHROMA SPIN-100 columns (Clontech). Spectrophotometric analysis was used for quantification of cRNA with acceptable A_{260}/A_{280} ratio of 1.9 to 2.1. After that, the cRNA was fragmented using Affymetrix defined protocol. Labeled and fragmented cRNA was hybridized to Affymetrix HGU-133 Plus 2 microarrays for 16 h at 45 °C using Affymetrix defined protocol. Microarrays were washed using a GeneChip® fluidics station 450 and stained initially with streptavidinphycoerytherin. For each sample the signal was further enhanced by incubation with biotinylated goat anti-streptavidin antibody followed by a second incubation with streptavidinphycoerytherin and a second round of intensities were measured. Microarrays were scanned with GeneChip® scanner controlled by Affymetrix Microarray Suite software.

A Custom CDF Version 14 with Entrez based gene definitions was used to annotate the arrays. The Raw fluorescence intensity values were normalized applying quantile normalization. Differential gene expression was analyzed based on loglinear mixed model ANOVA [186, 187], using a commercial software package SAS JMP7 Genomics, version 5, from SAS Institute (Cary, NC, USA). A false positive rate of $\alpha = 0.05$ with FDR correction was taken as the level of significance.

The overrepresentation analysis (ORA) is a microarray data analysis that uses predefined gene sets to identify a significant overrepresentation of genes in data sets [188, 189]. Pathways belonging to various cell functions such as cell cycle or apoptosis were obtained from public external databases (KEGG, `http://www.genome.jp/kegg/`). A Fisher's exact test was performed to detect the significantly regulated pathways.

Table 5.15: Commercial probes for TaqMan® quantitative PCR

Gene	Species	Entrez Gene ID	TaqMan® Assay ID
ACLY	human	47	Hs00982738_m1
CARM1 (*PRMT4*)	human	10498	Hs00406354_m1
CDK2	human	1017	Hs01548894_m1
CPT1A	human	1374	Hs00912671_m1
CPT1B	human	1375	Hs00992664_m1
CRHR1	human	1394	Hs00366363_m1
CRHR2	human	1395	Hs00266401_m1
CRTC2 (*TORC2*)	human	200186	Hs01064500_m1
FASN	human	2194	Hs01005622_m1
G6PD	human	2539	Hs00166169_m1
GLP1R	human	2740	Hs00157705_m1
GLS2	human	27165	Hs00203158_m1
GLUT1 (*SLC2A1*)	human	6513	Hs00892681_m1
GLUT2 (*SLC2A2*)	human	6514	Hs01096904_m1
KIF3B	human	9371	Hs01122781_m1
LDHa	human	3939	Hs00855332_g1
MEST	human	4232	Hs00853380_g1
NRIP1 (*RIP140*)	human	8204	Hs00534035_s1
PDK1	human	5163	Hs01561850_m1
PDK4	human	5166	Hs01037712_m1
PFKFB3	human	5209	Hs00998700_m1
PGC1α (*PPARGC1A*)	human	10891	Hs00173304_m1
PIK3CA	human	5290	Hs00907957_m1
SCD1	human	6319	Hs01682761_m1
TBP	human	6908	Hs00427620_m1
TBL1X	human	6907	Hs00183329_m1
TBL1XR1	human	79718	Hs01037550_m1
TSC22D4	human	81628	Hs00229526_m1

Table 5.16: Self-designed primers and probes for TaqMan® quantitative PCR

Gene	Species	Entrez Gene ID	Sequence	
Tbp	mouse	21374	Forward	TTGACCTAAAGACCATTGCACTTC
			Reverse	TTCTCATGATGACTGCAGCAAA
			Probe	FAM-5'-TGCAAGAAATGCTGAAT-ATAATCCCAAGCG-3'-TAMRA
Tbl1x	mouse	21372	Forward	ACGAGGTGAACTTTCTGGTATATCG
			Reverse	GGACTGGCTAATGTGACTTTCGA
			Probe	FAM-5'-ATCAGGTTTTTCCCACTC-TGCCTTCACG-3'-TAMRA

Gene Set Enrichment Analysis (GSEA), was used to determine whether defined lists (or sets) of genes exhibit a statistically significant bias in their distribution within a ranked gene list (see `http://www.broadinstitute.org/gsea/` for details [188].

Analyses were done in the R version 2.15 environments [190]. The ICC calculation was done using the irr-package.

5.18 Protein methods

5.18.1 Protein extraction from tissue

Tissue samples were snap-frozen in liquid nitrogen and stored at −80 °C. Pieces were cut on dry ice with a disposable scalpel and approximately 30 mg were homogenized in 400 µl protein extraction buffer by shaking with a stainless steel bead for 2–3 min at 30 Hz in a Tissue Lyser. Afterwards, 1/10 volume of protein extraction supplement buffer was added and samples were mixed for 1 h on a turning wheel at 4 °C and 7 rpm. Lysate was transferred to a new tube, centrifuged for 20 min at 13,000 rpm and supernatant was stored at −80 °C until further use.

5.18.2 Protein extraction from cell culture

Medium was aspirated, cells were washed once with DPBS and lyzed in 15–20 µl/cm² RIPA buffer with protease and phosphatase inhibitors. If required, cells were frozen after this step at −80 °C until further processing. Cells were scraped off the culture plate in RIPA buffer with a cell scraper, lysate was transferred to a 1.5 ml-tube and sonicated for 30 sec at low intensity in a Bioruptor® Plus sonicator. Finally, lysates were centrifuged at 13,000 rpm and 4 °C for 10 min and supernatant was transferred to a new tube and stored at −80 °C until further use.

5.18.3 Determination of protein concentration

Protein concentration was determined with the Pierce® BCA Protein Assay Kit on 96-well microtiter plates (Nunc F96). Protein samples were diluted 1:2 to 1:5 fold to not exceed the linear range of the standard curve. 10 µl of BSA standard (0.025–2 µg/µl) or diluted protein lysate were probed in duplicates with 200 µl of assay reagent per well.

5.18.4 SDS-polyacrylamide gel electrophoresis

10–20 µg of protein were mixed with water and 5× SDS loading dye to obtain a loading dye concentration of 1×, then denatured for 10 min at 95 °C before separating with SDS-polyacrylamide gels (8, 10 or 12 % separation gel) in SDS running buffer at 90–120 V for 90–120 min using a Mini-PROTEAN® 3 cell or Mini-PROTEAN® Tetra Cell with PowerPac Basic™ (Cat. No. 164-5050) from Bio-Rad. PageRuler™ prestained protein ladder was used as a size standard.

5.18.5 Immunoblotting

Transfer was done using a wet blot system. After separation, gels were carefully removed from glass plates and submerged in SDS transfer buffer. Meanwhile, a sandwich array with all components previously soaked in SDS transfer buffer was assembled in the transfer cassette: sponge pad, 1 gel-sized Whatman™ paper, gel-sized nitrocellulose membrane, gel, 1 gel-sized Whatman™ paper, sponge pad. Transfer was performed for 1:10 h at 80 V or 2:30 h at 70 V in SDS transfer buffer using a Mini Trans-Blot® Cell. The transfer sandwich was disassembled and the membrane was briefly stained with Ponceau S solution to assess quality of transfer. Staining was removed by 2–3 brief washes with TBS-T or PBS-T until no color remained. Subsequently, the membranes were blocked for 1 h at room temperature in corresponding blocking solution followed by incubation of primary antibody (see table 5.17 on the facing page) at 4 °C over night. Then, blots were washed 3 times for 5–10 min in TBS-T or PBS-T before adding HRP-conjugated secondary antibody (see table 5.18 on the next page) for 1 h at room temperature. Finally, blots were washed another 3 times for 5–10 min in TBS-T or PBS-T. ECL™ Western Blotting Detection Reagent mixture was applied to the membranes, incubated for 5 min, then membranes were put between to transparent plastic foils and chemoluminescence was imaged with a ChemiDoc™ XRS+ System with Image Lab™ software (Cat. No. 170-8265) from Bio-Rad.

5.18.6 Chromatin immunoprecipitation

Cross-linking: Capan-1 cells were seeded on five 15 cm-plates and grown to 80–90 % confluence within 2–3 days. Medium was then exchanged to 27 ml of regular culture medium, 3 ml of 3.7 % formaldehyde solution was added for cross-linking and mixed immediately. Plates were incubated on an orbital shaker at low speed for exactly 15 min. Reaction was stopped with 3 ml of 1.375 M glycine, mixed immediately and incubated on an orbital shaker at low speed for 5 min. Plates were then placed on ice, medium was removed and washed twice with 20 ml of ice-cold DPBS (completely removing wash from culture dish each time). Next, 2 ml of ice cold DPBS with 0.5 M PMSF was added, cells were scraped

Table 5.17: Incubation conditions for primary antibodies in immunoblotting

protein	company	Cat.-No.	diluent	dilution	origin	mouse	human
AKT	Cell Signaling	9272	5 % BSA in TBS-T	1:1000	rabbit	60 kDa	60 kDa
Ⓟ-AKT Ser-473	Cell Signaling	9271	5 % BSA in TBS-T	1:1000	rabbit	60 kDa	60 kDa
AMPK	Cell Signaling	2532	5 % BSA in TBS-T	1:1000	rabbit	64 kDa	62 kDa
Ⓟ-AMPK Thr-172	Cell Signaling	2535	5 % BSA in TBS-T	1:1000	rabbit	64 kDa	62 kDa
CDK2	Santa Cruz	sc-163	5 % BSA in TBS-T	1:1000	rabbit	39 kDa	34 kDa
CDK4	Cell Signaling	2906	5 % BSA in TBS-T	1:1000	mouse	34 kDa	34 kDa
Cyclin D1	Cell Signaling	2926	5 % BSA in TBS-T	1:1000	mouse	33 kDa	34 kDa
ERK-1/2	Cell Signaling	9102	5 % BSA in TBS-T	1:1000	rabbit	42 kDa 44 kDa	42 kDa 44 kDa
Ⓟ-ERK-1/2 Thr-202/Tyr-204	Cell Signaling	9101	5 % BSA in TBS-T	1:1000	rabbit	42 kDa 44 kDa	42 kDa 44 kDa
GSK3β	Cell Signaling	9315	5 % BSA in TBS-T	1:1000	rabbit	46 kDa	46 kDa
Ⓟ-GSK3β Ser-9	Cell Signaling	9336	5 % BSA in TBS-T	1:1000	rabbit	46 kDa	46 kDa
IRS1	Cell Signaling	3407	5 % BSA in TBS-T	1:500	rabbit	180 kDa	180 kDa
Ⓟ-IRS1 Tyr-895	Cell Signaling	3070	5 % BSA in TBS-T	1:500	rabbit	180 kDa	180 kDa
Ⓟ-IRS1 Ser-1101	Cell Signaling	2385	5 % BSA in TBS-T	1:500	rabbit	180 kDa	180 kDa
PI3K p110α	Cell Signaling	4249	5 % BSA in TBS-T	1:1000	rabbit	110 kDa	110 kDa
PTEN	Cell Signaling	9552	5 % BSA in TBS-T	1:1000	rabbit	54 kDa	54 kDa
Ⓟ-PTEN Ser-380 / Thr-382/383	Cell Signaling	9549	5 % BSA in TBS-T	1:1000	rabbit	54 kDa	54 kDa
TBL1X	Abcam	ab24548	5 % milk or 5 % BSA in PBS-T or TBS-T	1:1000	rabbit	57 kDa	64 kDa
TBL1XR1	Novus Biologicals	NB600-270	5 % milk or 5 % BSA in PBS-T or TBS-T	1:1000	rabbit	56 kDa	56 kDa
β-actin	Sigma	A5441	5 % milk or 5 % BSA in PBS-T or TBS-T	1:5000	mouse	42 kDa	42 kDa
VCP	Abcam	11433	5 % milk or 5 % BSA in PBS-T or TBS-T	1:5000	mouse	90 kDa	90 kDa

Table 5.18: Incubation conditions for secondary antibodies in immunoblotting

antibody	manufacturer	Cat. No.	diluent	dilution
goat anti-mouse IgG (H+L)-HRP	Bio-Rad	170-6516	5 % milk or 5 % BSA in TBS-T or PBS-T	1:5000
goat anti-rabbit IgG (H+L)-HRP	Bio-Rad	172-1019	5 % milk or 5 % BSA in TBS-T or PBS-T	1:5000

off, resuspended in the liquid and the material from all five cell culture dishes was pooled into one 15 ml-tube. Cells were centrifuged at 1500 rpm for 5 min at 4 °C.

Nuclei purification and chromatin fragmentation: The pellet was resuspended in 5 ml of ice cold ChIP swelling buffer, incubated on ice for 10 min, then homogenized by 10–20 up-down movements in a Dounce tissue grinder until no large visible particles remained. Homogenate was transferred to a new 15 ml-tube, incubated for 10 min at 4 °C to release the nuclei and then centrifuged at 2000 rpm for 5 min at 4 °C. The supernatant was removed, the pellet resuspended in 5 ml of ChIP Sucrose buffer A and homogenized by 10 up-down movements in a Dounce tissue grinder. The resulting nuclear suspension was then carefully layered over 5 ml of ChIP Sucrose buffer B and centrifuged at 3000 rpm for 15 min at 4 °C. Supernatant was carefully removed in 1 ml-steps, the nuclear pellet resuspended in 1 ml of MNase digestion buffer (EDTA-free) and transferred to a 1.5 ml DNA LoBind® tube (Eppendorf) using LoRetention pipette tips (Eppendorf). The pellet was centrifuged at 3000 rpm for 5 min at 4 °C, supernatant removed and resuspended in MNase digestion buffer to an OD_{260} of 0.2 (for measurement, 5 µl of nuclei were diluted in 1 ml of 1 M NaOH and analyzed using

a NanoDrop). For chromatin fragmentation, 8 µl of micrococcal nuclease (2000 gel units/µl, NEB) were added, inverted several times, incubated for 20 min at 37 °C and mixed by inverting every 3–5 min. The reaction was stopped by adding EDTA to a final concentration of 10 mM and putting the tube on ice. Nuclei were pelleted by centrifuging at 13,000 rpm for 1 min at 4 °C, supernatant discarded and resuspended in 1 ml of ChIP buffer (with protease inhibitors and 0.5 mM PMSF) and incubated on ice for 10 min. Lysis was checked under microscope (mix 10 µl nuclear suspension with 10 µl of 0.4 % trypan blue in PBS and put on coverslip). If lysis was not complete, samples were sonicated in a Bioruptor® Plus sonicator at high intensity for 3 cycles of 30 sec ON / 30 sec OFF. Sample was centrifuged at 13,000 rpm for 15 min at 4 °C and the chromatin-containing supernatant was transferred to a fresh 1.5 ml DNA LoBind® tube using LoRetention pipette tips. An aliquot of 50 µl was taken to check chromatin fragmentation, the remainder was snap-frozen in liquid nitrogen and stored at −80 °C until further use.

Analysis of chromatin digestion and concentration determination: The 50 µl sample was diluted with 100 µl of nuclease-free water and supplemented with 6 µl of 5 M NaCl and 2 µl RNase A (ThermoFischer Scientific). The sample was vortexed and then incubated at 37 °C for 30 min. Then 2 µl of ≈ 20 mg/ml proteinase K were added, vortexed and incubated at 55 °C for 2 h. The DNA was then purified with the MinElute PCR purification kit (Qiagen) with 50 µl elution volume and a 10 µl sample was analyzed on a 1 % agarose gel with 100 bp DNA marker (Fermentas). DNA fragments were between 150–900 bp corresponding to 1–5 nucleosomes.

Immunoprecipitation: The concentration of fragmented cross-linked chromatin was measured with a Qubit® 2.0 Fluorometer (Invitrogen™) using the Qubit® dsDNA HS Assay Kit (Invitrogen™) following manufacturer's instructions. For all subsequent steps DNA LoBind® tubes were used as well as LoRetention pipette tips for all steps where chromatin had to be pipetted. 10 µg of chromatin was used for each precipitation and filled up to a final volume of 500 µl with ChIP buffer plus protease inhibitors. As the 10 % input control, 1 µg of chromatin was dissolved in a total volume of 50 µl with ChIP buffer plus protease inhibitors and stored at −20 °C until further use.

Lysates were pre-cleared with 30 µl of ChIP-grade protein G agarose beads (pipetted with wide bore tips) and 4 µg Normal Rabbit IgG (Cell Signaling, Cat. No. 2729) for at least 2 h on a rotating wheel at 4 °C. Tubes were centrifuged at 6000 rpm for 1 min at 4 °C and supernatant was transferred to a new tube. Antibodies were added (negative control 1 µg Normal Rabbit IgG (Cell Signaling, Cat. No. 2729); positive control 10 µl Histone H3 antibody (Cell Signaling, Cat. No. 4620); sample: 10 µl TBL1X-antibody (Abcam, Cat. No. ab24548)) and incubated over night at 4 °C on a rotating wheel. The next morning, 30 µl ChIP-grade protein G agarose beads (pipetted with wide bore tips) were added and incubated for 2 h on a rotating wheel at 4 °C, then centrifuged at 6000 rpm for 1 min at 4 °C. Supernatant was aspirated and the beads were washed twice with 1 ml of ChIP wash buffer A, twice with 1 ml of ChIP wash buffer B, twice with 1 ml of ChIP wash buffer C and twice with 1 ml 1× TE with a 5 min rotation at room temperature for each washing step. After the last wash, beads were washed once more and the wash buffer was removed carefully and as completely as possible.

IP elution and reversal of crosslinks: DNA was eluted twice by adding 100 µl ChIP elution buffer, incubating at 65 °C and 1200 rpm on a shaking heating block for 15 min followed by centrifugation at 13,000 rpm for 1 min at room temperature. Both supernatants were collected and stored at −20 °C until further use. The 10 % input control was thawed and filled up to 200 µl with ChIP elution buffer. To all samples, 8 µl of 5 M NaCl was added and incubated at 65 °C over night at 950 rpm on a shaking heating block. Next morning, proteinase K was added to a final concentration of 1 mg/ml and incubated at 56 °C for 2 h at 950 rpm on a shaking heating block. Finally, RNase A was added to a final concentration of 100 µg/ml and incubated at 37 °C for 1 h followed by inactivation at 95 °C for 10 min.

DNA purification and PCR analysis: DNA was extracted with the MinElute PCR purification kit (Qiagen) following manufacturer's instructions. Enrichment of *PIK3CA* promoter fragment was performed on a StepOnePlus Real-Time PCR System. ChIP DNA was diluted 1:2 and 1 µl was mixed with 8.4 µl water, 0.3 µl 10 µM forward primer, 0.3 µl 10 µM reverse primer (see table 5.19) and 10 µl *Power* SYBR® Green PCR Master Mix. Samples were amplified using standard SYBR® Green protocol of the StepOne Software (10 min 95 °C; 40 cycles of 15 sec 95 °C, 1 min 60 °C; followed by 15 sec 95 °C, 1 min 60 °C, melt curve in 0.3 °C increments until 95 °C).

Table 5.19: ChIP primers for SYBR® Green quantitative PCR on human *PIK3CA* promoter

Primer	Sequence
Forward	TGTCAATTTTGTCCTTTGGGAACA
Reverse	CAGGACCTGAAAGGTTGCCT

5.19 Lipid methods

5.19.1 Lipid extraction from feces

Lipids were extracted from fecal matter by a modified version of Folch et al. [191]. Approximately 100 mg of frozen material was weighed into a 2 ml Safe-Lock tube (Eppendorf) and 1.5 ml of a chloroform/methanol mixture (2:1 ratio) pre-cooled to −80 °C was added together with a similarly pre-cooled stainless steel bead (Qiagen). The sample was homogenized in a Tissue Lyser for 1–2 min at 30 Hz until no visible large particles remained and then mixed for 20 min at room temperature on a rotating wheel. The homogenate was transferred to a fresh tube and centrifuged at 13,000 rpm for 30 min at 20 °C. The liquid phase was transferred to a fresh tube and 1/5 volume of 150 mM NaCl was added and mixed followed by centrifugation at 2000 rpm for 5 min at 20 °C. The lower phase was carefully transferred to a fresh tube, while avoiding contamination from the upper phase, and stored at −80 °C until further use. 40 µl of a chloroform/Triton® X-100 mixture (1:1 ratio) were placed in a fresh tube and mixed with 200 µl of the organic lipid extract. The chloroform was evaporated with an air-blow drier at room temperature until the weight of the tube did not change any more. 200 µl of water were added, mixed well by vortexing and the extract was stored in a glass vial at −20 °C until further use.

5.19.2 Triglyceride measurement

Triglycerides from fecal extracts were determined with the Serum Triglyceride Determination Kit (Sigma) that cleaves triglycerides into glycerol and fatty acids using the enzyme lipase. The Free Glycerol Reagent was dissolved with 40 ml of water and the Triglyceride Reagent with 10 ml of water, both without shaking or vortexing, and stored in dark bottles protected from light.

2 µl of lipid extract, or water, or Glycerol Standard dilutions (Sigma) were placed in two series of duplicates on a 96-well microtiter plate. The first series of duplicates was mixed with 100 µl of blank solution (4 volumes of Free Glycerol Reagent + 1 volume of water). The second series of duplicates was mixed with 100 µl of assay solution (4 volumes of Free Glycerol Reagent + 1 volume of Triglyceride Reagent). The plate was incubated for 5 min at 37 °C before measuring absorbance at 550 nm. Absorbances were converted to concentrations with the standard curves. Absorbance values of the blank solution (endogenous free glycerol in the samples) were subtracted from values measured with the assay solution (glycerol generated by the enzymatic reaction of the assay) to calculate triglyceride concentration, taking into account the initial sample weight and the dilution steps during the lipid extraction procedure.

5.19.3 Free fatty acid measurement

Determination of free fatty acids was done with the HR Series NEFA-HR (2) kit (Wako Diagnostics). The assay is based on a three-step enzymatic reaction:

$$\text{R–COOH (free fatty acid)} + \text{ATP} + \text{CoA–SH} \xrightarrow{\text{acyl-CoA synthetase}} \text{acyl-CoA} + \text{AMP} + \text{PP}_\text{i}$$

$$\text{acyl-CoA} + \text{O}_2 \xrightarrow{\text{acyl-CoA oxidase}} \text{2,3-}\textit{trans}\text{-enoyl-CoA} + \text{H}_2\text{O}_2$$

$$2\,\text{H}_2\text{O}_2 + \text{4-aminophenazone} + \text{3-methyl-}\textit{N}\text{-ethyl-}\textit{N}\text{-(β-hydroxyethyl)aniline} \xrightarrow{\text{peroxidase}} \text{quinoneimine} + 4\,\text{H}_2\text{O}$$

4 µl of lipid extract or water or serial dilutions of NEFA standard solution were pipetted in duplicates on a 96-well microtiter plate. 50 µl of color reagent solution A were added, mixed well and incubated for 10 min at 37 °C. Next, 100 µl of color reagent solution B were added, mixed well and incubated for 10 min at 37 °C before measuring absorbance at 550 nm.

5.20 Statistics

Statistics was done with Microsoft Excel (Student's *t*-test and Welch's *t*-test), GraphPad Prism version 5.04 for Windows (linear and non-linear regression models, one-way and two-way ANOVA) or SigmaPlot (two-way and three-way ANOVA). Data plotted in figures are mean ± standard error of the mean (SEM) unless stated otherwise.

5.21 Software

software	source
AxioVision SE64 Rel 4.8 for Axio Imager.M2	Carl Zeiss (Oberkochen, Germany)
BibDesk	http://bibdesk.sourceforge.net/
Bioconductor	Fred Hutchinson Cancer Research Center (Seattle, WA, USA)
BLAST	http://blast.ncbi.nlm.nih.gov/Blast.cgi
CellProfiler cell image analysis software	Broad Institute (Cambridge, MA, USA) [183–185]
Geneious	Biomatters, Ltd. (Auckland, New Zealand) [143]
GraphPad Prism version 5.04 for Windows	GraphPad Software, Inc. (La Jolla, CA, USA)
GSEA	http://www.broadinstitute.org/gsea/
ilastik v0.5.12	http://www.ilastik.org/ [192]
Illustrator	Adobe Systems (San Jose, CA, USA)
ImageJ	Wayne Rasband (NIH), Bethesda (MD, USA)
Image Lab™	Bio-Rad (München, Germany)
KEGG	http://www.genome.jp/kegg/
Living Image	Caliper LifeSciences (Rodgau, Germany)
Microarray Suite	Affymetrix (High Wycombe, United Kingdom)
Microsoft Office	Microsoft (Redmond, WA, USA)
MikroWin 2000 for Mithras LB 940	Berthold Technologies (Bad Wildbad, Germany)
Papers version 2.7.3	Mekentosj B.V. (Dordrecht, The Netherlands)
Photoshop	Adobe Systems (San Jose, CS, USA)
Primer-BLAST	http://www.ncbi.nlm.nih.gov/tools/primer-blast/
Pubmed	http://www.ncbi.nlm.nih.gov/pubmed
R version 2.15	http://www.r-project.org/ [190]
SAS® JMP 7	SAS® Institute (Cary, NC, USA)
SigmaPlot version 12.5	Systat Software, Inc. (Erkrath, Germany)
StepOnePlus™ system software	Life Technologies™, Applied Biosystems® (Darmstadt, Germany)
TEXShop	http://pages.uoregon.edu/koch/texshop/
TEXstudio	http://texstudio.sourceforge.net/
xcellence for Cellˆ R automated microscope	Olympus (Hamburg, Germany)
XF96 System Software for XF96 Extracellular Flux Analyzer	Seahorse Biosciences (Copenhagen, Denmark)
XELATEX typesetting software	http://www.xelatex.org/
ZEN for Cell Observer Z1	Carl Zeiss (Oberkochen, Germany)

Appendices

A Maps on global obesity and diabetes prevalence

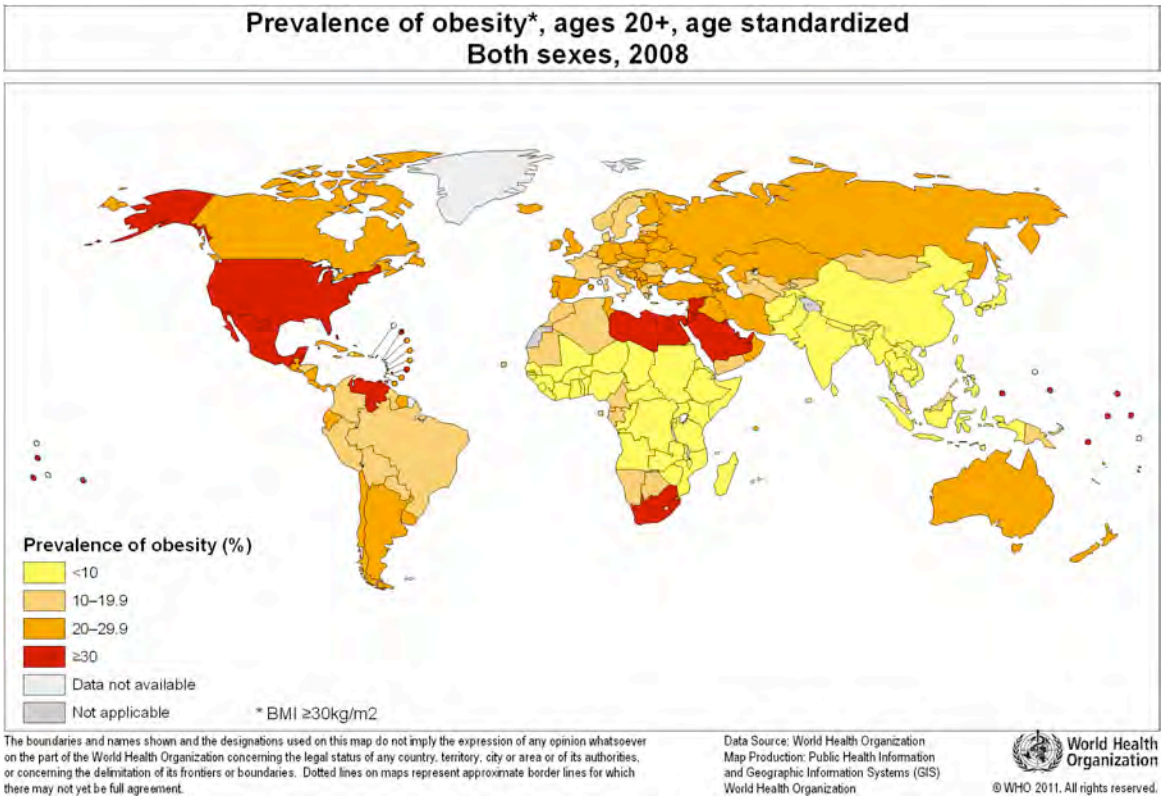

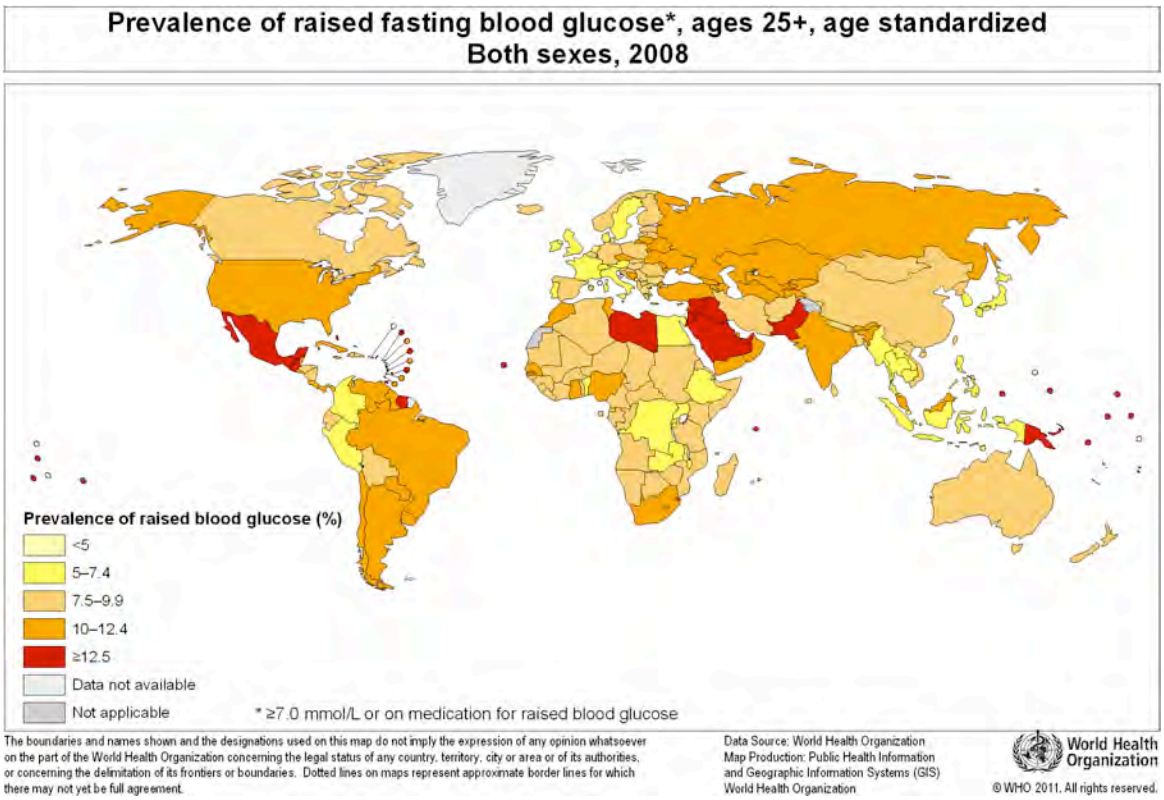

Figure A.1: Global prevalence of obesity and hyperglycemia

images obtained from [193] and [194]

B Sequence homology of human and murine TBL1X and TBL1XR1

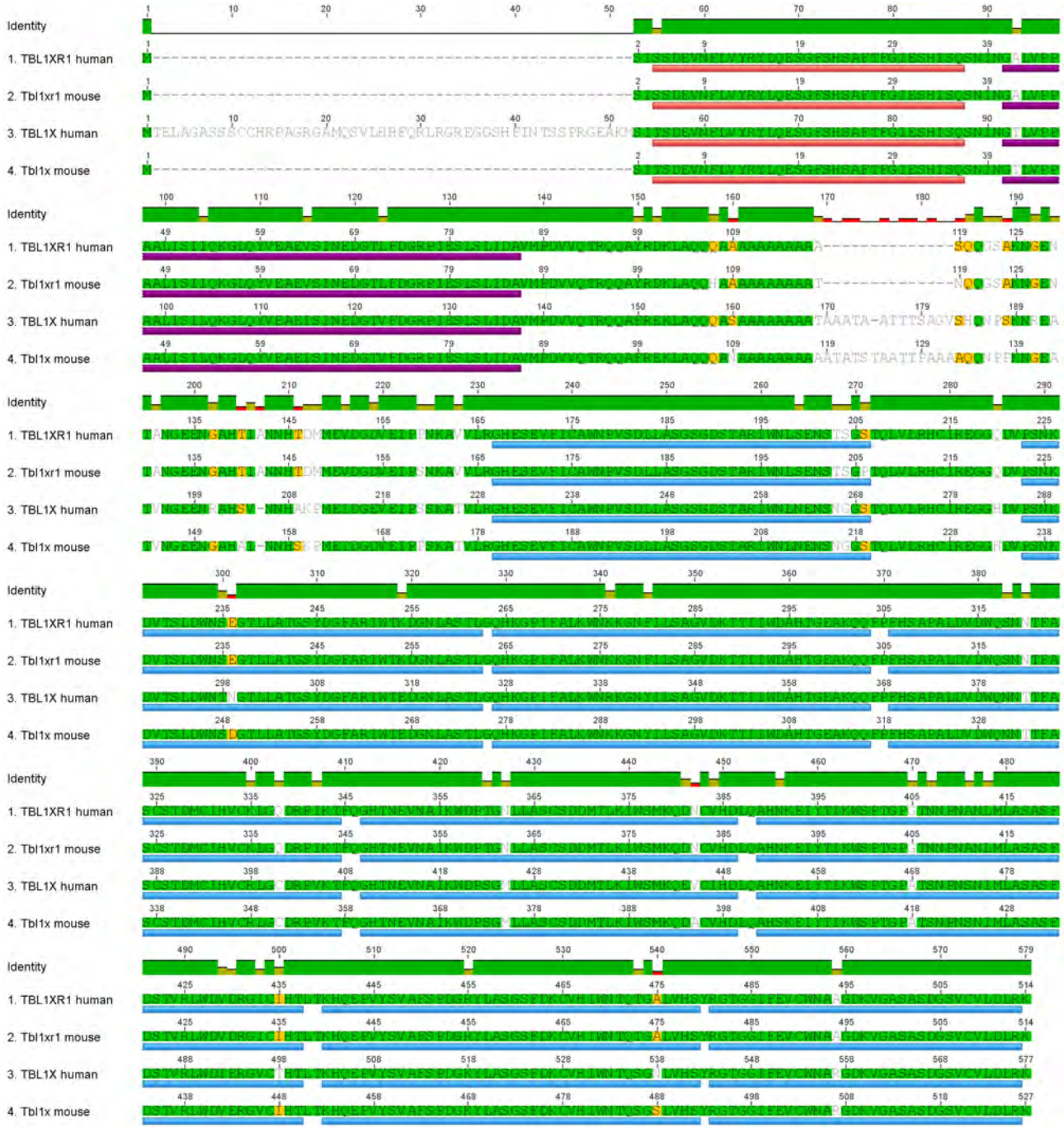

Figure B.1: Sequence alignment of human and murine TBL1X and TBL1XR1
red: LisH domain; purple: F-box-like domain; blue: WD40-repeat domain. Alignment and figure created with Geneious software [143].

C Tumor Stages

Table C.1: Tumor staging according to TNM classification of malignant tumors

"T" describes the size of the tumor and whether it has invaded nearby tissue; "N" describes regional lymph nodes that are involved; "M" describes distant metastasis; "G" describes the differentiation grade of the tumor cells; "R" describes the residual tumor after resection; Use of an "x" instead of a number or other suffix means that the parameter was not or could not be evaluated.

Stage	Description
Tis	*carcinoma/tumor in situ*, tumor has not yet invaded other tissues
T1	tumor ≤2 cm in size
T2	tumor >2 cm and ≤5 cm in size
T3	tumor >5 cm in size
T4	tumor exceeds organ boundary
N0	tumor cells absent from regional lymph nodes
N1	regional lymph node metastasis present; (at some sites: tumor spread to closest or small number of regional lymph nodes)
N2	tumor spread to an extent between N1 and N3 (N2 is not used at all sites)
N3	tumor spread to more distant or numerous regional lymph nodes (N3 is not used at all sites)
M0	no distant metastasis
M1	metastasis to distant organs (beyond regional lymph nodes)
G1	low grade, cells are well differentiated
G2	intermediate grade, cells are moderately differentiated
G3	high grade, cells are poorly differentiated
G4	anaplastic
R0	no residual tumor
R1	microscopic residual tumor
R2	macroscopic residual tumor

D Patient Data

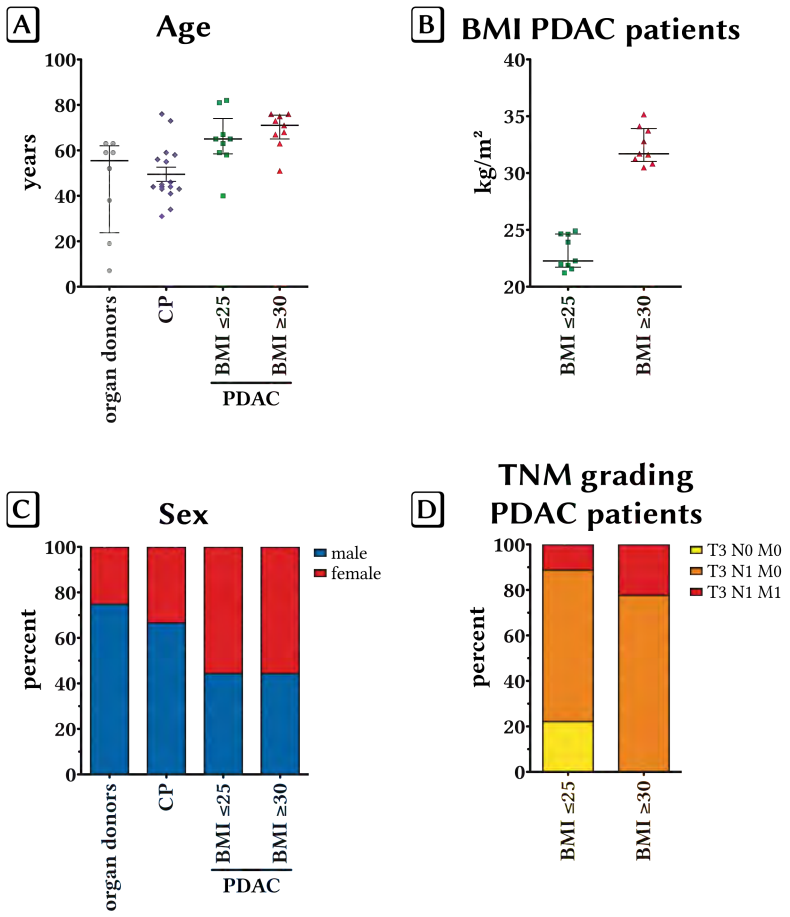

Figure D.1: Statistic parameters of human patients

A: age distribution of organ donors, CP and PDAC patients; B: BMI distribution of normal-weight and obese patients; C: sex distribution of organ donors, CP and PDAC patients; D: distribution of tumor grading of PCAD patients. Lines and error bars in A–B: median with interquartile range. CP: chronic pancreatitis, BMI: body mass index, PDAC: pancreatic ductal adenocarcinoma.

Table D.1: Details of human patients

organ donors (n = 8)

ID	age at explantation	sex
1166	63	♂
1207	19	♀
1220	38	♂
1234	63	♀
1242	7	♂
1348	52	♂
1366	59	♂
1384	59	♂

Chronic pancreatitis (n = 15)

ID	age at surgery	sex	operation	degree of pancreatitis
335	55	♀	pancreatic segmental resection	severe
346	45	♂	DPPHR	severe
359	31	♂	DPPHR	medium
475	76	♂	Whipple	mild
477	56	♂	DPPHR	severe
481	43	♀	DPPHR	severe
490	73	♀	pp-Whipple	mild
513	34	♂	pp-Whipple	medium
527	59	♂	pp-Whipple	medium/severe
528	46	♂	pp-Whipple	severe
546	44	♂	DPPHR	medium/severe
642	43	♀	DPPHR	severe
348	44	♂	DPPHR	severe
366	58	♂	resection	severe
401	41	♀	DPPHR	severe

cancer patients, BMI ≤ 25 (n = 9)

ID	age at surgery	sex	BMI	tumor classification
418	82	♀	24.65	T3 N0 M0 G3 R0
584	40	♀	21.97	T3 N1 M0 G2 R0
872	67	♂	24.91	T3 N1 M0 G2 R0
1157	65	♀	21.88	T3 N1 M1 G2 R1
1161	65	♂	21.22	T3 N1 M0 G3 R0
1201	59	♂	24.62	T3 N1 M0 G3 R0
1385	81	♀	22.27	T3 N1 M0 G2 R0
2979	63	♀	23.92	T3 N1 M0 G4
3054	58	♂	21.56	T3 N0 M0 G2 R1

cancer patients, BMI ≥ 30 (n = 9)

ID	age at surgery	sex	BMI	tumor classification
297	68	♀	30.82	T3 N1 M0 G1 R0
476	75	♂	34.11	T3 N1 M0 G3
744	67	♂	30.49	T3 N1 M0 G3 R0
1108	76	♂	32.79	T3 N1 M1 G2 R0
1640	73	♀	33.73	T3 N1 M0 G3 R1
1255	51	♀	31.62	T3 N1 M0 G2 R0
1544	71	♀	31.23	T3 N1 M0 G2 R0
1594	76	♂	31.70	T3 N1 M0 G3 R0
3060	63	♀	35.16	T3 N1 M1 G3 R1

Table D.2: Statistic parameters of human patients

organ donors

parameter	age at explantation
mean	44.25
standard deviation	21.45
minimum	7
1st quartile	32
median	55
3rd quartile	59
maximum	63

chronic pancreatitis

parameter	age at surgery
mean	49.50
standard deviation	12.52
minimum	31
1st quartile	43
median	44.50
3rd quartile	57.50
maximum	76

cancer patients, BMI ≤ 25

parameter	age at surgery	BMI
mean	63.89	23.04
standard deviation	12.42	1.42
minimum	40	21.22
1st quartile	58	21.90
median	64	22.85
3rd quartile	66	24.44
maximum	81	24.91

cancer patients, BMI ≥ 30

parameter	age at surgery	BMI
mean	68.44	32.33
standard deviation	7.88	1.52
minimum	51	30.49
1st quartile	67	31.24
median	71	31.66
3rd quartile	75	33.73
maximum	75	35.16

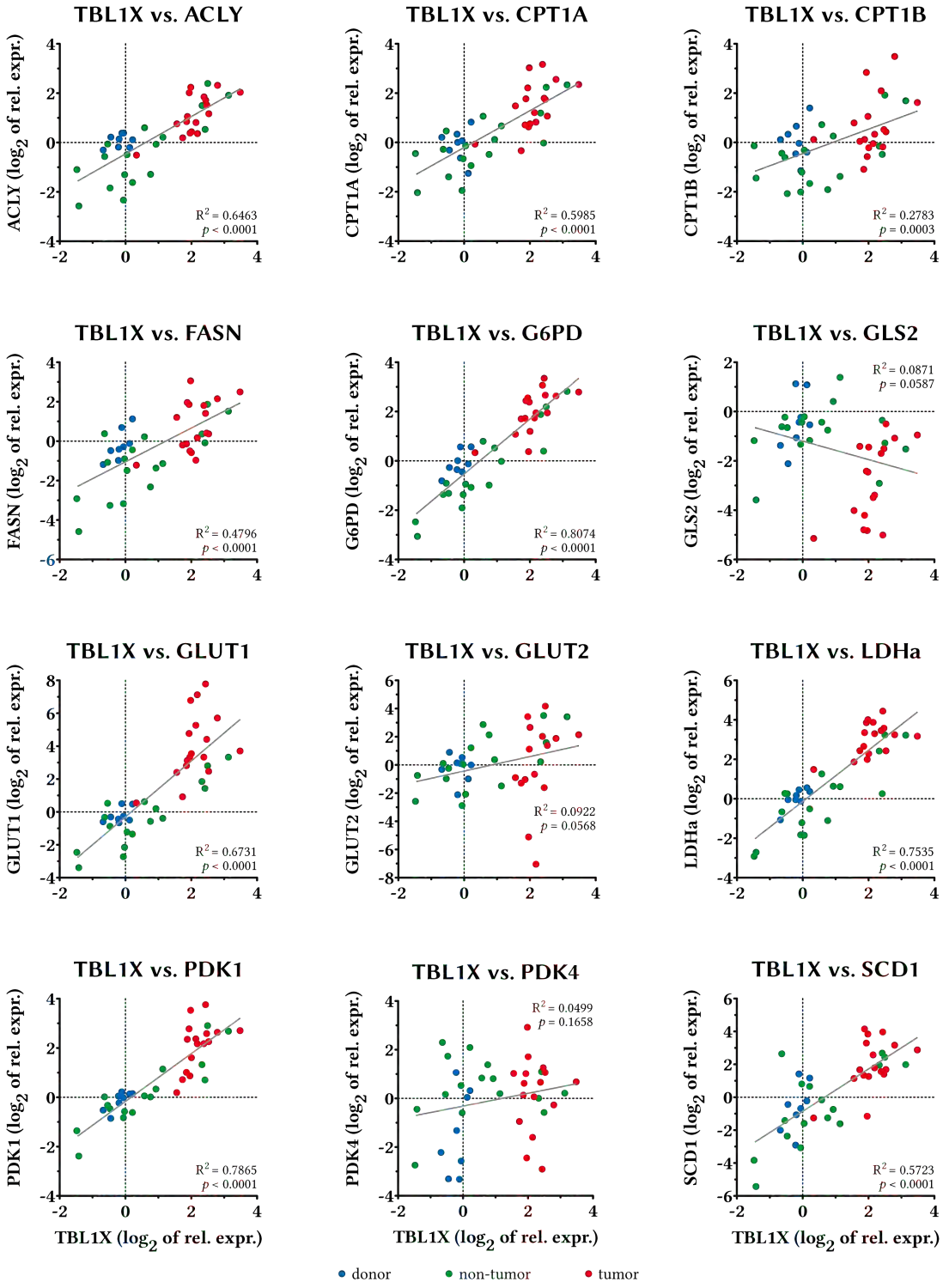

Figure D.2: Correlation of mRNA expression of *TBL1X* and metabolic genes in human patients

Plots show correlation of mRNA expression of *TBL1X* with metabolic genes from figure 3.6 on page 18. Each dot represents one sample from either organ donor (•), non-tumor tissue from cancer patient (•) or tumor tissue from cancer patient (•). Expression is normalized to 18S-rRNA and relative to a pooled organ donor sample. ACLY: ATP citrate lyase; CPT1A: carnitine palmitoyl transferase 1, liver isoform; CPT1B: carnitine palmitoyl transferase 1, muscle isoform; FASN: fatty acid synthase; G6PD: glucose-6-phosphate dehydrogenase; GLS2: glutaminase 2; GLUT1: glucose transporter 1 (SLC2A1); GLUT2: glucose transproter 2 (SLC2A2); LDHa: L-lactate dehydrogenase A chain; PDK1: pyruvate dehydrogenase kinase 1; PDK4: pyruvate dehydrogenase kinase 4; SCD1: stearyl-CoA desaturase. R^2: correlation coefficient of linear regression; p significance level for slope of regression line different from zero.

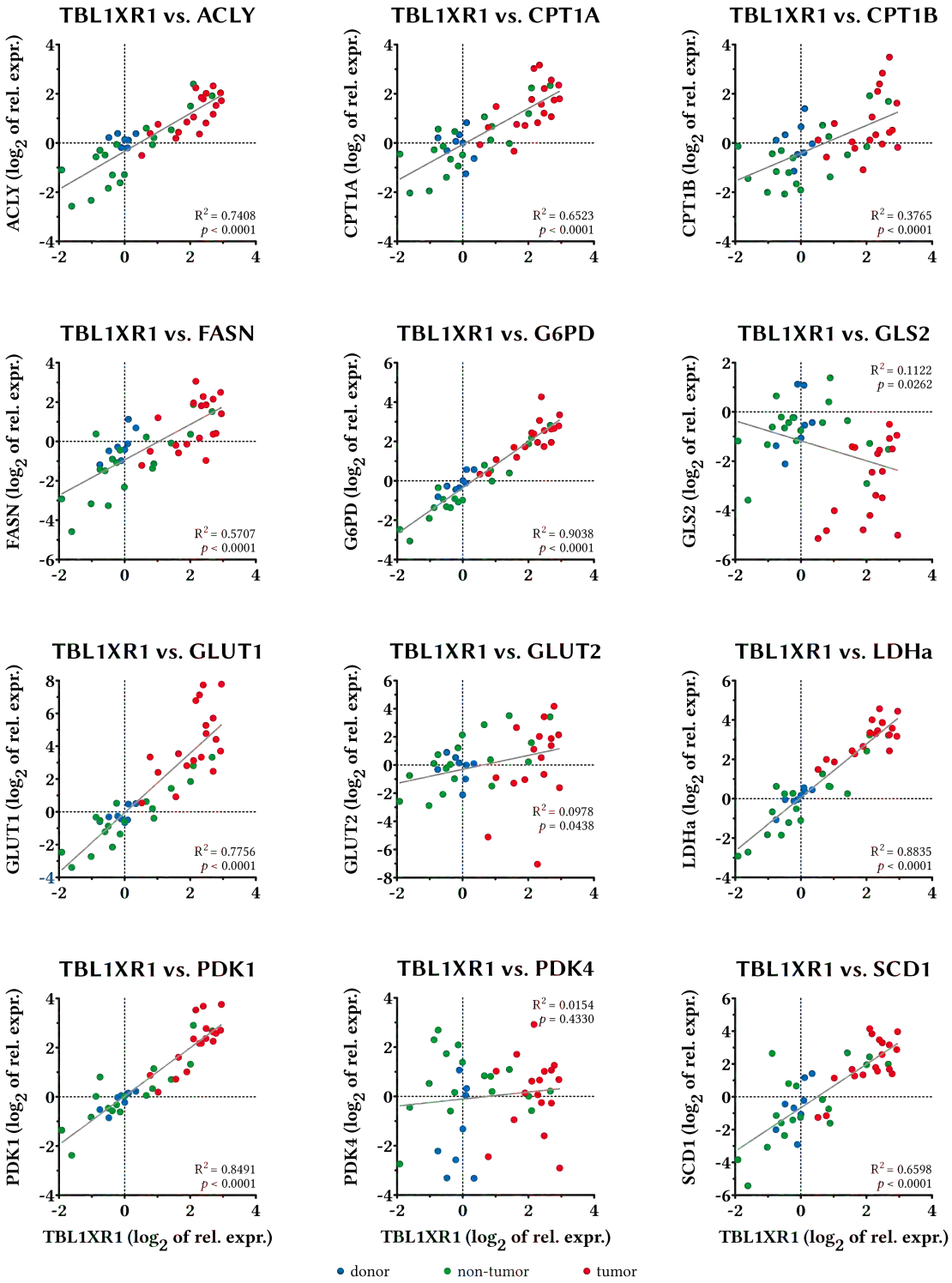

Figure D.3: Correlation of mRNA expression of *TBL1XR1* and metabolic genes in human patients

Plots show correlation of mRNA expression of TBL1XR1 with metabolic genes from figure 3.6 on page 18. Each dot represents one sample from either organ donor (•), non-tumor tissue from cancer patient (•) or tumor tissue from cancer patient (•). Expression is normalized to 18S-rRNA and relative to a pooled organ donor sample. ACLY: ATP citrate lyase; CPT1A: carnitine palmitoyl transferase 1, liver isoform; CPT1B: carnitine palmitoyl transferase 1, muscle isoform; FASN: fatty acid synthase; G6PD: glucose-6-phosphate dehydrogenase; GLS2: glutaminase 2; GLUT1: glucose transporter 1 (SLC2A1); GLUT2: glucose transproter 2 (SLC2A2); LDHa: L-lactate dehydrogenase A chain; PDK1: pyruvate dehydrogenase kinase 1; PDK4: pyruvate dehydrogenase kinase 4; SCD1: stearyl-CoA desaturase. R^2: correlation coefficient of linear regression; *p* significance level for slope of regression line different from zero.

E Details of HFD study on *p48$^{+/Cre}$; Kras$^{+/LSL-G12D}$* mice

Table E.1: Age and lifespan of mice on LFD/HFD study

†: animal was killed; ‡: animal died spontaneously; ◆: scheduled end of experiment; mor.: moribund; inv.: investigatory

animal number	genotype	diet	sex	age at start	time on diet	age at end	reason of death
76	*p48$^{+/Cre}$; Kras$^{+/LSL-G12D}$*	HFD	♂	9w 5d	11w 6d	21w 4d	◆, †
235	*p48$^{+/Cre}$; Kras$^{+/LSL-G12D}$*	HFD	♂	6w 5d	12w	18w 5d	◆, †
396	*p48$^{+/Cre}$; Kras$^{+/LSL-G12D}$*	HFD	♂	7w 5d	12w	19w 5d	◆, †
1741	*p48$^{+/Cre}$; Kras$^{+/LSL-G12D}$*	HFD	♂	6w 5d	12w	18w 5d	◆, †
167	*p48$^{+/Cre}$; Kras$^{+/LSL-G12D}$*	HFD	♂	6w 6d	1w 1d	8w	mor., †
74	*p48$^{+/Cre}$; Kras$^{+/LSL-G12D}$*	HFD	♂	9w 5d	2w 3d	12w 1d	mor., †
345	*p48$^{+/Cre}$; Kras$^{+/LSL-G12D}$*	HFD	♂	10w 2d	2w 3d	12w 5d	mor., †
382	*p48$^{+/Cre}$; Kras$^{+/LSL-G12D}$*	HFD	♂	7w 6d	2w 6d	10w 5d	mor., †
385	*p48$^{+/Cre}$; Kras$^{+/LSL-G12D}$*	HFD	♂	7w 6d	5w 1d	13w	mor., ‡
209	*p48$^{+/Cre}$; Kras$^{+/LSL-G12D}$*	HFD	♀	6w 6d	12w	18w 6d	◆, †
337	*p48$^{+/Cre}$; Kras$^{+/LSL-G12D}$*	HFD	♀	10w 2d	12w	22w 2d	◆, †
347	*p48$^{+/Cre}$; Kras$^{+/LSL-G12D}$*	HFD	♀	8w 5d	12w	20w 5d	◆, †
1639	*p48$^{+/Cre}$; Kras$^{+/LSL-G12D}$*	HFD	♀	8w 2d	12w	20w 2d	◆, †
1642	*p48$^{+/Cre}$; Kras$^{+/LSL-G12D}$*	HFD	♀	8w 1d	12w	20w 1d	◆, †
1922	*p48$^{+/Cre}$; Kras$^{+/LSL-G12D}$*	HFD	♀	8w	8w	16w	inv., †
1968	*p48$^{+/Cre}$; Kras$^{+/LSL-G12D}$*	HFD	♀	4w 6d	8w	12w 6d	inv., †
346	*p48$^{+/Cre}$; Kras$^{+/LSL-G12D}$*	HFD	♀	8w 5d	4w 2d	13w	mor., †
399	*p48$^{+/Cre}$; Kras$^{+/LSL-G12D}$*	HFD	♀	7w 1d	10w	17w 1d	mor., †
1665	*p48$^{+/Cre}$; Kras$^{+/LSL-G12D}$*	LFD	♂	7w 6d	12w	19w 6d	◆, †
1667	*p48$^{+/Cre}$; Kras$^{+/LSL-G12D}$*	LFD	♂	7w 6d	12w	19w 6d	◆, †
1970	*p48$^{+/Cre}$; Kras$^{+/LSL-G12D}$*	LFD	♂	4w 6d	12w	16w 6d	◆, †
376	*p48$^{+/Cre}$; Kras$^{+/LSL-G12D}$*	LFD	♂	7w 6d	2w 6d	10w 5d	mor., †
416	*p48$^{+/Cre}$; Kras$^{+/LSL-G12D}$*	LFD	♂	6w 1d	8w 2d	14w 3d	mor., †
69	*p48$^{+/Cre}$; Kras$^{+/LSL-G12D}$*	LFD	♀	9w 5d	11w 6d	21w 4d	◆, †
71	*p48$^{+/Cre}$; Kras$^{+/LSL-G12D}$*	LFD	♀	9w 5d	11w 6d	21w 4d	◆, †
73	*p48$^{+/Cre}$; Kras$^{+/LSL-G12D}$*	LFD	♀	9w 5d	11w 6d	21w 4d	◆, †
373	*p48$^{+/Cre}$; Kras$^{+/LSL-G12D}$*	LFD	♀	7w 6d	12w	19w 6d	◆, †
412	*p48$^{+/Cre}$; Kras$^{+/LSL-G12D}$*	LFD	♀	6w 1d	12w	18w 1d	◆, †
1758	*p48$^{+/Cre}$; Kras$^{+/LSL-G12D}$*	LFD	♀	6w 2d	12w	18w 2d	◆, †
380	*p48$^{+/Cre}$; Kras$^{+/LSL-G12D}$*	LFD	♀	7w 6d	11w	18w 6d	mor., †
63	wt	HFD	♂	11w 2d	12w	23w 2d	◆, †
81	*p48$^{+/Cre}$*	HFD	♂	9w 5d	11w 6d	21w 4d	◆, †
82	wt	HFD	♂	9w 5d	11w 6d	21w 4d	◆, †
168	wt	HFD	♂	6w 6d	12w	18w 6d	◆, †
233	wt	HFD	♂	6w 5d	12w	18w 5d	◆, †
344	*p48$^{+/Cre}$*	HFD	♂	10w 2d	12w	22w 2d	◆, †
397	*Trp53$^{+/LSL-R172H}$*	HFD	♂	7w 5d	12w	19w 5d	◆, †
1486	wt	HFD	♂	11w	12w	23w	◆, †
1488	wt	HFD	♂	11w	12w	23w	◆, †
1673	*p48$^{+/Cre}$*	HFD	♂	7w 5d	12w	19w 5d	◆, †
1742	*Kras$^{+/LSL-G12D}$*	HFD	♂	6w 5d	12w	18w 5d	◆, †
383	wt	HFD	♂	7w 6d	8w	15w 6d	◆, †
384	wt	HFD	♂	7w 6d	8w	15w 6d	◆, †
49	wt	HFD	♀	11w 6d	12w	23w 6d	◆, †
50	wt	HFD	♀	11w 6d	12w	23w 6d	◆, †

Table continued on next page

Table E.1 *continued:* Age and lifespan of mice on LFD/HFD study

†: animal was killed; ◆: scheduled end of experiment; wt: wild type

animal number	genotype	diet	sex	age at start	time on diet	age at end	reason of death
51	wt	HFD	♀	11w 6d	12w	23w 6d	◆, †
339	*p48 $^{+/Cre}$*	HFD	♀	10w 2d	12w	22w 2d	◆, †
366	*Trp53 $^{+/LSL-R172H}$*	HFD	♀	8w	12w	20w	◆, †
1640	wt	HFD	♀	8w 2d	12w	20w 2d	◆, †
1643	wt	HFD	♀	8w 1d	12w	20w 1d	◆, †
375	wt	LFD	♂	7w 6d	12w	19w 6d	◆, †
417	wt	LFD	♂	6w 1d	12w	18w 1d	◆, †
1487	wt	LFD	♂	11w	12w	23w	◆, †
1489	wt	LFD	♂	11w	12w	23w	◆, †
1664	wt	LFD	♂	7w 6d	12w	19w 6d	◆, †
1666	*Kras $^{+/LSL-G12D}$*	LFD	♂	7w 6d	12w	19w 6d	◆, †
1971	*Kras $^{+/LSL-G12D}$*	LFD	♂	4w 6d	12w	16w 6d	◆, †
52	wt	LFD	♀	11w 6d	12w	23w 6d	◆, †
53	wt	LFD	♀	11w 6d	12w	23w 6d	◆, †
54	wt	LFD	♀	11w 6d	12w	23w 6d	◆, †
72	wt	LFD	♀	9w 5d	11w 6d	21w 4d	◆, †
340	*p48 $^{+/Cre}$*	LFD	♀	10w 2d	12w	22w 2d	◆, †
350	*p48 $^{+/Cre}$*	LFD	♀	8w 5d	12w	20w 5d	◆, †
1759	wt	LFD	♀	6w 2d	12w	18w 2d	◆, †

Table E.2: Statistical analysis of area under curve for body weight change

Three-way ANOVA with Holm-Sidak post-test; DF: degrees of freedom; ΣS: sum of squares; MS: mean square; DM: difference of means; *F*: critical value of *F*-statistic; *t*: critical value of *t*-statistic; *p*: significance level, printed in green when significant (≤ 0.05); wt: wild type (all animals not carrying *p48 +/Cre* and *Kras +/LSL-G12D* alleles at the same time).

main effects

source of variation	DF	ΣS	MS	*F*	*p*
sex	1	143 824.403	143 824.403	7.345	0.010
genotype	1	75 209.485	75 209.485	3.841	0.057
diet	1	950 387.994	950 387.994	48.534	< 0.001
sex × genotype	1	78 675.438	78 675.438	4.018	0.051
sex × diet	1	879.985	879.985	0.045	0.833
genotype × diet	1	88 552.126	88 552.126	4.522	0.039
sex × genotype × diet	1	4 706.425	4 706.425	0.240	0.626
Residual	**43**	**842 027.450**	**19 582.034**		
Total	**50**	**2 868 950.889**	**57 379.018**		

pairwise multiple comparison procedures (Holm-Sidak method)

factor	comparison	DM	*t*	*p*
sex	♂ vs. ♀	114.231	2.710	0.010
genotype	wt vs. *p48 +/Cre; Kras +/LSL-G12D*	82.604	1.960	0.057
diet	LFD vs. HFD	293.642	6.967	< 0.001
diet within wt	LFD vs. HFD	383.274	7.734	< 0.001
diet within *p48 +/Cre; Kras +/LSL-G12D*	LFD vs. HFD	204.009	2.991	0.005
genotype within LFD	wt vs. *p48 +/Cre; Kras +/LSL-G12D*	7.028	0.113	0.910
genotype within HFD	wt vs. *p48 +/Cre; Kras +/LSL-G12D*	172.237	3.017	0.004

power of performed test with α = 0.05 for sex	0.698
power of performed test with α = 0.05 for genotype	0.362
power of performed test with α = 0.05 for diet	1.000
power of performed test with α = 0.05 for sex × genotype	0.382
power of performed test with α = 0.05 for sex × diet	0.050
power of performed test with α = 0.05 for genotype × diet	0.438

Table E.3: Statistical analysis of body weight change in male animals

Three-way ANOVA with Holm-Sidak post-test; DF: degrees of freedom; ΣS: sum of squares; MS: mean square; DM: difference of means; *F*: critical value of *F*-statistic; *t*: critical value of *t*-statistic; *p*: significance level, printed in green when significant (≤ 0.05); wt: wild type (all animals not carrying *p48* $^{+/Cre}$ and *Kras* $^{+/LSL-G12D}$ alleles at the same time).

main effects

source of variation	DF	ΣS	MS	*F*	*p*
time	11	83 314.110	7 574,010	49.740	< 0.001
genotype	1	13 925.054	13 925.054	91.448	< 0.001
diet	1	46 239.191	46 239.191	303.659	< 0.001
time × genotype	11	4 255.250	386.841	2.540	0.004
time × diet	11	6 006.143	546.013	3.586	< 0.001
genotype × diet	1	5 566.478	5 566.478	36.556	< 0.001
time × genotype × diet	11	923.647	83 968	0.551	0.867
Residual	**282**	**42 941.108**	**152.273**		
Total	**329**	**291 357.113**	**885.584**		

pairwise multiple comparison procedures (Holm-Sidak method)

factor	comparison	DM	*t*	*p*
genotype	wt vs. *p48* $^{+/Cre}$*; Kras* $^{+/LSL-G12D}$	14.651	9.563	< 0.001
diet	LFD vs. HFD	26.698	17.426	< 0.001
diet within wt	LFD vs. HFD	35.961	21.309	< 0.001
diet within *p48* $^{+/Cre}$*; Kras* $^{+/LSL-G12D}$	LFD vs. HFD	17.435	6.817	< 0.001
genotype within LFD	wt vs. *p48* $^{+/Cre}$*; Kras* $^{+/LSL-G12D}$	5.388	2.306	0.022
genotype within HFD	wt vs. *p48* $^{+/Cre}$*; Kras* $^{+/LSL-G12D}$	23.914	12.066	< 0.001
genotype at week 1	wt vs. *p48* $^{+/Cre}$*; Kras* $^{+/LSL-G12D}$	2.190	0.473	0.636
genotype at week 2	wt vs. *p48* $^{+/Cre}$*; Kras* $^{+/LSL-G12D}$	3.945	0.817	0.415
genotype at week 3	wt vs. *p48* $^{+/Cre}$*; Kras* $^{+/LSL-G12D}$	7.027	1.395	0.165
genotype at week 4	wt vs. *p48* $^{+/Cre}$*; Kras* $^{+/LSL-G12D}$	9.407	1.797	0.073
genotype at week 5	wt vs. *p48* $^{+/Cre}$*; Kras* $^{+/LSL-G12D}$	9.587	1.831	0.068
genotype at week 6	wt vs. *p48* $^{+/Cre}$*; Kras* $^{+/LSL-G12D}$	12.511	2.390	0.018
genotype at week 7	wt vs. *p48* $^{+/Cre}$*; Kras* $^{+/LSL-G12D}$	16.649	3.011	0.003
genotype at week 8	wt vs. *p48* $^{+/Cre}$*; Kras* $^{+/LSL-G12D}$	20.160	3.646	< 0.001
genotype at week 9	wt vs. *p48* $^{+/Cre}$*; Kras* $^{+/LSL-G12D}$	21.175	3.797	< 0.001
genotype at week 10	wt vs. *p48* $^{+/Cre}$*; Kras* $^{+/LSL-G12D}$	23.000	4.124	< 0.001
genotype at week 11	wt vs. *p48* $^{+/Cre}$*; Kras* $^{+/LSL-G12D}$	24.328	4.362	< 0.001
genotype at week 12	wt vs. *p48* $^{+/Cre}$*; Kras* $^{+/LSL-G12D}$	28.835	4.632	< 0.001
diet at week 1	LFD vs. HFD	7.526	1.626	0.105
diet at week 2	LFD vs. HFD	12.529	2.594	0.010
diet at week 3	LFD vs. HFD	18.727	3.709	< 0.001
diet at week 4	LFD vs. HFD	24.094	4.603	< 0.001
diet at week 5	LFD vs. HFD	24.044	4.593	< 0.001
diet at week 6	LFD vs. HFD	28.278	5.402	< 0.001
diet at week 7	LFD vs. HFD	32.588	5.894	< 0.001
diet at week 8	LFD vs. HFD	35.944	6.510	< 0.001
diet at week 9	LFD vs. HFD	33.246	5.961	< 0.001
diet at week 10	LFD vs. HFD	33.922	6.082	< 0.001
diet at week 11	LFD vs. HFD	34.440	6.175	< 0.001
diet at week 12	LFD vs. HFD	34.986	6.273	< 0.001

power of performed test with α = 0.05 for time	1.000
power of performed test with α = 0.05 for genotype	1.000
power of performed test with α = 0.05 for diet	1.000
power of performed test with α = 0.05 for time × genotype	0.788
power of performed test with α = 0.05 for time × diet	0.972
power of performed test with α = 0.05 for genotype × diet	1.000

Table E.4: Statistical analysis of body weight change in female animals

Three-way ANOVA with Holm-Sidak post-test; DF: degrees of freedom; ΣS: sum of squares; MS: mean square; DM: difference of means; *F*: critical value of *F*-statistic; *t*: critical value of *t*-statistic; *p*: significance level, printed in green when significant (≤ 0.05); wt: wild type (all animals not carrying *p48 +/Cre* and *Kras +/LSL-G12D* alleles at the same time).

main effects

source of variation	DF	ΣS	MS	*F*	*p*
time	11	73 776.009	6 706.910	26.748	< 0.001
genotype	1	18.486	18.486	0.0737	0.786
diet	1	59 945.730	59 945.730	239.075	< 0.001
time × genotype	11	164.709	14.974	0.060	1.000
time × diet	11	18 390.886	1 671.899	6.668	< 0.001
genotype × diet	1	2 977.714	2. 977.714	11.876	< 0.001
time × genotype × diet	11	689.547	62 686	0.250	0.993
Residual	**303**	**75 974.254**	**250.740**		
Total	**350**	**230 531.738**	**658.662**		

pairwise multiple comparison procedures (Holm-Sidak method)

factor	comparison	DM	*t*	*p*
genotype	wt vs. *p48 +/Cre; Kras +/LSL-G12D*	0.463	0.272	0.786
diet	LFD vs. HFD	26.381	15.462	< 0.001
diet within wt	LFD vs. HFD	32.261	13.636	< 0.001
diet within *p48 +/Cre; Kras +/LSL-G12D*	LFD vs. HFD	20.501	8.337	< 0.001
genotype within LFD	wt vs. *p48 +/Cre; Kras +/LSL-G12D*	6.343	2.578	0.010
genotype within HFD	wt vs. *p48 +/Cre; Kras +/LSL-G12D*	5.416	2.291	0.023
genotype at week 1	wt vs. *p48 +/Cre; Kras +/LSL-G12D*	0.051	0.009	0.993
genotype at week 2	wt vs. *p48 +/Cre; Kras +/LSL-G12D*	2.871	0.502	0.616
genotype at week 3	wt vs. *p48 +/Cre; Kras +/LSL-G12D*	0.996	0.174	0.862
genotype at week 4	wt vs. *p48 +/Cre; Kras +/LSL-G12D*	0.741	0.130	0.897
genotype at week 5	wt vs. *p48 +/Cre; Kras +/LSL-G12D*	1.571	0.271	0.787
genotype at week 6	wt vs. *p48 +/Cre; Kras +/LSL-G12D*	0.447	0.077	0.939
genotype at week 7	wt vs. *p48 +/Cre; Kras +/LSL-G12D*	2.015	0.348	0.728
genotype at week 8	wt vs. *p48 +/Cre; Kras +/LSL-G12D*	2.032	0.351	0.726
genotype at week 9	wt vs. *p48 +/Cre; Kras +/LSL-G12D*	0.944	0.157	0.875
genotype at week 10	wt vs. *p48 +/Cre; Kras +/LSL-G12D*	0.471	0.076	0.939
genotype at week 11	wt vs. *p48 +/Cre; Kras +/LSL-G12D*	1.231	0.195	0.845
genotype at week 12	wt vs. *p48 +/Cre; Kras +/LSL-G12D*	1.226	0.194	0.846
diet at week 1	LFD vs. HFD	5.546	0.970	0.333
diet at week 2	LFD vs. HFD	10.855	1.898	0.059
diet at week 3	LFD vs. HFD	12.042	2.105	0.036
diet at week 4	LFD vs. HFD	16.615	2.905	0.004
diet at week 5	LFD vs. HFD	16.602	2.865	0.004
diet at week 6	LFD vs. HFD	18.932	3.267	0.001
diet at week 7	LFD vs. HFD	26.404	4.556	< 0.001
diet at week 8	LFD vs. HFD	32.939	5.684	< 0.001
diet at week 9	LFD vs. HFD	33.408	5.533	< 0.001
diet at week 10	LFD vs. HFD	41.653	6.732	< 0.001
diet at week 11	LFD vs. HFD	47.177	7.480	< 0.001
diet at week 12	LFD vs. HFD	54.401	8.626	< 0.001

power of performed test with $\alpha = 0.05$ for time	1.000
power of performed test with $\alpha = 0.05$ for genotype	0.050
power of performed test with $\alpha = 0.05$ for diet	1.000
power of performed test with $\alpha = 0.05$ for time × genotype	0.050
power of performed test with $\alpha = 0.05$ for time × diet	1.000
power of performed test with $\alpha = 0.05$ for genotype × diet	0.927

Table E.5: Statistical analysis of area under curve for body fat

Three-way ANOVA with Holm-Sidak post-test; DF: degrees of freedom; ΣS: sum of squares; MS: mean square; DM: difference of means; *F*: critical value of *F*-statistic; *t*: critical value of *t*-statistic; *p*: significance level, printed in green when significant (≤ 0.05); wt: wild type (all animals not carrying *p48* $^{+/Cre}$ and *Kras* $^{+/LSL-G12D}$ alleles at the same time).

main effects

source of variation	DF	ΣS	MS	*F*	*p*
sex	1	9 567.586	9 567.586	2.903	0.096
genotype	1	72 904.245	72 904.245	22.122	< 0.001
diet	1	247 170.743	247 170.743	75.000	< 0.001
sex × genotype	1	2 532.970	2 532.970	0.769	0.386
sex × diet	1	12.277	12.277	0.004	0.952
genotype × diet	1	8 008.070	8 008.070	2.430	0.127
sex × genotype × diet	1	576.014	576.014	0.175	0.678
Residual	**42**	**138 415**	**3 295.597**		
Total	**49**	**591 708.284**	**12 075.679**		

pairwise multiple comparison procedures (Holm-Sidak method)

factor	comparison	DM	*t*	*p*
sex	♂ vs. ♀	29.643	1.704	0.096
genotype	wt vs. *p48* $^{+/Cre}$*; Kras* $^{+/LSL-G12D}$	81.827	4.703	< 0.001
diet	LFD vs. HFD	150.668	8.660	< 0.001

power of performed test with α = 0.05 for sex	0.255
power of performed test with α = 0.05 for genotype	0.998
power of performed test with α = 0.05 for diet	1.000
power of performed test with α = 0.05 for sex × genotype	0.050
power of performed test with α = 0.05 for sex × diet	0.050
power of performed test with α = 0.05 for genotype × diet	0.201

Table E.6: Statistical analysis of body fat in male animals

Three-way ANOVA with Holm-Sidak post-test; DF: degrees of freedom; ΣS: sum of squares; MS: mean square; DM: difference of means; *F*: critical value of *F*-statistic; *t*: critical value of *t*-statistic; *p*: significance level, printed in green when significant (≤ 0.05); wt: wild type (all animals not carrying *p48 +/Cre* and *Kras +/LSL-G12D* alleles at the same time).

main effects

source of variation	DF	ΣS	MS	*F*	*p*
time	3	5 958.696	1986.232	89.207	< 0.001
genotype	1	1 432.148	1 432.148	64.322	< 0.001
diet	1	3 012.171	3 012.171	135.285	< 0.001
time × genotype	3	337 768	112.589	5.057	0.003
time × diet	3	1 023.139	341.046	15.317	< 0.001
genotype × diet	1	20.847	20.847	0.936	0.336
time × genotype × diet	3	26.054	8.685	0.390	0.760
Residual	**95**	**2 115.207**	**22.265**		
Total	**110**	**19 768.469**	**179.713**		

pairwise multiple comparison procedures (Holm-Sidak method)

factor	comparison	DM	*t*	*p*
genotype	wt vs. *p48 +/Cre; Kras +/LSL-G12D*	8.023	8.020	< 0.001
diet	LFD vs. HFD	11.635	11.631	< 0.001
diet within wt	LFD vs. HFD	35.961	21.309	< 0.001
diet within *p48 +/Cre; Kras +/LSL-G12D*	LFD vs. HFD	17.435	6.817	< 0.001
genotype at week 0	wt vs. *p48 +/Cre; Kras +/LSL-G12D*	1.893	0.980	0.330
genotype at week 3	wt vs. *p48 +/Cre; Kras +/LSL-G12D*	7.575	3.923	< 0.001
genotype at week 7	wt vs. *p48 +/Cre; Kras +/LSL-G12D*	11.338	5.664	< 0.001
genotype at week 11	wt vs. *p48 +/Cre; Kras +/LSL-G12D*	11.286	5.292	< 0.001
diet at week 0	LFD vs. HFD	0.485	0.251	0.802
diet at week 3	LFD vs. HFD	13.539	7.012	< 0.001
diet at week 7	LFD vs. HFD	17.871	8.928	< 0.001
diet at week 11	LFD vs. HFD	14.646	6.868	< 0.001

power of performed test with α = 0.05 for time	1.000
power of performed test with α = 0.05 for genotype	1.000
power of performed test with α = 0.05 for diet	1.000
power of performed test with α = 0.05 for time × genotype	0.837
power of performed test with α = 0.05 for time × diet	1.000
power of performed test with α = 0.05 for genotype × diet	0.050

Table E.7: Statistical analysis of body fat in female animals

Three-way ANOVA with Holm-Sidak post-test; DF: degrees of freedom; ΣS: sum of squares; MS: mean square; DM: difference of means; *F*: critical value of *F*-statistic; *t*: critical value of *t*-statistic; *p*: significance level, printed in green when significant (≤ 0.05); wt: wild type (all animals not carrying *p48* $^{+/Cre}$ and *Kras* $^{+/LSL-G12D}$ alleles at the same time).

main effects

source of variation	DF	ΣS	MS	*F*	*p*
time	3	4 183.448	1 394.483	37.147	< 0.001
genotype	1	909.901	909.901	24.238	< 0.001
diet	1	4 520.685	4 520.685	120.423	< 0.001
time × genotype	3	184.831	61.610	1.641	0.185
time × diet	3	1 854.806	618.269	16.470	< 0.001
genotype × diet	1	246.921	246.921	6.578	0.012
time × genotype × diet	3	24.675	8.255	0.219	0.883
Residual	**96**	**3 603.847**	**37.540**		
Total	**111**	**15 508.330**	**139.715**		

pairwise multiple comparison procedures (Holm-Sidak method)

factor	comparison	DM	*t*	*p*
genotype	wt vs. *p48* $^{+/Cre}$*; Kras* $^{+/LSL-G12D}$	5.735	4.923	< 0.001
diet	LFD vs. HFD	12.782	10.974	< 0.001
diet within wt	LFD vs. HFD	15.770	9.630	< 0.001
diet within *p48* $^{+/Cre}$*; Kras* $^{+/LSL-G12D}$	LFD vs. HFD	9.765	5.911	< 0.001
genotype within LFD	wt vs. *p48* $^{+/Cre}$*; Kras* $^{+/LSL-G12D}$	2.747	1.661	0.100
genotype within HFD	wt vs. *p48* $^{+/Cre}$*; Kras* $^{+/LSL-G12D}$	8.722	5.318	< 0.001
diet at week 0	LFD vs. HFD	0.822	0.360	0.719
diet at week 3	LFD vs. HFD	10.758	4.720	< 0.001
diet at week 7	LFD vs. HFD	15.875	6.965	< 0.001
diet at week 11	LFD vs. HFD	23.675	9.568	< 0.001

power of performed test with α = 0.05 for time	1.000
power of performed test with α = 0.05 for genotype	0.999
power of performed test with α = 0.05 for diet	1.000
power of performed test with α = 0.05 for time × genotype	0.175
power of performed test with α = 0.05 for time × diet	1.000
power of performed test with α = 0.05 for genotype × diet	0.649

Table E.8: Statistical analysis of perigonadal fat weight

Three-way ANOVA with Holm-Sidak post-test; DF: degrees of freedom; ΣS: sum of squares; MS: mean square; DM: difference of means; *F*: critical value of *F*-statistic; *t*: critical value of *t*-statistic; *p*: significance level, printed in green when significant (≤ 0.05); wt: wild type (all animals not carrying *p48 +/Cre* and *Kras +/LSL-G12D* alleles at the same time).

main effects

source of variation	DF	ΣS	MS	*F*	*p*
sex	1	0.837	0.837	1,737	0.195
genotype	1	3.117	3.117	6.469	0.015
diet	1	23.225	23.225	48.207	< 0.001
sex × genotype	1	0.052	0.052	0.109	0.743
sex × diet	1	2.697	2.697	5.599	0.023
genotype × diet	1	0.018	0.018	0.038	0.847
sex × genotype × diet	1	1.289	1.289	2.676	0.110
Residual	**41**	**19.752**	**0.482**		
Total	**48**	**55.740**	**1.161**		

pairwise multiple comparison procedures (Holm-Sidak method)

factor	comparison	DM	*t*	*p*
sex	♂ vs. ♀	0.280	1.318	0.195
genotype	wt vs. *p48 +/Cre; Kras +/LSL-G12D*	0.541	2.543	0.015
diet	LFD vs. HFD	1.477	6.943	< 0.001
sex within LFD	♂ vs. ♀	0.784	2.495	0.017
sex within HFD	♂ vs. ♀	0.223	0.777	0.442
diet within ♂	LFD vs. HFD	0.974	3.104	0.003
diet within ♀	LFD vs. HFD	1.980	6.891	< 0.001

power of performed test with α = 0.05 for sex	0.125
power of performed test with α = 0.05 for genotype	0.627
power of performed test with α = 0.05 for diet	1.000
power of performed test with α = 0.05 for sex × genotype	0.050
power of performed test with α = 0.05 for sex × diet	0.547
power of performed test with α = 0.05 for genotype × diet	0.050

Table E.9: Statistical analysis of relative perigonadal fat weight

Three-way ANOVA with Holm-Sidak post-test; DF: degrees of freedom; ΣS: sum of squares; MS: mean square; DM: difference of means; *F*: critical value of *F*-statistic; *t*: critical value of *t*-statistic; *p*: significance level, printed in green when significant ($\lesssim 0.05$); wt: wild type (all animals not carrying *p48* $^{+/Cre}$ and *Kras* $^{+/LSL-G12D}$ alleles at the same time).

main effects

source of variation	DF	ΣS	MS	*F*	*p*
sex	1	50.257	50.257	0.327	0.571
genotype	1	845.489	845.489	5.501	0.024
diet	1	7 788.314	7 788.314	50.669	< 0.001
sex × genotype	1	193.738	193.738	1.260	0.268
sex × diet	1	2 202.455	2 202.455	14.329	< 0.001
genotype × diet	1	56.502	56.502	0.368	0.548
sex × genotype × diet	1	901.734	901.734	5.866	0.020
Residual	**41**	**6 302.085**	**153.709**		
Total	**48**	**19 612.242**	**408.588**		

pairwise multiple comparison procedures (Holm-Sidak method)

factor	comparison	DM	*t*	*p*
sex	♂ vs. ♀	2.173	0.572	0.571
genotype	wt vs. *p48* $^{+/Cre}$; *Kras* $^{+/LSL-G12D}$	8.911	2.345	0.024
diet	LFD vs. HFD	27.047	7.118	< 0.001

Three-way interaciton term analysis

Evaluated diet × sex across levels of genotype:
diet × sex interaction in wt: $p = 0.007$
diet × sex interaction in *p48* $^{+/Cre}$; *Kras* $^{+/LSL-G12D}$: $p = 0.356$

Simple, simple main effect in wt

The difference in the mean values among the different levels of diet evaluated within ♀ wt is greater than would be expected by chance ($p < 0.001$).

pairwise multiple comparison procedures (Holm-Sidak method)

factor	comparison	DM	*t*	*p*
sex within LFD wt	♂ vs. ♀	21.493	3.243	0.002
sex within HFD wt	♂ vs. ♀	25.679	4.284	< 0.001
diet within ♀ wt	LFD vs. HFD	48.329	7.293	< 0.001

Simple main effect tests in *p48* $^{+/Cre}$; *Kras* $^{+/LSL-G12D}$

The difference in the mean values among the different levels of diet evaluated within *p48* $^{+/Cre}$; *Kras* $^{+/LSL-G12D}$ (averaging over levels of sex) is greater than would be expected by chance ($p < 0.001$).

pairwise multiple comparison procedures (Holm-Sidak method)

factor	comparison	DM	*t*	*p*
diet within *p48* $^{+/Cre}$; *Kras* $^{+/LSL-G12D}$	LFD vs. HFD	29.350	4.775	< 0.001

power of performed test with $\alpha = 0.05$ for sex	0.050
power of performed test with $\alpha = 0.05$ for genotype	0.538
power of performed test with $\alpha = 0.05$ for diet	1.000
power of performed test with $\alpha = 0.05$ for sex × genotype	0.075
power of performed test with $\alpha = 0.05$ for sex × diet	0.961
power of performed test with $\alpha = 0.05$ for genotype × diet	0.050

Table E.10: Statistical analysis of liver weight

Three-way ANOVA with Holm-Sidak post-test; DF: degrees of freedom; ΣS: sum of squares; MS: mean square; DM: difference of means; *F*: critical value of *F*-statistic; *t*: critical value of *t*-statistic; *p*: significance level, printed in green when significant (≤ 0.05); wt: wild type (all animals not carrying *p48 +/Cre* and *Kras +/LSL-G12D* alleles at the same time).

main effects

source of variation	DF	ΣS	MS	*F*	*p*
sex	1	5.604	5.604	26.627	< 0.001
genotype	1	1.876	1.876	8.915	< 0.001
diet	1	1.098	1.098	5.219	0.027
sex × genotype	1	1.577	1.577	7.494	0.009
sex × diet	1	0.347	0.347	1.649	0.206
genotype × diet	1	0.152	0.152	0.722	0.400
sex × genotype × diet	1	0.510	0.510	2.422	0.127
Residual	**42**	**8.840**	**0.210**		
Total	**49**	**27.516**	**0.562**		

pairwise multiple comparison procedures (Holm-Sidak method)

factor	comparison	DM	*t*	*p*
sex	♂ vs. ♀	0.717	5.160	< 0.001
genotype	wt vs. *p48 +/Cre; Kras +/LSL-G12D*	0.415	2.986	0.005
diet	LFD vs. HFD	0.318	2.284	0.027
sex within wt	♂ vs. ♀	1.098	6.641	< 0.001
sex within *p48 +/Cre; Kras +/LSL-G12D*	♂ vs. ♀	0.337	1.507	0.139
genotype within ♂	wt vs. *p48 +/Cre; Kras +/LSL-G12D*	0.796	3.838	< 0.001
genotype within ♀	wt vs. *p48 +/Cre; Kras +/LSL-G12D*	0.035	0.186	0.853

power of performed test with α = 0.05 for sex	1.000
power of performed test with α = 0.05 for genotype	0.798
power of performed test with α = 0.05 for diet	0.510
power of performed test with α = 0.05 for sex × genotype	0.708
power of performed test with α = 0.05 for sex × diet	0.115
power of performed test with α = 0.05 for genotype × diet	0.050

Table E.11: Statistical analysis of relative liver weight

Three-way ANOVA with Holm-Sidak post-test; DF: degrees of freedom; ΣS: sum of squares; MS: mean square; DM: difference of means; *F*: critical value of *F*-statistic; *t*: critical value of *t*-statistic; *p*: significance level, printed in green when significant (≤ 0.05); wt: wild type (all animals not carrying *p48* $^{+/Cre}$ and *Kras* $^{+/LSL-G12D}$ alleles at the same time).

main effects

source of variation	DF	ΣS	MS	*F*	*p*
sex	1	303.498	303.498	6.024	0.018
genotype	1	86.769	86.769	1.722	0.197
diet	1	784.813	784.813	15.578	< 0.001
sex × genotype	1	352.281	352.281	6.993	0.011
sex × diet	1	297.683	297.683	5.909	0.019
genotype × diet	1	2.579	2.579	0.051	0.822
sex × genotype × diet	1	177.426	177.426	3.522	0.068
Residual	**42**	**2 115.941**	**50.380**		
Total	**49**	**4 685.693**	**95.626**		

pairwise multiple comparison procedures (Holm-Sidak method)

factor	comparison	DM	*t*	*p*
sex	♂ vs. ♀	5.280	2.454	0.018
genotype	wt vs. *p48* $^{+/Cre}$*; Kras* $^{+/LSL-G12D}$	2.823	1.312	0.197
diet	LFD vs. HFD	8.490	3.947	< 0.001
sex within wt	♂ vs. ♀	10.968	4.288	< 0.001
sex within *p48* $^{+/Cre}$*; Kras* $^{+/LSL-G12D}$	♂ vs. ♀	0.409	0.118	0.907
sex within LFD	♂ vs. ♀	0.051	0.016	0.987
sex within HFD	♂ vs. ♀	10.508	3.581	< 0.001
genotype within ♂	wt vs. *p48* $^{+/Cre}$*; Kras* $^{+/LSL-G12D}$	8.511	2.653	0.011
genotype within ♀	wt vs. *p48* $^{+/Cre}$*; Kras* $^{+/LSL-G12D}$	2.865	1.000	0.323
diet within ♂	LFD vs. HFD	3.261	1.017	0.315
diet within ♀	LFD vs. HFD	13.719	4.786	< 0.001

power of performed test with α = 0.05 for sex	0.588
power of performed test with α = 0.05 for genotype	0.123
power of performed test with α = 0.05 for diet	0.974
power of performed test with α = 0.05 for sex × genotype	0.670
power of performed test with α = 0.05 for sex × diet	0.577
power of performed test with α = 0.05 for genotype × diet	0.050

Table E.12: Statistical analysis of fasting glucose at 4 weeks

Three-way ANOVA with Holm-Sidak post-test; DF: degrees of freedom; ΣS: sum of squares; MS: mean square; DM: difference of means; *F*: critical value of *F*-statistic; *t*: critical value of *t*-statistic; *p*: significance level, printed in green when significant (≤ 0.05); wt: wild type (all animals not carrying *p48 +/Cre* and *Kras +/LSL-G12D* alleles at the same time).

main effects

source of variation	DF	ΣS	MS	*F*	*p*
sex	1	33.995	33.995	0.056	0.814
genotype	1	2 910.365	2 910.365	4.766	0.034
diet	1	9 214.140	9 214.140	15.098	< 0.001
sex × genotype	1	135.904	135.904	0.223	0.639
sex × diet	1	586.829	586.829	0.961	0.332
genotype × diet	1	230.635	230.635	0.378	0.542
sex × genotype × diet	1	199.940	199.940	0.327	0.057
Residual	**50**	**30 532.799**	**610.656**		
Total	**57**	**48 576.224**	**852.214**		

pairwise multiple comparison procedures (Holm-Sidak method)

factor	comparison	DM	*t*	*p*
sex	♂ vs. ♀	1.636	0.236	0.814
genotype	wt vs. *p48 +/Cre; Kras +/LSL-G12D*	15.136	2.183	0.034
diet	LFD vs. HFD	26.931	3.884	< 0.001

power of performed test with α = 0.05 for sex	0.050
power of performed test with α = 0.05 for genotype	0.466
power of performed test with α = 0.05 for diet	0.971
power of performed test with α = 0.05 for sex × genotype	0.050
power of performed test with α = 0.05 for sex × diet	0.050
power of performed test with α = 0.05 for genotype × diet	0.050

Table E.13: Statistical analysis of fasting glucose at 8 weeks

Three-way ANOVA with Holm-Sidak post-test; DF: degrees of freedom; ΣS: sum of squares; MS: mean square; DM: difference of means; *F*: critical value of *F*-statistic; *t*: critical value of *t*-statistic; *p*: significance level, printed in green when significant (≤ 0.05); wt: wild type (all animals not carrying *p48* $^{+/Cre}$ and *Kras* $^{+/LSL-G12D}$ alleles at the same time).

main effects

source of variation	DF	ΣS	MS	*F*	*p*
sex	1	1 396.657	1 396.657	5.326	0.026
genotype	1	4 321.869	4 321.869	16.482	< 0.001
diet	1	11 077.399	11 077.399	42.245	< 0.001
sex × genotype	1	1 393.664	1 393.664	5.315	0.026
sex × diet	1	1 748.876	1 748.876	6.670	0.013
genotype × diet	1	2 523.466	2 523.466	9.624	< 0.001
sex × genotype × diet	1	1 194.880	1 194.880	4.557	0.038
Residual	**44**	**11 537.470**	**262.215**		
Total	**51**	**49 807.077**	**976.609**		

pairwise multiple comparison procedures (Holm-Sidak method)

factor	comparison	DM	*t*	*p*
sex	♂ vs. ♀	11.103	2.308	0.026
genotype	wt vs. *p48* $^{+/Cre}$*; Kras* $^{+/LSL-G12D}$	19.532	4.060	< 0.001
diet	LFD vs. HFD	31.270	6.500	< 0.001

Three-way interaciton term analysis

Evaluated diet × sex across levels of genotype:
diet × sex interaction in wt: $p = 0.001$
diet × sex interaction in *p48* $^{+/Cre}$*; Kras* $^{+/LSL-G12D}$: $p = 0.902$

Simple, simple main effect in wt

The difference in the mean values among the different levels of diet evaluated within ♂ wt is greater than would be expected by chance ($p < 0.001$).

pairwise multiple comparison procedures (Holm-Sidak method)

factor	comparison	DM	*t*	*p*
sex within HFD wt	♂ vs. ♀	44.890	5.734	< 0.001
diet within ♂ wt	LFD vs. HFD	68.890	8.799	< 0.001
diet within ♀ wt	LFD vs. HFD	23.500	2.715	0.009

power of performed test with $\alpha = 0.05$ for sex	0.522
power of performed test with $\alpha = 0.05$ for genotype	0.982
power of performed test with $\alpha = 0.05$ for diet	1.000
power of performed test with $\alpha = 0.05$ for sex × genotype	0.521
power of performed test with $\alpha = 0.05$ for sex × diet	0.645
power of performed test with $\alpha = 0.05$ for genotype × diet	0.834

Table E.14: Statistical analysis of random-fed glucose at 12 weeks

Three-way ANOVA with Holm-Sidak post-test; DF: degrees of freedom; ΣS: sum of squares; MS: mean square; DM: difference of means; *F*: critical value of *F*-statistic; *t*: critical value of *t*-statistic; *p*: significance level, printed in green when significant (≤ 0.05); wt: wild type (all animals not carrying *p48 +/Cre* and *Kras +/LSL-G12D* alleles at the same time).

main effects

source of variation	DF	ΣS	MS	*F*	*p*
sex	1	60.902	60.902	0.040	0.843
genotype	1	4 841.720	4 841.720	3.176	0.082
diet	1	6 043.120	6 043.120	3.964	0.053
sex × genotype	1	0.152	0.152	0.0000999	0.992
sex × diet	1	93.639	93.639	0.0614	0.805
genotype × diet	1	5 714.254	5 714.254	3.749	0.060
sex × genotype × diet	1	512.191	512.191	0.375	0.543
Residual	**42**	**64 022.845**	**1 524.353**		
Total	**49**	**89 493.120**	**1 826.390**		

power of performed test with α = 0.05 for sex	0.050
power of performed test with α = 0.05 for genotype	0.287
power of performed test with α = 0.05 for diet	0.376
power of performed test with α = 0.05 for sex × genotype	0.352
power of performed test with α = 0.05 for sex × diet	0.050
power of performed test with α = 0.05 for genotype × diet	0.050

Table E.15: Statistical analysis of fasting insulin at 4 weeks

Three-way ANOVA with Holm-Sidak post-test; DF: degrees of freedom; ΣS: sum of squares; MS: mean square; DM: difference of means; *F*: critical value of *F*-statistic; *t*: critical value of *t*-statistic; *p*: significance level, printed in green when significant (≤ 0.05); wt: wild type (all animals not carrying *p48 +/Cre* and *Kras +/LSL-G12D* alleles at the same time).

main effects

source of variation	DF	ΣS	MS	*F*	*p*
sex	1	0.232	0.232	1.721	0.197
genotype	1	0.062	0.062	0.457	0.503
diet	1	0.126	0.126	0.935	0.503
sex × genotype	1	0.003	0.003	0.022	0.883
sex × diet	1	0.123	0.123	0.910	0.346
genotype × diet	1	0.020	0.020	0.149	0.702
sex × genotype × diet	1	0.044	0.044	0.326	0.572
Residual	**38**	**5.117**	**0.135**		
Total	**45**	**6.015**	**0.134**		

power of performed test with α = 0.05 for sex	0.123
power of performed test with α = 0.05 for genotype	0.050
power of performed test with α = 0.05 for diet	0.050
power of performed test with α = 0.05 for sex × genotype	0.050
power of performed test with α = 0.05 for sex × diet	0.050
power of performed test with α = 0.05 for genotype × diet	0.050

Table E.16: Statistical analysis of fasting insulin at 8 weeks

Three-way ANOVA with Holm-Sidak post-test; DF: degrees of freedom; ΣS: sum of squares; MS: mean square; DM: difference of means; *F*: critical value of *F*-statistic; *t*: critical value of *t*-statistic; *p*: significance level, printed in green when significant (≤ 0.05); wt: wild type (all animals not carrying *p48* $^{+/Cre}$ and *Kras* $^{+/LSL-G12D}$ alleles at the same time).

main effects

source of variation	DF	ΣS	MS	*F*	*p*
sex	1	0.664	0.664	3.253	0.080
genotype	1	0.818	0.818	4.008	0.053
diet	1	0.005	0.005	0.026	0.872
sex × genotype	1	0.771	0.771	3.775	0.060
sex × diet	1	0.006	0.006	0.032	0.860
genotype × diet	1	0.024	0.024	0.117	0.734
sex × genotype × diet	1	0.058	0.058	0.283	0.598
Residual	**36**	**7.352**	**0.204**		
Total	**43**	**10.954**	**0.255**		

power of performed test with α = 0.05 for sex	0.294
power of performed test with α = 0.05 for genotype	0.378
power of performed test with α = 0.05 for diet	0.050
power of performed test with α = 0.05 for sex × genotype	0.353
power of performed test with α = 0.05 for sex × diet	0.050
power of performed test with α = 0.05 for genotype × diet	0.050

Table E.17: Statistical analysis of random-fed insulin at 12 weeks

Three-way ANOVA with Holm-Sidak post-test; DF: degrees of freedom; ΣS: sum of squares; MS: mean square; DM: difference of means; *F*: critical value of *F*-statistic; *t*: critical value of *t*-statistic; *p*: significance level, printed in green when significant (≤ 0.05); wt: wild type (all animals not carrying *p48* $^{+/Cre}$ and *Kras* $^{+/LSL-G12D}$ alleles at the same time).

main effects

source of variation	DF	ΣS	MS	*F*	*p*
sex	1	1 731.990	1 731.990	1.292	0.262
genotype	1	1 611.692	1 611.692	1.202	0.279
diet	1	1 883.171	1 883.171	1.405	0.243
sex × genotype	1	1 688.362	1 688.362	1.260	0.268
sex × diet	1	1 452.859	1 452.859	1.084	0.304
genotype × diet	1	1 408.133	1 408.133	1.051	0.311
sex × genotype × diet	1	1 536.438	1 536.438	1.146	0.290
Residual	**42**	**56 293.980**	**1 340.333**		
Total	**49**	**75 866.930**	**1 548.305**		

power of performed test with α = 0.05 for sex	0.0778
power of performed test with α = 0.05 for genotype	0.0685
power of performed test with α = 0.05 for diet	0.0896
power of performed test with α = 0.05 for sex × genotype	0.0745
power of performed test with α = 0.05 for sex × diet	0.0562
power of performed test with α = 0.05 for genotype × diet	0.0528

F Microarray of Capan-1 cells

Table F.1: Overrepresentation analysis for TBL1X knockdown on GOPB pathways

Pathways belonging to various cell functions were obtained from public external databases (`http://www.geneontology.org/GO`) and a Fisher's exact test was performed to detect the significantly regulated pathways. Enrichment score: measure of pathway cluster enrichment over the other clusters; count: number of regulated genes within the pathway; raw p value: significance of pathway enrichment; list total: number of genes within the analyzed list of target genes having at least one GOBP annotation; pop hits: number of genes available on the entire microarray, annotated by the considered GOBP category or annotation cluster; pop total: number of genes available on the entire microarray having at least one GOBP annotation; Bonferroni: adjusted p value by Bonferroni method; Benjamini: adjusted p value by Benjamini method; FDR: false discovery rate.

Annotation Cluster 1	**Enrichment Score: 4.024**									
GOBP term	**count**	**%**	**raw p value**	**list total**	**pop hits**	**pop total**	**fold enrichment**	**Bonferroni**	**Benjamini**	**FDR [%]**
GO:0007049 cell cycle	71	8.17	8.05×10^{-8}	635	776	13528	1.949	2.18×10^{-4}	2.18×10^{-4}	1.43×10^{-4}
GO:0000278 mitotic cell cycle	39	4.49	4.61×10^{-6}	635	370	13528	2.246	0.0124	0.0062	0.0082
GO:0022403 cell cycle phase	42	4.83	4.82×10^{-6}	635	414	13528	2.161	0.0129	0.0043	0.0086
GO:0022402 cell cycle process	52	5.98	5.15×10^{-6}	635	565	13528	1.961	0.0138	0.0035	0.0092
GO:0051329 interphase of mitotic cell cycle	16	1.84	8.65×10^{-5}	635	103	13528	3.309	0.2087	0.0257	0.1539
GO:0051325 interphase	16	1.84	1.21×10^{-4}	635	106	13528	3.216	0.2786	0.0321	0.2146
GO:0048285 organelle fission	24	2.76	4.77×10^{-4}	635	229	13528	2.233	0.7250	0.0945	0.8459
GO:0007067 mitosis	23	2.65	6.66×10^{-4}	635	220	13528	2.227	0.8349	0.1207	1.1782
GO:0000280 nuclear division	23	2.65	6.66×10^{-4}	635	220	13528	2.227	0.8349	0.1207	1.1782
GO:0000087 M phase of mitotic cell cycle	23	2.65	8.47×10^{-4}	635	224	13528	2.187	0.8991	0.1418	1.4977
GO:0000082 G1/S transition of mitotic cell cycle	10	1.15	0.0011	635	56	13528	3.804	0.9467	0.1674	1.9101
GO:0051301 cell division	27	3.11	0.0015	635	295	13528	1.950	0.9833	0.2032	2.6550
GO:0000279 M phase	29	3.34	0.0017	635	329	13528	1.878	0.9902	0.2162	2.9992

Table F.2: Overrepresentation analysis for TBL1X knockdown on KEGG pathways

Pathways belonging to various cell functions were obtained from public external databases (`http://www.genome.jp/kegg/`) and a Fisher's exact test was performed to detect the significantly regulated pathways. count: number of regulated genes within the pathway; raw *p* value: significance of pathway enrichment; list total: number of genes within the analyzed list of target genes having at least one KEGG annotation; pop hits: number of genes available on the entire microarray, annotated by the considered KEGG category or annotation cluster; pop total: number of genes available on the entire microarray having at least one KEGG annotation; Bonferroni: adjusted *p* value by Bonferroni method; Benjamini: adjusted *p* value by Benjamini method; FDR: false discovery rate.

KEGG pathway	count	%	raw *p* value	list total	pop hits	pop total	fold enrichment	Bonferroni	Benjamini	FDR [%]
hsa04115 p53 signaling pathway	15	1.46	1.74×10^{-5}	286	68	5085	3.922	0.0030	0.0030	0.0213
hsa04120 ubiquitin mediated proteolysis	15	1.46	0.0205	286	137	5085	1.947	0.9732	0.7007	22.3944
hsa04110 cell cycle	14	1.37	0.0220	286	125	5085	1.991	0.9795	0.6218	23.8511
hsa04144 endocytosis	18	1.76	0.0279	286	184	5085	1.739	0.9929	0.6279	29.2695
hsa00564 glycerophospholipid metabolism	9	0.88	0.0350	286	68	5085	2.353	0.9980	0.6463	35.393
hsa04010 MAPK signaling pathway	23	2.25	0.0426	286	267	5085	1.532	0.9995	0.6629	41.3316

Table F.3: Overrepresentation analysis for TBL1XR1 knockdown on KEGG pathways

Pathways belonging to various cell functions were obtained from public external databases (`http://www.genome.jp/kegg/`) and a Fisher's exact test was performed to detect the significantly regulated pathways. count: number of regulated genes within the pathway; raw *p* value: significance of pathway enrichment; list total: number of genes within the analyzed list of target genes having at least one KEGG annotation; pop hits: number of genes available on the entire microarray, annotated by the considered KEGG category or annotation cluster; pop total: number of genes available on the entire microarray having at least one KEGG annotation; Bonferroni: adjusted *p* value by Bonferroni method; Benjamini: adjusted *p* value by Benjamini method; FDR: false discovery rate.

KEGG pathway	count	%	raw *p* value	list total	pop hits	pop total	fold enrichment	Bonferroni	Benjamini	FDR [%]
hsa04115 p53 signaling pathway	10	1.18	0.0053	249	68	5085	3.003	0.5885	0.5885	6.2924
hsa04350 TGFβ signaling pathway	11	1.3	0.0092	249	87	5085	2.582	0.786	0.5374	10.6721
hsa04114 oocyte meiosis	12	1.42	0.0176	249	110	5085	2.228	0.9474	0.6253	19.3929
hsa04070 phosphatidylinositol signaling system	9	1.06	0.0266	249	74	5085	2.484	0.9887	0.6737	27.957
hsa04910 insulin signaling pathway	13	1.53	0.0310	249	135	5085	1.967	0.9947	0.6487	31.8110
hsa04310 Wnt signaling pathway	14	1.65	0.0319	249	151	5085	1.893	0.9954	0.5920	32.5494
hsa04110 cell cycle	12	1.42	0.0405	249	125	5085	1.960	0.9989	0.5756	39.4626
hsa05200 pathways in cancer	24	2.83	0.0475	249	328	5085	1.494	0.9997	0.5545	44.6651

Table F.4: GSEA for TBL1X knockdown on KEGG pathways

Gene Set Enrichment Analysis (GSEA), was used to determine whether defined lists (or sets) of genes exhibit a statistically significant bias in their distribution within a ranked gene list. Pathways belonging to various cell functions such as cell cycle or apoptosis were obtained from public external databases (KEGG, `http://www.genome.jp/kegg/`). 140 of 204 gene sets were downregulated in TBL1X knockdown compared to shNC-treated cells. Of these, 24 were significantly enriched at an FDR < 25 % and are shown in this table. A guide to interpret GSEA results is available at `http://www.broadinstitute.org/gsea/doc/GSEAUserGuideFrame.html?_Interpreting_GSEA_Results`

gene set	size	enrichment score	normalized enrichment score	nominal *p* value	FDR *q* value	FWER *p* value	rank at max
hsa04914 progesterone-mediated oocyte maturation	81	-0.5778	-1.8797	0.0000	0.1155	0.098	1998
hsa04110 cell cycle	119	-0.5344	-1.8163	0.0000	0.1392	0.221	2217
hsa05212 pancreatic cancer	69	-0.5710	-1.7736	0.0065	0.1522	0.327	2330
hsa05142 chagas disease (american trypanosomiasis)	99	-0.5198	-1.7390	0.0016	0.1615	0.437	2897
hsa05222 small cell lung cancer	82	-0.5289	-1.7110	0.0000	0.1749	0.545	717
hsa05218 melanoma	71	-0.5296	-1.6756	0.0064	0.2016	0.660	1429
hsa04622 RIG-I-like receptor signaling pathway	65	-0.5278	-1.6397	0.0100	0.2441	0.784	1743
hsa04662 B-cell receptor signaling pathway	74	-0.5151	-1.6367	0.0067	0.2205	0.798	1586
hsa05131 shigellosis	57	-0.5376	-1.6349	0.0083	0.1990	0.802	2388
hsa05215 prostate cancer	87	-0.4971	-1.6235	0.0061	0.1977	0.830	3040
hsa04360 axon guidance	127	-0.4658	-1.6156	0.0047	0.1911	0.841	2503
hsa04114 oocyte meiosis	105	-0.4812	-1.6114	0.0047	0.1811	0.855	1848
hsa04621 NOD-like receptor signaling pathway	56	-0.5253	-1.6087	0.0066	0.1706	0.862	3040
hsa05221 acute myeloid leukemia	56	-0.5232	-1.5963	0.0215	0.1734	0.880	1448
hsa04660 T-cell receptor signaling pathway	107	-0.4647	-1.5775	0.0079	0.1879	0.914	1486
hsa04810 regulation of actin cytoskeleton	207	-0.4262	-1.5730	0.0041	0.1821	0.920	2388
hsa00604 glycosphingolipid biosynthesis – ganglio series	15	-0.6566	-1.5588	0.0509	0.1907	0.932	3505
hsa00564 glycerophospholipid metabolism	74	-0.4870	-1.5507	0.0177	0.1920	0.946	1592
hsa04620 Toll-like receptor signaling pathway	94	-0.4638	-1.5504	0.0143	0.1824	0.946	3037
hsa05145 toxoplasmosis	122	-0.4516	-1.5457	0.0148	0.1792	0.951	1871
hsa04210 apoptosis	85	-0.4758	-1.5275	0.0146	0.1951	0.975	717
hsa05100 bacterial invasion of epithelial cells	68	-0.4792	-1.5094	0.0302	0.2137	0.990	1453
hsa04141 protein processing in endoplasmic reticulum	159	-0.4236	-1.5054	0.0105	0.2100	0.990	2379
hsa05200 pathways in cancer	318	-0.3842	-1.4864	0.0013	0.2301	0.995	1783

Table F.5: GSEA for TBL1XR1 knockdown on KEGG pathways

Gene Set Enrichment Analysis (GSEA), was used to determine whether defined lists (or sets) of genes exhibit a statistically significant bias in their distribution within a ranked gene list. Pathways belonging to various cell functions such as cell cycle or apoptosis were obtained from public external databases (KEGG, `http://www.genome.jp/kegg/`). 147 of 204 gene sets were downregulated in TBL1XR1 knockdown compared to shNC-treated cells. Of these, 43 were significantly enriched at an FDR < 25 % and the top 25 are shown in this table. A guide to interpret GSEA results is available at `http://www.broadinstitute.org/gsea/doc/GSEAUserGuideFrame.html?_Interpreting_GSEA_Results`

gene set	size	enrichment score	normalized enrichment score	nominal *p* value	FDR *q* value	FWER *p* value	rank at max
hsa04810 regulation of actin cytoskeleton	207	-0.5136	-2.0129	0.0000	0.0128	0.011	1773
hsa04971 gastric acid secretion	71	-0.5899	-1.9861	0.0000	0.0126	0.022	2388
hsa05212 pancreatic cancer	69	-0.5584	-1.8920	0.0015	0.0303	0.078	1445
hsa04350 TGFβ signaling pathway	82	-0.5303	-1.8628	0.0015	0.0322	0.110	1083
hsa00450 selenocompound metabolism	17	-0.6975	-1.7921	0.0091	0.0650	0.252	1804
hsa04510 focal adhesion	197	-0.4490	-1.7500	0.0000	0.0886	0.380	1773
hsa04270 vascular smooth muscle contraction	108	-0.4823	-1.7334	0.0000	0.0884	0.430	2005
hsa04972 pancreatic secretion	91	-0.4955	-1.7308	0.0000	0.0795	0.441	2395
hsa03060 protein export	23	-0.6204	-1.7224	0.0139	0.0756	0.460	1886
hsa00360 phenylalanine metabolism	17	-0.6664	-1.6799	0.0202	0.1026	0.596	1306
hsa05215 prostate cancer	87	-0.4758	-1.6669	0.0015	0.1081	0.652	1445
hsa05211 renal cell carcinoma	67	-0.4876	-1.6512	0.0148	0.1145	0.707	1971
hsa04664 Fc epsilon RI signaling pathway	75	-0.4724	-1.6112	0.0076	0.1500	0.823	2005
hsa04730 long-term depression	65	-0.4819	-1.6067	0.0110	0.1444	0.833	2388
hsa05220 chronic myeloid leukemia	72	-0.4631	-1.5906	0.0176	0.1539	0.878	1540
hsa04964 proximal tubule bicarbonate reclamation	23	-0.5879	-1.5886	0.0260	0.1474	0.883	64
hsa05210 colorectal cancer	62	-0.4762	-1.5786	0.0110	0.1513	0.905	1445
hsa04520 adherens junction	72	-0.4665	-1.5775	0.0154	0.1447	0.910	2553
hsa04914 progesterone-mediated oocyte maturation	81	-0.4554	-1.5771	0.0106	0.1376	0.911	2670
hsa00670 one carbon pool by folate	17	-0.6220	-1.5738	0.0374	0.1344	0.921	660
hsa05130 pathogenic escherichia coli infection	48	-0.4872	-1.5514	0.0155	0.1531	0.952	1740
hsa00910 nitrogen metabolism	23	-0.5724	-1.5435	0.0379	0.1562	0.963	1722
hsa00600 sphingolipid metabolism	36	-0.5118	-1.5236	0.0417	0.1725	0.976	1426
hsa05218 melanoma	71	-0.4454	-1.5167	0.0249	0.1747	0.980	1445
hsa04310 Wnt signaling pathway	146	-0.4000	-1.5131	0.0100	0.1718	0.981	1601

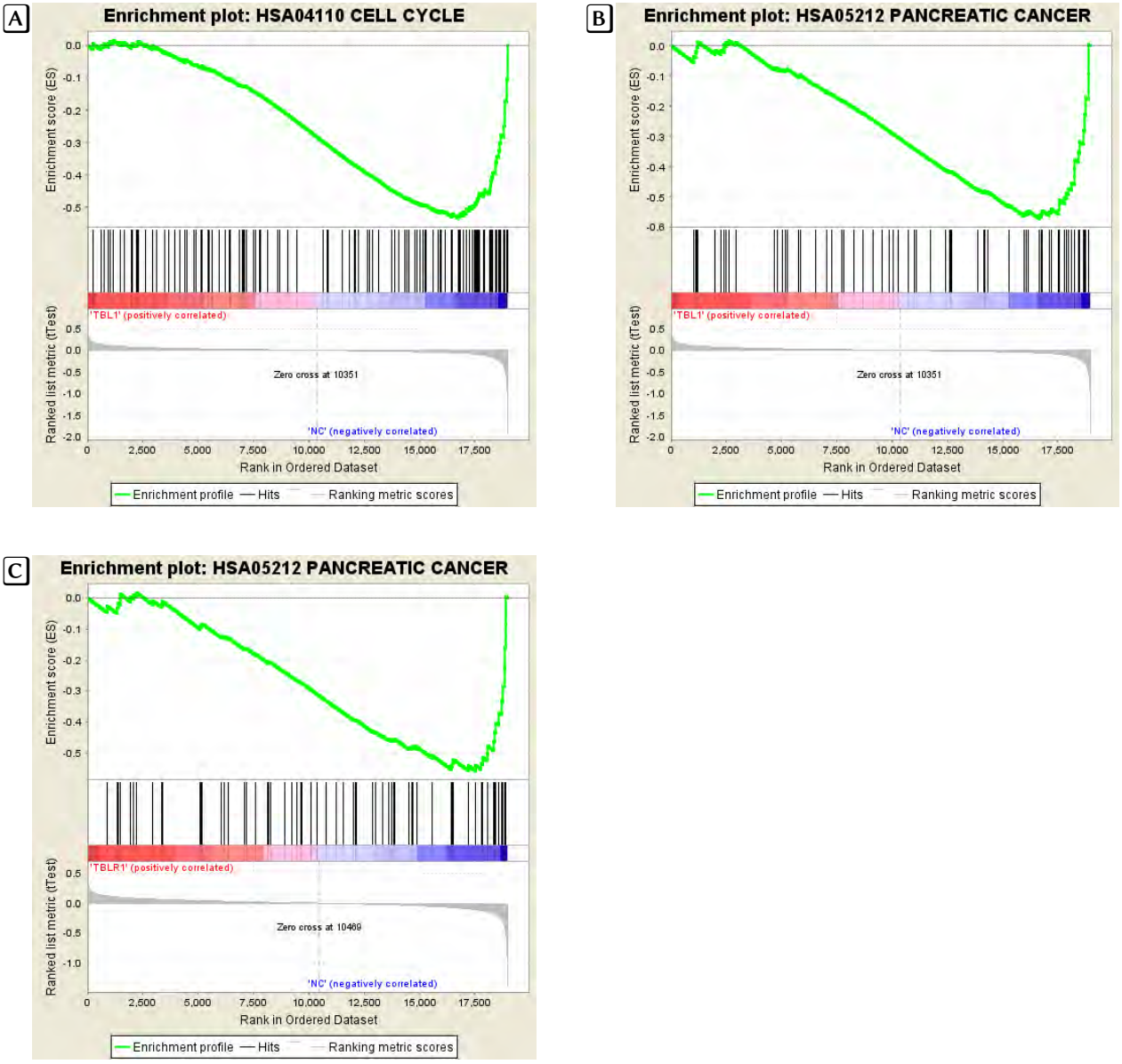

Figure F.1: Enrichment plots of GSEA analysis

Enrichment plots from GSEA for "hsa04110 cell cycle" (A) and "hsa05215 pancreatic cancer" (B) in TBL1X knockdown and for "hsa05215 pancreatic cancer" in TBL1XR1 knockdown (C). A guide to interpret GSEA results and enrichment plots is available at `http://www.broadinstitute.org/gsea/doc/GSEAUserGuideFrame.html?_Interpreting_GSEA_Results`

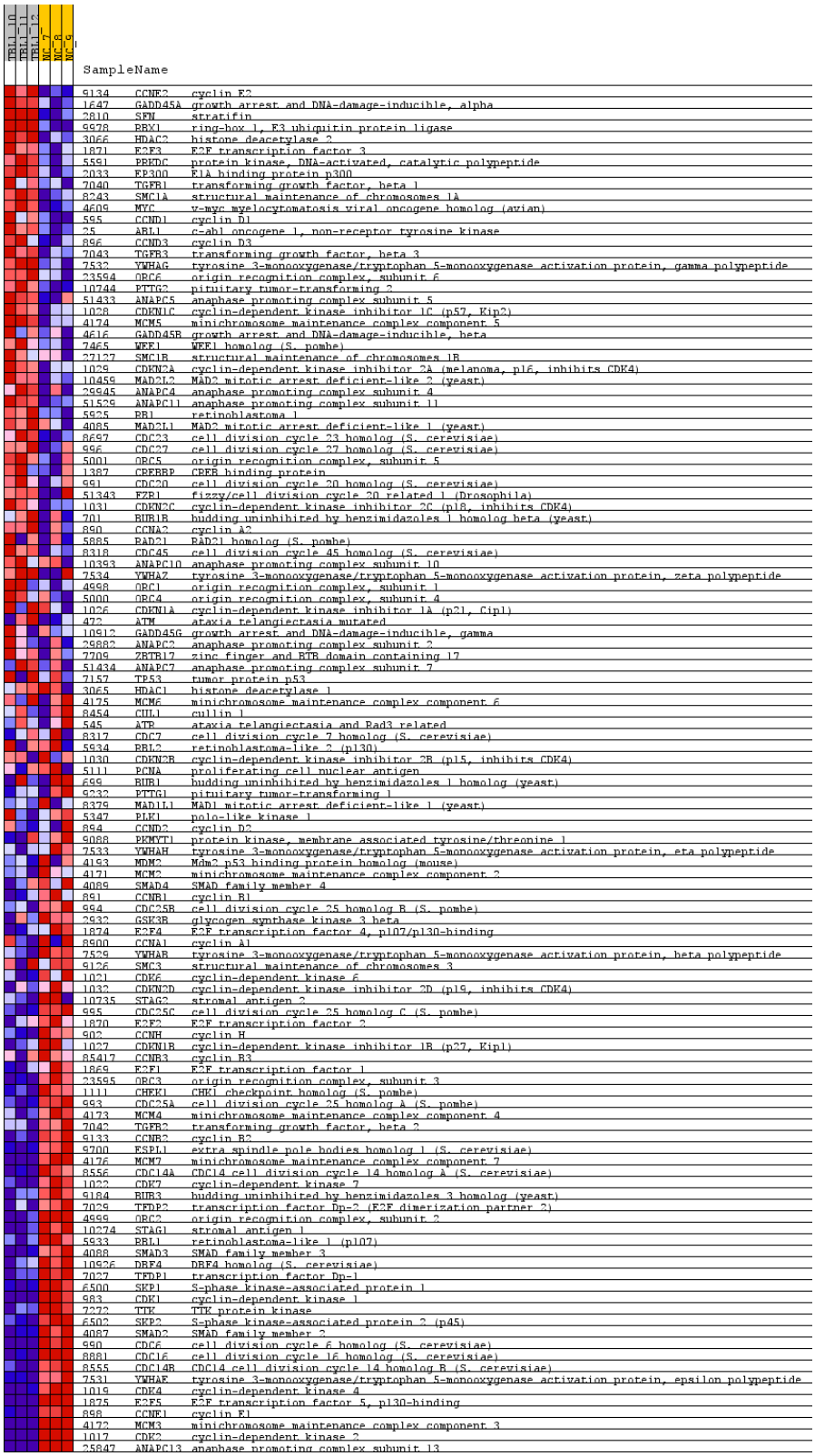

Figure F.2: Heat map from GSEA for gene set "hsa04110 cell cycle" in TBL1X knockdown

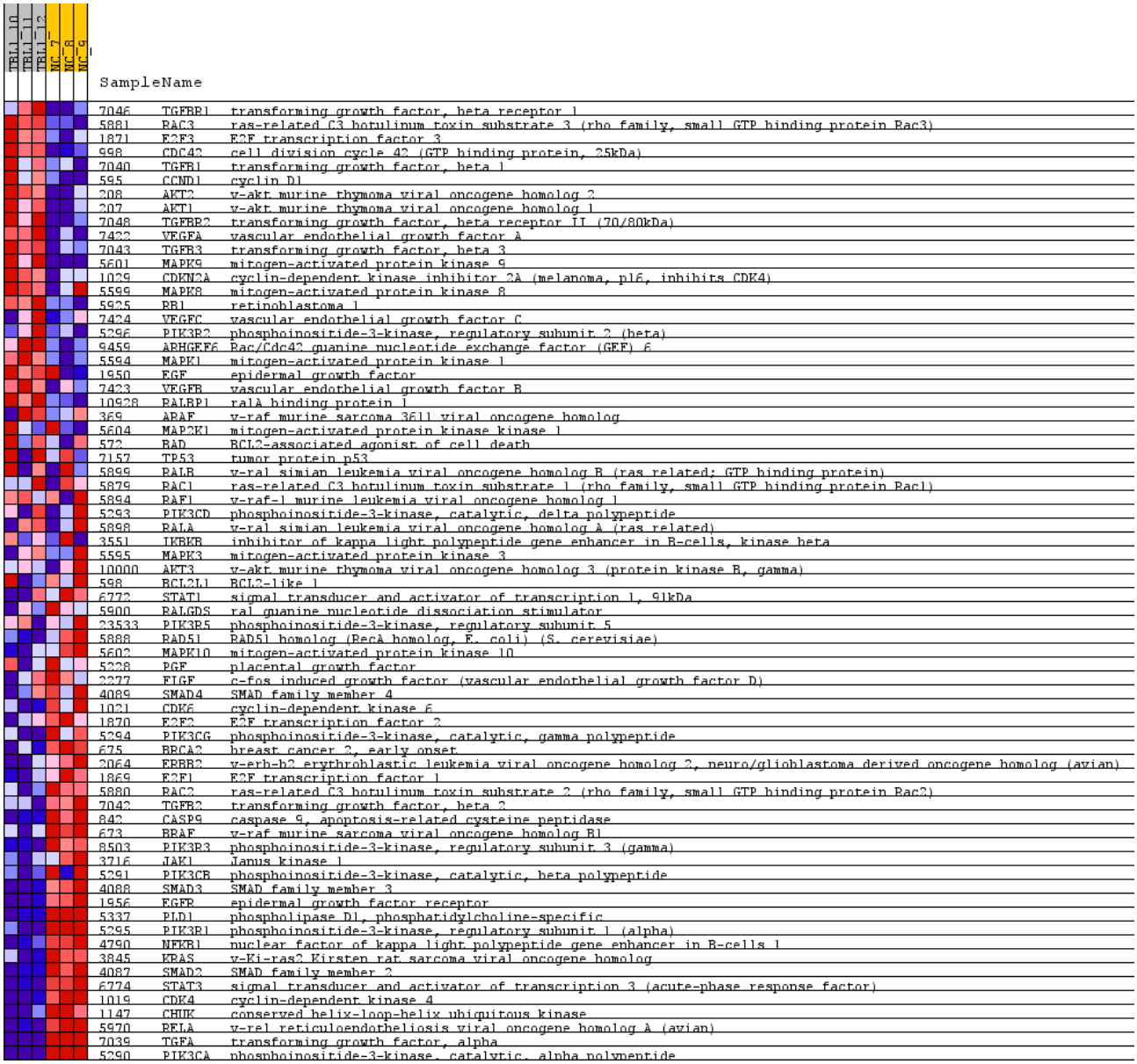

Figure F.3: Heat map from GSEA for gene set "hsa05212 pancreatic cancer" in TBL1X knockdown

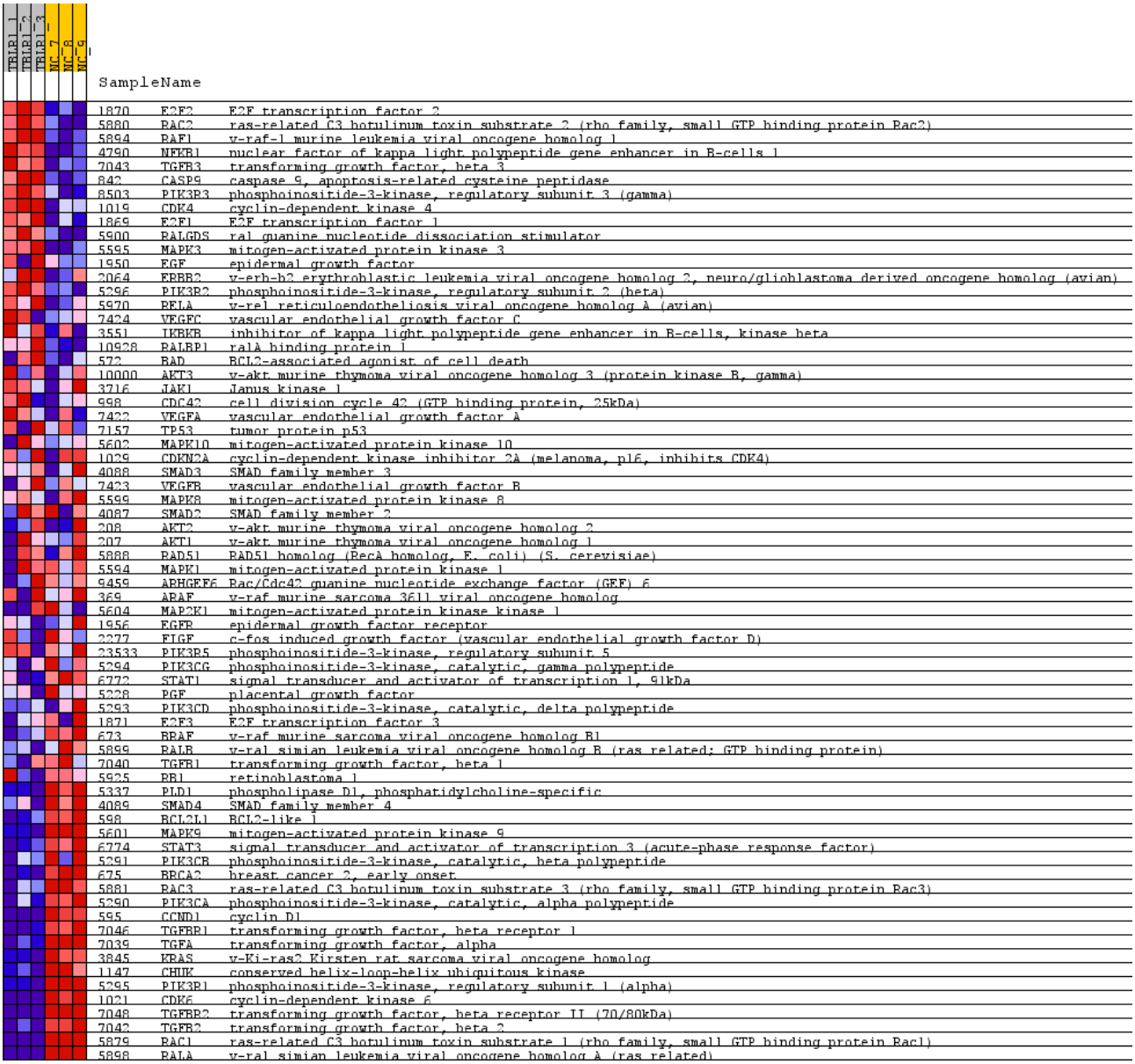

Figure F.4: Heat map from GSEA for gene set "hsa05212 pancreatic cancer" in TBL1XR1 knockdown

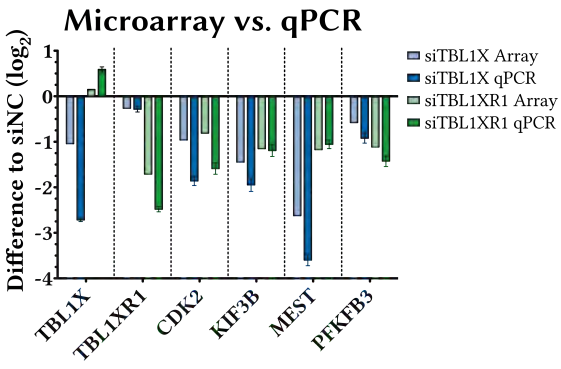

Figure F.5: Validation of microarray

RNA used for microarray was reverse transcribed to cDNA and gene expression was analyed with TaqMan® quantitative PCR. Besides TBL1X and TBL1XR1 four other genes with strong regulation in the microarray were chosen. CDK2: cyclin dependent kinase 2; KIF3B: Kinesin-like protein KIF3B; MEST: Mesoderm-specific transcript homolog protein; PFKFB3: 6-phosphofructo-2-kinase/fructose-2,6-bisphosphatase 3. Data plotted as mean ± SEM.

G Seahorse extracellular flux measurement

Cells take up oxygen and nutrients and convert them to energy that is stored as ATP. Byproducts of cellular energy metabolism are heat, lactate and CO_2 that are dissipated to the extracellular environment.

Measuring the oxygen consumption rate (OCR) in cells can give valuable insight into their physiological state. Cells, especially cancer cells, also use glycolysis to generate ATP independent of oxygen availability by converting glucose to lactate. Production of the latter results in an efflux of protons to the extracellular medium, causing acidification of the medium which can be measured by changes in pH, providing the extracellular acidification rate (ECAR).

G.1 Mito Stress Test Kit

In this assay the cells are metabolically challenged by subsequently adding three different chemicals that shift the bioenergetic profile of the cell (figure G.1).

First, oxygen consumption is measured under basal conditions. Then oligomycin is injected into the culture medium which inhibits ATP synthesis by blocking the proton channel of the F_0 portion ATP synthase (Complex V). This way, it can be distinguished between the percentage of oxygen consumption used for ATP synthesis and the percentage of oxygen consumption required to overcome the natural proton leak across the inner mitochondrial membrane.

The second injection is FCCP (carbonyl cyanide-*p*-trifluoromethoxyphenylhydrazone), an ionophore that serves as an uncoupling agent. It disrupts ATP synthesis by transporting hydrogen ions across the mitochondrial membrane instead of the proton channel of ATP synthase (Complex V). The resulting collapse of the mitochondrial membrane potential leads to a rapid consumption of energy and oxygen, without the generation of ATP as the cell tries to maintain its membrane potential.

The third injection is a combination of the Complex I inhibitor rotenone and the Complex III inhibitor antimycin A. This combination blocks mitochondrial respiration resulting in a decrease in OCR. This way the non-mitochondrial oxygen consumption can be determined.

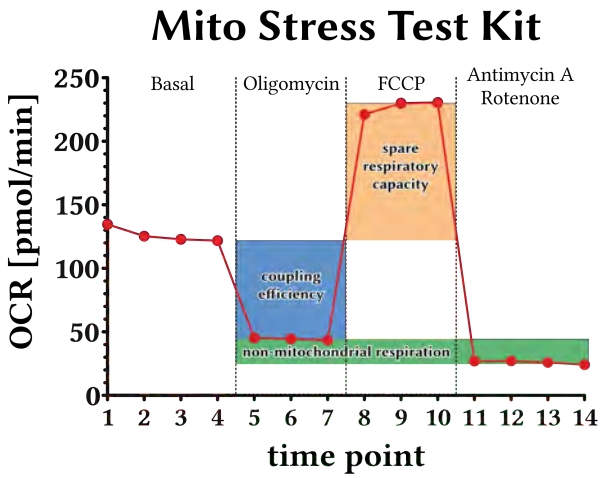

Figure G.1: Mito Stress Test Kit

Besides the basal respiration and cellular response to the indicated chemicals, several other parameters can be determined. Non-mitochondrial respiration is the difference in OCR after application of oligomycin and after injection of antimycin A and rotenone and accounts for the fraction of oxygen that is consumed by non-mitochondrial processes. The coupling efficiency is the percentage of oxygen that is used to produce ATP via Complex V. The spare respiratory capacity is the difference in OCR under basal conditions and after application of FCCP. This is the actual 'stress test' measure of the assay, as it provides an idea of a cell's maximum ATP production and thus its ability to respond to stress in form of an increase in energy demand. Figure is adapted from the Mito Stress Test Kit manual from Seahorse Bioscience.

G.2 Glycolysis Stress Test Kit

This assay measures the three key parameters of glycolytic function: Glycolysis, Glycolytic Capacity, and Glycolytic Reserve (figure G.2).

First, the cells are incubated under basal conditions without glucose and ECAR is measured. Next, glucose is injected into the culture medium to a final concentration of 10 mM. It is taken up by the cells and catabolized through the glycolytic pathway to lactate, producing ATP and protons. The extrusion of protons into the surrounding medium produces a rapid increase in ECAR. This glucose-induced response is reported as the rate of glycolysis

Next, oligomycin is injected which inhibits ATP synthesis by blocking the proton channel of the F_0 portion of the mitochondrial ATP synthase (Complex V). This inhibition of mitochondrial ATP production forces the cell to shift its energy production to glycolysis to meet its ATP demands, resulting in an increase in ECAR revealing the maximum glycolytic capacity of the cell.

The final injection is 2-deoxyglucose, a glucose analog which inhibits glycolysis through competitive binding to glucose hexokinase, the first enzyme in the glycolytic pathway. The resulting decrease in ECAR gives the non-glycolytic acidification and further confirms that the ECAR observed in the experiment is due to glycolysis.

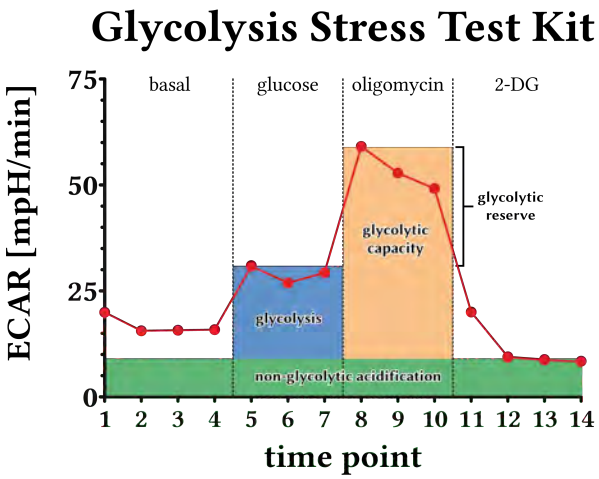

Figure G.2: Glycolysis Stress Test Kit

Besides the basal acidification rate and cellular response to the indicated chemicals, several other parameters can be determined. Non-glycolytic acidification is due to basal proton extrusion as well as CO_2 release to the media followed by its hydration to carbonic acid and bicarbonate. Glycolysis rate is the difference in ECAR after glucose injection and after application of 2-deoxyglucose. Glycolytic capacity is the difference in ECAR after 2-deoxyglucose injection and after application of oligomycin. The difference between glycolytic capacity and glycolysis rate is the glycolytic reserve, the cells ability to increase its glycolytic flux to meet an increase in energy demand. Figure is adapted from the Glycolysis Stress Test Kit manual from Seahorse Bioscience.

H Statistical analysis of subcutaneous shTBL1X-Panc02 allografts

Table H.1: Statistical analysis of subcutaneous shTBL1X-Panc02 allografts growth

Two-way ANOVA with Holm-Sidak post-test was performed using SigmaPlot. Analysis was either done on all experimental groups or only on NaCl control vs. 20 $^{mg}/_{kg}$ gemcitabine (GEM-20) since this was the dosage where the synergistic effect of TBL1X-knockdown and chemotherapeutic treatment was most prominent. Significant values ($p \leq 0.05$) are printed in green.

		absolute tumor volume		relative tumor volume	
	source of variation	**all groups**	**NaCl/GEM-20**	**all groups**	**NaCl/GEM-20**
	shRNA	< 0.001	0.002	0.086	0.192
	gemcitabine	0.023	0.254	< 0.001	0.006
	interaction	0.189	0.486	0.769	0.464

		absolute tumor volume		relative tumor volume	
	Holm-Sidak post-tests	**all groups**	**NaCl/GEM-20**	**all groups**	**NaCl/GEM-20**
	shNC vs. shTBL1X	< 0.001	0.002	0.086	0.192
	NaCl vs. GEM-20	0.449	0.254	0.006	0.006
	NaCl vs. GEM-60	0.037		0.028	
	NaCl vs. GEM-120	0.050		< 0.001	
	GEM-20 vs. GEM-60	0.477		0.441	
	GEM-20 vs. GEM-120	0.461		0.363	
	GEM-60 vs. GEM-120	0.843		0.114	
within shNC	**NaCl vs. GEM-20**	0.356	0.211	0.251	0.115
within shNC	**NaCl vs. GEM-60**	0.009		0.240	
within shNC	**NaCl vs. GEM-120**	0.014		0.006	
within shNC	**GEM-20 vs. GEM-60**	0.315		0.833	
within shNC	**GEM-20 vs. GEM-120**	0.322		0.239	
within shNC	**GEM-60 vs. GEM-120**	0.814		0.300	
within shTBL1X	**NaCl vs. GEM-20**	0.987	0.735	0.015	0.012
within shTBL1X	**NaCl vs. GEM-60**	0.986		0.106	
within shTBL1X	**NaCl vs. GEM-120**	0.978		0.009	
within shTBL1X	**GEM-20 vs. GEM-60**	0.994		0.601	
within shTBL1X	**GEM-20 vs. GEM-120**	0.979		0.811	
within shTBL1X	**GEM-60 vs. GEM-120**	0.964		0.591	
within NaCl	**shNC vs. shTBL1X**	< 0.001	0.050	0.619	0.661
within GEM-20	**shNC vs. shTBL1X**	0.010	0.050	0.112	0.166
within GEM-60	**shNC vs. shTBL1X**	0.165		0.303	
within GEM-120	**shNC vs. shTBL1X**	0117		0.755	

Table H.2: Statistical analysis of subcutaneous shTBL1X-Panc02 allografts proliferation

Two-way ANOVA with Holm-Sidak post-test was performed using SigmaPlot. Significant values ($p \leq 0.05$) are printed in green.

main effects

source of variation	DF	ΣS	MS	*F*	*p*
shRNA	1	408.868	408.868	14.609	0.092
gemcitabine	1	17.665	17.665	0.631	0.441
shRNA × gemcitabine	1	82.100	82.100	2.933	0.110
Residual	**13**	**363.847**	**27.988**		
Total	**16**	**849.752**	**53.110**		

pairwise multiple comparison procedures (Holm-Sidak method)

factor	comparison	DM	*t*	*p*
shRNA	shNC vs. shTBL1X	9.854	3.822	0.002
gemcitabine	NaCl vs. GEM-20	2.048	0.794	0.441
shRNA within NaCl	shNC vs. shTBL1X	14.270	3.815	0.002
shRNA within GEM-20	shNC vs. shTBL1X	5.438	1.532	0.149
gemcitabine within shNC	NaCl vs. GEM-20	6.464	1.821	0.092
gemcitabine within shTBL1X	NaCl vs. GEM-20	2.367	0.633	0.538

power of performed test with $\alpha = 0.05$ for shRNA	0.939
power of performed test with $\alpha = 0.05$ for gemcitabine	0.050
power of performed test with $\alpha = 0.05$ for shRNA × gemcitabine	0.240

J Current literature on TBL1X and TBL1XR1

Table J.1: Relevant publications on TBL1X and TBL1XR1

reference	key findings
Bassi et al. (1999) [85]	identification of the *TBL1X* gene and association with X-linked late-onset sensorineural deafness
Guenther et al. (2000) [87]	TBL1X is part of the SMRT/HDAC3 co-repressor complex
Zhang et al. (2002) [88]	GPS2 and TBL1X interact cooperatively with repression domain 1 of NCoR to form a heterotrimeric structure
Yoon et al. (2003) [89]	function of TBL1X and TBL1XR1 in the NCoR complex
Tomita et al. (2003) [195]	TBL1XR1 forms a complex with NCoR and is recruited to target gene promoters of the oncoproteins PML and PLZF
Perissi et al. (2004) [90]	function of TBL1X and TBL1XR1 as exchange factors for nuclear receptor corepressors
Tomita et al. (2004) [196]	unliganded thyroid hormone receptor interacts with TBL1XR1 and recruits TBL1XR1 to its chromatinized target promoter
Yoon et al. (2005) [197]	TBL1X and TBL1XR1 bind preferentially to hypoacetylated histones H2B and H4
Ishizuka and Lazar (2005) [198]	characterization of binding regions of NCoR for TBL1X and TBL1XR1
Gerlitz et al. (2005) [199]	The LisH domain of TBL1X is important for nuclear import of TBL1X
Zhang et al. (2006) [200]	TBL1XR1 regulates the expression of nuclear hormone receptor co-repressors
Liu et al. (2007) [100]	TBL1XR1 is upregulated in lung squamous cell carcinoma
Li and Wang (2008) [92]	TBL1X and TBL1XR1 interact with β-catenin upon Wnt activation
Perissi et al. (2008) [91]	TBL1X and TBL1XR1 are differently phosphorylated thus exerting their distinct functions
Choi et al. (2008) [201]	the LisH motif of TBL1X and TBL1XR1 is required for histone binding, oligomerization, and transcriptional repression
Parker et al. (2008) [101]	deletion of *TBL1XR1* is a recurrent abnormality in ETV6-RUNX1 positive acute lymphoblastic leukemia
Huang et al. (2009) [202]	TLR2 signaling leads to rapid activation of CaMKII and phosphorylation of TBL1XR1
Kadota et al. (2009) [102]	*TBL1XR1* is amplified in breast cancer and knockdown leads to reduced cell migration, invasion, and tumorigenesis in a mouse xenograft model
Dimitrova et al. (2010) [203]	TBL1X protects β-catenin from Siah-1-mediated ubiquitination
Toropainen et al. (2010) [204]	Myc expression is depended on TBL1X
Foulds et al. (2010) [205]	*TBL1X* is a target gene of human steroid receptor RNA activator
Keutgens et al. (2010) [206]	TBL1XR1 is involved in the degradation of the oncogene Bcl-3
Chung et al. (2011) [207]	a SNP in the *TBL1X* gene is associated with autism spectrum disorder
Ramadoss et al. (2011) [208]	TBL1X binds to NF-κB and facilitates its recruitment to target gene promoters
Kulozik et al. (2011) [105]	TBL1X and TBL1XR1 regulate hepatic lipid metabolism via PPARα
Choi et al. (2011) [93]	TBL1X and TBL1XR1 are SUMOylated in a Wnt signaling-dependent manner and recruited to Wnt target gene promoters

Table continued on next page

Table J.1 *continued:* relevant publications on TBL1X and TBL1XR1

reference	key findings
Scott et al. (2012) [103]	fusion of *TBL1XR1* and *TP63* is a recurrent event in B-cell non-Hodgkin lymphoma
Gonzalez-Aguilar et al. (2012) [104]	*TBL1XR1* is frequently mutated in primary central nervous system lymphomas
O'Roak et al. (2012) [209]	recurrent disruptive mutations of TBL1XR1 may contribute to 1 % of sporadic autism spectrum disorders
Han et al. (2013) [210]	miRNA 483-5p modulates the levels of proteins of the MeCP2-interacting corepressor complexes, including HDAC4 and TBL1X
Rohm et al. (2013) [106]	TBL1XR1 controls lipid mobilization in white adipose tissue
García-Ibarbia et al. (2013) [211]	*TBL1X* gene and other Wnt target genes are differently methylated in osteoporotic hip fractures compared to osteoarthritis
Huang et al. (2014) [151]	*TBL1XR1* is a predicted target gene of miRNA 205 and is downregulated in lung squamous cell carcinoma
Daniels et al. (2014) [152]	TBL1XR1 is a coactivator of androgen receptor in prostate cancer cells
Olsson et al. (2014) [153]	deletions or uniparental isodisomies of *TBL1XR1* were significantly more common in B-cell precursor acute lymphoblastic leukemia patients who relapsed compared with those remaining in complete remission
Liu et al. (2014) [156]	TBL1XR1 is highly expressed in esophageal squamous cell carcinoma, positively correlated with disease stage and negatively correlated with patient survival; it regulates lymphangiogenesis and lymphatic metastasis and induces VEGF-C expression
Chen et al. (2014) [155]	*TBL1XR1* fuses to retinoid acid receptor alpha in a variant t(3;17)(q26;q21) translocation of acute promyelocytic leukemia
de Oliveira et al. (2014) [212]	*TBL1X* and *PIK3CA* genes are differentially regulated in the SOD1(G93A) amyotrophic lateral sclerosis animal model
Wang et al. (2014) [157]	TBL1XR1 is upregulated in cervical cancer, correlates with the clinical stage, survival time and recurrence, and promotes epithelial-mesenchymal transition
Jones et al. (2014) [154]	TBL1XR1 knockdown in acute lymphoblastic leukemia precursor cell lines results in reduced glucocorticoid receptor recruitment to glucocorticoid responsive genes leading to decreased glucocorticoid signaling
Bi et al. (2014) [213]	SUMOylation stabilizes GPS2 protein through promoting its interaction with TBL1X and reducing its ubiquitination

Acknowledgments

I want to thank Prof. Dr. Stephan Herzig for giving me the opportunity to perform this study as a member of his great research team and for his constant multifaceted support, Dr. Oliver Strobel for the extensive and productive collaboration and Dr. Karin Müller-Decker for her valuable advice and profound knowledge.

Special thanks go to Oksana Seibert, Annika Zota and Yvonne Feuchter for their great help in the lab, their valuable assistance during all the mouse experiments and to Daniela Strzoda, Katharina Sowodniok, Alexandra Tuch and Anja Reimann, for their help in the lab. I have never before met so many technicians in one place that were at the same time competent, nice and always fun to work with.

Karin Ruf and Susann Wendler did a tremendous job with all the histology work from embedding through cutting to staining. Thanks also to Maria Muciek for performing the gene expression microarrays and to Carsten Sticht for analyzing them and answering all my questions.

I am moreover obliged to Adam Rose for performing the radioactive 2-deoxyglucose uptake assay on my behalf and to Xiaoyue Wang for her invaluable assistance with the chromatin immunoprecipitation.

I further want to thank Michaela Schäfer for her assistance with the subcutaneous injections as well as helpful and amusing discussions. A big thank you goes once more to Michaela and also to Adriano Maida, Ashley Eheim and Anastasia Bachmann for proofreading the manuscript of this thesis.

My appreciation also goes to all the other present and former members of the Herzig and the Strobel group for their friendly support during the past four years and for maintaining a nice working atmosphere, namely – in alphabetic order by family name – Carolyn Algire, Carsten Bahr, Irem Bayindir, Mauricio Berriel Diaz, Maik Brune, Roldan de Guia, Claudia Dittner, Bilgen Ekim Üstünel, Alexander Ernst, Kilian Friedrich, Philipp Gmach, Tatiana Golea, Laura Graser, Fabian Ilmberger, Julia Jäger, Allan Jones, Asrar Ali Khan, Dagmar Kindler, Milen Kirilov, Stefan Kleinsorg, Anja Krones-Herzig, Philipp Kulozik, Sarah Lerch, Daša Medrikova, Bettina Meissburger, Karin Mössenböck, Katharina Niopek, Marcos Rios Garcia, Maria Rohm, Florian Rösch, Tobias Schafmeier, Alisa Schmidt, Jonas Schumacher, Sandra Seum, Tjeerd Sijmonsma, Anke Sommerfeld, Aishwarya Sundaram, and Alexandros Vegiopoulos.

My gratitude also goes to the Heidelberg Life-Science Lab at the DKFZ, especially to its founder Dr. Thomas Schutz and its current director Dr. Katrin Platzer as well as Hannah Novatschkova and all the other great people there. My membership in this marvelous organization during my high school time was crucial in nourishing my scientific interest and making the final decision to study biology rather than medicine, chemistry or physics. All the things that I learned there, both scientifically and non-scientifically, during my time as a participant in high school and also later as a mentor while already studying at university, are an invaluable resource that influenced my CV in so many ways.

Most of all I would like to say thank you to my parents for always supporting me in my scientific curiosity, be it with my extracurricular activities in the Heidelberg Life-Science Lab during my high school time, or later at university.

I also owe a huge thank you to Thorsten who always supported me during the last four years, especially during the stressful crazy last year. Thank you for always believing in me, cheering me up, pushing me when I needed to be pushed, and never entirely losing patience with me.

Without the help and support of all these people, this work would not have been possible.

References

[1] Ahmed A Elayat, Mostafa M el Naggar, and Mohammad Tahir. An immunocytochemical and morphometric study of the rat pancreatic islets. *J. Anat.*, 186 (Pt 3):629–637, June 1995. PMID 7559135.

[2] Haiyong Han and Daniel D Von Hoff. SnapShot: Pancreatic Cancer. *CCELL*, 23(3):424–424.e1, March 2013.

[3] Nabeel Bardeesy and Ronald A Depinho. Pancreatic cancer biology and genetics. *Nat Rev Cancer*, 2(12):897–909, December 2002. PMID 12459728.

[4] Peter Kaatsch, Claudia Spix, Alexander Katalinic, Stefan Hentschel, Nadia Baras, Benjamin Barnes, Joachim Bertz, Jörg Haberland, Klaus Kraywinkel, Antje Laudi, and Ute Wolf. Krebs in Deutschland 2007/2008. Robert Koch-Institut und die Gesellschaft der epidemiologischen Krebsregister in Deutschland e. V., Berlin, 2012. Available from: `http://edoc.rki.de/docviews/abstract.php?lang=ger&id=1846`.

[5] Shinichi Yachida, Siân Jones, Ivana Bozic, Tibor Antal, Rebecca Leary, Baojin Fu, Mihoko Kamiyama, Ralph H Hruban, James R Eshleman, Martin A Nowak, Victor E Velculescu, Kenneth W Kinzler, Bert Vogelstein, and Christine A Iacobuzio-Donahue. Distant metastasis occurs late during the genetic evolution of pancreatic cancer. *Nature*, 467(7319):1114–1117, October 2010. PMID 20981102.

[6] Peter Kaatsch, Claudia Spix, Stefan Hentschel, Alexander Katalinic, Sabine Luttmann, Sandra Caspritz, Josef Cernaj, Anke Ernst, Juliane Folkerts, Jutta Hansmann, Kristine Kranzhöfer, Eva Krieghoff-Henning, Beatrice Kunz, Andrea Penzkofer, Kornelia Treml, Kerstin Wittenberg, Nadia Baras, Benjamin Barnes, Joachim Bertz, Nina Buttmann-Schweiger, Stefan Dahm, Manuela Franke, Jörg Haberland, Klaus Kraywinkel, Antje Wienecke, and Ute Wolf. Krebs in Deutschland 2009/2010. Robert Koch-Institut und die Gesellschaft der epidemiologischen Krebsregister in Deutschland e. V., Berlin, November 2013. Available from: `http://www.krebsdaten.de/Krebs/DE/Content/Publikationen/Krebs_in_Deutschland/krebs_in_deutschland_node.html`.

[7] United States Department of Health and Human Services, Centers for Disease Control and Prevention and National Cancer Institute. National Program of Cancer Registries Early Release Cancer Statistics: 1999-2010, WONDER On-line Database [online]. Available from: `http://wonder.cdc.gov/cancer.html` [cited 16.07.2014].

[8] Medspace. Pancreatic Cancer [online]. Available from: `http://emedicine.medscape.com/article/280605-overview` [cited 16.07.2014].

[9] Haojie Huang, Jaroslaw Daniluk, Yan Liu, Jun Chu, Z Li, Baoan Ji, and C D Logsdon. Oncogenic K-Ras requires activation for enhanced activity. *Oncogene*, 33(4):532–535, January 2014. PMID 23334325.

[10] Jaroslaw Daniluk, Yan Liu, Defeng Deng, Jun Chu, Haojie Huang, Sebastian Gaiser, Zobeida Cruz-Monserrate, Huamin Wang, Baoan Ji, and Craig D Logsdon. An NF-κB pathway-mediated positive feedback loop amplifies Ras activity to pathological levels in mice. *J Clin Invest*, 122(4):1519–1528, April 2012. PMID 22406536.

[11] Ralph H Hruban, N Volkan Adsay, Jorge Albores-Saavedra, Carolyn Compton, Elizabeth S Garrett, Steven N Goodman, Scott E Kern, David S Klimstra, Günter Klöppel, Daniel S Longnecker, Jutta Lüttges, and G Johan A Offerhaus. Pancreatic intraepithelial neoplasia: a new nomenclature and classification system for pancreatic duct lesions. *Am. J. Surg. Pathol.*, 25(5):579–586, May 2001. PMID 11342768.

[12] Robb E Wilentz, Christine A Iacobuzio-Donahue, Pedram Argani, Denis M McCarthy, Jennifer L Parsons, Charles J Yeo, Scott E Kern, and Ralph H Hruban. Loss of expression of Dpc4 in pancreatic intraepithelial neoplasia: evidence that DPC4 inactivation occurs late in neoplastic progression. *Cancer Res*, 60(7):2002–2006, April 2000. PMID 10766191.

[13] Matthias Löhr, Günter Klöppel, Patrick Maisonneuve, Albert B Lowenfels, and Jutta Lüttges. Frequency of K-ras mutations in pancreatic intraductal neoplasias associated with pancreatic ductal adenocarcinoma and chronic pancreatitis: a meta-analysis. *Neoplasia*, 7(1):17–23, January 2005. PMID 15720814.

[14] Anirban Maitra, N Volkan Adsay, Pedram Argani, Christine A Iacobuzio-Donahue, Angelo De Marzo, John L Cameron, Charles J Yeo, and Ralph H Hruban. Multicomponent analysis of the pancreatic adenocarcinoma progression model using a pancreatic intraepithelial neoplasia tissue microarray. *Mod. Pathol.*, 16(9):902–912, September 2003. PMID 13679454.

[15] Sunil R Hingorani, Emanuel F Petricoin, Anirban Maitra, Vinodh Rajapakse, Catrina King, Michael A Jacobetz, Sally Ross, Thomas P Conrads, Timothy D Veenstra, Ben A Hitt, Yoshiya Kawaguchi, Don Johann, Lance A Liotta, Howard C Crawford, Mary E Putt, Tyler Jacks, Christopher V E Wright, Ralph H Hruban, Andrew M Lowy, and David A Tuveson. Preinvasive and invasive ductal pancreatic cancer and its early detection in the mouse. *Cancer Cell*, 4(6):437–450, December 2003. PMID 14706336.

[16] Sunil R Hingorani, Lifu Wang, Asha S Multani, Chelsea Combs, Therese B Deramaudt, Ralph H Hruban, Anil K Rustgi, Sandy Chang, and David A Tuveson. Trp53R172H and KrasG12D cooperate to promote chromosomal instability and widely metastatic pancreatic ductal adenocarcinoma in mice. *Cancer Cell*, 7(5):469–483, May 2005. PMID 15894267.

[17] Andrew J Aguirre, Nabeel Bardeesy, Manisha Sinha, Lyle Lopez, David A Tuveson, James Horner, Mark S Redston, and Ronald A Depinho. Activated Kras and Ink4a/Arf deficiency cooperate to produce metastatic pancreatic ductal adenocarcinoma. *Genes Dev*, 17(24):3112–3126, December 2003. PMID 14681207.

[18] John P Morris, Sam C Wang, and Matthias Hebrok. KRAS, Hedgehog, Wnt and the twisted developmental biology of pancreatic ductal adenocarcinoma. *Nat Rev Cancer*, 10(10):683–695, October 2010. PMID 20814421.

[19] Catherine Carrière, Elliott S Seeley, Tobias Goetze, Daniel S Longnecker, and Murray Korc. The Nestin progenitor lineage is the compartment of origin for pancreatic intraepithelial neoplasia. *Proc Natl Acad Sci USA*, 104(11):4437–4442, March 2007. PMID 17360542.

[20] Carmen Guerra, Alberto J Schuhmacher, Marta Cañamero, Paul J Grippo, Lena Verdaguer, Lucía Pérez-Gallego, Pierre Dubus, Eric P Sandgren, and Mariano Barbacid. Chronic pancreatitis is essential for induction of pancreatic ductal adenocarcinoma by K-Ras oncogenes in adult mice. *CCELL*, 11(3):291–302, March 2007. PMID 17349585.

[21] Nils Habbe, Guanglu Shi, Robert A Meguid, Volker Fendrich, Farzad Esni, Huiping Chen, Georg Feldmann, Doris A Stoffers, Stephen F Konieczny, Steven D Leach, and Anirban Maitra. Spontaneous induction of murine pancreatic intraepithelial neoplasia (mPanIN) by acinar cell targeting of oncogenic Kras in adult mice. *Proc Natl Acad Sci USA*, 105(48):18913–18918, December 2008. PMID 19028870.

[22] Sharon Y Gidekel Friedlander, Gerald C Chu, Eric L Snyder, Nomeda Girnius, Gregory Dibelius, Denise Crowley, Eliza Vasile, Ronald A Depinho, and Tyler Jacks. Context-dependent transformation of adult pancreatic cells by oncogenic K-Ras. *Cancer Cell*, 16(5):379–389, November 2009. PMID 19878870.

[23] Christopher L Wolfgang, Joseph M Herman, Daniel A Laheru, Alison P Klein, Michael A Erdek, Elliot K Fishman, and Ralph H Hruban. Recent progress in pancreatic cancer. *CA Cancer J Clin*, 63(5):318–348, September 2013. PMID 23856911.

[24] Cristina Bosetti, E Lucenteforte, D T Silverman, G Petersen, Paige M Bracci, B T Ji, E Negri, D Li, H A Risch, S H Olson, S Gallinger, A B Miller, H B Bueno-de Mesquita, R Talamini, J Polesel, P Ghadirian, P A Baghurst, W Zatonski, E Fontham, William R Bamlet, E A Holly, P Bertuccio, Y T Gao, M Hassan, H Yu, R C Kurtz, M Cotterchio, J Su, P Maisonneuve, E J Duell, P Boffetta, and C La Vecchia. Cigarette smoking and pancreatic cancer: an analysis from the International Pancreatic Cancer Case-Control Consortium (Panc4). *Ann Oncol*, 23(7):1880–1888, July 2012. PMID 22104574.

[25] Patrick Maisonneuve and Albert B Lowenfels. Epidemiology of pancreatic cancer: an update. *Dig Dis*, 28(4-5):645–656, 2010. PMID 21088417.

[26] E Lucenteforte, C La Vecchia, D Silverman, G M Petersen, Paige M Bracci, B T Ji, Cristina Bosetti, D Li, S Gallinger, A B Miller, H B Bueno-de Mesquita, R Talamini, J Polesel, P Ghadirian, P A Baghurst, W Zatonski, E Fontham, William R Bamlet, E A Holly, Y T Gao, E Negri, M Hassan, M Cotterchio, J Su, P Maisonneuve, P Boffetta, and E J Duell. Alcohol consumption and pancreatic cancer: a pooled analysis in the International Pancreatic Cancer Case-Control Consortium (PanC4). *Ann Oncol*, 23 (2):374–382, February 2012. PMID 21536662.

[27] E J Duell, E Lucenteforte, S H Olson, Paige M Bracci, D Li, H A Risch, D T Silverman, B T Ji, S Gallinger, E A Holly, E H Fontham, P Maisonneuve, H B Bueno-de Mesquita, P Ghadirian, R C Kurtz, E Ludwig, H Yu, A B Lowenfels, D Seminara, G M Petersen, C La Vecchia, and P Boffetta. Pancreatitis and pancreatic cancer risk: a pooled analysis in the International Pancreatic Cancer Case-Control Consortium (PanC4). *Ann Oncol*, 23(11):2964–2970, November 2012. PMID 22767586.

[28] P Ghadirian, P Boyle, A Simard, J Baillargeon, P Maisonneuve, and C Perret. Reported family aggregation of pancreatic cancer within a population-based case-control study in the Francophone community in Montreal, Canada. *Int J Pancreatol*, 10(3-4): 183–196, November 1991. PMID 1787333.

[29] Richard Wooster, Susan L Neuhausen, Jonathan Mangion, Yvette Quirk, Deborah Ford, Nadine Collins, Kim Nguyen, Sheila Seal, Thao Tran, Diane Averill, Patty Fields, Gill Marshall, Steven Narod, Gilbert M Lenoir, Henry Lynch, Jean Feunteun, Peter Devillee, Cees J Cornelisse, Fred H Menko, Peter A Daly, Wilma Ormiston, Ross McManus, Carole Pye, Cathryn M Lewis, Lisa A Cannon-Albright, Julian Peto, Bruce A J Ponder, Mark H Skolnick, Douglas F Easton, David E Goldgar, and Michael R Stratton. Localization of a breast cancer susceptibility gene, BRCA2, to chromosome 13q12-13. *Science*, 265(5181):2088–2090, September 1994. PMID 8091231.

[30] Edward Giovannucci and Dominique Michaud. The role of obesity and related metabolic disturbances in cancers of the colon, prostate, and pancreas. *Gastroenterology*, 132(6):2208–2225, May 2007. PMID 17498513.

[31] Debra T Silverman, Christine A Swanson, Gridley Gridley, Sholom Wacholder, Raymond S Greenberg, Linda M Brown, Richard B Hayes, G Maria Swanson, Janet B Schoenberg, Linda M Pottern, Ann G Schwartz, Joseph F Fraumeni, and Robert N Hoover. Dietary and nutritional factors and pancreatic cancer: a case-control study based on direct interviews. *J Natl Cancer Inst*, 90(22):1710–1719, November 1998. PMID 9827525.

[32] Anthony J G Hanley, Kenneth C Johnson, Paul J Villeneuve, Yang Mao, and Canadian Cancer Registries Epidemiology Research Group. Physical activity, anthropometric factors and risk of pancreatic cancer: results from the Canadian enhanced cancer surveillance system. *Int J Cancer*, 94(1):140–147, October 2001. PMID 11668489.

[33] Sai Yi Pan, Kenneth C Johnson, Anne-Marie Ugnat, Shi Wu Wen, Yang Mao, and Canadian Cancer Registries Epidemiology Research Group. Association of obesity and cancer risk in Canada. *Am. J. Epidemiol.*, 159(3):259–268, February 2004. PMID 14742286.

[34] Carey A Eberle, Paige M Bracci, and Elizabeth A Holly. Anthropometric factors and pancreatic cancer in a population-based case-control study in the San Francisco Bay area. *Cancer causes & control : CCC*, 16(10):1235–1244, December 2005. PMID 16215874.

[35] Eugenia E Calle, Carmen Rodriguez, Kimberly Walker-Thurmond, and Michael J Thun. Overweight, obesity, and mortality from cancer in a prospectively studied cohort of U.S. adults. *N Engl J Med*, 348(17):1625–1638, April 2003. PMID 12711737.

[36] James Everhart. Diabetes Mellitus as a Risk Factor for Pancreatic Cancer. *JAMA*, 273(20):1605–1609, May 1995. PMID 7745774.

[37] R Huxley, A Ansary-Moghaddam, A Berrington de González, F Barzi, and M Woodward. Type-II diabetes and pancreatic cancer: a meta-analysis of 36 studies. *Br J Cancer*, 92(11):2076–2083, June 2005. PMID 15886696.

[38] Suresh T Chari, Cynthia L Leibson, Kari G Rabe, Lawrence J Timmons, Jeanine Ransom, Mariza de Andrade, and Gloria M Petersen. Pancreatic cancer-associated diabetes mellitus: prevalence and temporal association with diagnosis of cancer. *Gastroenterology*, 134(1):95–101, January 2008. PMID 18061176.

[39] G David Batty, Martin J Shipley, Michael Marmot, and George Davey Smith. Diabetes status and post-load plasma glucose concentration in relation to site-specific cancer mortality: findings from the original Whitehall study. *Cancer causes & control : CCC*, 15(9):873–881, November 2004. PMID 15577289.

[40] Susan M Gapstur, Peter H Gann, William Lowe, Kiang Liu, Laura Colangelo, and Alan Dyer. Abnormal glucose metabolism and pancreatic cancer mortality. *JAMA*, 283(19):2552–2558, May 2000. PMID 10815119.

[41] Eugenia E Calle and Rudolf Kaaks. Overweight, obesity and cancer: epidemiological evidence and proposed mechanisms. *Nat Rev Cancer*, 4(8):579–591, August 2004. PMID 15286738.

[42] Susen Becker, Laure Dossus, and Rudolf Kaaks. Obesity related hyperinsulinaemia and hyperglycaemia and cancer development. *Arch. Physiol. Biochem.*, 115(2):86–96, May 2009. PMID 19485704.

[43] Oliver Stoeltzing, Wenbiao Liu, Niels Reinmuth, Fan Fan, Alexander A Parikh, Corazon D Bucana, Douglas B Evans, Gregg L Semenza, and Lee M Ellis. Regulation of hypoxia-inducible factor-1alpha, vascular endothelial growth factor, and angiogenesis by an insulin-like growth factor-I receptor autocrine loop in human pancreatic cancer. *Am J Pathol*, 163(3):1001–1011, September 2003. PMID 12937141.

[44] Yongfen Min, Yasushi Adachi, Hiroyuki Yamamoto, Hideto Ito, Fumio Itoh, Choon-Taek Lee, Sorena Nadaf, David P Carbone, and Kohzoh Imai. Genetic blockade of the insulin-like growth factor-I receptor: a promising strategy for human pancreatic cancer. *Cancer Res*, 63(19):6432–6441, October 2003. PMID 14559833.

[45] Donghui Li, Sai-Ching J Yeung, Manal M Hassan, Marina Konopleva, and James L Abbruzzese. Antidiabetic therapies affect risk of pancreatic cancer. *Gastroenterology*, 137(2):482–488, August 2009. PMID 19375425.

[46] Haim Werner, Doron Weinstein, and Itay Bentov. Similarities and differences between insulin and IGF-I: structures, receptors, and signalling pathways. *Arch. Physiol. Biochem.*, 114(1):17–22, February 2008. PMID 18465355.

[47] Michael Brownlee. Biochemistry and molecular cell biology of diabetic complications. *Nature*, 414(6865):813–820, December 2001. PMID 11742414.

[48] M Takada, T Koizumi, H Toyama, Y Suzuki, and Y Kuroda. Differential expression of RAGE in human pancreatic carcinoma cells. *Hepatogastroenterology*, 48(42):1577–1578, November 2001. PMID 11813576.

[49] Moriatsu Takada, Kenro Hirata, Tetsuo Ajiki, Yasuyuki Suzuki, and Yoshikazu Kuroda. Expression of receptor for advanced glycation end products (RAGE) and MMP-9 in human pancreatic cancer cells. *Hepatogastroenterology*, 51(58):928–930, July 2004. PMID 15239215.

[50] Rui Kang, Tara Loux, Daolin Tang, Nicole E Schapiro, Philip Vernon, Kristen M Livesey, Alyssa Krasinskas, Michael T Lotze, and Herbert J Zeh. The expression of the receptor for advanced glycation endproducts (RAGE) is permissive for early pancreatic neoplasia. *Proc Natl Acad Sci USA*, 109(18):7031–7036, May 2012. PMID 22509024.

[51] Carolyn Algire, Lilian Amrein, Mahvash Zakikhani, Lawrence Panasci, and Michael Pollak. Metformin blocks the stimulative effect of a high-energy diet on colon carcinoma growth in vivo and is associated with reduced expression of fatty acid synthase. *Endocr Relat Cancer*, 17(2):351–360, June 2010. PMID 20228137.

[52] Carolyn Algire, Olga Moiseeva, Xavier Deschenes-Simard, Lilian Amrein, Luca A Petruccelli, Elena Birman, Benoît Viollet, Gerardo Ferbeyre, and Michael N Pollak. Metformin reduces endogenous reactive oxygen species and associated DNA damage. *Cancer Prev Res (Phila)*, January 2012. PMID 22262811.

[53] J Khasawneh, M D Schulz, A Walch, Jan Rozman, Martin Hrabe de Angelis, Martin Klingenspor, A Buck, M Schwaiger, D Saur, R M Schmid, Günter Klöppel, Bence Sipos, F R Greten, and M C Arkan. Inflammation and mitochondrial fatty acid beta-oxidation link obesity to early tumor promotion. *Proc Natl Acad Sci USA*, 106(9):3354–3359, March 2009. PMID 19208810.

[54] Stuart P Weisberg, Daniel McCann, Manisha Desai, Michael Rosenbaum, Rudolph L Leibel, and Anthony W Ferrante. Obesity is associated with macrophage accumulation in adipose tissue. *J Clin Invest*, 112(12):1796–1808, December 2003. PMID 14679176.

[55] Francisca Lago, Carlos Diéguez, Juan Gómez-Reino, and Oreste Gualillo. Adipokines as emerging mediators of immune response and inflammation. *Nat Clin Pract Rheumatol*, 3(12):716–724, December 2007. PMID 18037931.

[56] Bincy Philip, Christina L Roland, Jaroslaw Daniluk, Yan Liu, Deyali Chatterjee, Sobeyda B Gomez, Baoan Ji, Haojie Huang, Huamin Wang, Jason B Fleming, Craig D Logsdon, and Zobeida Cruz-Monserrate. A high-fat diet activates oncogenic Kras and COX2 to induce development of pancreatic ductal adenocarcinoma in mice. *Gastroenterology*, 145(6):1449–1458, December 2013. PMID 23958541.

[57] Goodarz Danaei, Mariel M Finucane, Yuan Lu, Gitanjali M Singh, Melanie J Cowan, Christopher J Paciorek, John K Lin, Farshad Farzadfar, Young-Ho Khang, Gretchen A Stevens, Mayuree Rao, Mohammed K Ali, Leanne M Riley, Carolyn A Robinson, Majid Ezzati, and Global Burden of Metabolic Risk Factors of Chronic Diseases Collaborating Group (Blood Glucose). National, regional, and global trends in fasting plasma glucose and diabetes prevalence since 1980: systematic analysis of health examination surveys and epidemiological studies with 370 country-years and 2·7 million participants. *Lancet*, 378(9785):31–40, July 2011. PMID 21705069.

[58] Mariel M Finucane, Gretchen A Stevens, Melanie J Cowan, Goodarz Danaei, John K Lin, Christopher J Paciorek, Gitanjali M Singh, Hialy R Gutierrez, Yuan Lu, Adil N Bahalim, Farshad Farzadfar, Leanne M Riley, Majid Ezzati, and Global Burden of Metabolic Risk Factors of Chronic Diseases Collaborating Group (Body Mass Index). National, regional, and global trends in body-mass index since 1980: systematic analysis of health examination surveys and epidemiological studies with 960 country-years and 9·1 million participants. *Lancet*, 377(9765):557–567, February 2011. PMID 21295846.

[59] Gretchen A Stevens, Gitanjali M Singh, Yuan Lu, Goodarz Danaei, John K Lin, Mariel M Finucane, Adil N Bahalim, Russell K McIntire, Hialy R Gutierrez, Melanie Cowan, Christopher J Paciorek, Farshad Farzadfar, Leanne Riley, Majid Ezzati, and Global Burden of Metabolic Risk Factors of Chronic Diseases Collaborating Group (Body Mass Index). National, regional, and global trends in adult overweight and obesity prevalences. *Popul Health Metr*, 10(1):22, 2012. PMID 23167948.

[60] B M Popkin and M M Slining. New dynamics in global obesity facing low- and middle-income countries. *Obes Rev*, 14 Suppl 2:11–20, November 2013. PMID 24102717.

[61] World Health Organization (WHO). Global Health Observatory (GHO) – Obesity [online]. Available from: `http://www.who.int/gho/ncd/risk_factors/obesity_text/en/` [cited 16.02.2014].

[62] World Health Organization (WHO). Global Health Observatory (GHO) – Overweight and obesity [online]. Available from: `http://www.who.int/gho/ncd/risk_factors/overweight/en/index.html` [cited 16.02.2014].

[63] World Health Organization (WHO). Diabetes Programme [online]. Available from: `http://www.who.int/diabetes/en/` [cited 16.02.2014].

[64] Centers for Disease Control and Prevention. National Center for Chronic Disease Prevention and Health Promotion. Division of Diabetes Translation. Diabetes Data and Trends [online]. Available from: `http://apps.nccd.cdc.gov/DDTSTRS/default.aspx` [cited 16.02.2014].

[65] S3-Leitlinie zum exokrinen Pankreaskarzinom. Leitlinienprogramm Onkologie der AWMF, Deutschen Krebsgesellschaft e.V. und Deutschen Krebshilfe e.V., October 2013. Available from: `http://leitlinienprogramm-onkologie.de/uploads/tx_sbdownloader/LL_Pankreas_OL_Langversion.pdf`.

[66] Cancer Facts & Figures 2013. American Cancer Society, Atlanta, 2013. Available from: `http://www.cancer.org/research/cancerfactsstatistics/cancerfactsfigures2013/index`.

[67] Helmut Oettle, Stefan Post, Peter Neuhaus, Klaus Gellert, Jan Langrehr, Karsten Ridwelski, Harald Schramm, Joerg Fahlke, Carl Zuelke, Christof Burkart, Klaus Gutberlet, Erika Kettner, Harald Schmalenberg, Karin Weigang-Koehler, Wolf-Otto Bechstein, Marco Niedergethmann, Ingo Schmidt-Wolf, Lars Roll, Bernd Doerken, and Hanno Riess. Adjuvant chemotherapy with gemcitabine vs observation in patients undergoing curative-intent resection of pancreatic cancer: a randomized controlled trial. *JAMA*, 297(3):267–277, January 2007. PMID 17227978.

[68] H Ueno, T Kosuge, Y Matsuyama, J Yamamoto, A Nakao, S Egawa, R Doi, M Monden, T Hatori, M Tanaka, M Shimada, and K Kanemitsu. A randomised phase III trial comparing gemcitabine with surgery-only in patients with resected pancreatic cancer: Japanese Study Group of Adjuvant Therapy for Pancreatic Cancer. *Br J Cancer*, 101(6):908–915, September 2009. PMID 19690548.

[69] John P Neoptolemos, Deborah D Stocken, Helmut Friess, Claudio Bassi, Janet A Dunn, Helen Hickey, Hans Beger, Laureano Fernandez-Cruz, Christos Dervenis, François Lacaine, Massimo Falconi, Paolo Pederzoli, Akos Pap, David Spooner, David J Kerr, Markus W Büchler, and European Study Group for Pancreatic Cancer. A randomized trial of chemoradiotherapy and chemotherapy after resection of pancreatic cancer. *N Engl J Med*, 350(12):1200–1210, March 2004. PMID 15028824.

[70] Deborah D Stocken, Markus W Büchler, Christos Dervenis, Claudio Bassi, H Jeekel, J H G Klinkenbijl, K E Bakkevold, T Takada, H Amano, John P Neoptolemos, and Pancreatic Cancer Meta-analysis Group. Meta-analysis of randomised adjuvant therapy trials for pancreatic cancer. *Br J Cancer*, 92(8):1372–1381, April 2005. PMID 15812554.

[71] John P Neoptolemos, Deborah D Stocken, Claudio Bassi, Paula Ghaneh, David Cunningham, David Goldstein, Robert Padbury, Malcolm J Moore, Steven Gallinger, Christophe Mariette, Moritz N Wente, Jakob R Izbicki, Helmut Friess, Markus M Lerch, Christos Dervenis, Attila Oláh, Giovanni Butturini, Ryuichiro Doi, Pehr A Lind, David Smith, Juan W Valle, Daniel H Palmer, John A Buckels, Joyce Thompson, Colin J McKay, Charlotte L Rawcliffe, Markus W Büchler, and European Study Group for Pancreatic Cancer. Adjuvant chemotherapy with fluorouracil plus folinic acid vs gemcitabine following pancreatic cancer resection: a randomized controlled trial. *JAMA*, 304(10):1073–1081, September 2010. PMID 20823433.

[72] John P Neoptolemos, Deborah D Stocken, C Tudur Smith, Claudio Bassi, Paula Ghaneh, E Owen, Malcolm J Moore, Robert Padbury, Ryuichiro Doi, David Smith, and Markus W Büchler. Adjuvant 5-fluorouracil and folinic acid vs observation for pancreatic cancer: composite data from the ESPAC-1 and -3(v1) trials. *Br J Cancer*, 100(2):246–250, January 2009. PMID 19127260.

[73] Nuno M F S A Cerqueira, Pedro A Fernandes, and Maria J Ramos. Understanding ribonucleotide reductase inactivation by gemcitabine. *Chemistry*, 13(30):8507–8515, 2007. PMID 17636467.

[74] Mark S Duxbury, Hiromichi Ito, Eric Benoit, Michael J Zinner, Stanley W Ashley, and Edward E Whang. Retrovirally mediated RNA interference targeting the M2 subunit of ribonucleotide reductase: A novel therapeutic strategy in pancreatic cancer. *Surgery*, 136(2):261–269, August 2004. PMID 15300189.

[75] Eugene J Koay, Mark J Truty, Vittorio Cristini, Ryan M Thomas, Rong Chen, Deyali Chatterjee, Ya'an Kang, Priya R Bhosale, Eric P Tamm, Christopher H Crane, Milind Javle, Matthew H Katz, Vijaya N Gottumukkala, Marc A Rozner, Haifa Shen, Jeffery E Lee, Huamin Wang, Yuling Chen, William Plunkett, James L Abbruzzese, Robert A Wolff, Gauri R Varadhachary, Mauro Ferrari, and Jason B Fleming. Transport properties of pancreatic cancer describe gemcitabine delivery and response. *J Clin Invest*, March 2014. PMID 24614108.

[76] Y Nakano, S Tanno, K Koizumi, T Nishikawa, K Nakamura, M Minoguchi, T Izawa, Y Mizukami, T Okumura, and Y Kohgo. Gemcitabine chemoresistance and molecular markers associated with gemcitabine transport and metabolism in human pancreatic cancer cells. *Br J Cancer*, 96(3):457–463, February 2007. PMID 17224927.

[77] Rui Wang, Long Cheng, Jun Xia, Zishu Wang, Qiong Wu, and Zhiwei Wang. Gemcitabine Resistance is Associated with Epithelial-Mesenchymal Transition and Induction of HIF-1 in Pancreatic Cancer Cells. *Curr Cancer Drug Targets*, February 2014. PMID 24575976.

[78] Takayuki Asano, Yixin Yao, Jijiang Zhu, Donghui Li, James L Abbruzzese, and Shrikanth A G Reddy. The PI 3-kinase/Akt signaling pathway is activated due to aberrant Pten expression and targets transcription factors NF-kappaB and c-Myc in pancreatic cancer cells. *Oncogene*, 23(53):8571–8580, November 2004. PMID 15467756.

[79] Sylvia S W Ng, Ming-Sound Tsao, Sue Chow, and David W Hedley. Inhibition of phosphatidylinositide 3-kinase enhances gemcitabine-induced apoptosis in human pancreatic cancer cells. *Cancer Res*, 60(19):5451–5455, October 2000. PMID 11034087.

[80] Victor M Bondar, Bridget Sweeney-Gotsch, Michael Andreeff, Gordon B Mills, and David J McConkey. Inhibition of the phosphatidylinositol 3'-kinase-AKT pathway induces apoptosis in pancreatic carcinoma cells in vitro and in vivo. *Molecular Cancer Therapeutics*, 1(12):989–997, October 2002. PMID 12481421.

[81] Peter J Watson, Louise Fairall, and John W R Schwabe. Nuclear hormone receptor co-repressors: structure and function. *Mol. Cell. Endocrinol.*, 348(2):440–449, January 2012. PMID 21925568.

[82] Jeremy Turner and Merlin Crossley. Cloning and characterization of mCtBP2, a co-repressor that associates with basic Krüppel-like factor and other mammalian transcriptional regulators. *EMBO J*, 17(17):5129–5140, September 1998. PMID 9724649.

[83] G Chinnadurai. CtBP, an unconventional transcriptional corepressor in development and oncogenesis. *Mol Cell*, 9(2):213–224, February 2002. PMID 11864595.

[84] Peter J Watson, Louise Fairall, Guilherme M Santos, and John W R Schwabe. Structure of HDAC3 bound to co-repressor and inositol tetraphosphate. *Nature*, 481(7381):335–340, January 2012. PMID 22230954.

[85] Maria T Bassi, Rajkumar S Ramesar, Barbara Caciotti, Ingrid M Winship, Alessandro De Grandi, Mirko Riboni, Philip L Townes, Peter Beighton, Andrea Ballabio, and Giuseppe Borsani. X-linked late-onset sensorineural deafness caused by a deletion involving OA1 and a novel gene containing WD-40 repeats. *Am. J. Hum. Genet.*, 64(6):1604–1616, June 1999. PMID 10330347.

[86] Jiwen Li, Jin Wang, Jianxiang Wang, Zafar Nawaz, Johnson M Liu, Jun Qin, and Jiemin Wong. Both corepressor proteins SMRT and N-CoR exist in large protein complexes containing HDAC3. *EMBO J*, 19(16):4342–4350, August 2000. PMID 10944117.

[87] Matthew G Guenther, William S Lane, Wolfgang Fischle, Eric Verdin, Mitchell A Lazar, and Ramin Shiekhattar. A core SMRT corepressor complex containing HDAC3 and TBL1, a WD40-repeat protein linked to deafness. *Genes Dev*, 14(9):1048–1057, May 2000. PMID 10809664.

[88] Jinsong Zhang, Markus Kalkum, Brian T Chait, and Robert G Roeder. The N-CoR-HDAC3 nuclear receptor corepressor complex inhibits the JNK pathway through the integral subunit GPS2. *Mol Cell*, 9(3):611–623, March 2002. PMID 11931768.

[89] Ho-Geun Yoon, Doug W Chan, Zhi-Qing Huang, Jiwen Li, Joseph D Fondell, Jun Qin, and Jiemin Wong. Purification and functional characterization of the human N-CoR complex: the roles of HDAC3, TBL1 and TBLR1. *EMBO J*, 22(6):1336–1346, March 2003. PMID 12628926.

[90] Valentina Perissi, Aneel Aggarwal, Christopher K Glass, David W Rose, and Michael G Rosenfeld. A corepressor/coactivator exchange complex required for transcriptional activation by nuclear receptors and other regulated transcription factors. *Cell*, 116(4):511–526, February 2004. PMID 14980219.

[91] Valentina Perissi, Claudio Scafoglio, Jie Zhang, Kenneth A Ohgi, David W Rose, Christopher K Glass, and Michael G Rosenfeld. TBL1 and TBLR1 phosphorylation on regulated gene promoters overcomes dual CtBP and NCoR/SMRT transcriptional repression checkpoints. *Mol Cell*, 29(6):755–766, March 2008. PMID 18374649.

[92] Jiong Li and Cun-Yu Wang. TBL1-TBLR1 and beta-catenin recruit each other to Wnt target-gene promoter for transcription activation and oncogenesis. *Nat Cell Biol*, 10(2):160–169, February 2008. PMID 18193033.

[93] Hyo-Kyoung Choi, Kyung-Chul Choi, Jung-Yoon Yoo, Meiying Song, Suk Jin Ko, Chul Hoon Kim, Jin-Hyun Ahn, Kyung-Hee Chun, Jong In Yook, and Ho-Geun Yoon. Reversible SUMOylation of TBL1-TBLR1 Regulates β-Catenin-Mediated Wnt Signaling. *Mol Cell*, 43(2):203–216, July 2011. PMID 21777810.

[94] Patrick W Heiser, Janet Lau, Makoto M Taketo, Pedro L Herrera, and Matthias Hebrok. Stabilization of beta-catenin impacts pancreas growth. *Development*, 133(10):2023–2032, May 2006. PMID 16611688.

[95] Karl Willert and Katherine A Jones. Wnt signaling: is the party in the nucleus? *Genes Dev*, 20(11):1394–1404, June 2006. PMID 16751178.

[96] Randall T Moon, Aimee D Kohn, Giancarlo V De Ferrari, and Ajamete Kaykas. WNT and beta-catenin signalling: diseases and therapies. *Nat. Rev. Genet.*, 5(9):691–701, September 2004. PMID 15372092.

[97] John P Morris, David A Cano, Shigeki Sekine, Sam C Wang, and Matthias Hebrok. Beta-catenin blocks Kras-dependent reprogramming of acini into pancreatic cancer precursor lesions in mice. *J Clin Invest*, 120(2):508–520, February 2010. PMID 20071774.

[98] Min Yu, David T Ting, Shannon L Stott, Ben S Wittner, Fatih Ozsolak, Suchismita Paul, Jordan C Ciciliano, Malgorzata E Smas, Daniel Winokur, Anna J Gilman, Matthew J Ulman, Kristina Xega, Gianmarco Contino, Brinda Alagesan, Brian W Brannigan, Patrice M Milos, David P Ryan, Lecia V Sequist, Nabeel Bardeesy, Sridhar Ramaswamy, Mehmet Toner, Shyamala Maheswaran, and Daniel A Haber. RNA sequencing of pancreatic circulating tumour cells implicates WNT signalling in metastasis. *Nature*, 487(7408):510–513, July 2012. PMID 22763454.

[99] Marina Pasca di Magliano, Andrew V Biankin, Patrick W Heiser, David A Cano, Pedro J A Gutierrez, Therese Deramaudt, Davendra Segara, Amanda C Dawson, James G Kench, Susan M Henshall, Robert L Sutherland, Andrzej Dlugosz, Anil K Rustgi, and Matthias Hebrok. Common activation of canonical Wnt signaling in pancreatic adenocarcinoma. *PLoS ONE*, 2(11): e1155, January 2007. PMID 17982507.

[100] Yan Liu, Wenyue Sun, Kaitai Zhang, Hongwei Zheng, Ying Ma, Dongmei Lin, Xinyu Zhang, Lin Feng, Wendong Lei, Ziqiang Zhang, Suping Guo, Naijun Han, Wei Tong, Xiaoli Feng, Yanning Gao, and Shujun Cheng. Identification of genes differentially expressed in human primary lung squamous cell carcinoma. *Lung Cancer*, 56(3):307–317, June 2007. PMID 17316888.

[101] Helen Parker, Qian An, Kerry Barber, Marian Case, Teresa Davies, Zoë Konn, Adam Stewart, Sarah Wright, Mike Griffiths, Fiona M Ross, Anthony V Moorman, Andy G Hall, Julie A Irving, Christine J Harrison, and Jon C Strefford. The complex genomic profile of ETV6-RUNX1 positive acute lymphoblastic leukemia highlights a recurrent deletion of TBL1XR1. *Genes Chromosomes Cancer*, 47(12):1118–1125, December 2008. PMID 18767146.

[102] Mitsutaka Kadota, Misako Sato, Beverly Duncan, Akira Ooshima, Howard H Yang, Natacha Diaz-Meyer, Sheryl Gere, Shun-Ichiro Kageyama, Junya Fukuoka, Takuya Nagata, Kazuhiro Tsukada, Barbara K Dunn, Lalage M Wakefield, and Maxwell P Lee. Identification of novel gene amplifications in breast cancer and coexistence of gene amplification with an activating mutation of PIK3CA. *Cancer Res*, 69(18):7357–7365, September 2009. PMID 19706770.

[103] David W Scott, Karen L Mungall, Susana Ben-Neriah, Sanja Rogic, Ryan D Morin, Graham W Slack, King L Tan, Fong Chun Chan, Raymond S Lim, Joseph M Connors, Marco A Marra, Andrew J Mungall, Christian Steidl, and Randy D Gascoyne. TBL1XR1/TP63: a novel recurrent gene fusion in B-cell non-Hodgkin lymphoma. *Blood*, 119(21):4949–4952, May 2012. PMID 22496164.

[104] Alberto Gonzalez-Aguilar, Ahmed Idbaih, Blandine Boisselier, Naïma Habbita, Marta Rossetto, Alice Laurenge, Aurélie Bruno, Anne Jouvet, Marc Polivka, Clovis Adam, Dominique Figarella-Branger, Catherine Miquel, Anne Vital, Hervé Ghesquières, Rémy Gressin, Vincent Delwail, Luc Taillandier, Olivier Chinot, Pierre Soubeyran, Emmanuel Gyan, Sylvain Choquet, Caroline Houillier, Carole Soussain, Marie-Laure Tanguy, Yannick Marie, Karima Mokhtari, and Khê Hoang-Xuan. Recurrent mutations of MYD88 and TBL1XR1 in primary central nervous system lymphomas. *Clin Cancer Res*, 18(19):5203–5211, October 2012. PMID 22837180.

[105] Philipp Kulozik, Allan Jones, Frits Mattijssen, Adam J Rose, Anja Reimann, Daniela Strzoda, Stefan Kleinsorg, Christina Raupp, Jürgen Kleinschmidt, Karin Müller-Decker, Walter Wahli, Carsten Sticht, Norbert Gretz, Christian von Loeffelholz, Martin Stockmann, Andreas Pfeiffer, Sigrid Stöhr, Geesje M Dallinga-Thie, Peter P Nawroth, Mauricio Berriel Diaz, and Stephan Herzig. Hepatic deficiency in transcriptional cofactor TBL1 promotes liver steatosis and hypertriglyceridemia. *Cell Metab*, 13 (4):389–400, April 2011. PMID 21459324.

[106] Maria Rohm, Anke Sommerfeld, Daniela Strzoda, Allan Jones, Tjeerd P Sijmonsma, Gottfried Rudofsky, Christian Wolfrum, Carsten Sticht, Norbert Gretz, Maximilian Zeyda, Lukas Leitner, Peter P Nawroth, Thomas M Stulnig, Mauricio Berriel Diaz, Alexandros Vegiopoulos, and Stephan Herzig. Transcriptional cofactor TBLR1 controls lipid mobilization in white adipose tissue. *Cell Metab*, 17(4):575–585, April 2013. PMID 23499424.

[107] Rania Elakoum, Guillaume Gauchotte, Abderrahim Oussalah, Marie-Pierre Wissler, Christelle Clément-Duchêne, Jean-Michel Vignaud, Jean-Louis Guéant, and Farès Namour. CARM1 and PRMT1 are dysregulated in lung cancer without hierarchical features. *Biochimie*, 97:210–218, February 2014. PMID 24211191.

[108] Lu Wang, Zibo Zhao, Mark B Meyer, Sandeep Saha, Menggang Yu, Ailan Guo, Kari B Wisinski, Wei Huang, Weibo Cai, J Wesley Pike, Ming Yuan, Paul Ahlquist, and Wei Xu. CARM1 methylates chromatin remodeling factor BAF155 to enhance tumor progression and metastasis. *Cancer Cell*, 25(1):21–36, January 2014. PMID 24434208.

[109] Mauricio Berriel Diaz, Anja Krones-Herzig, Dagmar Metzger, Anja Ziegler, Alexandros Vegiopoulos, Martin Klingenspor, Karin Müller-Decker, and Stephan Herzig. Nuclear receptor cofactor receptor interacting protein 140 controls hepatic triglyceride metabolism during wasting in mice. *Hepatology*, 48(3):782–791, September 2008. PMID 18712775.

[110] Inka Zschiedrich, Ulrike Hardeland, Anja Krones-Herzig, Mauricio Berriel Diaz, Alexandros Vegiopoulos, Johannes Müggenburg, Dirk Sombroek, Thomas G Hofmann, Rainer Zawatzky, Xiaolei Yu, Norbert Gretz, Mark Christian, Roger White, Malcolm G Parker, and Stephan Herzig. Coactivator function of RIP140 for NFkappaB/RelA-dependent cytokine gene expression. *Blood*, 112(2):264–276, July 2008. PMID 18469200.

[111] Marion Lapierre, Sandrine Bonnet, Caroline Bascoul-Mollevi, Imade Ait-Arsa, Stéphan Jalaguier, Maguy Del Rio, Michela Plateroti, Paul Roepman, Marc Ychou, Julie Pannequin, Frédéric Hollande, Malcolm Parker, and Vincent Cavaillès. RIP140 increases APC expression and controls intestinal homeostasis and tumorigenesis. *J Clin Invest*, March 2014. PMID 24667635.

[112] Alan Cheng and Alan R Saltiel. More TORC for the gluconeogenic engine. *Bioessays*, 28(3):231–234, March 2006. PMID 16479585.

[113] Sylvia N Schreiber, Roger Emter, M Benjamin Hock, Darko Knutti, Jessica Cardenas, Michael Podvinec, Edward J Oakeley, and Anastasia Kralli. The estrogen-related receptor alpha (ERRalpha) functions in PPARgamma coactivator 1alpha (PGC-1alpha)-induced mitochondrial biogenesis. *Proc Natl Acad Sci USA*, 101(17):6472–6477, April 2004. PMID 15087503.

[114] Eiko Kanaya, Takuma Shiraki, and Hisato Jingami. The nuclear bile acid receptor FXR is activated by PGC-1alpha in a ligand-dependent manner. *Biochem J*, 382(Pt 3):913–921, September 2004. PMID 15202934.

[115] Sonali Bhalla, Cengiz Ozalp, Sungsoon Fang, Lingjin Xiang, and Jongsook Kim Kemper. Ligand-activated pregnane X receptor interferes with HNF-4 signaling by targeting a common coactivator PGC-1alpha. Functional implications in hepatic cholesterol and glucose metabolism. *J Biol Chem*, 279(43):45139–45147, October 2004. PMID 15322103.

[116] Kavita Bhalla, Bor Jang Hwang, Ruby E Dewi, Lihui Ou, William Twaddel, Hong-Bin Fang, Scott B Vafai, Francesca Vazquez, Pere Puigserver, Laszlo Boros, and Geoffrey D Girnun. PGC1α promotes tumor growth by inducing gene expression programs supporting lipogenesis. *Cancer Res*, 71(21):6888–6898, November 2011. PMID 21914785.

[117] G Deblois, J St-Pierre, and V Giguère. The PGC-1/ERR signaling axis in cancer. *Oncogene*, 32(30):3483–3490, July 2013. PMID 23208510.

[118] Otto Warburg, Franz Wind, and Erwin Negelein. The Metabolism of tumors in the body. *J. Gen. Physiol.*, 8(6):519–530, March 1927. PMID 19872213.

[119] Guido Kroemer and Jacques Pouyssegur. Tumor Cell Metabolism: Cancer's Achilles' Heel. *Cancer Cell*, 13(6):472–482, June 2008.

[120] Ralph J DeBerardinis, Julian J Lum, Georgia Hatzivassiliou, and Craig B Thompson. The biology of cancer: metabolic reprogramming fuels cell growth and proliferation. *Cell Metab*, 7(1):11–20, January 2008. PMID 18177721.

[121] C Muñoz-Pinedo, N El Mjiyad, and J-E Ricci. Cancer metabolism: current perspectives and future directions. *Cell Death Dis*, 3: e248, 2012. PMID 22237205.

[122] Georgia Hatzivassiliou, Fangping Zhao, Daniel E Bauer, Charalambos Andreadis, Anthony N Shaw, Dashyant Dhanak, Sunil R Hingorani, David A Tuveson, and Craig B Thompson. ATP citrate lyase inhibition can suppress tumor cell growth. *CCELL*, 8 (4):311–321, October 2005. PMID 16226706.

[123] Hui Qin Wang, Deborah A Altomare, Kristine L Skele, Poulikos I Poulikakos, Francis P Kuhajda, Antonio Di Cristofano, and Joseph R Testa. Positive feedback regulation between AKT activation and fatty acid synthase expression in ovarian carcinoma cells. *Oncogene*, 24(22):3574–3582, May 2005. PMID 15806173.

[124] Pedro Vizán, Gema Alcarraz-Vizán, Santiago Díaz-Moralli, Olga N Solovjeva, Wilma M Frederiks, and Marta Cascante. Modulation of pentose phosphate pathway during cell cycle progression in human colon adenocarcinoma cell line HT29. *Int J Cancer*, 124(12):2789–2796, June 2009. PMID 19253370.

[125] Wenwei Hu, Cen Zhang, Rui Wu, Yvonne Sun, Arnold Levine, and Zhaohui Feng. Glutaminase 2, a novel p53 target gene regulating energy metabolism and antioxidant function. *Proc Natl Acad Sci USA*, 107(16):7455–7460, April 2010. PMID 20378837.

[126] Brendan D Manning and Lewis C Cantley. AKT/PKB signaling: navigating downstream. *Cell*, 129(7):1261–1274, June 2007. PMID 17604717.

[127] Valeria R Fantin, Julie St-Pierre, and Philip Leder. Attenuation of LDH-A expression uncovers a link between glycolysis, mitochondrial physiology, and tumor maintenance. *CCELL*, 9(6):425–434, June 2006. PMID 16766262.

[128] Alfonso Mora, Christopher Lipina, François Tronche, Calum Sutherland, and Dario R Alessi. Deficiency of PDK1 in liver results in glucose intolerance, impairment of insulin-regulated gene expression and liver failure. *Biochem J*, 385(Pt 3):639–648, February 2005. PMID 15554902.

[129] Natalia Scaglia, Jeffrey W Chisholm, and R Ariel Igal. Inhibition of stearoylCoA desaturase-1 inactivates acetyl-CoA carboxylase and impairs proliferation in cancer cells: role of AMPK. *PLoS ONE*, 4(8):e6812, 2009. PMID 19710915.

[130] Roland Buettner, Jürgen Schölmerich, and L Cornelius Bollheimer. High-fat diets: modeling the metabolic disorders of human obesity in rodents. *Obesity (Silver Spring)*, 15(4):798–808, April 2007. PMID 17426312.

[131] Angela M Valverde, Cecilia Mur, Sebastián Pons, Alberto M Alvarez, Morris F White, C Ronald Kahn, and Manuel Benito. Association of insulin receptor substrate 1 (IRS-1) y895 with Grb-2 mediates the insulin signaling involved in IRS-1-deficient brown adipocyte mitogenesis. *Mol Cell Biol*, 21(7):2269–2280, April 2001. PMID 11259577.

[132] Yu Li, Timothy J Soos, Xinghai Li, Jiong Wu, Matthew Degennaro, Xiaojian Sun, Dan R Littman, Morris J Birnbaum, and Roberto D Polakiewicz. Protein kinase C Theta inhibits insulin signaling by phosphorylating IRS1 at Ser(1101). *J Biol Chem*, 279(44):45304–45307, October 2004. PMID 15364919.

[133] Chien Li, Peilin Chen, Joan Vaughan, Amy Blount, Alon Chen, Pauline M Jamieson, Jean Rivier, M Susan Smith, and Wylie Vale. Urocortin III is expressed in pancreatic beta-cells and stimulates insulin and glucagon secretion. *Endocrinology*, 144(7): 3216–3224, July 2003. PMID 12810578.

[134] Chien Li, Peilin Chen, Joan Vaughan, Kuo-Fen Lee, and Wylie Vale. Urocortin 3 regulates glucose-stimulated insulin secretion and energy homeostasis. *Proc Natl Acad Sci USA*, 104(10):4206–4211, March 2007. PMID 17360501.

[135] K Lewis, C Li, M H Perrin, A Blount, K Kunitake, C Donaldson, J Vaughan, T M Reyes, J Gulyas, W Fischer, L Bilezikjian, J Rivier, P E Sawchenko, and W W Vale. Identification of urocortin III, an additional member of the corticotropin-releasing factor (CRF) family with high affinity for the CRF2 receptor. *Proc Natl Acad Sci USA*, 98(13):7570–7575, June 2001. PMID 11416224.

[136] Peilin Chen, Joan Vaughan, Cindy Donaldson, Wylie Vale, and Chien Li. Injection of Urocortin 3 into the ventromedial hypothalamus modulates feeding, blood glucose levels, and hypothalamic POMC gene expression but not the HPA axis. *Am J Physiol Endocrinol Metab*, 298(2):E337–45, February 2010. PMID 19952342.

[137] L I Partecke, M Sendler, A Kaeding, F U Weiss, J Mayerle, A Dummer, T D Nguyen, N Albers, S Speerforck, M M Lerch, C D Heidecke, W von Bernstorff, and A Stier. A Syngeneic Orthotopic Murine Model of Pancreatic Adenocarcinoma in the C57/BL6 Mouse Using the Panc02 and 6606PDA Cell Lines. *Eur Surg Res*, 47(2):98–107, June 2011. PMID 21720167.

[138] Fanjie Zhang and Rebecca L Aft. Chemosensitizing and cytotoxic effects of 2-deoxy-D-glucose on breast cancer cells. *J Cancer Res Ther*, 5 Suppl 1:S41–3, September 2009. PMID 20009293.

[139] Fahimeh Aghaee, Jalil Pirayesh Islamian, and Behzaad Baradaran. Enhanced radiosensitivity and chemosensitivity of breast cancer cells by 2-deoxy-d-glucose in combination therapy. *J Breast Cancer*, 15(2):141–147, June 2012. PMID 22807930.

[140] Esther Castellano, Clare Sheridan, May Zaw Thin, Emma Nye, Bradley Spencer-Dene, Markus E Diefenbacher, Christopher Moore, Madhu S Kumar, Miguel M Murillo, Eva Grönroos, Francois Lassailly, Gordon Stamp, and Julian Downward. Requirement for Interaction of PI3-Kinase p110α with RAS in Lung Tumor Maintenance. *Cancer Cell*, 24(5):617–630, November 2013. PMID 24229709.

[141] Stefan Eser, Nina Reiff, Marlena Messer, Barbara Seidler, Kathleen Gottschalk, Melanie Dobler, Maren Hieber, Andreas Arbeiter, Sabine Klein, Bo Kong, Christoph W Michalski, Anna Melissa Schlitter, Irene Esposito, Alexander J Kind, Lena Rad, Angelika E Schnieke, Manuela Baccarini, Dario R Alessi, Roland Rad, Roland M Schmid, Günter Schneider, and Dieter Saur. Selective Requirement of PI3K/PDK1 Signaling for Kras Oncogene-Driven Pancreatic Cell Plasticity and Cancer. *Cancer Cell*, February 2013. PMID 23453624.

[142] J Alan Diehl, Mangeng Cheng, Martine F Roussel, and Charles J Sherr. Glycogen synthase kinase-3beta regulates cyclin D1 proteolysis and subcellular localization. *Genes Dev*, 12(22):3499–3511, November 1998. PMID 9832503.

[143] A J Drummond, B Ashton, M Cheung, A Cooper, J Heled, M Kearse, R Moir, S Stones-Havas, S Sturrock, T Thierer, and A Wilson. Geneious.

[144] Dietrich Rothenbacher, Michael Löw, Philip D Hardt, Hans-Ulrich Klör, Hartwig Ziegler, and Hermann Brenner. Prevalence and determinants of exocrine pancreatic insufficiency among older adults: results of a population-based study. *Scand. J. Gastroenterol.*, 40(6):697–704, June 2005. PMID 16036530.

[145] Hella Jürgens, Wiltrud Haass, Tamara R Castañeda, Annette Schürmann, Corinna Koebnick, Frank Dombrowski, Bärbel Otto, Andrea R Nawrocki, Philipp E Scherer, Jochen Spranger, Michael Ristow, Hans-Georg Joost, Peter J Havel, and Matthias H Tschöp. Consuming fructose-sweetened beverages increases body adiposity in mice. *Obes. Res.*, 13(7):1146–1156, July 2005. PMID 16076983.

[146] Satomi Nishikawa, Akira Yasoshima, Kunio Doi, Hiroyuki Nakayama, and Koji Uetsuka. Involvement of sex, strain and age factors in high fat diet-induced obesity in C57BL/6J and BALB/cA mice. *Exp. Anim.*, 56(4):263–272, July 2007. PMID 17660680.

[147] Ling-Ling Hwang, Chien-Hua Wang, Tzu-Ling Li, Shih-Dar Chang, Li-Chun Lin, Ching-Ping Chen, Chiung-Tong Chen, Keng-Chen Liang, Ing-Kang Ho, Wei-Shiung Yang, and Lih-Chu Chiou. Sex differences in high-fat diet-induced obesity, metabolic alterations and learning, and synaptic plasticity deficits in mice. *Obesity (Silver Spring)*, 18(3):463–469, March 2010. PMID 19730425.

[148] Yoshiya Kawaguchi, Bonnie Cooper, Maureen Gannon, Michael Ray, Raymond J MacDonald, and Christopher V E Wright. The role of the transcriptional regulator Ptf1a in converting intestinal to pancreatic progenitors. *Nat. Genet.*, 32(1):128–134, September 2002. PMID 12185368.

[149] Mikio Hoshino, Shoko Nakamura, Kiyoshi Mori, Takeshi Kawauchi, Mami Terao, Yoshiaki V Nishimura, Akihisa Fukuda, Toshimitsu Fuse, Naoki Matsuo, Masaki Sone, Masahiko Watanabe, Haruhiko Bito, Toshio Terashima, Christopher V E Wright, Yoshiya Kawaguchi, Kazuwa Nakao, and Yo-Ichi Nabeshima. Ptf1a, a bHLH transcriptional gene, defines GABAergic neuronal fates in cerebellum. *Neuron*, 47(2):201–213, July 2005. PMID 16039563.

[150] Gabrielle S Sellick, Karen T Barker, Irene Stolte-Dijkstra, Christina Fleischmann, Richard J Coleman, Christine Garrett, Anna L Gloyn, Emma L Edghill, Andrew T Hattersley, Peter K Wellauer, Graham Goodwin, and Richard S Houlston. Mutations in PTF1A cause pancreatic and cerebellar agenesis. *Nat. Genet.*, 36(12):1301–1305, December 2004. PMID 15543146.

[151] Wei Huang, Yi Jin, Yunfeng Yuan, Chunxue Bai, Ying Wu, Hongguang Zhu, and Shaohua Lu. Validation and target gene screening of hsa-miR-205 in lung squamous cell carcinoma. *Chin. Med. J.*, 127(2):272–278, 2014. PMID 24438615.

[152] Garrett Daniels, Yirong Li, Lan Lin Gellert, Albert Zhou, Jonathan Melamed, Xinyu Wu, Xinming Zhang, David Zhang, Daniel Meruelo, Susan K Logan, Ross Basch, and Peng Lee. TBLR1 as an androgen receptor (AR) coactivator selectively activates AR target genes to inhibit prostate cancer growth. *Endocr Relat Cancer*, 21(1):127–142, February 2014. PMID 24243687.

[153] L Olsson, A Castor, M Behrendtz, A Biloglav, E Forestier, K Paulsson, and B Johansson. Deletions of IKZF1 and SPRED1 are associated with poor prognosis in a population-based series of pediatric B-cell precursor acute lymphoblastic leukemia diagnosed between 1992 and 2011. *Leukemia*, 28(2):302–310, February 2014. PMID 23823658.

[154] Courtney L Jones, Teena Bhatla, Roy Blum, Jinhua Wang, Steven W Paugh, Xin Wen, Wallace Bourgeois, Danielle S Bitterman, Elizabeth A Raetz, Debra J Morrison, David T Teachey, William E Evans, Michael J Garabedian, and William L Carroll. Loss of TBL1XR1 Disrupts Glucocorticoid Receptor Recruitment to Chromatin and Results in Glucocorticoid Resistance in a B-Lymphoblastic Leukemia Model. *J Biol Chem*, June 2014. PMID 24895125.

[155] Yirui Chen, Shouyun Li, Chunlin Zhou, Chengwen Li, Kun Ru, Qing Rao, Haiyan Xing, Zheng Tian, Kejing Tang, Yingchang Mi, Baohong Wang, Min Wang, and Jianxiang Wang. TBLR1 fuses to retinoid acid receptor alpha in a variant t(3;17)(q26;q21) translocation of acute promyelocytic leukemia. *Blood*, April 2014. PMID 24782508.

[156] Liping Liu, Chuyong Lin, Weijiang Liang, Shu Wu, Aibin Liu, Jueheng Wu, Xin Zhang, Pengli Ren, Mengfeng Li, and Libing Song. TBL1XR1 promotes lymphangiogenesis and lymphatic metastasis in esophageal squamous cell carcinoma. *Gut*, March 2014. PMID 24667177.

[157] J Wang, J Ou, Y Guo, T Dai, X Li, J Liu, M Xia, L Liu, and M He. TBLR1 is a novel prognostic marker and promotes epithelial-mesenchymal transition in cervical cancer. *Br J Cancer*, May 2014. PMID 24874481.

[158] Hans Clevers. Wnt/beta-catenin signaling in development and disease. *Cell*, 127(3):469–480, November 2006. PMID 17081971.

[159] Maamoun M Al-Aynati, Nikolina Radulovich, Robert H Riddell, and Ming-Sound Tsao. Epithelial-cadherin and beta-catenin expression changes in pancreatic intraepithelial neoplasia. *Clin Cancer Res*, 10(4):1235–1240, February 2004. PMID 14977820.

[160] Gang Zeng, Matt Germinaro, Amanda Micsenyi, Navjot K Monga, Aaron Bell, Ajit Sood, Vanita Malhotra, Neena Sood, Vandana Midda, Dulabh K Monga, Demetrius M Kokkinakis, and Satdarshan P S Monga. Aberrant Wnt/beta-catenin signaling in pancreatic adenocarcinoma. *Neoplasia*, 8(4):279–289, April 2006. PMID 16756720.

[161] Richard Possemato, Kevin M Marks, Yoav D Shaul, Michael E Pacold, Dohoon Kim, Kıvanç Birsoy, Shalini Sethumadhavan, Hin-Koon Woo, Hyun G Jang, Abhishek K Jha, Walter W Chen, Francesca G Barrett, Nicolas Stransky, Zhi-Yang Tsun, Glenn S Cowley, Jordi Barretina, Nada Y Kalaany, Peggy P Hsu, Kathleen Ottina, Albert M Chan, Bingbing Yuan, Levi A Garraway, David E Root, Mari Mino-Kenudson, Elena F Brachtel, Edward M Driggers, and David M Sabatini. Functional genomics reveal that the serine synthesis pathway is essential in breast cancer. *Nature*, 476(7360):346–350, August 2011. PMID 21760589.

[162] P Rodriguez-Viciana, P H Warne, R Dhand, B Vanhaesebroeck, I Gout, M J Fry, M D Waterfield, and J Downward. Phosphatidylinositol-3-OH kinase as a direct target of Ras. *Nature*, 370(6490):527–532, August 1994. PMID 8052307.

[163] Tsutomu Kodaki, Rüdiger Woscholski, Bengt Hallberg, Pablo Rodriguez-Viciana, Julian Downward, and P J Parker. The activation of phosphatidylinositol 3-kinase by Ras. *Curr. Biol.*, 4(9):798–806, September 1994. PMID 7820549.

[164] Esther Castellano and Julian Downward. RAS Interaction with PI3K: More Than Just Another Effector Pathway. *Genes Cancer*, 2(3):261–274, March 2011. PMID 21779497.

[165] Juan Angel Fresno Vara, Enrique Casado, Javier de Castro, Paloma Cejas, Cristóbal Belda-Iniesta, and Manuel González-Barón. PI3K/Akt signalling pathway and cancer. *Cancer Treat. Rev.*, 30(2):193–204, April 2004. PMID 15023437.

[166] Rosemary A Fryer, Blake Barlett, Christine Galustian, and Angus G Dalgleish. Mechanisms underlying gemcitabine resistance in pancreatic cancer and sensitisation by the iMiDTM lenalidomide. *Anticancer Res*, 31(11):3747–3756, November 2011. PMID 22110196.

[167] Chunning Zheng, Xuelong Jiao, Yingsheng Jiang, and Shaochuan Sun. ERK1/2 activity contributes to gemcitabine resistance in pancreatic cancer cells. *J. Int. Med. Res.*, 41(2):300–306, April 2013. PMID 23569008.

[168] Scott M Wilhelm, Christopher Carter, Liya Tang, Dean Wilkie, Angela McNabola, Hong Rong, Charles Chen, Xiaomei Zhang, Patrick Vincent, Mark McHugh, Yichen Cao, Jaleel Shujath, Susan Gawlak, Deepa Eveleigh, Bruce Rowley, Li Liu, Lila Adnane, Mark Lynch, Daniel Auclair, Ian Taylor, Rich Gedrich, Andrei Voznesensky, Bernd Riedl, Leonard E Post, Gideon Bollag, and Pamela A Trail. BAY 43-9006 exhibits broad spectrum oral antitumor activity and targets the RAF/MEK/ERK pathway and receptor tyrosine kinases involved in tumor progression and angiogenesis. *Cancer Res*, 64(19):7099–7109, October 2004. PMID 15466206.

[169] Scott Wilhelm, Christopher Carter, Mark Lynch, Timothy Lowinger, Jacques Dumas, Roger A Smith, Brian Schwartz, Ronit Simantov, and Susan Kelley. Discovery and development of sorafenib: a multikinase inhibitor for treating cancer. *Nat Rev Drug Discov*, 5(10):835–844, October 2006. PMID 17016424.

[170] Lillian L Siu, Ahmad Awada, Chris H Takimoto, Martine Piccart, Brian Schwartz, Tom Giannaris, Chetan Lathia, Oana Petrenciuc, and Malcolm J Moore. Phase I trial of sorafenib and gemcitabine in advanced solid tumors with an expanded cohort in advanced pancreatic cancer. *Clin Cancer Res*, 12(1):144–151, January 2006. PMID 16397036.

[171] Hedy Lee Kindler, Kristen Wroblewski, James A Wallace, Michael J Hall, Gershon Locker, Sreenivasa Nattam, Edem Agamah, Walter M Stadler, and Everett E Vokes. Gemcitabine plus sorafenib in patients with advanced pancreatic cancer: a phase II trial of the University of Chicago Phase II Consortium. *Invest New Drugs*, 30(1):382–386, February 2012. PMID 20803052.

[172] Niranjan Awasthi, Changhua Zhang, Stefan Hinz, Margaret A Schwarz, and Roderich E Schwarz. Enhancing sorafenib-mediated sensitization to gemcitabine in experimental pancreatic cancer through EMAP II. *J. Exp. Clin. Cancer Res.*, 32:12, 2013. PMID 23497499.

[173] Rene Hennig, Jacinthe Ventura, Ralf Segersvard, Erin Ward, Xian-Zhong Ding, Sambasiva M Rao, Borko D Jovanovic, Takeshi Iwamura, Mark S Talamonti, Richard H Bell, and Thomas E Adrian. LY293111 improves efficacy of gemcitabine therapy on pancreatic cancer in a fluorescent orthotopic model in athymic mice. *Neoplasia*, 7(4):417–425, April 2005. PMID 15967119.

[174] Malcolm J Moore, David Goldstein, John Hamm, Arie Figer, Joel R Hecht, Steven Gallinger, Heather J Au, Pawel Murawa, David Walde, Robert A Wolff, Daniel Campos, Robert Lim, Keyue Ding, Gary Clark, Theodora Voskoglou-Nomikos, Mieke Ptasynski, Wendy Parulekar, and National Cancer Institute of Canada Clinical Trials Group. Erlotinib plus gemcitabine compared with gemcitabine alone in patients with advanced pancreatic cancer: a phase III trial of the National Cancer Institute of Canada Clinical Trials Group. *J. Clin. Oncol.*, 25(15):1960–1966, May 2007. PMID 17452677.

[175] R Palorini, F P Cammarata, F Cammarata, C Balestrieri, A Monestiroli, M Vasso, C Gelfi, L Alberghina, and F Chiaradonna. Glucose starvation induces cell death in K-ras-transformed cells by interfering with the hexosamine biosynthesis pathway and activating the unfolded protein response. *Cell Death Dis*, 4:e732, 2013. PMID 23868065.

[176] Brandon Faubert, Gino Boily, Said Izreig, Takla Griss, Bozena Samborska, Zhifeng Dong, Fanny Dupuy, Christopher Chambers, Benjamin J Fuerth, Benoît Viollet, Orval A Mamer, Daina Avizonis, Ralph J DeBerardinis, Peter M Siegel, and Russell G Jones. AMPK is a negative regulator of the Warburg effect and suppresses tumor growth in vivo. *Cell Metab*, 17(1):113–124, January 2013. PMID 23274086.

[177] Krushna C Patra, Qi Wang, Prashanth T Bhaskar, Luke Miller, Zebin Wang, Will Wheaton, Navdeep Chandel, Markku Laakso, William J Muller, Eric L Allen, Abhishek K Jha, Gromoslaw A Smolen, Michelle F Clasquin, R Brooks Robey, and Nissim Hay. Hexokinase 2 Is Required for Tumor Initiation and Maintenance and Its Systemic Deletion Is Therapeutic in Mouse Models of Cancer. *Cancer Cell*, July 2013. PMID 23911236.

[178] Farzin Haque, Dan Shu, Yi Shu, Luda S Shlyakhtenko, Piotr G Rychahou, B Mark Evers, and Peixuan Guo. Ultrastable synergistic tetravalent RNA nanoparticles for targeting to cancers. *Nano Today*, 7(4):245–257, August 2012. PMID 23024702.

[179] Yi Shu, Fengmei Pi, Ashwani Sharma, Mehdi Rajabi, Farzin Haque, Dan Shu, Markos Leggas, B Mark Evers, and Peixuan Guo. Stable RNA nanoparticles as potential new generation drugs for cancer therapy. *Adv. Drug Deliv. Rev.*, 66:74–89, February 2014. PMID 24270010.

[180] Maria Rohm. *Transcriptional co-factor TBLR1 controls lipid mobilization in white adipose tissue*. PhD thesis, Ruprecht-Karls-Universität, Heidelberg, 2012.

[181] Stephan Herzig, Fanxin Long, Ulupi S Jhala, Susan Hedrick, Rebecca Quinn, Anton Bauer, Dorothea Rudolph, Gunther Schutz, Cliff Yoon, Pere Puigserver, Bruce M Spiegelman, and Marc Montminy. CREB regulates hepatic gluconeogenesis through the coactivator PGC-1. *Nature*, 413(6852):179–183, September 2001. PMID 11557984.

[182] Markus Schmitt and Michael Pawlita. High-throughput detection and multiplex identification of cell contaminations. *Nucleic Acids Res*, 37(18):e119, October 2009. PMID 19589807.

[183] Michael R Lamprecht, David M Sabatini, and Anne E Carpenter. CellProfiler: free, versatile software for automated biological image analysis. *BioTechniques*, 42(1):71–75, January 2007. PMID 17269487.

[184] Anne E Carpenter, Thouis R Jones, Michael R Lamprecht, Colin Clarke, In Han Kang, Ola Friman, David A Guertin, Joo Han Chang, Robert A Lindquist, Jason Moffat, Polina Golland, and David M Sabatini. CellProfiler: image analysis software for identifying and quantifying cell phenotypes. *Genome Biol*, 7(10):R100, 2006. PMID 17076895.

[185] Lee Kamentsky, Thouis R Jones, Adam Fraser, Mark-Anthony Bray, David J Logan, Katherine L Madden, Vebjorn Ljosa, Curtis Rueden, Kevin W Eliceiri, and Anne E Carpenter. Improved structure, function and compatibility for CellProfiler: modular high-throughput image analysis software. *Bioinformatics*, 27(8):1179–1180, April 2011. PMID 21349861.

[186] Wen-Ping Hsieh, Tzu-Ming Chu, Russell D Wolfinger, and Greg Gibson. Mixed-model reanalysis of primate data suggests tissue and species biases in oligonucleotide-based gene expression profiles. *Genetics*, 165(2):747–757, October 2003. PMID 14573485.

[187] J Roy. SAS for Mixed Models. *J Biopharm Stat*, 17:363–365, 2007.

[188] Aravind Subramanian, Pablo Tamayo, Vamsi K Mootha, Sayan Mukherjee, Benjamin L Ebert, Michael A Gillette, Amanda Paulovich, Scott L Pomeroy, Todd R Golub, Eric S Lander, and Jill P Mesirov. Gene set enrichment analysis: a knowledge-based approach for interpreting genome-wide expression profiles. *Proc Natl Acad Sci USA*, 102(43):15545–15550, October 2005. PMID 16199517.

[189] Theodora Manoli, Norbert Gretz, Hermann-Josef Gröne, Marc Kenzelmann, Roland Eils, and Benedikt Brors. Group testing for pathway analysis improves comparability of different microarray datasets. *Bioinformatics*, 22(20):2500–2506, October 2006. PMID 16895928.

[190] RDC Team. *R: A language and environment for statistical computing*. R foundation for Statistical Computing, Vienna, Austria, 2005. ISBN 3-900051-07-0.

[191] Jordi Folch, M Lees, and G H Sloane Stanley. A simple method for the isolation and purification of total lipides from animal tissues. *J Biol Chem*, 226(1):497–509, May 1957. PMID 13428781.

[192] Christoph Sommer, Christoph Straehle, Ullrich Köthe, and Fred A Hamprecht. ilastik: Interactive Learning and Segmentation Toolkit. In *8th IEEE International Symposium on Biomedical Imaging (ISBI)*, 2011.

[193] World Health Organization (WHO). Prevalence of obesity, ages 20+, age standardized, both sexes, 2008 [online]. Available from: `http://gamapserver.who.int/mapLibrary/Files/Maps/Global_Obesity_BothSexes_2008.png` [cited 16.02.2014].

[194] World Health Organization (WHO). Prevalence of raised fasting blood glucose, ages 25+, age standardized, both sexes, 2008 [online]. Available from: `http://gamapserver.who.int/mapLibrary/Files/Maps/Global_BloodGlucosePrevalence_BothSexes_2008.png` [cited 16.02.2014].

[195] Akihiro Tomita, Daniel R Buchholz, Keiko Obata, and Yun-Bo Shi. Fusion protein of retinoic acid receptor alpha with promyelocytic leukemia protein or promyelocytic leukemia zinc finger protein recruits N-CoR-TBLR1 corepressor complex to repress transcription in vivo. *J Biol Chem*, 278(33):30788–30795, August 2003. PMID 12794076.

[196] Akihiro Tomita, Daniel R Buchholz, and Yun-Bo Shi. Recruitment of N-CoR/SMRT-TBLR1 corepressor complex by unliganded thyroid hormone receptor for gene repression during frog development. *Mol Cell Biol*, 24(8):3337–3346, April 2004. PMID 15060155.

[197] Ho-Geun Yoon, Youngsok Choi, Philip A Cole, and Jiemin Wong. Reading and function of a histone code involved in targeting corepressor complexes for repression. *Mol Cell Biol*, 25(1):324–335, January 2005. PMID 15601853.

[198] Takahiro Ishizuka and Mitchell A Lazar. The nuclear receptor corepressor deacetylase activating domain is essential for repression by thyroid hormone receptor. *Mol Endocrinol*, 19(6):1443–1451, June 2005. PMID 15695367.

[199] Gabi Gerlitz, Enbal Darhin, Giovanna Giorgio, Brunella Franco, and Orly Reiner. Novel functional features of the Lis-H domain: role in protein dimerization, half-life and cellular localization. *Cell Cycle*, 4(11):1632–1640, November 2005. PMID 16258276.

[200] Xin-Min Zhang, Qing Chang, Lin Zeng, Judy Gu, Stuart Brown, and Ross S Basch. TBLR1 regulates the expression of nuclear hormone receptor co-repressors. *BMC Cell Biol.*, 7:31, 2006. PMID 16893456.

[201] Hyo-Kyoung Choi, Kyung-Chul Choi, Hee-Bum Kang, Han-Cheon Kim, Yoo-Hyun Lee, Seungjoo Haam, Hyoung-Gi Park, and Ho-Geun Yoon. Function of multiple Lis-Homology domain/WD-40 repeat-containing proteins in feed-forward transcriptional repression by silencing mediator for retinoic and thyroid receptor/nuclear receptor corepressor complexes. *Mol Endocrinol*, 22 (5):1093–1104, May 2008. PMID 18202150.

[202] Wendy Huang, Serena Ghisletti, Valentina Perissi, Michael G Rosenfeld, and Christopher K Glass. Transcriptional integration of TLR2 and TLR4 signaling at the NCoR derepression checkpoint. *Mol Cell*, 35(1):48–57, July 2009. PMID 19595715.

[203] Yoana N Dimitrova, Jiong Li, Young-Tae Lee, Jessica Rios-Esteves, David B Friedman, Hee-Jung Choi, William I Weis, Cun-Yu Wang, and Walter J Chazin. Direct ubiquitination of beta-catenin by Siah-1 and regulation by the exchange factor TBL1. *J Biol Chem*, 285(18):13507–13516, April 2010. PMID 20181957.

[204] Sari Toropainen, Sami Väisänen, Sami Heikkinen, and Carsten Carlberg. The down-regulation of the human MYC gene by the nuclear hormone 1alpha,25-dihydroxyvitamin D3 is associated with cycling of corepressors and histone deacetylases. *J Mol Biol*, 400(3):284–294, July 2010. PMID 20493879.

[205] Charles E Foulds, Anna Tsimelzon, Weiwen Long, Andrew Le, Sophia Y Tsai, Ming-Jer Tsai, and Bert W O'Malley. Research resource: expression profiling reveals unexpected targets and functions of the human steroid receptor RNA activator (SRA) gene. *Mol Endocrinol*, 24(5):1090–1105, May 2010. PMID 20219889.

[206] Aurore Keutgens, Kateryna Shostak, Pierre Close, Xin Zhang, Benoît Hennuy, Marie Aussems, Jean-Paul Chapelle, Patrick Viatour, André Gothot, Marianne Fillet, and Alain Chariot. The repressing function of the oncoprotein BCL-3 requires CtBP, while its polyubiquitination and degradation involve the E3 ligase TBLR1. *Mol Cell Biol*, 30(16):4006–4021, August 2010. PMID 20547759.

[207] Ren-Hua Chung, Deqiong Ma, Kai Wang, Dale J Hedges, James M Jaworski, John R Gilbert, Michael L Cuccaro, Harry H Wright, Ruth K Abramson, Ioanna Konidari, Patrice L Whitehead, Gerard D Schellenberg, Hakon Hakonarson, Jonathan L Haines, Margaret A Pericak-Vance, and Eden R Martin. An X chromosome-wide association study in autism families identifies TBL1X as a novel autism spectrum disorder candidate gene in males. *Mol Autism*, 2(1):18, 2011. PMID 22050706.

[208] Sivakumar Ramadoss, Jiong Li, Xiangming Ding, Khalid Al Hezaimi, and Cun-Yu Wang. Transducin β-like protein 1 recruits nuclear factor κB to the target gene promoter for transcriptional activation. *Mol Cell Biol*, 31(5):924–934, March 2011. PMID 21189284.

[209] Brian J O'Roak, Laura Vives, Wenqing Fu, Jarrett D Egertson, Ian B Stanaway, Ian G Phelps, Gemma Carvill, Akash Kumar, Choli Lee, Katy Ankenman, Jeff Munson, Joseph B Hiatt, Emily H Turner, Roie Levy, Diana R O'Day, Niklas Krumm, Bradley P Coe, Beth K Martin, Elhanan Borenstein, Deborah A Nickerson, Heather C Mefford, Dan Doherty, Joshua M Akey, Raphael Bernier, Evan E Eichler, and Jay Shendure. Multiplex targeted sequencing identifies recurrently mutated genes in autism spectrum disorders. *Science*, 338(6114):1619–1622, December 2012. PMID 23160955.

[210] Kihoon Han, Vincenzo Alessandro Gennarino, Yoontae Lee, Kaifang Pang, Kazue Hashimoto-Torii, Sanaa Choufani, Chandrasekhar S Raju, Michael C Oldham, Rosanna Weksberg, Pasko Rakic, Zhandong Liu, and Huda Y Zoghbi. Human-specific regulation of MeCP2 levels in fetal brains by microRNA miR-483-5p. *Genes Dev*, 27(5):485–490, March 2013. PMID 23431031.

[211] Carmen García-Ibarbia, Jesús Delgado-Calle, Iñigo Casafont, Javier Velasco, Jana Arozamena, María I Pérez-Núñez, María A Alonso, María T Berciano, Fernando Ortiz, José L Pérez-Castrillón, Agustín F Fernández, Mario F Fraga, María T Zarrabeitia, and José A Riancho. Contribution of genetic and epigenetic mechanisms to Wnt pathway activity in prevalent skeletal disorders. *Gene*, 532(2):165–172, December 2013. PMID 24096177.

[212] Gabriela P de Oliveira, Jessica R Maximino, Mariana Maschietto, Edmar Zanoteli, Renato D Puga, Leandro Lima, Dirce M Carraro, and Gerson Chadi. Early gene expression changes in skeletal muscle from SOD1(G93A) amyotrophic lateral sclerosis animal model. *Cell Mol Neurobiol*, 34(3):451–462, April 2014. PMID 24442855.

[213] Hailian Bi, Shujing Li, Miao Wang, Zhaojun Jia, Alan K Chang, Pengsha Pang, and Huijian Wu. SUMOylation of GPS2 protein regulates its transcription-suppressing function. *Mol Biol Cell*, June 2014. PMID 24943844.

Index